Title
Utilizing Stable Isotope Labeling to Measure Changes in Global, Ontology-Grouped, and Individual Protein Flux Rates in Skeletal Muscle

Author
Bizieff, Alec

Publication Date
2023

Peer reviewed|Thesis/dissertation

Utilizing Stable Isotope Labeling to Measure Changes in Global, Ontology-Grouped, and Individual Protein Flux Rates in Skeletal Muscle

By

Alec Bizieff

A dissertation submitted in partial satisfaction of the

requirements for the degree of

Doctor of Philosophy

in

Metabolic Biology

in the

Graduate Division

of the

University of California, Berkeley

Committee in Charge:

Professor Marc Hellerstein, Chair
Professor Anders Näar
Professor Irina Conboy

Summer 2023

Abstract

Utilizing Stable Isotope Labeling to Measure Changes in Global, Ontology-Grouped, and Individual Protein Flux Rates in Skeletal Muscle

By

Alec Bizieff

Doctor of Philosophy in Metabolic Biology

University of California, Berkeley

Professor Marc Hellerstein, Chair

Proteins are the ultimate focal point for organismal composition and the basis for many biological functions that occur within. It is well known that proteins in a biological system are not static; there is flux through synthesis and degradation pathways, resulting in a dynamic steady-state that underlies both stable and adaptive levels of proteins. For many biological functions to occur, the rate of either protein synthesis or degradation deviates from normal to allow for changes to occur. Accordingly, when protein pool size adjusts to new levels a kinetic signature in the form of a fraction of newly synthesized proteins may be present at each stage. In the Hellerstein Lab, we utilize an innovative methodology and approach to measure this signature directly *in-vivo* with stable isotope labeling.

The approach used in this study to measure protein dynamics *in-vivo* involves administering deuterium (^2H) from deuterated "heavy" water (^2H_2O) to research subjects or experimental animals. During the labeling period, newly synthesized proteins will incorporate the available ^2H into amino acids in newly synthesized protein molecules, resulting in "heavy" proteins. These are functionally identical to their non-^2H-incorporated "light" counterparts and only differ in subtle alterations in the pattern and amount of deuterium atoms in the constituent amino acids of which a peptide chain is composed. Protein mass isotopomers are then quantified through analysis by high-performance liquid chromatography (HPLC) coupled single (MS) and tandem (MS/MS) mass spectrometry and protein flux rates are calculated by use of Mass Isotopomer Distribution Analysis (MIDA). With this approach, we investigated here non-invasive biomarkers of Duchenne muscular dystrophy (DMD) as well as the unique stages of muscle tissue regeneration and effects on tissues distant from acute injury.

DMD is the most severe form of muscular dystrophy, with debilitating symptoms that cause patients to succumb to their complications early in life. Currently, there are a few approved treatments for DMD, but these therapies mainly treat the symptoms of the disease and have shown mild improvements in a clinical population so far. DMD is one of the most studied genetic diseases, as there is a pressing demand for proper treatment or therapy for this indication. Here, we have discovered and validated a clinical biomarker of whole muscle protein synthesis,

which is a key marker of skeletal muscle health in DMD, from non-invasive methods. This marker was first discovered in a clinical population, but then reverse translated to an animal model of DMD to validate that it is a faithful marker of whole muscle protein synthesis rates. Our data clearly demonstrate that certain muscle-specific proteins can escape into circulation from the dystrophic muscle and be captured from urinary excretion to understand changes in whole-muscle protein flux rates. These findings may provide crucial information to clinicians and researchers alike about a key metric that can determine disease progression or response to treatment.

Both skeletal and smooth muscle tissue have the capacity to regenerate after injury or damage to help maintain optimal functional properties. This regenerative capacity is an important process, and its dysregulation is implicated in many diseases, such as muscular dystrophy and pathological atrophy. Muscle regeneration is a widely studied topic, but no one has utilized the method of *in-vivo* stable isotope labeling to categorize the global, ontology-grouped, and individual flux rates of proteins at each sequential unique stage of regeneration. In the work presented here, we examine how protein flux rates change over time as skeletal muscle tissue regenerates from an acute injury. Also, we explore the relationship between protein flux measurements and abundance-based gene expressions to understand their correlation.

There is evidence to support the notion that other muscle tissue that is not directly injured will respond to systemic circulating factors from acute tissue injury and enter an altered functional state. Therefore, we also explore the effect that acute local injury has on distant muscle tissue that is undamaged. Our data show clear changes in global, ontology-grouped, and individual protein flux changes at each unique stage of muscle regeneration, and that there is no correlation between measured protein flux changes in regenerating muscle and gene expression of the same proteins. Interestingly, changes are further demonstrated in global, ontology-grouped, and individual protein fluxes in muscle that are distant to local acute injury, which do not reflect the same tissue gene expression rates. This data provides further evidence that other muscle tissue that is not directly injured will respond to systemic circulating factors from acute tissue injury. Therefore, setting up future experiments to deepen our understanding of the systemic communication network that our body utilizes during injury or regenerative events.

Table of Contents

Acknowledgments

To say this work was done in solitude would be a lie. It simply could not have been achieved without the dedicated effort of many other individuals besides myself. From direct contributions to the work produced in this document to the intangible things like support and encouragement, many were able to leave their mark on my work in one way or another. Unfortunately, it is hard to quantify the impact from, and therefore acknowledge, every single person who helped me to get to where I am today. However, I did my best to keep tabs on those who made a meaningful influence on my graduate studies and tried to acknowledge their contributions in the following passages. Thank you all to those mentioned (and not mentioned) for all that you have done for me to help me complete this degree. Your efforts are much appreciated.

Dr. Marc Hellerstein, MD, PhD

Obviously, the principal investigator (PI) for a graduate student's project should get the most, and therefore, first acknowledgment for their contributions to the student's work. Marc is no exception to this rule. The work that was done over the course of my graduate degree was heavily influenced and primarily guided by Marc. Therefore, on a conceptual level, this work has as much credit to me as to him as well.

Marc is hands down the smartest individual that I have ever interacted with, much less had the ability to directly learn from over the course of my time at Berkeley. To have an M.D. and PhD from separate Ivy League institutions, become a tenured professor at one of the world's premier research universities, start and run his own start-up biotech company based on an analytical model that he conceived, on top of conducting groundbreaking clinically based research year after year is nothing short of a laundry list of momentous achievements. There are times when I believed that he contained an entire encyclopedia's worth of information in his head that could be readily called upon no matter what scientific topic was being discussed. It was truly astonishing that someone could have such a detailed an in-deptht understanding of human metabolic disease and their underlying biochemical processes as Marc does. However, for him, it is just another routine day of speaking with research collaborators, funding agencies, his fellow professors of Morgan Hall, or sharing his thoughts in lab meeting. Needless to say, Marc's intelligence speaks for itself, and I knew that he was more than capable of providing the correct insight and guidance to take me from a newbie graduate student to a seasoned PhD candidate.

It was not only Marc's intellect that made me decide to join the Hellerstein Lab, but more so the research. His focus on translational research is unlike any other in the department and his commitment to producing relevant and applicable research in the field of metabolic diseases is unparalleled. I am a firm believer in the adage, "If it doesn't translate to a clinical population, then so what?" and was glad to find a mentor that shared a similar sentiment. The unique opportunity to be directly involved with clinical based research studies is something that will stand out as special for me during my time at Berkeley. For me, the Hellerstein Lab was the perfect synergy of biological concepts overlaid on germane clinical based studies. Seeing my work translate into improving the quality of life of another person is an experience that is almost exclusively fulfilled by the work done in the Hellerstein Lab.

In summary, I am thankful for the impact that Marc has had on my work and truly believe that I wouldn't have been able to do it without his input. His lab set the scaffolding for which I was able to construct this work from and deliver this completed project.

Dr. Anders Näar, PhD

Another key influence on my time as a graduate student here at UC Berkeley was the presence of Dr. Anders Näar. I will be honest, if I hadn't joined the Hellerstein Lab, my other choice would have been the lab of Dr. Näar. Unfortunately, I joined the department right around the same time he came over from Harvard and the Näar Lab was still the "new kid on the block" that had not established themselves into the department stalwart they are today. Also, at the time, I was too naive to understand what microRNA were and how they are implicated in all kinds of human health and disease. Knowing what I do now, which is still not much, I would have given the Näar Lab a strong consideration (but most likely would have still ended up where I am now).

From being a part of my oral qualification exam, to offering to work collaboratively on a high-impact research paper, Dr. Näar's input and feedback have always helped shape the trajectory and outcome of my work as a graduate student. In fact, his influence on my work started almost from the first day that I joined the department. My early interest in Duchenne muscular dystrophy, which happened to turn into one of the sections below in this dissertation, was sparked by a relatively new project he was working on at the time. Our paths crossed and we struck up a conversation about the current research and therapies behind the disease. It ended up with a strong mentor-mentee relationship that I was able to gain key insight into that field of study. Overall, my project would not have been what is it today without the ample help and support that Dr. Näar has provided. For that, I am grateful to have crossed paths with such a soft spoken but knowledgeable individual that has helped me along almost every step of my graduate journey.

Dr. Irina M Conboy PhD

If the credit for the first half of my dissertation goes to Dr. Näar, then the second half goes to Dr. Irina Conboy. She was the brainchild that sparked my motivation to study the dynamics of skeletal muscle regeneration in the scope of *in-vivo* necrotic damage. In fact, she provided me with access to many of the resources and academic works that started my journey down this path of regeneration biology. Therefore, I am fortunate to have Dr. Conboy as my out of department thesis committee member, otherwise I would not have been exposed to it and decided to pursue one half of my entire dissertation.

My respect for Dr. Conboy does not stop at her intellectual horsepower. At first glance, she is a seemingly sweet woman with a strong Eastern European accent. However, after spending no more than a few minutes with Dr. Conboy, anyone will be left puzzled how she can fit such a large personality into such a small stature. She is lively and full of energy, generally finds herself at the center of all conversations but also ready to set someone straight at all times. One of my fondest moments of Dr. Conboy is when she was invited to give a presentation in front of my entire department, professors and all. At some point in her slide presentation, a fellow professor raised their hand and proposed that there was no evidence behind one of the claims she had made. She sharply yet gracefully refuted that point with concrete evidence that was hidden elsewhere in her presentation, almost as if she was waiting for that comment to be made. The end result of that exchange was a collective unspoken shock from the entire department to the embarrassment that she just dealt out, but the aftermath was a solidified respect by many for Dr. Conboy as a "take-no-shit" academic mind. Dr. Conboy's impact on my time at Berkeley has been immense and I am grateful to have her as another mentor for my project. I will always remember her not only for her great work in the field of regeneration biology, but also as one of my favorite personalities that I directly interacted with on campus.

Kelvin Lee

Again, the results of my work were not generated in a vacuum. Besides the direct mentorship of Dr. Hellerstein, I was able to benefit from the contributions of the senior staff scientists in the Hellerstein Lab, such as Kelvin. Every leader has their "right-hand man" as someone they trust to call upon when they need a second opinion; Michael Jordan had Scottie Pipen, Steve Jobs had Steve Wozniak, and Marc Hellerstein has Kelvin Lee. In his own right, Kelvin has the brains and skills to run an academic lab of his own. However, he decides to use his intellect to guide many of the clinical collaborations that the Hellerstein Lab undertakes and provide an expert opinion on all things Mass Isotopomer Distribution Analysis (MIDA) related.

Outside of his readily apparent intelligence, Kelvin is one of the smoothest and most laid-back type of guys I know, especially for the workload he handles for this lab. Unfortunately, the remote work demands in the post-pandemic era only permitted Kelvin to come into the lab once a week or so, primarily for lab meetings. This drastically shortened the face-to-face interactions that I was able to have with him. However, in the time that we did talk in person, he was always a pleasant conversation to have. From the newest mass spectrometry techniques to which Tight End to play in Fantasy Football this week, Kelvin is one of the people you can talk to about anything and everything under the sun. And while his role was mainly reserved for attending to the clinical collaborators, he would always provide poignant feedback that was relevant and actionable when I would present my data in lab meetings. Therefore, a lot of my work can be attributed to Kelvin's thoughts and ideas, and for that I am grateful to have someone like him on the Hellerstein Lab team.

Shubha Shankaran

Along with Kelvin, Shubha makes up the other half of the senior scientists in the Hellerstein Lab. Despite having similar job roles mainly handling clinical collaborations, Shubha has still found time to make a substantial impact on my work. When I first settled on joining the Hellerstein Lab, Shubha was the first person I directly worked with on a project. She took my hand and led me from being a novel graduate student to directly contributing to a major clinical research study. In fact, the outcomes of that project are included in this dissertation below.

I was able to learn so much from Shubha in the field of clinical research and musculoskeletal disease in a short time. She played the day-to-day role of my direct mentor when Marc was not readily available. I could always rely on her to provide a thorough and detail filled answer to any research question I had about my own topic. I can recall having 45-minute discussions with her over simple methods development processes, going into fine detail about each step and the current literature that surrounded it. Much like the other senior members of the Hellerstein Lab, Shubha was a walking encyclopedia of pertinent information, of which I greatly benefited from having access to. She laid a lot of the foundation on which I was able to build my research studies upon and her expertise and knowledge in the field helped drive the projects laid out in this dissertation to completion. I am very fortunate to have someone like Shubha readily accessible to talk about anything with and cannot believe that my degree would have turned out the way it did without her presence in the Hellerstein Lab.

Maggie Cheng

If all of my mentors are responsible in part for steering me on the right path in my degree, then Maggie is responsible in part for putting in the work to get me there. As one part of my undergraduate duo, Maggie's contributions to my projects are invaluable. It is truly astonishing the magnification power an extra set of capable hands can produce on the overall productivity and output of my work. Having Maggie work alongside me for the past two years has been nothing but a pleasure. Her easy-going demeanor mixed with her willingness to learn and put in the work has made her nothing less than an ideal fit for an undergraduate volunteer. I have heard horror stories from other graduate students about poorly performing undergraduates detracting from their progress in the lab. However, I am confident to say that Maggie exceeded my expectations and was a massive benefit to have working for me. Taking an undergraduate volunteer is a bit of a gamble, due to the reasons previously mentioned, however, I believe that my time and energy investment paid off great dividends with Maggie and I am grateful for the work she has contributed to my dissertation projects.

Thankfully, at the time of writing this dissertation, Maggie will spend another year in the Hellerstein Lab, finishing up her honors thesis, of which she conceived herself. That way she has time to finish up my manuscript revision experiments for me alongside completing her own project. All jokes aside, Maggie has a bright future ahead of her wherever she decides to take her career. I am confident that she will make great contributions to whatever path she decides to take in life and that her efforts as well as strong character traits will take her to great achievements. Overall, it was a pleasure to work with Maggie, and I hope we will stay in touch as we both progress into the next stages of our career and beyond.

Kelvin Chang

Along with Maggie, Kelvin completes the duo of undergraduate volunteers that made a significant impact on the work provided in this dissertation. Having one extra set of capable hands does wonders for a graduate student's productivity, but two sets is almost like having a cheat code enabled. Kelvin's intellect along with his easy-going attitude made it a great experience to work with him. He was easy to teach and rarely would I have to explain things more than once to him. I could trust he knew what to do in the lab and let him operate with a great deal of autonomy as an undergraduate. That is pretty impressive for an undergraduate since it was ultimately my work that was on the line here. However, I knew that it was in safe hands and that I could trust Kelvin (and Maggie too) to get the work done properly and on time. Whether it was staying later than expected on a school night or coming in on the weekends to help out with an experiment, Kelvin was always there when I needed the extra set of hands. His dedication to the work and enthusiasm to put in extra effort are things that I am grateful to have as an undergraduate volunteer.

Kelvin has a bright future ahead of him as a research scientist at Genentech. As of the time of writing this dissertation, he just completed his time as an undergraduate at UC Berkeley and is starting a contract position at Genentech this summer. Regardless of the path he decides to take for his career, I am sure that Kelvin will have an immediate and lasting impact wherever he ends up. It was a great pleasure to work with Kelvin and I am sure he will put his intellect and demeanor to good use in his current and future roles in industry. I also hope to stay in contact with Kelvin, as he one day might be able to get me a job at Genentech.

Naveed Ziari

Oh man, what a character Naveed is. If you ask anyone else in the department about their thoughts on him, they will most likely laugh and share a colorful, yet stereotypical "Naveed" type story with you. As a fellow graduate student in the Hellerstein Lab, Naveed was a quintessential part of my experience in graduate school, and it wouldn't be the same without him. On a daily basis, he was probably the person I talked to the most in the whole department. And when I say talked to, it could be about *ANYTHING*. From NBA basketball playoffs, to Bitcoin, to geopolitics, Naveed is the kind of person that can hold a conversation with anyone about anything and everything. It was always a small surprise to see him in the lab every morning and hear whatever ridiculous story happened to him the day before. Although after spending nearly 4 years working with him, Naveed never ceases to bring in a new story almost every morning that seems to top the ridiculousness of the last one.

In all seriousness, Naveed is genuinely intellectually talented and has unparalleled knowledge of MIDA and mass spectrometry that will prove to be a coveted skillset one day. Although his project is fundamentally different from mine, Naveed was still able to help with various aspects of the work in this dissertation, including bioinformatics analysis. His genius with software engineering is a massive benefit to have in the Hellerstein Lab and has proven valuable to fellow members, including myself. However, I would say Naveed's main contributions to my work in this dissertation are more as a fellow "brother in arms" to battle the pits of academia alongside with. I could go on to describe some of his antics in detail, but I believe the best way to sum up Naveed's impact on my time as a graduate student is like so; the best cure for digging through the trenches of laboratory work is laughter and without Naveed's presence, my time at UC Berkeley wouldn't be as lively or enjoyable as it was.

Hussein Mohammad

Now you talk about one of my all-time favorite people in the Hellerstein Lab, Hussein is definitely in contention for the top spot. He's the kind of guy that you just have to experience being around to know what I mean. His story of immigrating from Eastern Africa to the US is fascinating and shows the character this guy has. Being the resident mass spectrometry technician in the Hellerstein Lab, I actually have to credit Hussein with doing the most work for my dissertation projects. Without his assistance, none of this would have been possible. I mean that. He operates multiple close to half-a-million-dollar machines and is the central point that the majority of the work in the Hellerstein Lab goes through. Without his knowledge and expertise, there would be no MIDA experiments to be run.

But it is not only his necessary presence in the lab that is what I appreciate about Hussein. He is the coolest dude in this department hands down. I mean that in both definitions of the word. His life story is inspiring and some of the decisions he had to make in order to benefit the rest of his family are downright deserving of a medal. You will have to ask him about it for the full details. But he is also the calmest, soft-spoken individual I have ever met in science. I legitimately cannot recall a time that I witnessed Hussein visibly frustrated or upset. His constant attitude of stoicism is impressive especially when you factor in his job responsibilities. That is why I am fortunate to have Hussein as a part of the Hellerstein Lab. Without him, the work done here would probably not exist and I for sure would be missing my daily dose of calm Hussein energy to help keep a level head in the lab.

Edna Nyangau

As one of the researcher technicians in the Hellerstein Laboratory, Edna played a vital role in generating the data for my projects. As with Hussein, I don't think I would be where I am today without her help. Her knowledge and dependability are what make her a crucial part of the success the Hellerstein Lab has achieved over the years. She is pretty much responsible for the majority of clinical collaboration samples that are processed in the lab. She knows more about the GC/MS and the Q-Trap MS than the rest of the laboratory combined. But what truly makes her an exceptional person to work with is her resilience and dependability. You can find her in the lab on nights and weekends pretty much consistently. Despite the fragile nature of some mass spectrometry machines, she is always there to fix things when they break. I know every time I submit samples for her to run on the mass spectrometer for me, I can count on her to run them promptly and to return accurate results.

However, what makes Edna so unique as an individual is not only her scientific prowess, but also her vibrant personality. At first glance, she is quiet and projects a reserved demeanor. But once you get to know her, Edna is as vivacious and outgoing as anyone else I know. She is quick to make friends with anyone and also not afraid to tell them what's on her mind. That is one of the things I respect the most about her. She tells it like it is and isn't afraid of what others might think. Along with science, she has a passion for the arts and creativity. I feel like this is a perfect way for her to show her true colors and project her form of self expression. Overall, I admire and respect Edna both as a researcher and as an individual. Her efforts have certainly helped me to reach the finish line of my degree and her presence has left an impression that will not soon be forgotten.

Mark Fitch

Although Mark retired about halfway through my degree, I still owe him a lot of acknowledgements for the assistance he provided me with during my time in the Hellerstein Lab. A wise and sagely individual, Mark symbolized a father-like figure for most people in the lab. His tenure and experience made him a wealth of technical knowledge for all the experiments that go on in the laboratory. He is the only exception to Edna in terms of GC/MS knowledge. In fact, he most likely taught her the vast majority of information he knew about the machines. No matter what the question was, if it had to do with something that was going on inside the walls of the Hellerstein Lab, Mark was the guy to ask. He was pretty much the glue that kept the laboratory running smoothly on a daily basis in terms of technical oversight and operations.

What I liked most about Mark was his personality and the way he treated people. He seemed to consistently be in a state of relaxation no matter the external circumstances. Like he had seen it all and nothing new could be thrown his way to phase him. He was always ready to help and share his advice when someone needed it, regardless of what he was doing at the time. It was comforting to know that "I could always ask Mark" whenever I embarked upon a new project in the lab or got stumped on how to troubleshoot a protocol. These are the reasons I am grateful to have Mark be a part of the Hellerstein Lab. Also, because he is one of the last true Oakland A's baseball fans left. That truly shows his long-term commitment to something. Overall, Mark was a great mentor for the in's and out's of daily laboratory work. He was an even better person to be around, and I thoroughly enjoyed being in his presence, whether it was to fix a faulty experiment or to grieve about last night's ball game.

Marcy Matthews

If Mark Fitch is the “lab dad” of the Hellerstein Lab, then Marcy is the “lab mom”. She handled all of the day-to-day operations that occurred in the lab with an organized and poised manner. She was always available to help whenever someone needed her assistance. I felt that the first half of my degree I was over burdening her with constant questions to get myself up to speed on the laboratory work, however, I then realized that Marcy generally enjoyed helping whoever she could, no matter what she was doing at the time. That is pretty impressive given that she usually had her hands tied up doing her own laboratory work. Marcy was like a laboratory “swiss army knife”, who could pretty much handle anything thrown her way. From troubleshooting the spectrometer for protein assay protocols to handling laboratory supply ordering and everything in between, Marcy was a true Renaissance woman.

The best part about Marcy is no matter what the task was, she seemed to always do it with a smile on her face. Her bubbly personality would make anyone feel as if they were right at home, even if it was their first day on the job. This is how Marcy treated me, and everyone she dealt with, and I am grateful to have her as someone to both look up to and simultaneously joke around with in the lab. When she announced her temporary departure from the Hellerstein Lab to take care of her on-the-way second child, there was a uniform sense of sadness along with panic. Sadness that we won’t have Marcy’s infectious attitude to bring the lab up a few beats on the daily, but also a panic set in as to how we could cover all of her responsibilities. This just goes to show how much of an impact Marcy had on the lab and how her presence truly was missed upon her departure. Therefore, it was a pleasure to work alongside and become friends with Marcy, and I hope she finds her way back to the Hellerstein Lab one day if it suits her.

Tyler Field

Being the last, but definitely not the least, acknowledgement for their contributions to my work as a graduate student is Tyler. He is an integral part of the Hellerstein Lab that, upon Marcy’s departure, absorbed the role of day-to-day operations in the lab. As is a common theme amongst Hellerstein Lab members, Tyler truly embodied the laid-back, easy-going personality that is becoming more of a rarity in the life sciences. His love for professional sports, mainly the NBA, made it easy to establish a connection with him since my early days in the Hellerstein Lab. Since then, it grew over time to be one of the strongest connections that I still have in the department. Although we may be on different working schedules now, mine more of a strict 9 -5 and his being early mornings or late nights, when we do cross paths in the lab it's like nothing has changed. Being so, I am lucky to still be in contact with Tyler and hope to maintain this as we both move forward in our lives.

As I mentioned, once Marcy left, Tyler took on most of her responsibilities as a laboratory technician. Which is beyond remarkable since he already had his own workstream of duties to complete. But by adding on the remainder of the work to be done in the lab, now pretty much all of the daily processes are done by him. It is of no surprise that he can take on this amount of responsibility and still handle his work as he is one of the most dependable and trustworthy people in this lab. What he does to make sure this lab functions on a daily basis is just a reflection of that. Therefore, I am grateful for Tyler’s presence in this lab and as someone I can enjoy having a friendly conversation with whenever we see each other. Without him, the Hellerstein Lab would not function to the degree it does today, and I certainly wouldn’t enjoy the same connection with someone when the Golden State Warriors play the Sacramento Kings.

Introduction

Overview of a Stable Isotope (^2H_2O) Labeling Method and Workflow to Measure Protein Flux Rates *In-Vivo*

Proteins comprise many of the necessary components of vital processes in biological systems. The function of proteins includes (but are not limited to) reaction catalyzing enzymes, signaling molecules, cell surface receptors, transcription factors, cellular chaperons, and integral components of organelles and their functions. Proteins are the endpoint of informational flow in a biological system. DNA, which harbors and produces the message when prompted, is translated into the intermediary "messenger" RNA, which acts as a transient medium to shuttle the information signal to a ribosome for the production of protein [1]. Proteins are produced and regulated in a highly specific manner, to ensure proper cellular dynamics depending on intracellular or extracellular stimulus. Ultimately, the interaction of many proteins dictates the behavior of the cell it comprises; the interaction of many cells dictates the behavior of a tissue they are a part of; and interaction of many tissues dictates the behavior of the organism they make up. Therefore, proteins are the ultimate focal point for organismal composition and the basis for many biological functions that occur within. Interestingly, proteins actually govern their own existence by modulating their own synthesis and breakdown by other pre-existing predecessor cellular proteins. Needless to say, there is an ever-increasing demand for expanding our knowledge on the maintenance of protein homeostasis (proteostasis) as a critical component of proper cellular functioning and adaptation to constantly changing environmental signals.

It is well known and accepted that proteins are not static entities. They exist in a delicate balance between synthesis and degradation signals. In healthy organisms, the interplay between protein synthesis and degradation biological signals, such as post-translational modification, regulation of protein folding, and influence from other proteins, promotes cellular processes that help maintain properly functioning tissues. This action of protein homeostasis is termed "proteostasis" and controls cellular protein turnover by the dynamic equilibrium between protein synthesis and degradation. Specifically, it is a disruption of proteostasis, by either abnormal protein synthesis or degradation, that can lead to deleterious symptom manifestation of many diseases [2]. Traditionally, researchers of biological systems have used abundance-based measurements to understand expression levels of proteins, or their genetic precursors as a proxy for protein expression. Some of these measurements include western blot or immunofluorescence for proteins and reverse transcription quantitative polymerase chain reaction (RT-qPCR) or next generation sequencing (NGS) for genes. While a great amount of information can be learned from these measurements, they all miss the temporal dimension that is crucial to truly understanding protein dynamics in a living organism. Therefore, it is warranted to utilize measurements that can capture this information of a protein's dynamic interaction with its environment over time to better understand the biological system it constitutes. Fortunately, there have been various methods developed to do exactly this, as we will discuss in further detail below.

Being able to measure a protein not only as a static abundance value at a single cross-sectional time point, but also as a dynamic component over the timeline of its existence in a biological system will provide researchers and medical professionals alike with a greater depth of knowledge on the true driving forces behind human health and disease. There have been a few

transformative technologies in the field of stable isotope labeling that have helped progress these efforts forward. Traditional stable isotope labeling of proteins generally requires infusion of a stable isotope, such as ^{13}Carbon or ^{18}Oxygen that can incorporate itself into newly synthesized proteins from the onset of label enrichment [3]. While these methods are fruitful in the data they can produce, it is generally not very feasible to implement them in a clinical setting. The requirement of multiple intravenous infusions to administer these stable isotopes is invasive to the research subjects and more resource intensive for researchers. Therefore, it is necessary to develop a method that can provide the time-dependent information of stable isotope labeling without all the painstaking steps required to administer them. Stable isotope labeling with deuterium (^{2}H) in the form of "heavy water" (^2H_2O) [4], developed by the Hellerstein laboratory at UC Berkeley, has provided ease, breadth, and accuracy for these efforts.

The monomeric precursors of biopolymers can become labeled with deuterium covalently through enzymatic reactions involving proton exchange with solvent water. For protein synthesis, ^{2}H incorporation occurs in free, unbound amino acids and this includes both non-essential and essential amino acids that assemble into proteins [4]. Beyond the domain of proteomics, the Hellerstein lab has also developed methods for measuring flux rates of other important polymers including fatty acids [5], nucleic acids [6], and many other biomolecules. This is where another pioneering technology from the Hellerstein lab comes into play: mass isotopomer distribution analysis (MIDA) [7, 8]. By using a high-performance liquid chromatography coupled to a mass spectrometer (HPLC/MS), we can detect the incorporation of ^{2}H into any organic monomeric unit, a peptide for example, that constitutes a larger polymer unit, like a protein. The incorporation of ^{2}H into an organic monomeric unit is not a binary action. ^{2}H can incorporate at potentially multiple spots in an organic monomer and the likelihood of incorporation is dependent upon the organism's body water enrichment of ^2H_2O. Knowing this information, we can use MIDA to calculate the rate of turnover (synthesis or degradation) of a polymer based on all the individual identifying monomeric units (unique to one polymer) we can detect via HPLC/MS. This is achieved by comparing the labeled mass isotopomer species for a given identifying monomeric unit against an unlabeled mass isotopomer species of the same monomeric unit to determine the extent of ^{2}H label incorporation that occurred in the presence of a given body water enrichment of ^2H_2O. Combined with identifying multiple mass isotopomer species to empower MIDA, HPLC/MS analysis can provide us with the ability to characterize the dynamics of biological systems at a global scale through non-biased "-omics" techniques.

Current "-omics" approaches, including genomics (DNA), transcriptomics (RNA), proteomics (proteins), lipidomics (lipids), and metabolomics (metabolites), have become increasingly important for the characterization of biological processes at a global scale. Employing these techniques allows for a more comprehensive understanding of the outcomes of fundamental cellular biology. In the past couple of decades, there has been an increased emphasis placed on the value these approaches can provide [9]. Instead of relying on a handful of traditional markers of cellular functions, a broad spectrum of analytes can provide an all-encompassing picture of what is occurring inside an organism. Two (of the many) advantages of an HPLC/MS can synergistically combine to produce the revolutionary analysis known as "dynamic proteomics": a technique that incorporates ^{2}H labeling with the simultaneous identification and analysis of hundreds to thousands of proteins *in-vivo*. Dynamic proteomics takes traditional quantitative proteomics, which only measures static abundance of proteins, to another dimension by measuring the turnover rate of hundreds to thousands of proteins at the

same time. This allows for non-hypothesis driven, global determination of the flux through pathways of interest.

In summation, dynamic proteomics analysis is a powerful tool that can be used from *in-vitro* applications to pre-clinical animal models all the way up to clinical studies. Utilizing HPLC/MS analysis allows us to simultaneously take a non-hypothesis, global analysis of biological processes in a tissue, while also enabling a targeted approach to better understanding the turnover of individual proteins of interest. Our objective for this work is to implement dynamic proteomics to better understand important biological processes from an extra-dimensional perspective, following both a non-hypothesis based and targeted approach. This analytical approach provides significant advancement to the field of proteomics, which can be used to better elucidate the cellular mechanisms that underlie many biological processes.

References:

1. Crick F. Central Dogma of Molecular Biology. *Nature*. 1970;227(5258):561-563. doi:10.1038/227561a0

2. Balch WE, Morimoto RI, Dillin A, Kelly JW. Adapting Proteostasis for Disease Intervention. *Science*. 2008;319(5865):916-919. doi:10.1126/science.1141448

3. Gevaert K, Impens F, Ghesquière B, Van Damme P, Lambrechts A, Vandekerckhove J. Stable isotopic labeling in proteomics. *Proteomics*. 2008;8(23-24):4873-4885. doi:10.1002/pmic.200800421

4. Holmes WE, Angel TE, Li KW, Hellerstein MK. Chapter Seven - Dynamic Proteomics: In Vivo Proteome-Wide Measurement of Protein Kinetics Using Metabolic Labeling. In: Metallo CM, ed. *Methods in Enzymology*. Vol 561. Metabolic Analysis Using Stable Isotopes. Academic Press; 2015:219-276. doi:10.1016/bs.mie.2015.05.018

5. Hellerstein MK, Christiansen M, et al. Measurement of de novo hepatic lipogenesis in humans using stable isotopes. *J Clin Invest* 87:1841-52, 1991. PMID: 2022750; PMCID: PMC295308

6. Busch R, Neese RA, Awada M, Hayes GM, Hellerstein MK. Measurement of cell proliferation by heavy water labeling. *Nat Protoc*. 2007;2(12):3045-3057. doi:10.1038/nprot.2007.420

7. Hellerstein MK, Neese RA. Mass isotopomer distribution analysis: a technique for measuring biosynthesis and turnover of polymers. *Am J Physiol*. 1992;263(5 Pt 1):E988-1001. doi:10.1152/ajpendo.1992.263.5.E988

8. Hellerstein MK, Neese RA. Mass isotopomer distribution analysis at eight years: theoretical, analytic, and experimental considerations. *Am J Physiol*. 1999;276(6):E1146-1170. doi:10.1152/ajpendo.1999.276.6.E1146

9. Hasin Y, Seldin M, Lusis A. Multi-omics approaches to disease. *Genome Biology*. 2017;18(1):83. doi:10.1186/s13059-017-1215-1

Section 1

Duchenne Muscular Dystrophy (DMD) Disease Etiology and Current Therapies

Review of the Existing Literature

DMD Inheritance

Duchenne Muscular Dystrophy (DMD) is an X chromosome linked genetic disease that affects the growth and development of both voluntary (skeletal) and involuntary (cardiac, respiratory, and digestive) muscles [1]. The prevalence of DMD is about 1 in 3,500-5,000 births and seems to be equally distributed among different regions in the world [2, 3, 4, 5]. DMD disproportionately affects males, due to the simple Mendelian inheritance pattern of sex-linked genetics. Female cases of DMD are less than 1 in 1 million female births globally [6], however, female carriers of the disease (dystrophin gene mutation on one X chromosome) can display abnormal musculoskeletal or cardiorespiratory symptoms that are mild and do not affect their daily lives [7]. DMD is the most severe version of muscular dystrophy, with the greatest impact on a patient's health, quality of life, and overall lifespan [8]. Other common muscular dystrophies are Becker muscular dystrophy (BMD) and Limb Girdle muscular dystrophy (LGMD) that have similar origins as DMD, but generally have less severe symptom manifestation [9]. Therefore, the scope of this literature review will mainly be focused on DMD in male patients since it is the most common form of the disease that presents the most severe symptoms. We plan to take an all-encompassing approach to DMD by covering the symptoms of the disease, its cause and etiology, how DMD is studied with pre-clinical animal models, how DMD is diagnosed, early-stage biomarkers and physical hallmarks of DMD, and a prospective look at the future of DMD therapies.

What is Dystrophin

DMD is characterized by a loss of an integral muscle protein, dystrophin, which causes the phenotype of dystrophin-deficient muscle mentioned above [10,11,12]. Dystrophin is the product of the dystrophin gene and acts as part of a larger intercellular scaffolding network in the myofiber that anchors contractile components, primarily intracellular actin filaments, to extracellular structures through the sarcolemma [13]. Collectively, dystrophin and its other binding partners form a necessary structure of the muscle known as the dystrophin-associated protein complex (DAPC) [13]. Parts of the DAPC interact with and influence many important structures in the muscle, including the sarcolemma, cytoskeleton (mainly actin filaments), channel proteins, and signaling proteins either directly or indirectly [13]. Given the implication of dystrophin into a larger complex that is involved with multiple cellular functions, it is easy to see how dystrophin deficiency in DMD can cause so many of the symptoms discussed below. Of its many functions, the DAPC primarily acts as a "shock absorber" for the stress of repeated muscle contractions to prevent them from disrupting the sarcolemma. However, without dystrophin, the DAPC loses its functional presence, and the stress is placed on the sarcolemma instead [12,14]. Over time and with repeated contractions, the stress accumulated on the sarcolemma causes it to break down and become more permeable, leading to symptom manifestation, as well as other tissue homeostasis disrupting events. Probably the most detrimental part of DMD is the reduced regenerative

capacity of satellite cells [15]. Failure to complete a regenerative event of damaged muscle from local satellite cells eventually leads to exhaustion of satellite cell's regenerative capacity and further damaged tissue is replaced with fibrotic scar tissue instead of healthy new myofibers. This contributes greatly to the phenotype of fibrotic non-functional tissue development that replaces healthy muscle and is a hallmark phenotype of DMD patients [16].

What Causes Dystrophin Deficiency

DMD is caused by mutations in the gene that encodes for the protein dystrophin, which serves as an important link between the sarcolemma (muscle membrane) and contracting components in the muscle. There are many different genetic mutations that can cause DMD, such as point mutations (base pair deletion or insertion), whole exon duplications, or whole exon deletions (which are the most common form of mutation) [17, 18]. Deletions and duplications can cluster in "hotspot" regions on the dystrophin gene, which are located at exons 45–55 and 3–9 and account for over 50% of all DMD cases [19, 20]. There can be one or multiple mutations to the dystrophin gene that can cause DMD, and the type of mutation that causes the disease can determine the severity of the symptoms. For example, in more than 90% of diagnosed cases, "out-of-frame" reading frame mutations will lead to DMD, but "in-frame" reading frame mutations lead to a less severe form of muscular dystrophy known as Becker muscular dystrophy (BMD). Reading frame mutations in this disease will be dependent upon which exons are affected [18,21]. Ultimately, the type of mutation on the dystrophin gene will affect the overall functionality and quality of the dystrophin protein produced, thus affecting the phenotype and symptoms of disease [8,18]. However, DMD is a complex disease, and its pathology is not fully determined by one single gene. Genetic variants that alter the expression and function of *CD40*, *THBS1*, *SPP1*, *ACTN3*, *LTBP4*, and *TCTEX1D* have all been associated with slower disease progression in DMD patients to do the protective mechanisms these genes affect [22, 23]. It is also interesting to note that 1 out of 3 DMD cases is caused by *de novo* germline mutations [24, 25, 26].

DMD Phenotype

DMD is a progressively deteriorating disease where symptoms continually worsen over the course of a patient's life. This congenital disease is present from birth, but the majority of life-impacting symptoms do not first appear until around ages 3 - 5 [27]. This is in part due to the nature of the disease being highly dependent upon an individual's environment and activity levels. A young child is not physically very active until that age, and therefore will not accumulate the physical symptoms of DMD from repeated stress placed on dystrophin-deficient muscles. The specific pathology of the disease will be discussed in detail later in this review, but it is important to understand the natural progression of the disease based on a subject's activity levels throughout life. DMD eventually leads to loss of ambulation, assisted ventilation, and premature death in affected patients. Some important milestones for disease progression are listed as follows: most patients are wheelchair dependent by 10 - 12 years old, need assisted ventilation by their early 20's, and succumb to cardiac or respiratory failure by their early 40's [27].

The phenotypic response to dystrophin deficiency in skeletal muscle includes, but is not limited exclusively to:

Weakening of the Sarcolemma (Outer Membrane of Muscle Tissue)

- When a muscle undergoes a contraction-relaxation cycle, force is produced and requires the efficient handling of the mechanical stress placed on the sarcolemma. In healthy muscle, this mechanical stress is absorbed by the cytoskeleton, sarcolemma, and extracellular matrix through the DAPC. In DMD, the absence of a critical DAPC component, dystrophin, places the stress of repeated muscle contractions mainly on the sarcolemma. This leads to weakening of the muscle membrane and makes it highly susceptible to contraction-mediated damage [9]. Tears in the sarcolemma, termed "delta-lesions", can form in the muscle of DMD patients and are visible with electron microscopy [28]. These tears can lead to further disease progression by allowing influx of extracellular components that mediate inflammation and disrupt tissue homeostasis. Also, intracellular components can escape into the cytoplasm, leading to higher detection of enzymes like muscle-specific creatine kinase (CK-M) in the blood of DMD patients [29]. To further demonstrate this point, muscle damage is correlated with repeated bouts of stress placed on it, therefore, the muscles that experience the most stress, such as the involuntary cardiorespiratory system, are affected earlier and more severely than other muscles [30].

Improper Nitric Oxide Signaling (NOS) of Vasodilation Leading to Tissue Ischemia

- Along with its mechanical properties, dystrophin has other important physiological influences on skeletal muscle. Mainly its association with neuronal nitric oxide synthase (nNOS), which helps mediate blood flow to the tissue by producing nitric oxide to induce vasodilation in the surrounding vasculature [31]. Disruption of vasodilation in DMD leads to functional ischemia and muscle damage because nNOS cannot properly localize to the DAPC, and therefore produce nitric oxide to induce proper blood flow [32]. Along with modulating proper blood flow in the muscle, NO has also been implicated in increasing glucose uptake into the cell [33, 34], reducing inflammation [35], and regulating mitochondrial respiration [36]. Therefore, nNOS regulation is paramount to proper muscle function and maintenance of homeostasis.

Free Radical Damage

- Dystrophic muscle has been shown to produce significantly more damaging free radical species than healthy skeletal muscle. Reactive oxygen species (ROS) are produced by enzymes in the muscle when the microtubule lattice becomes disorganized, which is the case in DMD when the dystrophin-microtubule association is disrupted [37, 38]. Along with ROS, there are reactive nitrogen species (RNS) that are also produced in DMD by delocalization of nNOS from the DAPC [39]. The dystrophic muscle is also less efficient at removing these free radical species due to a reduction in the potent antioxidant glutathione when compared to healthy muscle [40]. Therefore, unregulated free radical production can lead to a myriad of persistent damage within the tissue [41].

Mitochondrial Dysfunction

- Along with free radical damage coming from aberrant enzyme activity, another source that contributes to free radical damage within the dystrophic muscle is mitochondrial dysfunction [42]. There are several different ways in which the mitochondria can become dysfunctional in DMD, such as swelling from extracellular calcium influx [42], disorganized microtubule lattice [43], and faulty mitophagy processes to clean up defective

mitochondria [44]. Outside of free radical production, mitochondria can affect DMD symptom progression through abnormal bioenergetics. The stresses placed on mitochondria from dystrophic muscle led to decreased ATP production, which in turn reduces availability of energy substrates for other processes in the muscle [42, 45, 46]. This starts a positive-feedback cycle where lack of ATP availability prevents compensatory cellular mechanisms from the muscle to help restore ATP production of the mitochondria, which leads to further mitochondrial dysfunction and a reduction of the energy substrate.

Overloading of Cytosol with Calcium

- Intramuscular cytosolic calcium levels are tightly regulated to provide proper contraction-relaxation cycling and homeostasis of other cellular processes. In DMD, the delta-lesions in the sarcolemma allow for extracellular calcium to influx into the cytosol, disrupting this equilibrium [47]. Calcium overloading of the muscle directly contributes to cell death pathways mediated by calcium-dependent proteases and phospholipases [47, 48], as well as previously mentioned mitochondria dysfunction. The sarcoplasmic reticulum, an organelle that is tasked with maintaining calcium levels in the muscle cell during contraction-relaxation cycles, has both faulty calcium releasing channels and uptake receptors [49, 50, 51], therefore leading to poor maintenance of calcium homeostasis in the dystrophic muscle.

Impairment/Inability to Complete a Regenerative Event from Satellite Cells (stem cells in muscle tissue)

- Muscle wasting, fibrosis, and fatty tissue deposition are all hallmark consequences of satellite cell failure to regenerate tissue. It is well known and documented that satellite cell (muscle-specific stem cell) functions are disrupted in DMD due to a myriad of reasons [15, 52]. However, there is a new theory that the DAPC has a direct link to satellite cell activation [53], and thus its absence in DMD would mediate these regenerative issues. Regardless of its etiology, exhaustion of satellite cell regeneration capacity over time is one of the main drivers behind the long-term symptoms experienced by DMD patients.

All of these phenotypes of DMD skeletal muscle contribute to the severe loss of muscle function and atrophy as a patient ages. This list is non-comprehensive, while there are many other symptoms from dystrophin deficiency that are not listed here, these are some of the most severe and noteworthy symptoms of the disease. Although it is not uniformly agreed upon what is the root cause of the disease, one hypothesis stands out as the front runner to explain many clinical findings of DMD: the sarcolemmal damage model [10].

Mouse Model of DMD (the *mdx* mouse)

The *C57BL/10ScSn-Dmdmdx/J* (*mdx*) mouse has become the standard pre-clinical model for DMD examination because of its similar genotype to humans. Therefore, many of the discoveries in the field of DMD have been made by working with this model over the last 4 decades. The traditional *mdx* mouse model arose spontaneously from a healthy C57BL10ScSn colony, with a single point mutation in exon 23 of the dystrophin gene leading to an in-frame mutation and truncated protein produced [54, 55]. Since then, there have been many iterations of animal models for DMD, including various transgenic rodents and dogs [56]. Each model comes

with its own advantages and disadvantages; therefore, it is advisable to make sure the model that is selected can best represent the aspect of DMD that is being studied. However, despite the seemingly endless availability of new and improved animal models, the standard *mdx* mouse model is still the most tested and by far has the most published literature around it. Therefore, making it a "gold standard" to assess the genotypic and phenotypic response to DMD.

Mdx mice undergo a phase of constant muscle cell degeneration and regeneration, known as the "dystrophic phase", which reflects the same mechanism of dystrophin deficiency that is experienced in humans [57, 58]. During this phase, the muscle undergoes sarcolemmal degradation, extracellular infiltration, active myofiber necrosis, variance in myofiber size, and present central nuclei from recent myofiber regeneration [59, 60]. These symptoms peak around 3 - 4 weeks of age, and generally plateau for the rest of the animal's life. The severe symptoms of DMD in humans, such as muscle weakness and accumulation of non-functional fibrotic tissue, do not generally occur in *mdx* mice in the peripheral limbs until about 2 years of age [61]. Also, many cardiac related issues are not reported in young *mdx* mice, with onset of symptoms being about 10 months of age [62]. Therefore, *mdx* mice do not demonstrate the same impairment on lifespan as human DMD patients, with *mdx* mice living as long as their healthy companions. Overall, the *mdx* mouse exhibits the same mechanisms of disease progression as human DMD patients, but only experiences mild symptoms that are mildly life influencing in comparison to the severity of that in humans. Nonetheless, these animal models are still a good way to study various aspects of DMD *in-vivo* because of their similarity in disease mechanisms as human patients.

Diagnosis of DMD

Diagnosis of this disease generally involves genetic screening, and while this disease is congenital, individuals generally are not diagnosed until around ages 3-5 due to delay in symptom manifestation. The full guidelines for genetic diagnosis of DMD are well outlined and should be followed by researchers and medical practitioners [62]. In brief, the genetic diagnosis of DMD is done in a stepwise fashion, to save the time and money of patients and families [48, 63]. First, an individual must be suspected of having DMD by the presence of early symptoms that are discussed below. The first round of genetic testing uses multiplex ligation-dependent probe amplification (MLPA) or array comparative genomic hybridization (array CGH) to confirm the presence, or deletion, of the 79 exons in the dystrophin gene. It is estimated that around ~75% of all DMD patients harbor either deletions or duplications to one or multiple exons in the dystrophin gene that are the major contributor to DMD progression [45]. Therefore, MLPA and array CGH are the preferred front-line genetic diagnostic tools to diagnose most disease patients after one test. If a mutation is not identified this way, small mutation analysis using Sanger sequencing of all 79 exons is required. It is important to note that the type of mutation will influence the symptoms and overall progression of disease [64]. This spectrum on which dystrophin deficiency occurs can be explained by the simple "reading frame rule". "Out-of-frame" mutations that alter the overall production of dystrophin, such as exon duplication or deletion, will lead to DMD 90% of the time. While "in-frame" mutations that come from single base pair mutations, such as base pair in-dels, will lead to Becker muscular dystrophy (BMD) [45]. Therefore, the diagnosis of dystrophin deficiency is complex and multifactorial to determine how an individual's symptoms will progress.

Earlier Biomarkers of DMD

There have been efforts to establish earlier diagnosis of this disease using biomarker screens [66] or physical assessments [65], however, lack of awareness of early symptom manifestation is generally what leads to delayed diagnosis. Generally, individuals with DMD will start to present the following physical symptoms around 2 - 4 years of age: delayed motor functioning skills development, general muscle weakness, calve muscle hypertrophy, and Gower's syndrome (use of the upper body to raise to upright from the floor as a compensatory mechanism of weak hip and leg muscles) [63]. Other symptoms in about 30% of DMD patients are cognitive impairments, such as delay in speech or memory development [65]. Along with physical symptoms of disease, elevated plasma CK-M levels are seen in DMD patients from birth [66]. Incorporation of both early physical signs and biomarker screening of DMD onset could lead to earlier genetic testing, and therefore earlier treatment of the disease. Therefore, it is warranted and necessary to improve the way that DMD can be assessed to diagnose and treat it earlier in a patient's life, which can lead to better disease management outcomes and overall improved quality of life for the patient [65].

Importance of Proteomics for Biomarkers

Although proteomics analysis is not utilized for the diagnosis of DMD, it provides critical information that can be used to track disease progression and measure an individual's response to therapy or pharmacological intervention. Unfortunately, the commonly used proteomics procedures require invasive methods of sample collection, such as muscle biopsies or blood drawing [67]. To date, these methods of sample collection are also employed by clinical investigators, causing a serious issue concerning ethical treatment of DMD subjects. Invasive procedures, especially muscle biopsies, are viewed as unethical in a DMD patient. Therefore, it is warranted to develop a non-invasive protocol to properly measure and track the progression of DMD and other musculoskeletal diseases with little to no harm to the patient. Urine serves as a potential candidate for this exact purpose. It is easy to collect in large sample quantities and does not require painful procedures such as skin puncturing with a needle. In recent literature, it is observed that human DMD patients have certain muscle proteins with an altered quantitative measurement in their urine when compared to that of healthy individuals [68, 69]. Therefore, it is suggested that urine has the potential to be a new non-invasive modality of sample collection for proteomics analysis.

Proposing Non-Invasive Biomarker

The possible explanation of muscle proteins being found in urine is due to a loss of muscle membrane integrity from the lack of dystrophin. The lipid bilayer of the sarcolemma is not strong enough on its own to counteract the forces put on it with muscle contraction. Therefore, the DMD muscle becomes more permeable and develops a "leaky" characteristic that allows certain proteins, metabolites, and enzymes to enter circulation from muscles [1, 58, 70]. Recent literature has found that Titin fragments, pieces of a large sarcomere protein specific to skeletal muscle, have been found in higher quantities in both *mdx* mice and DMD patients in comparison to healthy individuals [71, 72]. Titin is one of the largest single proteins in the body, but readily undergoes protease digestion during the disruption of tissue homeostasis from dystrophin deficiency. This allows its fragments to escape from the muscle, through the damaged sarcolemma, and into the circulation. Since many proteins in systemic circulation can be filtered out through the kidneys and excreted, it would be interesting to see if the presence of Titin fragments is higher in *mdx* or DMD patients. In fact, *Rouillon et al.* showed Titin fragments are

present in higher quantities in the urine of both *mdx* mice and human DMD patients, thus presenting an attractive opportunity to further explore it as a biomarker of disease [69]. Over the past few years, there has been great progress in the development of Titin as a non-invasive biomarker of DMD in both an animal model and a clinical setting [68, 73, 74, 75]. This work has culminated in the development of a commercially available enzyme linked immunosorbent assay (ELISA) for urinary Titin as a way for researchers to diagnose the disease in preclinical animal models [76]. This justifies further research to examine if other intracellular components that leak into circulation from the muscle can be quantified by a "virtual biopsy" and provide more information on what is occurring inside the dystrophic muscle.

Importance of Non-Invasive Dynamic Proteomics

Current proteomics sample collection techniques involve invasive procedures that require the use of needles and other skin puncturing modalities. These must be done either early in life or multiple times across a patient's lifespan to effectively track and measure the progression of the disease. Despite recent advances in biopsy technologies and techniques [77], these procedures are still resource intensive and time-consuming for young individuals and those suffering from debilitating musculoskeletal illness. Therefore, it is understandable to move away from the outdated invasive skin puncture procedures and develop a non-invasive methodology to accurately assess DMD. Although proteomics data is not currently used to evaluate DMD, it can provide an alternative way to obtain critical information only available to clinical investigators or researchers from a muscle biopsy. Along with quantitative data, we plan to use these target muscle proteins to provide information regarding the dynamic flux of protein synthesis and degradation occurring in the dystrophin-deficient muscle. Applying a stable isotope, such as deuterium (^{2}H), that can be incorporated into newly synthesized nonessential amino acids will provide us with information regarding the fractional synthesis rate (FSR) of various proteins of interest, if they are able to be quantified in urine. This information could be useful to clinicians and medical professionals alike to assess the progression and severity of an individual's disease condition. Previous work from a research group in the Hellerstein lab shows that certain muscle-specific proteins can reflect whole muscle protein synthesis rates when taken from circulation [78]. This sets the stage for expansion of virtual biopsies to include more specific proteins that can be easily obtained and show direct clinical relevance to DMD in non-invasive samples, such as urine.

DMD Therapies

Although there are currently no complete cures for this inheritable disease, therapies exist to help patients deal with their symptoms by improving overall daily quality of life and extending lifespan [79, 80, 81]. The current standard of care for most DMD patients involves glucocorticoid prescription, physical therapy, dietary intervention, and potentially surgery. Glucocorticoid treatment is generally prescribed to all diagnosed DMD patients to help maintain inflammation in skeletal muscle associated with disease progression [82]. While this treatment is robust in achieving a reduction in inflammation, glucocorticoids have other side effects that are associated with long-term treatment and therefore must be considered when prescribing [83]. Non-pharmacological treatments like physical therapy and dietary interventions can show great improvement in symptom management for DMD patients [84, 85]. While these forms of treatment are easy to implement and have little negative side effects, they can only improve the symptoms and do not directly address the root cause of DMD.

Recently, there has been a large focus on developing potential cures for dystrophin deficiency that is seen in all forms of muscular dystrophy by leveraging various cutting-edge technologies. Since disease severity is primarily determined by the ability of the dystrophin gene to be produced in a functional manner, there has been an effort to restore the reading frame of "out-of-frame" mutations via exon skipping on the dystrophin gene [86]. This is primarily mediated by antisense oligonucleotides (ASOs) that directly target specific exons on the dystrophin gene to "skip" them in the translation sequence and restore the reading frame to produce a truncated but still functioning dystrophin protein [87]. The focus is to restore at least partially functional dystrophin production to reduce the severity of symptoms DMD patients may face, and to make them closer to those of the milder BMD form. However, clinical results of this treatment modality are still sparse at the time of writing this thesis and show modest results at best. Also, this therapy is specific to the type of mutation an individual has and therefore is not a one size fits all treatment. More work needs to be done to properly determine the therapeutic value of these treatments.

Another newly emerging strategy to combat DMD is through upregulation of a surrogate protein Utrophin that is also a member of the DAPC and has similar roles as dystrophin [88]. In fact, Utrophin is generally found to be upregulated in DMD patients already as a compensatory mechanism for loss of dystrophin, but it is not enough to rescue the phenotype of disease. Therefore, pharmacological compounds that demonstrate Utrophin upregulation in preclinical animal models, like the *mdx* mouse, have been examined in a clinical setting as well. So far clinical trials have shown poor bioavailability and little to no therapeutic effect of these treatments in DMD patients [89]. However, the mechanism of action of these treatments is well understood and potentially other compounds can be made to target the same therapeutic pathway for Utrophin upregulation.

In my opinion, the most attractive potential treatment for DMD that is being produced is adeno-associated virus (AAV) vector-mediated gene therapy. AAV's have a broad research and medical purpose, primarily focusing on delivering genetic therapies to target tissues. In the scope of DMD, AAV based gene therapy is directed towards delivering gene sequences that help the muscle produce a smaller version of dystrophin termed "micro-dystrophin" [90]. This micro-dystrophin can act as a replacement for regular dystrophin, and in theory compensate for dystrophin deficiency by completing the same role in the muscle. There has been great success of this therapy in preclinical models of disease, showing robust recovery of disease phenotype in animals [90]. However, there is currently little data available on this technology in DMD patients. The studies that have been done are small in patient number and require an extended period of treatment time to show any treatment effect. Therefore, this treatment shows potential to significantly reduce or eliminate the symptoms of DMD in patients, but first more robust testing must be done to prove its therapeutic ability.

References:

1. Houang EM, Sham YY, Bates FS, Metzger JM. Muscle membrane integrity in Duchenne muscular dystrophy: recent advances in copolymer-based muscle membrane stabilizers. *Skeletal Muscle*. 2018;8(1):31. doi:10.1186/s13395-018-0177-7

2. Mendell JR, Shilling C, Leslie ND, et al. Evidence-based path to newborn screening for Duchenne muscular dystrophy. *Ann Neurol*. 2012;71(3):304-313. doi:10.1002/ana.23528

3. Ryder S, Leadley RM, Armstrong N, et al. The burden, epidemiology, costs and treatment for Duchenne muscular dystrophy: an evidence review. *Orphanet J Rare Dis*. 2017;12(1):79. doi:10.1186/s13023-017-0631-3

4. Mah JK, Korngut L, Dykeman J, Day L, Pringsheim T, Jette N. A systematic review and meta-analysis on the epidemiology of Duchenne and Becker muscular dystrophy. *Neuromuscul Disord*. 2014;24(6):482-491. doi:10.1016/j.nmd.2014.03.008

5. Bladen CL, Rafferty K, Straub V, et al. The TREAT-NMD Duchenne muscular dystrophy registries: conception, design, and utilization by industry and academia. *Hum Mutat*. 2013;34(11):1449-1457. doi:10.1002/humu.22390

6. Satre V, Monnier N, Devillard F, Amblard F, Lunardi J. Prenatal diagnosis of DMD in a female foetus affected by Turner syndrome. *Prenat Diagn*. 2004;24(11):913-917. doi:10.1002/pd.1031

7. Ishizaki M, Kobayashi M, Adachi K, Matsumura T, Kimura E. Female dystrophinopathy: Review of current literature. *Neuromuscul Disord*. 2018;28(7):572-581. doi:10.1016/j.nmd.2018.04.005

8. Mercuri E, Bönnemann CG, Muntoni F. Muscular dystrophies. *Lancet*. 2019;394(10213):2025-2038. doi:10.1016/S0140-6736(19)32910-1

9. Emery AE. The muscular dystrophies. *The Lancet*. 2002;359(9307):687-695. doi:10.1016/S0140-6736(02)07815-7

10. Moser H. Duchenne muscular dystrophy: pathogenetic aspects and genetic prevention. *Hum Genet*. 1984;66(1):17-40. doi:10.1007/BF00275183

11. Hoffman EP, Brown RH, Kunkel LM. Dystrophin: the protein product of the Duchenne muscular dystrophy locus. *Cell*. 1987;51(6):919-928. doi:10.1016/0092-8674(87)90579-4

12. Petrof BJ, Shrager JB, Stedman HH, Kelly AM, Sweeney HL. Dystrophin protects the sarcolemma from stresses developed during muscle contraction. *Proceedings of the National Academy of Sciences*. 1993;90(8):3710-3714. doi:10.1073/pnas.90.8.3710

13. Gao Q, McNally EM. The Dystrophin Complex: structure, function and implications for therapy. *Compr Physiol*. 2015;5(3):1223-1239. doi:10.1002/cphy.c140048

14. Ervasti JM, Ohlendieck K, Kahl SD, Gaver MG, Campbell KP. Deficiency of a glycoprotein component of the dystrophin complex in dystrophic muscle. *Nature*. 1990;345(6273):315-319. doi:10.1038/345315a0

15. Morgan JE, Zammit PS. Direct effects of the pathogenic mutation on satellite cell function in muscular dystrophy. *Experimental Cell Research*. 2010;316(18):3100-3108. doi:10.1016/j.yexcr.2010.05.014

16. Kharraz Y, Guerra J, Pessina P, Serrano AL, Muñoz-Cánoves P. Understanding the Process of Fibrosis in Duchenne Muscular Dystrophy. *BioMed Research International*. 2014;2014:e965631. doi:10.1155/2014/965631

17. Magri F, Govoni A, D'Angelo MG, et al. Genotype and phenotype characterization in a large dystrophinopathic cohort with extended follow-up. *J Neurol*. 2011;258(9):1610-1623. doi:10.1007/s00415-011-5979-z

18. Aartsma-Rus A, Van Deutekom JCT, Fokkema IF, Van Ommen GJB, Den Dunnen JT. Entries in the Leiden Duchenne muscular dystrophy mutation database: an overview of mutation types and paradoxical cases that confirm the reading-frame rule. *Muscle Nerve*. 2006;34(2):135-144. doi:10.1002/mus.20586

19. Nakamura A, Shiba N, Miyazaki D, et al. Comparison of the phenotypes of patients harboring in-frame deletions starting at exon 45 in the Duchenne muscular dystrophy gene indicates potential for the development of exon skipping therapy. *J Hum Genet*. 2017;62(4):459-463. doi:10.1038/jhg.2016.152

20. Nakamura A, Fueki N, Shiba N, et al. Deletion of exons 3-9 encompassing a mutational hot spot in the DMD gene presents an asymptomatic phenotype, indicating a target region for multiexon skipping therapy. *J Hum Genet*. 2016;61(7):663-667. doi:10.1038/jhg.2016.28

21. Aartsma-Rus A, Ginjaar IB, Bushby K. The importance of genetic diagnosis for Duchenne muscular dystrophy. *J Med Genet*. 2016;53(3):145-151. doi:10.1136/jmedgenet-2015-103387

22. Bello L, Pegoraro E. The "Usual Suspects": Genes for Inflammation, Fibrosis, Regeneration, and Muscle Strength Modify Duchenne Muscular Dystrophy. *J Clin Med*. 2019;8(5):649. doi:10.3390/jcm8050649

23. Spitali P, Zaharieva I, Bohringer S, et al. TCTEX1D1 is a genetic modifier of disease progression in Duchenne muscular dystrophy. *Eur J Hum Genet*. 2020;28(6):815-825. doi:10.1038/s41431-019-0563-6

24. Garcia S, de Haro T, Zafra-Ceres M, Poyatos A, Gomez-Capilla JA, Gomez-Llorente C. Identification of de novo Mutations of Duchénnè/Becker Muscular Dystrophies in Southern Spain. *Int J Med Sci*. 2014;11(10):988-993. doi:10.7150/ijms.8391

25. Yu H, Chen YC, Liu GL, Wu ZY. A De novo Mutation in Dystrophin Causing Muscular Dystrophy in a Female Patient. *Chin Med J (Engl)*. 2017;130(19):2273-2278. doi:10.4103/0366-6999.215338

26. Caskey CT, Nussbaum RL, Cohan LC, Pollack L. Sporadic occurrence of Duchenne muscular dystrophy: evidence for new mutation. *Clin Genet*. 1980;18(5):329-341. doi:10.1111/j.1399-0004.1980.tb02293.x

27. Duan D, Goemans N, Takeda S, Mercuri E, Aartsma-Rus A. Duchenne muscular dystrophy. *Nat Rev Dis Primers*. 2021;7(1):1-19. doi:10.1038/s41572-021-00248-3

28. Mokri B, Engel AG. Duchenne dystrophy: electron microscopic findings pointing to a basic or early abnormality in the plasma membrane of the muscle fiber. *Neurology*. 1975;25(12):1111-1120. doi:10.1212/wnl.25.12.1111

29. Aartsma-Rus A, van Putten M. Assessing functional performance in the mdx mouse model. *J Vis Exp*. 2014;(85):51303. doi:10.3791/51303

30. Stedman HH, Sweeney HL, Shrager JB, et al. The mdx mouse diaphragm reproduces the degenerative changes of Duchenne muscular dystrophy. *Nature*. 1991;352(6335):536-539. doi:10.1038/352536a0

31. Brenman JE, Chao DS, Xia H, Aldape K, Bredt DS. Nitric oxide synthase complexed with dystrophin and absent from skeletal muscle sarcolemma in Duchenne muscular dystrophy. *Cell*. 1995;82(5):743-752. doi:10.1016/0092-8674(95)90471-9

32. Sander M, Chavoshan B, Harris SA, et al. Functional muscle ischemia in neuronal nitric oxide synthase-deficient skeletal muscle of children with Duchenne muscular dystrophy. *Proc Natl Acad Sci U S A*. 2000;97(25):13818-13823. doi:10.1073/pnas.250379497

33. Hong YH, Betik AC, McConell GK. Role of nitric oxide in skeletal muscle glucose uptake during exercise. *Exp Physiol*. 2014;99(12):1569-1573. doi:10.1113/expphysiol.2014.079202

34. Kellogg DL, McCammon KM, Hinchee-Rodriguez KS, Adamo ML, Roman LJ. Neuronal nitric oxide synthase mediates insulin- and oxidative stress-induced glucose uptake in skeletal muscle myotubes. *Free Radic Biol Med*. 2017;110:261-269. doi:10.1016/j.freeradbiomed.2017.06.018

35. Kaminski HJ, Andrade FH. Nitric oxide: biologic effects on muscle and role in muscle diseases. *Neuromuscul Disord*. 2001;11(6-7):517-524. doi:10.1016/s0960-8966(01)00215-2

36. Tengan CH, Rodrigues GS, Godinho RO. Nitric Oxide in Skeletal Muscle: Role on Mitochondrial Biogenesis and Function. *Int J Mol Sci*. 2012;13(12):17160-17184. doi:10.3390/ijms131217160

37. Prins KW, Humston JL, Mehta A, Tate V, Ralston E, Ervasti JM. Dystrophin is a microtubule-associated protein. *J Cell Biol*. 2009;186(3):363-369. doi:10.1083/jcb.200905048

38. Khairallah RJ, Shi G, Sbrana F, et al. Microtubules underlie dysfunction in duchenne muscular dystrophy. *Sci Signal*. 2012;5(236):ra56. doi:10.1126/scisignal.2002829

39. Li D, Yue Y, Lai Y, Hakim CH, Duan D. Nitrosative stress elicited by nNOSμ delocalization inhibits muscle force in dystrophin-null mice. *J Pathol*. 2011;223(1):88-98. doi:10.1002/path.2799

40. Dudley RWR, Khairallah M, Mohammed S, Lands L, Des Rosiers C, Petrof BJ. Dynamic responses of the glutathione system to acute oxidative stress in dystrophic mouse (mdx) muscles. *Am J Physiol Regul Integr Comp Physiol*. 2006;291(3):R704-710. doi:10.1152/ajpregu.00031.2006

41. Di Meo S, Venditti P. Evolution of the Knowledge of Free Radicals and Other Oxidants. *Oxidative Medicine and Cellular Longevity*. 2020;2020:e9829176. doi:10.1155/2020/9829176

42. Timpani CA, Hayes A, Rybalka E. Revisiting the dystrophin-ATP connection: How half a century of research still implicates mitochondrial dysfunction in Duchenne Muscular Dystrophy aetiology. *Medical Hypotheses*. 2015;85(6):1021-1033. doi:10.1016/j.mehy.2015.08.015

43. Ramos SV, Hughes MC, Delfinis LJ, Bellissimo CA, Perry CGR. Mitochondrial bioenergetic dysfunction in the D2.mdx model of Duchenne muscular dystrophy is associated with microtubule disorganization in skeletal muscle. *PLoS One*. 2020;15(10):e0237138. doi:10.1371/journal.pone.0237138

44. Reid AL, Alexander MS. The Interplay of Mitophagy and Inflammation in Duchenne Muscular Dystrophy. *Life*. 2021;11(7):648. doi:10.3390/life11070648

45. Percival JM, Siegel MP, Knowels G, Marcinek DJ. Defects in mitochondrial localization and ATP synthesis in the mdx mouse model of Duchenne muscular dystrophy are not alleviated by PDE5 inhibition. *Hum Mol Genet*. 2013;22(1):153-167. doi:10.1093/hmg/dds415

46. Rybalka E, Timpani CA, Cooke MB, Williams AD, Hayes A. Defects in Mitochondrial ATP Synthesis in Dystrophin-Deficient Mdx Skeletal Muscles May Be Caused by Complex I Insufficiency. *PLOS ONE*. 2014;9(12):e115763. doi:10.1371/journal.pone.0115763

47. Turner PR, Westwood T, Regen CM, Steinhardt RA. Increased protein degradation results from elevated free calcium levels found in muscle from mdx mice. *Nature*. 1988;335(6192):735-738. doi:10.1038/335735a0

48. Millay DP, Sargent MA, Osinska H, et al. Genetic and pharmacologic inhibition of mitochondrial-dependent necrosis attenuates muscular dystrophy. *Nat Med*. 2008;14(4):442-447. doi:10.1038/nm1736

49. Kyrychenko S, Poláková E, Kang C, et al. Hierarchical accumulation of RyR post-translational modifications drives disease progression in dystrophic cardiomyopathy. *Cardiovasc Res*. 2013;97(4):666-675. doi:10.1093/cvr/cvs425

50. Bellinger AM, Reiken S, Carlson C, et al. Hypernitrosylated ryanodine receptor calcium release channels are leaky in dystrophic muscle. *Nat Med*. 2009;15(3):325-330. doi:10.1038/nm.1916

51. Kushnir A, Wajsberg B, Marks AR. Ryanodine receptor dysfunction in human disorders. *Biochim Biophys Acta Mol Cell Res*. 2018;1865(11 Pt B):1687-1697. doi:10.1016/j.bbamcr.2018.07.011

52.Blau HM, Webster C, Pavlath GK. Defective myoblasts identified in Duchenne muscular dystrophy. *Proceedings of the National Academy of Sciences*. 1983;80(15):4856-4860. doi:10.1073/pnas.80.15.4856

53. Chang NC, Sincennes MC, Chevalier FP, et al. The Dystrophin Glycoprotein Complex Regulates the Epigenetic Activation of Muscle Stem Cell Commitment. *Cell Stem Cell*. 2018;22(5):755-768.e6. doi:10.1016/j.stem.2018.03.022

54. Bulfield G, Siller WG, Wight PA, Moore KJ. X chromosome-linked muscular dystrophy (mdx) in the mouse. *Proc Natl Acad Sci U S A*. 1984;81(4):1189-1192.

55. Sicinski P, Geng Y, Ryder-Cook AS, Barnard EA, Darlison MG, Barnard PJ. The molecular basis of muscular dystrophy in the mdx mouse: a point mutation. *Science*. 1989;244(4912):1578-1580. doi:10.1126/science.2662404

56.McGreevy JW, Hakim CH, McIntosh MA, Duan D. Animal models of Duchenne muscular dystrophy: from basic mechanisms to gene therapy. *Dis Model Mech*. 2015;8(3):195-213. doi:10.1242/dmm.018424

57. MacLennan PA, Edwards RH. Protein turnover is elevated in muscle of mdx mice in vivo. *Biochem J*. 1990;268(3):795-797.

58. Dadgar S, Wang Z, Johnston H, et al. Asynchronous remodeling is a driver of failed regeneration in Duchenne muscular dystrophy. *J Cell Biol*. 2014;207(1):139-158. doi:10.1083/jcb.201402079

59. Carnwath JW, Shotton DM. Muscular dystrophy in the mdx mouse: histopathology of the soleus and extensor digitorum longus muscles. *J Neurol Sci*. 1987;80(1):39-54. doi:10.1016/0022-510x(87)90219-x

60. Dangain J, Vrbova G. Muscle development in mdx mutant mice. *Muscle Nerve*. 1984;7(9):700-704. doi:10.1002/mus.880070903

61. DiMario JX, Uzman A, Strohman RC. Fiber regeneration is not persistent in dystrophic (MDX) mouse skeletal muscle. *Dev Biol*. 1991;148(1):314-321. doi:10.1016/0012-1606(91)90340-9

62. Quinlan JG, Hahn HS, Wong BL, Lorenz JN, Wenisch AS, Levin LS. Evolution of the mdx mouse cardiomyopathy: physiological and morphological findings. *Neuromuscul Disord*. 2004;14(8-9):491-496. doi:10.1016/j.nmd.2004.04.007

63. Birnkrant DJ, Bushby K, Bann CM, et al. Diagnosis and management of Duchenne muscular dystrophy, part 1: diagnosis, and neuromuscular, rehabilitation, endocrine, and gastrointestinal and nutritional management. *Lancet Neurol*. 2018;17(3):251-267. doi:10.1016/S1474-4422(18)30024-3

64. Monaco AP, Bertelson CJ, Liechti-Gallati S, Moser H, Kunkel LM. An explanation for the phenotypic differences between patients bearing partial deletions of the DMD locus. *Genomics*. 1988;2(1):90-95. doi:10.1016/0888-7543(88)90113-9

65. Aartsma-Rus A, Hegde M, Ben-Omran T, et al. Evidence-Based Consensus and Systematic Review on Reducing the Time to Diagnosis of Duchenne Muscular Dystrophy. *J Pediatr*. 2019;204:305-313.e14. doi:10.1016/j.jpeds.2018.10.043

66. Szigyarto CAK, Spitali P. Biomarkers of Duchenne muscular dystrophy: current findings. *Degener Neurol Neuromuscul Dis*. 2018;8:1-13. doi:10.2147/DNND.S121099

67. Mousa NO, Osman A, Fahmy N, et al. Duchenne Muscular Dystrophy (DMD) Treatment: Past and Present Perspectives. In: *Muscular Dystrophy - Research Updates and Therapeutic Strategies*. IntechOpen; 2020. doi:10.5772/intechopen.92765

68. Awano H, Matsumoto M, Nagai M, et al. Diagnostic and clinical significance of the titin fragment in urine of Duchenne muscular dystrophy patients. *Clinica Chimica Acta*. 2018;476:111-116. doi:10.1016/j.cca.2017.11.024

69. Rouillon J, Zocevic A, Leger T, et al. Proteomics profiling of urine reveals specific titin fragments as biomarkers of Duchenne muscular dystrophy. *Neuromuscul Disord*. 2014;24(7):563-573. doi:10.1016/j.nmd.2014.03.012

70. Ozawa E, Hagiwara Y, Yoshida M. Creatine kinase, cell membrane and Duchenne muscular dystrophy. *Mol Cell Biochem*. 1999;190(1):143-151. doi:10.1023/A:1006974613418

71. Hathout Y, Marathi RL, Rayavarapu S, et al. Discovery of serum protein biomarkers in the mdx mouse model and cross-species comparison to Duchenne muscular dystrophy patients. *Hum Mol Genet*. 2014;23(24):6458-6469. doi:10.1093/hmg/ddu366

72. Oonk S, Spitali P, Hiller M, et al. Comparative mass spectrometric and immunoassay-based proteome analysis in serum of Duchenne muscular dystrophy patients. *Proteomics Clin Appl*. 2016;10(3):290-299. doi:10.1002/prca.201500044

73. Maruyama N, Asai T, Abe C, et al. Establishment of a highly sensitive sandwich ELISA for the N-terminal fragment of titin in urine. *Sci Rep*. 2016;6(1):39375. doi:10.1038/srep39375

74. Robertson AS, Majchrzak MJ, Smith CM, et al. Dramatic elevation in urinary amino terminal titin fragment excretion quantified by immunoassay in Duchenne muscular dystrophy patients and in dystrophin deficient rodents. *Neuromuscul Disord*. 2017;27(7):635-645. doi:10.1016/j.nmd.2017.05.009

75. Kanda K, Sakuma J, Akimoto T, Kawakami Y, Suzuki K. Detection of titin fragments in urine in response to exercise-induced muscle damage. *PLoS One*. 2017;12(7):e0181623. doi:10.1371/journal.pone.0181623

76. Shirakawa T, Ikushima A, Maruyama N, et al. A sandwich ELISA kit reveals marked elevation of titin N-terminal fragment levels in the urine of mdx mice. *Animal Models and Experimental Medicine*. 2022;5(1):48-55. doi:10.1002/ame2.12204

77. Barthelemy F, Woods JD, Nieves-Rodriguez S, et al. A well-tolerated core needle muscle biopsy process suitable for children and adults. *Muscle & Nerve*. 2020;62(6):688-698. doi:10.1002/mus.27041

78. Shankaran M, King CL, Angel TE, et al. Circulating protein synthesis rates reveal skeletal muscle proteome dynamics. *J Clin Invest*. 2016;126(1):288-302. doi:10.1172/JCI79639

79. Eagle M, Bourke J, Bullock R, et al. Managing Duchenne muscular dystrophy--the additive effect of spinal surgery and home nocturnal ventilation in improving survival. *Neuromuscul Disord*. 2007;17(6):470-475. doi:10.1016/j.nmd.2007.03.002

80. Moxley RT, Pandya S, Ciafaloni E, Fox DJ, Campbell K. Change in natural history of Duchenne muscular dystrophy with long-term corticosteroid treatment: implications for management. *J Child Neurol*. 2010;25(9):1116-1129. doi:10.1177/0883073810371004

81. Saito T, Kawai M, Kimura E, et al. Study of Duchenne muscular dystrophy long-term survivors aged 40 years and older living in specialized institutions in Japan. *Neuromuscul Disord*. 2017;27(2):107-114. doi:10.1016/j.nmd.2016.11.012

82. Schram G, Fournier A, Leduc H, et al. All-cause mortality and cardiovascular outcomes with prophylactic steroid therapy in Duchenne muscular dystrophy. *J Am Coll Cardiol*. 2013;61(9):948-954. doi:10.1016/j.jacc.2012.12.008

83. Oray M, Abu Samra K, Ebrahimiadib N, Meese H, Foster CS. Long-term side effects of glucocorticoids. *Expert Opinion on Drug Safety*. 2016;15(4):457-465. doi:10.1517/14740338.2016.1140743

84. Dhargave P, Nalini A, Nagarathna R, et al. Effect of Yoga and Physiotherapy on Pulmonary Functions in Children with Duchenne Muscular Dystrophy - A Comparative Study. *Int J Yoga*. 2021;14(2):133-140. doi:10.4103/ijoy.IJOY_49_20

85. Bushby K, Bourke J, Bullock R, Eagle M, Gibson M, Quinby J. The multidisciplinary management of Duchenne muscular dystrophy. *Current Paediatrics*. 2005;15(4):292-300. doi:10.1016/j.cupe.2005.04.001

86. Takeda S, Clemens PR, Hoffman EP. Exon-Skipping in Duchenne Muscular Dystrophy. *J Neuromuscul Dis*. 8(Suppl 2):S343-S358. doi:10.3233/JND-210682

87. Matsuo M. Antisense Oligonucleotide-Mediated Exon-skipping Therapies: Precision Medicine Spreading from Duchenne Muscular Dystrophy. *JMA J*. 2021;4(3):232-240. doi:10.31662/jmaj.2021-0019

88. Blake DJ, Tinsley JM, Davies KE. Utrophin: A Structural and Functional Comparison to Dystrophin. *Brain Pathology*. 1996;6(1):37-47. doi:10.1111/j.1750-3639.1996.tb00781.x

89. Muntoni F, Tejura B, Spinty S, et al. A Phase 1b Trial to Assess the Pharmacokinetics of Ezutromid in Pediatric Duchenne Muscular Dystrophy Patients on a Balanced Diet. *Clin Pharmacol Drug Dev*. 2019;8(7):922-933. doi:10.1002/cpdd.642

90. Duan D. Systemic AAV Micro-dystrophin Gene Therapy for Duchenne Muscular Dystrophy. *Mol Ther*. 2018;26(10):2337-2356. doi:10.1016/j.ymthe.2018.07.011

Chapter 1

Profoundly Lower Biomarkers of Muscle Mass and Rate of Contractile Protein Synthesis from Urine of Boys with Duchenne muscular dystrophy

*William J. Evans [1, 2], *Mahalakshmi Shankaran [1], Edward C. Smith [2], Carl Morris [3], Edna Nyangau [1], Alec Bizieff [1], Marcy Matthews [1], Hussein Mohamed [1], and Marc Hellerstein [1]

[1] Department of Nutritional Sciences, University of California, Berkeley, CA

[2] Duke Medical Center, Duke University, Raleigh, NC

[3] Solid Biosciences, Inc, Cambridge, MA

*These authors contributed equally to this work as first authors

Full Publication: Evans WJ, Shankaran M, Smith EC, Morris C, Nyangau E, Bizieff A, Matthews M, Mohamed H, Hellerstein M. Profoundly lower muscle mass and rate of contractile protein synthesis in boys with Duchenne muscular dystrophy. *J Physiol*. 2021 Dec;599(23):5215-5227. doi: 10.1113/JP282227.

My contribution to this work included sample processing, data collection, data analysis, and manuscript writing.

Address Correspondence:

William J. Evans, PhD
Department of Nutritional Sciences and Toxicology, Morgan Hall
University of California Berkeley
William.Evans@berkeley.edu

Abstract

Skeletal muscle in boys with Duchenne muscular dystrophy (DMD) undergoes a progressive loss of functional mass, with fibrosis and lipid accumulation. Here we use two non-invasive, stable isotope-based methods from urine samples to simultaneously measure the fractional rate of muscle protein synthesis (FSR) and the total functional skeletal muscle mass (MM) in 10 DMD subjects (6-17 yrs) and 9 age-matched healthy male subjects. Functional MM was profoundly reduced in DMD subjects compared to controls (17% vs 41% of body weight, $p < 0.0001$), particularly in older, non-ambulant patients in whom functional MM was extraordinarily low (< 13% body weight). We explored the urine proteome to measure the FSR of skeletal muscle-derived proteins. Titin and myosin light chain FSRs were substantially lower in DMD subjects compared to controls (27% and 11% of control, respectively, $p < 0.0001$). There were no differences in albumin FSR, and no differences were observed for muscle-derived sarcoplasmic proteins (creatine kinase M-type and carbonic anhydrase-3) measured in plasma. These data demonstrate that both functional MM and muscle protein synthesis rates can be quantified non-invasively and are markedly reduced in DMD subjects, suggesting that contractile but not sarcoplasmic protein synthesis is affected by a lack of dystrophin. These non-invasive measurements from urine samples provide potential biomarkers of disease progression and therapeutic efficacy in patients with DMD or other neuromuscular disorders.

Introduction

Duchenne muscular dystrophy (DMD) is an X-chromosome-linked disease that is characterized by a mutation in the gene that codes for the muscle protein, dystrophin. DMD patients show a progressive loss of muscle strength and functional capacity. In addition, DMD patients also undergo a progressive loss of functional muscle mass (MM) that is associated with increased muscle fibrosis and lipid accumulation [1]. The use of magnetic resonance imaging (MRI) to characterize these changes with DMD has shown that an increasing proportion of non-contractile tissue in skeletal muscle is associated with diminished strength and function [2] with a large degree of heterogeneity among individual muscle groups in the same boy and between patients [3]. MRI provides estimates of regional muscle mass, but unless a whole-body MRI is performed, it does not provide an assessment of whole-body functional MM. Moreover, non-ambulatory patients, obese patients, and patients with severe muscle contractures may not be able to participate in studies that require MRI. The ability to measure accurately and inexpensively the total amount of MM in patients with DMD has not, however, been previously available.

The D_3-creatine (D_3Cr) dilution method measures total body creatine pool size, about 98% of which is sequestered in skeletal muscle. By this method, an oral tracer dose of D_3Cr is administered, absorbed and, once in circulation, transported against a large concentration gradient into the sarcomere. Creatine is turned over in muscle through the non-enzymatic and physically constant conversion of creatine to creatinine, which is rapidly excreted into urine. The enrichment of urinary D_3creatinine (D_3Crn) thereby reveals the enrichment of intramyocellular D_3Cr, which provides a noninvasive measurement of total body MM, based on the dilution of

administered D_3Cr. The method has been previously validated in rodents [4, 5], adult humans [6, 7], and recently, in premature infants [8].

While the D_3Cr dilution measures MM, it does not provide an assessment of muscle protein synthesis rates. The fractional synthesis rate (FSR) of muscle proteins has most often been determined using a muscle biopsy along with a primed, constant infusion of a labeled amino acid such as leucine or phenylalanine [9]. The use of heavy water labeling combined with tandem mass spectrometric analysis provides the ability to measure FSRs of 100s of proteins simultaneously. Skeletal muscle "leaks" myocellular proteins into the circulation, particularly in DMD [10]. Proteins or peptides synthesized only in skeletal muscle can thereby be isolated from body fluids to measure their isotopic enrichment and labeling pattern and, from this, determine muscle protein FSRs [11] without a muscle biopsy. In patients with DMD, urine is also enriched with peptides and proteins synthesized only in skeletal muscle. For example, urinary excretion of the muscle protein titin is dramatically elevated in DMD [12].

In the present study, we measured both MM using the D_3-creatine dilution method and the rate of muscle protein synthesis with heavy water based on muscle proteins released into body fluids, including carbonic anhydrase-3 (CA3) and creatine phosphokinase-muscle type (CK-MM), in blood and urine from patients with DMD and healthy, age-matched male controls. We also used the dilution of heavy water to determine total body water content as a separate estimate of lean body mass [13].

Results

IRB Study Approval This study was approved by the Duke University Institutional Review Board. Parents signed an approved consent form and all subjects provided assent. Ten subjects (7 – 17 years old) with DMD and nine healthy male control subjects (8 – 16 years old) were enrolled. DMD subjects participated in this study during a normally scheduled clinical visit. Three of the subjects with DMD were non-ambulant. The subject characteristics are shown in Table 1.

Dosing of Tracers Subjects weighing < 50 kg ingested 15 mg and those weighing $\geq$ 50 kg ingested 30 mg of D_3Cr dissolved in 2ml 70% ^2H_2O. Study schedule is shown in Figure 1. A saliva sample was collected 2 hours after the dose for the measurement of ^2H_2O and calculation of total body water content. After the saliva sample was collected, three doses of approximately 0.7 ml/kg of 70% ^2H_2O were ingested on the first day and again on days 2, 3, and 4. Two doses of 0.7 ml/kg of 70% ^2H_2O were ingested daily on days 5 – 14. The dosing schedule of ^2H_2O was designed to achieve and maintain body ^2H_2O enrichment at 1.5 – 2% through day 14 (Supplementary Figure 1).

Sample Collection In addition to the 2-hour sample, saliva was collected on days 7 and 10 for determination of ^2H enrichment in body water during labeling with ^2H_2O. Fasting urine samples were collected on days 2, 3, and 4 for determination of D_3Crn enrichment, total creatine and creatinine concentrations, and ^2H enrichment in body water during the period of labeling with ^2H_2O. On day 14, blood and urine samples were collected for determination of the ^2H enrichment in newly synthesized proteins to determine FSR. All samples were stored frozen until analysis.

Body composition by dual energy x-ray absorptiometry (DXA) was measured in the DMD cohort only on the initial day of dosing. Measurements of functional capacity were performed on the DMD cohort and included time to rise from supine, time to walk/run 10 m, grip strength, and 6-minute walk distance.

D_3-Creatine Dilution We have previously observed that a small amount of the orally ingested D_3Cr is "spilled" into urine in some human subjects. As a result, an algorithm has been created to correct for D_3Cr loss in urine using the urine creatine/creatinine measured in the fasting condition[7]. For the control subjects, the average urine Cr and Crn concentrations was 1.9 μM and 15.2 mM, and for DMD 5.4 mM and 6.9 mM, respectively. The urine Cr/Crn ratios were 12 times greater in DMD than in controls (Table 2). Muscle mass values and muscle mass/body weight were substantially higher in the healthy controls compared to the DMD subjects, as shown in Figure 1A, Figure 2, and Table 3. Remarkably, the three non-ambulant DMD subjects, aged 14-17 years, had 13%, 3%, and 5% muscle mass relative to body weight. In healthy control subjects, muscle mass was strongly associated with body weight ($r = 0.825$, $p = 0.006$) while there was no relationship between muscle mass and weight in DMD ($r = 0.517$, $p = 0.126$). Initial saliva samples for determination of TBW were inadequate for measurement in two controls and one DMD subject. FFM was significantly lower in the DMD cohort compared to controls (Figure 1B). In all subjects, MM was strongly related to FFM measured by TBW ($r = 0.9121$, $p<0.001$), as shown in Figure 1C. In healthy control subjects, MM was significantly associated with FFM ($r = 0.864$, $p = 0.006$) and in DMD ($r = 0.773$, $p = 0.025$). Body composition represented as %MM, %FFM and %fat relative to body weight is shown in Figure 2. In DMD, %MM and %FFM was substantially lower compared to controls. DXA lean mass was measured in the DMD cohort and was unrelated to MM ($r = 0.54$, $p = 0.11$). A negative relationship between time to rise from supine and MM was observed in the 6 ambulant DMD subjects ($r = -0.881$, $p<0.01$) with no relationship seen between MM and 6-minute walk distance or grip strength.

Muscle Protein Synthesis The FSR of several proteins (Supplementary Table 1) was measured in plasma and urine of controls and DMD subjects following labeling with ^2H_2O for 14 days. The FSR of titin was determined from ^2H enrichment of titin peptides in urine samples. As previously reported [12], urinary peptides derived from titin were in far greater abundance in the DMD cohort compared with control subjects (two control subjects had very low abundance and their titin FSR values could not be determined). The FSR of titin was significantly lower in DMD subjects compared to control subjects (Figure 3A). The FSR of myosin light chain 1/3, another muscle-derived protein, was also significantly lower in the urine of DMD subjects compared to control subjects (Figure 3B), whereas several other urinary proteins were either fully turned over or not different between the two groups. The FSR of muscle-derived proteins isolated from plasma, CK-MM and CA-3 in plasma samples, were not significantly different in DMD subjects compared to control subjects (Figures 3C, 3D). The relationship between the different biomarkers, as well as with muscle mass, fat-free mass and plasma testosterone is shown in Table 4.

Discussion

Here we used two complementary non-invasive methods to quantitatively measure total body MM and the rate of muscle protein synthesis in subjects with DMD. The rates of synthesis of contractile proteins were markedly lower in DMD subjects compared to controls, while those of sarcoplasmic proteins were not different. Total body MM was profoundly reduced in DMD subjects compared to controls. Remarkably, the non-ambulant and oldest boys DMD subjects had MM values that were between 3-13% of body weight. Muscle mass was also a much lower relative component of FFM in DMD compared with controls, likely reflecting the increasing amounts of fibrosis and lipid accumulation within muscle and the decreasing amount of functional (contractile) muscle observed as DMD progresses[14]. The calculation of creatine pool size to MM is based on an average of 4.3 g of creatine/kg of muscle [4, 5]. While this calculation is derived from healthy muscle and may not be the same in dystrophic muscle, it provides an estimate of functional muscle. Intramyocellular CK-MM and Cr are co-located with contractile proteins [15, 16] and, as a result, muscle Cr is undiluted by lipid and/or fibrotic tissue and the measurement of Cr pool size provides an estimate of functional MM. Skeletal muscle of patients with DMD undergoes a progressive loss of functional mass that is associated with increased muscle fibrosis and lipid accumulation [1]. Increasing non-contractile tissue in skeletal muscle estimated by magnetic resonance imaging (MRI) is associated with diminished strength and functional capacity [2]. MRI has provided a better understanding of the nature and the extent of increasing muscle fibrosis and fat accumulation and the resultant negative effects on muscle function in DMD [17], however this method is expensive, time consuming, and only provides estimates of regional muscle mass. Unless whole-body MRI is performed, it does not provide an assessment of functional muscle in the whole body. As observed previously [18], our data demonstrate large differences in FFM, %FFM and % body fat between DMD subjects and controls. Body composition has been measured in DMD using DXA or bioelectrical impedance each of which provide estimates of FFM but not MM [19, 20.] Our data demonstrate that FFM does not provide an accurate estimate of MM, particularly in DMD. Although we observed a significant overall relationship between FFM estimated by TBW and MM in all subjects (r^2 = 0.832, $P < 0.0001$) with a stronger relationship in controls vs DMD ($r^2 = 0.746$, $p = 0.006$) than in DMD ($r^2 = 0.598$, $p = 0.025$), we report, for the first time, that MM was on average 34±9% of FFM and 17±10% of body weight in DMD compared to 41±9% and 56±9% in control, indicating that FFM substantially overestimates MM, particularly in DMD, and should not be used as a surrogate for MM. In the oldest (non-ambulant) subject with DMD, FFM was 62.3% while MM was, remarkably, 5% of body weight and only 8% of FFM. The D_3Cr dilution method is a non-invasive and accurate method to assess creatine pool size which is associated with the contractile component of skeletal muscle. We have previously demonstrated that the D_3Cr muscle mass, but not DXA lean mass, is strongly related to functional capacity, risk of disability and falls in a large cohort of very old men [19]. Importantly, the progression of loss of function in DMD can be rapid in some patients with rapid decreases in muscle strength, functional capacity, and contractile tissue over the course of a single year [20, 21]. Although functional correlates could only be tested in ambulant DMD subjects, we observed a significant correlation between D_3Cr MM and the functional metric time to rise from a supine position ($r^2 = 0.776$, $p<0.01$).

We observed a relatively low spillage or oral D_3Cr into urine, based on the creatine/creatinine ratio (Table 2) in all of the subjects with the exception of the older DMD subjects with very low muscle mass. The high ratio was due to high urinary Cr and relatively low urinary Crn values. The lower urinary Crn levels reflect the low amount of muscle, but the higher

urinary Cr values likely result from continued normal production of hepatic and renal Cr but a very small amount of muscle for transport into the sarcomere and, as a result, excess excretion of Cr. A previously validated correction algorithm to account for Cr spillage was applied to all subjects [7]. This data confirms a previous report [22] demonstrating an increase in the serum Cr/Crn ratio with age in DMD because of increasing Cr and decreasing Crn concentrations.

$^{2}H_2O$ aliquots were ingested daily by all subjects, enriching the total body water pool and allowing continuous labeling of newly synthesized proteins to determine the FSR of skeletal muscle proteins [11]. There is little information on the effects of dystrophin deficiency on muscle protein FSR in humans. In the only clinical study that measured muscle protein FSR in DMD, Rennie et al [9] showed that the rate of muscle protein synthesis in DMD patients was 77% lower than that of healthy adult men. In that study, muscle biopsies were obtained before and after a primed-constant infusion of ^{13}C-leucine was administered to measure incorporation into mixed muscle. The investigators concluded that low MM in DMD was a result of a greatly reduced rate of muscle protein synthesis rather than accelerated rate of degradation. This method provides only an assessment of mixed muscle protein synthesis measured during the short period of the infusion, unlike the use of $^{2}H_2O$ which provides an integrated value for FSR during the 2-week labeling period, including both fed and fasted states. We observed an approximately 73% lower rate of titin and 89% lower rate of myosin light chain 1/3 synthesis in DMD subjects compared to healthy controls and no differences in the rate of synthesis of sarcoplasmic proteins, CKMM and CA3. Titin is a massive protein attached to the *z*-disk and *m*-line of the sarcomere and is involved in muscle force production. Myosin light chain 1/3 is an essential contractile protein found in type II fibers [23]. Circulating peptide fragments of myosin light chain proteins and both circulating and urinary titin fragments have been reported to be significantly elevated in patients with DMD [12, 24], however the present data indicate much lower synthesis rates for both of these contractile proteins compared with controls. We also observed a strong correlation between FSR values of titin and myosin light chain 1/3. In contrast, the rates of synthesis of sarcoplasmic proteins not involved in muscle force production may not be affected by a lack of dystrophin. Abundance of circulating CK and CA3 has been suggested as biomarkers of progression of DMD [25], however, increased levels of muscle-derived proteins may only reflect the total amount of muscle and leakiness of the sarcolemma in DMD, rather than a metabolic flux due to a lack of dystrophin.

We also report significantly lower total testosterone levels in corticosteroid treated DMD subjects compared to controls. Both hormonal factors may affect muscle protein FSR, although a contractile protein specific effect of testosterone or corticosteroids has not been previously reported. There was no difference in the FSR of albumin indicating that neither hormonal status, nor DMD, influenced the FSR of this protein by the liver. The substantially lower FSRs of contractile proteins likely contribute to the much lower amount of functional muscle mass observed in DMD in this study. Gene expression of lumican has been shown to be higher in muscle from DMD subjects compared to that of healthy (but not age or sex-matched) control subjects [26], but lumican FSR was also lower in DMD compared to control subjects. Lumican is a proteoglycan that interacts with collagen in extracellular matrix development. Together these data suggest that the rate of synthesis of extracellular matrix proteins is depressed in DMD and may not explain the large increases in muscle fibrosis associated with disease progression. A prolonged half-life of these proteins may point to more cross-linked collagens and a slower breakdown rate for matrix proteins in DMD.

Conclusions

We report, for the first time, that functional skeletal MM and the FSRs of contractile proteins were substantially lower in DMD subjects compared with healthy, age-matched controls. The measurement of functional MM and the muscle protein synthesis rates can be performed non-invasively and accurately in patients with DMD using only urine samples. Muscle mass by the D_3Cr dilution method decreases with age in DMD, and these data suggest that this measurement may provide a facile indicator of disease progression. Determination of the FSR of skeletal muscle proteins using the "virtual biopsy" method [11] provides a determination of metabolic flux that may provide complementary information to the static concentration of individual proteins. Moreover, because this method measures only newly synthesized protein, FSR determination can provide a rapid assessment of the effects of novel pharmacological therapies that may be targeted more specifically at contractile proteins. The use of non-invasive urine or blood samples for complex metabolic markers of disease progression will allow more frequent measurements in DMD patients or patients with other neuromuscular diseases.

Materials and Methods

D_3-Creatine Dilution Morning fasting urine samples were used to determine creatine (Cr) and creatinine (Crn) concentrations as well as D_3Crn enrichment using methods described in detail elsewhere [7]. Briefly, 100 µl of urine or standards for the determination of a standard curve was added to 100 µl internal standard and 200 µl acetonitrile. Samples were centrifuged to precipitate proteins, and aliquots of the supernatant were diluted 50-fold using 70% acetonitrile for liquid chromatography/mass spectrometry analysis performed on a Sciex 6500 QTRAP (AB Sciex LLC, Framingham, MA) operating in multiple reaction monitoring mode. Quantitation of Cr and Crn concentrations to calculate Cr/Crn ratios was performed using an external standard curve using an internal standard mixture of D_5-labelled Cr and Crn following transitions (132.1/44.1) and (114.1/44.1). Quantitation of D_3Crn enrichment was performed with internal isotope ratios using a standard curve for D_3Crn enrichment and measured multiple reaction monitoring transitions 114.1/44.1 corresponding to the M0 peak of Crn and 117.1/47.1 which corresponds to D_3Crn. Spillage of D_3Cr dose was estimated from Cr/Crn ratio values using an algorithm [7]. Urine D_3Crn enrichment corrected for spillage of D_3Cr was used to calculate total body creatine and muscle mass (4.3 g creatine/kg muscle) as previously described [6, 7].

FSR of Muscle Proteins FSR of muscle-derived proteins, including titin and myosin light chain 1/3 as well as other circulating proteins, were determined from the deuterium enrichment patterns of urinary peptides from these proteins. Urinary proteins were extracted from neat samples as previously described [27]. Urine samples ranging from 175ul-2ml were subjected to either organic precipitation or spin-column filtration. Protein concentration was determined by Bradford assay (Bio-Rad, CA) with BSA as standards and 100ug protein was digested in-solution by trypsin prior to LC/MS analysis. As previously reported [12], urinary peptides derived from titin were in far greater abundance in DMD samples compared with control subjects. FSR of muscle-derived proteins in plasma, carbonic anhydrase-3 (CA3) and creatine kinase MM (CK-MM), as well as lumican, an extracellular matrix protein and fibrogenesis marker, were determined by LC/MS-MS analysis at the end of 14 days of ^2H_2O labeling. These proteins were

immuno-precipitated from 1ml plasma samples followed by digestion with trypsin prior to LC/MS analysis using methods described previously [11, 28].

LC/MS analysis of trypsin-digested peptides from plasma and urine samples were carried out on a 6550 QTOF (quadrupole time-of-flight) mass spectrometer with a 1260 Chip Cube nano ESI source (Agilent Technologies, Santa Clara, CA). Peptides were separated using a Polaris HR chip consisting of enrichment and analytical columns packed with a Polaris C18-A stationary phase. Mobile phases were 5% vol/vol acetonitrile and 0.1% formic acid in water and 95% acetonitrile and 0.1% formic acid in water. Peptides were eluted at a 350 nl/min flow rate with a 27-min LC gradient. Each sample was analyzed once for protein/peptide identification in data-dependent MS/MS mode and once for peptide isotope analysis in MS mode. Acquired MS/MS spectra were extracted and searched using Spectrum Mill Proteomics Workbench software (Agilent Technologies) and human protein database (UniProt.org). Search results were validated with a global false discovery rate of 1%. A filtered list of peptides was collapsed into a nonredundant peptide formula database containing peptide elemental composition, mass, and retention time. This was used to extract mass isotope abundances (M_0–M_3) of each peptide from MSonly acquisition files with MassHunter Qualitative Analysis software (Agilent Technologies). An in-house software was used to calculate peptide elemental composition and curve fit parameters for predicting peptide isotope enrichment (EM_0) based on precursor body water enrichment (p) and the number (n) of amino acid C-H positions per peptide actively incorporating hydrogen (H) and deuterium (D) from body water. Subsequent data handling was performed using python-based scripts, with input of body water precursor enrichment for each subject, to yield fractional synthesis data at the protein level. Additional details of the FSR calculations and data filtering criteria were described in detail previously [11, 14]. The FSR data includes proteins with ≥ 2 peptides that were measured in at least 4 subjects per group and were not fully turned over in both groups after 14 days of ^2H_2O labeling.

Acknowledgments

This work was supported by Duchenne United Kingdom and Solid BioSciences. We thank Shalendar Bhasin for providing testosterone analysis and Valeria Ricotti for helping to organize and implement this project. We thank the study participants and their families for their full cooperation in this complex study.

Competing Interests

WJE and MH are listed as co-inventors on patents for the D_3creatine dilution method. However, they do not control the IP nor do they derive any income from the use of this method. The other authors declare no competing interests.

References

1. Liu, G.C., Jong, Y.J., Chiang, C.H. & Jaw, T.S. Duchenne muscular dystrophy: MR grading system with functional correlation. *Radiology* **186**, 475-480 (1993).

2. Akima, H., *et al.* Relationships of thigh muscle contractile and non-contractile tissue with function, strength, and age in boys with Duchenne muscular dystrophy. *Neuromuscul Disord* **22**, 16-25 (2012).

3. Chrzanowski, S.M., *et al.* Multi-slice MRI reveals heterogeneity in disease distribution along the length of muscle in Duchenne muscular dystrophy. *Acta Myol* **36**, 151-162 (2017).

4. Stimpson, S.A., *et al.* Longitudinal changes in total body creatine pool size and skeletal muscle mass using the D-creatine dilution method. *J Cachexia Sarcopenia Muscle* (2013).

5. Stimpson, S.A., *et al.* Total-body creatine pool size and skeletal muscle mass determination by creatine-(methyl-D3) dilution in rats. *J Appl Physiol (1985)* **112**, 19401948 (2012).

6. Clark, R.V., *et al.* Total body skeletal muscle mass: estimation by creatine (methyl-d3) dilution in humans. *J Appl Physiol (1985)* **116**, 1605-1613 (2014).

7. Shankaran, M., *et al.* Dilution of oral D3 -Creatine to measure creatine pool size and estimate skeletal muscle mass: development of a correction algorithm. *J Cachexia Sarcopenia Muscle* **9**, 540-546 (2018).

8. Scottoline, B., *et al.* Deuterated, D3-creatine and heavy water dilution to measure total body muscle and lean mass in neonates: Validation of a novel, non-invasive method. *Pediatric Academic Societies Meeting* **Abstract (accepted)** (2019).

9. Rennie, M.J., *et al.* Effects of Duchenne muscular dystrophy on muscle protein synthesis. *Nature* **296**, 165-167 (1982).

10. Hathout, Y., *et al.* Clinical utility of serum biomarkers in Duchenne muscular dystrophy. *Clin Proteomics* **13**, 9 (2016).

11. Shankaran, M., *et al.* Circulating protein synthesis rates reveal skeletal muscle proteome dynamics. *J Clin Invest* **126**, 288-302 (2016).

12. Robertson, A.S., *et al.* Dramatic elevation in urinary amino terminal titin fragment excretion quantified by immunoassay in Duchenne muscular dystrophy patients and in dystrophin deficient rodents. *Neuromuscul Disord* **27**, 635-645 (2017).

13. Lukaski, H.C. & Johnson, P.E. A simple, inexpensive method of determining total body water using a tracer dose of D2O and infrared absorption of biological fluids. *Am J Clin Nutr* **41**, 363-370 (1985).

14. Klingler, W., Jurkat-Rott, K., Lehmann-Horn, F. & Schleip, R. The role of fibrosis in Duchenne muscular dystrophy. *Acta Myol* **31**, 184-195 (2012).

15. Wallimann, T., Moser, H. & Eppenberger, H.M. Isoenzyme-specific localization of M-line bound creatine kinase in myogenic cells. *J Muscle Res Cell Motil* **4**, 429-441 (1983).

16. Hill, D.K. The location of creatine phosphate in frog's striated muscle. *J Physiol* **164**, 3150 (1962).
c
17. Barnard, A.M., *et al.* MR biomarkers predict clinical function in Duchenne muscular dystrophy. *Neurology* **94**, e897-e909 (2020).

18. Skalsky, A.J., Han, J.J., Abresch, R.T., Shin, C.S. & McDonald, C.M. Assessment of regional body composition with dual-energy X-ray absorptiometry in Duchenne muscular dystrophy: correlation of regional lean mass and quantitative strength. *Muscle Nerve* **39**, 647-651 (2009).

19. Cawthon, P.M., *et al.* Strong Relation between Muscle Mass Determined by D3-creatine Dilution, Physical Performance and Incidence of Falls and Mobility Limitations in a Prospective Cohort of Older Men. *J Gerontol A Biol Sci Med Sci* (2018).

20. Willcocks, R.J., *et al.* Leg muscle MRI in identical twin boys with duchenne muscular dystrophy. *Muscle Nerve* (2018).

21. Mendell, J.R., *et al.* Eteplirsen for the treatment of Duchenne muscular dystrophy. *Annals of Neurology* **74**, 637-647 (2013).

22. Boca, S.M., *et al.* Discovery of Metabolic Biomarkers for Duchenne Muscular Dystrophy within a Natural History Study. *PLoS One* **11**, e0153461 (2016).

23. Ravenscroft, G., *et al.* Bi-allelic mutations in MYL1 cause a severe congenital myopathy. *Hum Mol Genet* **27**, 4263-4272 (2018).

24. Burch, P.M., *et al.* Muscle-Derived Proteins as Serum Biomarkers for Monitoring Disease Progression in Three Forms of Muscular Dystrophy. *J Neuromuscul Dis* **2**, 241-255 (2015).

25. Strandberg, K., *et al.* Blood-derived biomarkers correlate with clinical progression in Duchenne muscular dystrophy. *J Neuromuscul Dis* **7**, 231-246 (2020).

26. Haslett, J.N., *et al.* Gene expression comparison of biopsies from Duchenne muscular dystrophy (DMD) and normal skeletal muscle. *Proc Natl Acad Sci U S A* **99**, 15000-15005 (2002).

27. Afkarian, M., *et al.* Optimizing a proteomics platform for urine biomarker discovery. *Mol Cell Proteomics* **9**, 2195-2204 (2010).

28. Decaris, M.L., *et al.* Identifying nonalcoholic fatty liver disease patients with active fibrosis by measuring extracellular matrix remodeling rates in tissue and blood. *Hepatology* **65**, 78-88 (2017).

Figure Legend

Figure 1 Study Design All subjects received an initial dose of D_3-creatine (D_3Cr) dissolved in ^2H_2O to determine total body water and muscle mass. Two hours after the dose, saliva was sampled. Following this saliva sample, ^2H_2O was ingested daily for deuterium labeling of all newly synthesized proteins. Urine was collected 2 days after dosing of D_3Cr for determination of D_3-creatinine enrichment. Saliva was sampled on days 7, 10, and 14 to measure enrichment of ^2H_2O. On day 14 blood and urine were collected for determination of protein fractional synthetic rate. DMD subjects underwent strength, functional testing, and DXE measurement of lean body mass.

Figure 2 Subject Physical Measurements A.) Muscle mass by D_3creatine dilution in DMD and age-matched control males (*$p < 0.0001$), **B.)** FFM by total body water in DMD and control (*$p < 0.0001$), **C.)** Correlation of muscle mass vs FFM in all subjects, open circles, DMD and closed circles, control ($r = 0.912$, $p < 0.0001$).

Figure 3 Body Composition Body composition values for control and DMD using D_3creatine dilution for muscle mass (MM) and total body water for fat-free mass (FFM). DMD vs Control: %MM $p< 0.001$, %FFM $p<0.05$, %Fat, $p < 0.05$.

Figure 4 Selected Protein Turnover Rates Average fractional synthetic rate (%/day) for contractile proteins **A)** titin and **B)** myosin light chain 1/3 (from urine, $p < 0.0001$) and **C)** sarcoplasmic proteins creatine kinase M and **D)** carbonic anhydrase 3 (from plasma, no significant difference).

Supplementary Figures

Figure S1 Body Water Enrichment Body water enrichment curve for control and DMD subjects. All subjects consumed daily aliquots of ^2H_2O.

Figures and Tables

Table 1 Subject Characteristics

Subject Characteristics	Control	DMD
Number	9	10
Age (years)	12.1 ± 3.2	11.6 ± 3.3
Weight (kg)	53.7 ± 20.7	39.3 ± 18.0
Height (cm)	156.2 ± 17.8	135.3 ± 17.3*
BMI (kg/m^2)	21.2 ± 4.9	21.3 ± 7.1
Plasma Total Testosterone (ng/dL)	162.4 ± 182.2	28.2 ± 57.6*

*$p<0.05$ compared to Control.

Table 2 Urine Concentrations Creatine, Creatinine and Creatine/Creatinine Ratio

Group	Urine Cr (mM)	Urine Crn (mM)	Cr/Crn
Control	1.94 ± 3.13	15.21 ± 5.23	0.12 ± 0.2
DMD	5.41 ± 3.85*	6.94 ± 3.02***	0.99 ± 0.84**

*p<0.05, **p<0.01, ***p<0.001 compared to Control.

Table 3 Relative Body Composition Values of Muscle Mass and Fat Free Mass

	Control	DMD	t-test
% Muscle Mass / Body Weight	41% ± 9% (9)	17% ± 10% (10)	$p < 0.0001$
% Fat Free Mass / Body Weight	74% ± 9% (8)	54% ± 19% (9)	$p < 0.05$
% Muscle Mass / Fat Free Mass	56% ± 9% (8)	34% ± 12% (9)	$p < 0.005$

Data are presented as mean ± SD (range) (n).

Table 4 Correlation matrix of muscle mass (D_3creatine dilution), fat free mass (TBW), circulating testosterone and the fractional synthetic rate (FSR) of contractile proteins from urine and sarcoplasmic proteins from plasma.

Pearson Correlation	Muscle Mass (kg)	Fat Free Mass (kg)	Titin FSR/day	Myosin light chain 1/3 FSR/day	CK-M FSR/day	CA-3 FSR/day	Lumican FSR/day
Fat Free Mass (kg)	r = 0.912*****						
Urine Titin (FSR/day)	r = 0.630**	r = 0.524*					
Urine Myosin light chain 1/3 (FSR/day)	r = 0.923****	r = 0.652	r = 0.891***				
Plasma CK-M (FSR/day)	r = 0.146	r =0.096	r = 0.418	r = 0.076			
Plasma CA-3 (FSR/day)	r = 0.388	r = 0.243	r = 0.292	r = 0.333	r = -0.515*		
Plasma Lumican (FSR/day)	r = 0.572*	r = 0.492*	r = 0.361	r = 0.457	r = -0.236	r = 0.299	
Plasma Total Testosterone (ng/dL)	r = 0.687***	r = 0.785****	r = 0.444	r = 0.491	r = 0.348	r = -0.071	r = 0.346

FSRs of lumican, fibronectin, and gelsolin (from urine) are also included.
*p<0.05,
**p<0.01,
***p<0.005,
****p<0.0005,
*****p<0.0001

Table 5 FSR per day represented as Mean ± SD (n) for proteins measured in urine or immunoprecipitated from plasma

	Control FSR/day	DMD FSR/day	t-test p-value significant after B-H correction
Proteins in urine	-	-	-
Titin	19.2% ± 0.3% (7)	4.7% ± 1.0% (10)	Yes
Myosin light chain 1/3, skeletal muscle isoform	6.3% ± 0.8% (4)	0.7% ± 0.2% (5)	Yes
Golgi membrane protein 1	2.1% ± 0.4% (7)	1.2% ± 0.3% (9)	Yes
Fibronectin	3.4% ± 0.5% (8)	5.6% ± 0.7% (6)	Yes
Glutaminyl-peptide cyclotransferase *	32.9% ± 1.8% (5)	8.5% ± 1.4% (8)	Yes
Semenogelin-1	7.7% ± 1.5% (7)	3.4% ± 1.0% (8)	Yes
Gelsolin *	32.9% ± 0.6% (8)	13.3% ± 1.1% (5)	Yes
Prostaglandin-H2 D-isomerase *	32.9% ± 1.3% (9)	15.6% ± 1.0% (10)	Yes
Collagen alpha-2(XI) chain	5.1% ± 0.9% (7)	2.7% ± 1.2% (7)	Yes
Collagen alpha-2(V) chain	2.8% ± 1.4% (7)	0.8% ± 0.5% (8)	Yes
Immunoglobulin lambda constant 2 *	32.9% ± 0.7% (8)	15.7% ± 1.3% (8)	Yes
Non-secretory ribonuclease	4.3% ± 1.2% (6)	11.0% ± 2.1% (10)	No
Albumin	2.9% ± 0.5% (9)	4.3% ± 0.8% (10)	No
Sulfhydryl oxidase 1	2.7% ± 0.7% (4)	1.1% ± 0.3% (4)	No

Monocyte differentiation antigen CD14 *	32.9% ± 1.0% (7)	5.6% ± 4.3% (6)	No
Alpha-1-antitrypsin *	30.3% ± 0.9% (7)	6.5% ± 3.4% (10)	No
Collagen alpha-1(I) chain	3.7% ± 1.1% (9)	2.4% ± 0.4% (10)	No
Collagen alpha-1(III) chain	3.3% ± 1.2% (7)	1.1% ± 0.4% (10)	No
Immunoglobulin kappa light chain *	32.9% ± 0.6% (9)	20.3% ± 2.5% (10)	No
Actin, cytoplasmic 1	1.9% ± 0.7% (6)	3.7% ± 1.4% (9)	No
Immunoglobulin heavy constant gamma 1	3.5% ± 0.8% (9)	5.1% ± 1.5% (10)	No
Collagen alpha-2(I) chain	7.5% ± 1.1% (9)	4.9% ± 1.8% (10)	No
Secreted and transmembrane protein 1 *	21.2% ± 1.4% (9)	32.9% ± 1.0% (6)	No
Inactive tyrosine-protein kinase PEAK1	6.1% ± 0.5% (7)	4.2% ± 1.8% (4)	No
Immunoglobulin heavy constant gamma 2	3.2% ± 1.2% (7)	5.7% ± 2.8% (8)	No
Androglobin	3.7% ± 0.7% (6)	4.8% ± 1.0% (8)	No
Prothrombin	10.2% ± 2.9% (6)	19.7% ± 2.0% (10)	No
Hemoglobin subunit beta	3.8% ± 2.9% (7)	2.0% ± 1.5% (7)	No
Collagen alpha-1(V) chain	2.3% ± 0.4% (7)	1.8% ± 0.7% (6)	No
Clusterin *	27.9% ± 2.8% (4)	32.9% ± 1.0% (10)	No
Peptidoglycan recognition protein 1 *	32.9% ± 0.8% (5)	24.8% ± 2.5% (6)	No
Collagen alpha-1(VI) chain	11.0% ± 2.1% (7)	16.6% ± 2.8% (9)	No

Immunoglobulin lambda-like polypeptide 5*	33.2% ± 0.8% (7)	18.4% ± 1.6% (8)	No
CD99 antigen	18.2% ± 1.8% (6)	13.7% ± 0.8% (8)	No
CD59 glycoprotein	8.5% ± 0.6% (9)	9.1% ± 0.7% (10)	No
Prosaposin *	32.9% ± 3.0% (4)	17.8% ± 1.6% (8)	No
Serotransferrin	8.4% ± 2.1% (9)	7.2% ± 1.1% (9)	No
Vitelline membrane outer layer protein 1 homolog *	32.9% ± 1.5% (7)	19.0% ± 4.9% (4)	No
Keratin, type II cytoskeletal 1	2.4% ± 1.5% (5)	1.8% ± 1.4% (6)	No
Cystatin-C	3.9% ± 1.3% (4)	4.8% ± 2.2% (7)	No
Vasorin	10.6% ± 2.8% (7)	12.9% ± 3.3% (9)	No
Lysosomal alpha-glucosidase	6.0% ± 3.0% (4)	7.3% ± 2.8% (5)	No
Hemoglobin subunit delta	3.0% ± 0.8% (5)	2.6% ± 2.6% (4)	No
Collagen alpha-1(II) chain	2.1% ± 0.7% (9)	2.2% ± 1.3% (8)	No
Apolipoprotein D	11.1% ± 1.3% (5)	11.7% ± 1.3% (8)	No
CD44 antigen	7.6% ± 0.8% (7)	7.5% ± 1.2% (9)	No
Basement membrane-specific heparan sulfate proteoglycan core protein	24.0% ± 1.4% (8)	26.0% ± 1.5% (8)	No
Myosin-14 *	31.5% ± 0.5% (8)	33.6% ± 0.8% (7)	No
Polymeric immunoglobulin receptor	14.8% ± 1.9% (8)	15.4% ± 2.6% (6)	No
Carbonic anhydrase 1	2.1% ± 0.6% (4)	2.1% ± 2.3% (4)	No

Proteins immunoprecipitated from plasma	-	-	-
Creatine kinase M-type	2.8% ± 1.9% (9)	2.0% ± 0.3% (10)	No
Carbonic anhydrase-3	2.0% ± 1.6% (9)	1.4% ± 0.4% (10)	No
Lumican	4.0% ± 2.0% (9)	2.6% ± 0.4% (10)	No

Data are presented as mean ± SD (n). * Indicates that this protein was > 85% turned over resulting in a possible underestimate of FSR

Figure 1 Study Design

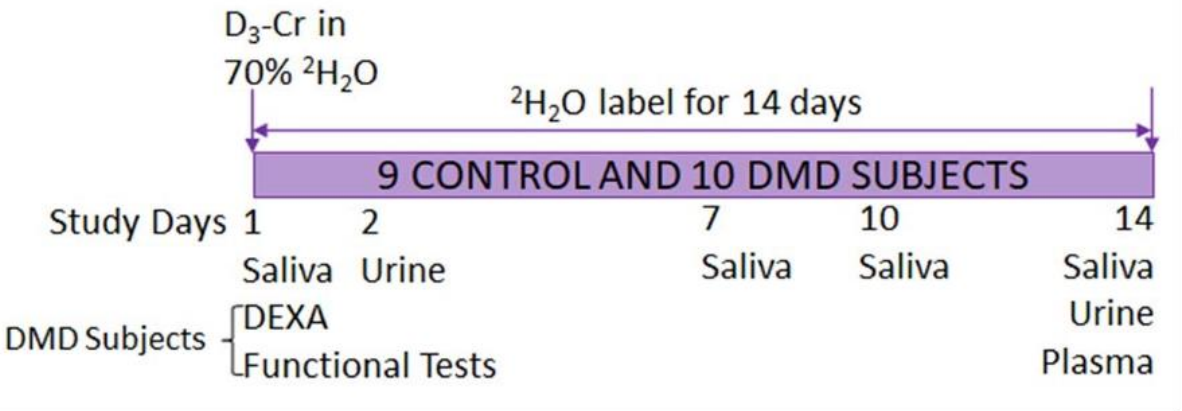

<u>Figure 2</u> Subject Physical Measurements

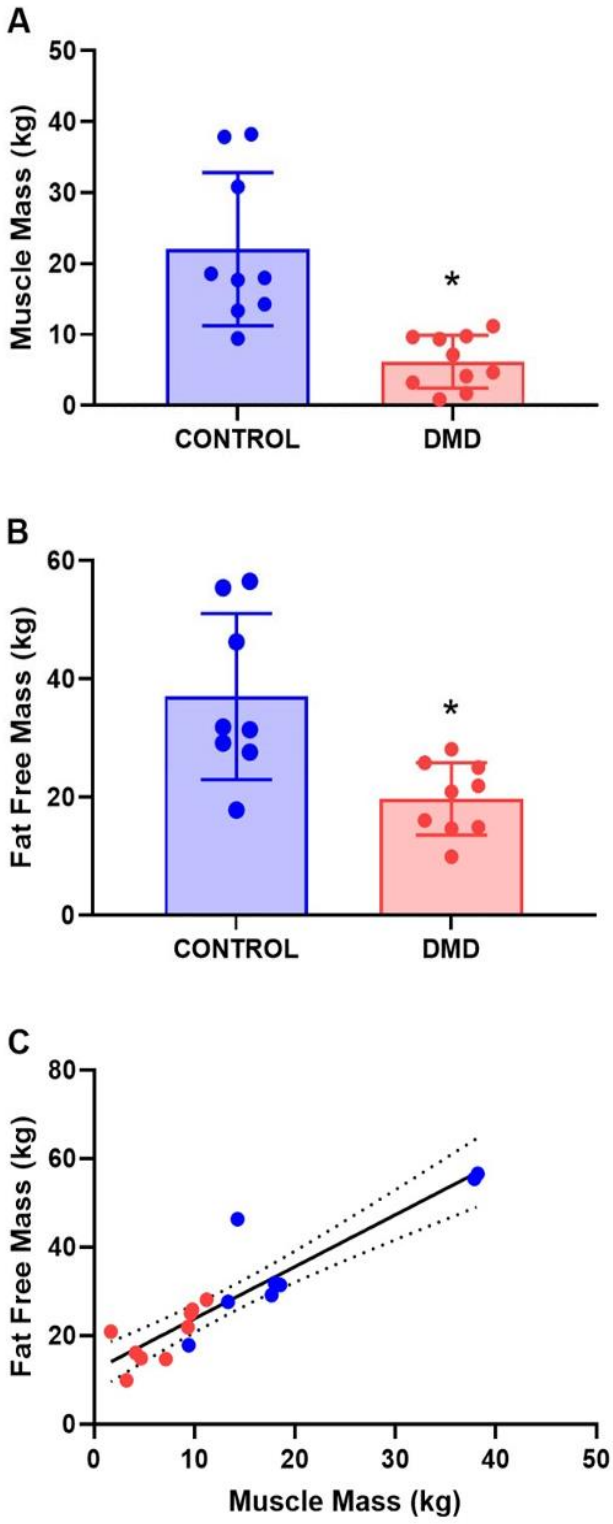

Figure 3 Body Composition

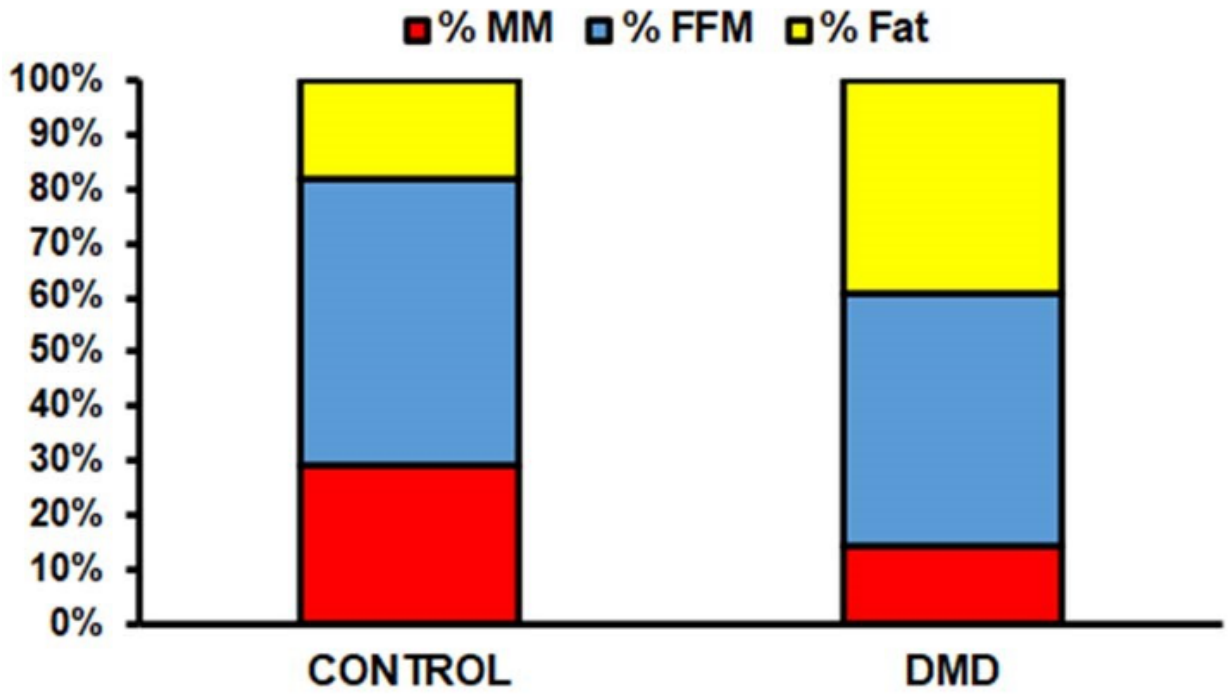

Figure 4 Selected Protein Turnover Rates

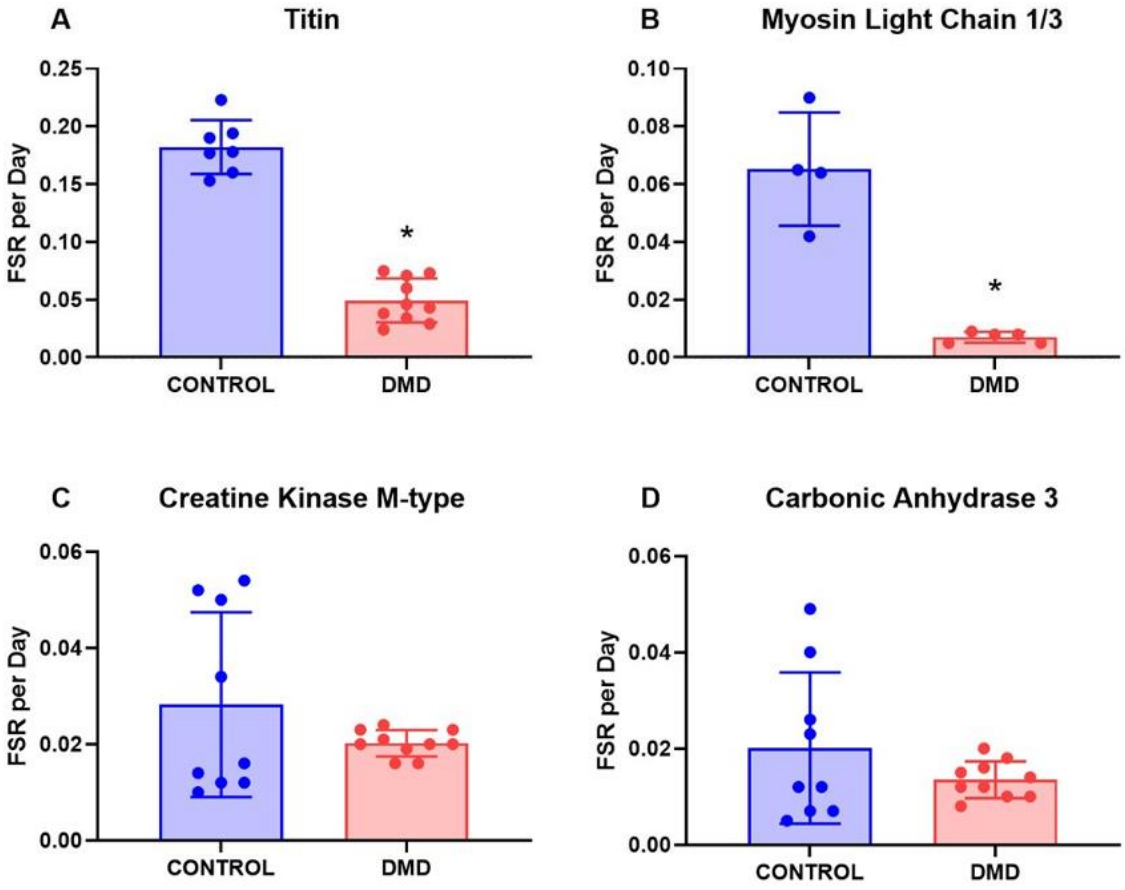

Figure S1 Body Water Enrichment

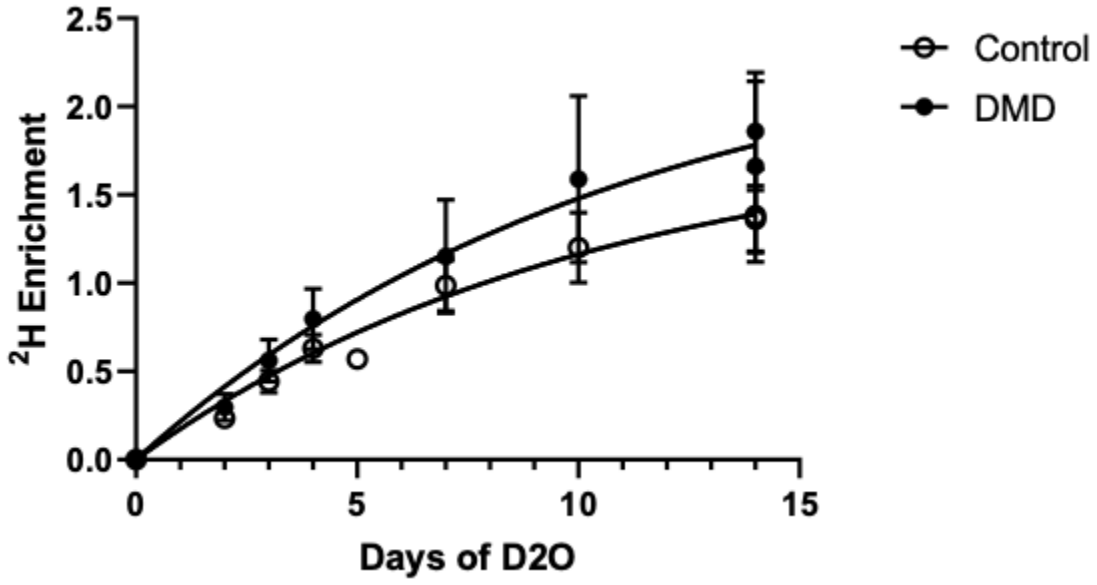

Chapter 2

Development of a Virtual Biopsy of Whole Muscle Protein FSR from Non-Invasive Collection Methods in *mdx* Mice

Alec Bizieff [1], Maggie Cheng [1], Kelvin Chang [1], Hussein Mohammed [1], and Marc K. Hellerstein[1]

[1] Department of Nutritional Sciences & Toxicology, University of California, Berkeley

Correspondence:
Marc K. Hellerstein
march@berkeley.edu
University of California, Berkeley
Berkeley, CA, United States

Abstract

Musculoskeletal diseases, like muscular dystrophy or pathological atrophy, have a serious impact on patients' quality of life. Symptoms range in variety and severity, but most share a unifying root cause of a decrease in maintaining proper tissue function. The effects of disease and treatment on whole muscle protein turnover rates are not well characterized. In this work, we employed an approach that couples deuterated water (^2H_2O) administration with liquid chromatography-mass spectrometry (LC-MS) to measure *in-vivo* protein turnover. We then examined protein extracts from urinary samples of a pre-clinical animal model of Duchenne muscular dystrophy (DMD), the *mdx* mouse, for muscle-specific proteins to serve as potential biomarkers of change in whole muscle protein flux rates. We report two muscle-specific proteins, Myosin-4 and Titin, that were found in urinary protein extracts and well reflect changes in parent muscle proteins and whole muscle protein turnover rates. In summary, certain urinary-derived muscle-specific proteins reflect the change in protein flux rates that are observed in the parent muscle tissue of the *mdx* mouse.

Introduction

Healthy skeletal muscle tissue is maintained in a biological system by a continual balance between protein synthesis and protein degradation. This process, termed proteostasis, may be impaired in various musculoskeletal diseases, and dysregulation can further exacerbate the development of deleterious disease symptoms [2]. One of the most debilitating and currently incurable musculoskeletal diseases is Duchenne muscular dystrophy (DMD) [3]. Characterized by a loss of an integral protein, dystrophin, that serves as a link between the sarcolemma and contracting components in the muscle, DMD causes severe loss of muscle function and atrophy as a patient ages [1]. Therefore, it is warranted to obtain as much knowledge as possible about the pathology of this disease and how it affects biological processes down to a subcellular level.

There have been many accomplishments in the field of DMD therapies in the past few decades [5, 6, 7]. However, there currently is not a non-invasive method for measuring muscle protein synthesis rates (FSR) reliably because muscle biopsies are generally contraindicated in DMD. The utilization of stable isotope labeling techniques can be powerful for obtaining relevant information about DMD. In one of the only clinical studies that measures muscle protein FSR in DMD patients with stable isotopes, we concluded that the significantly lower muscle mass in DMD was due to a decrease in muscle protein synthesis rate, not an increase in muscle degradation [4]. Therefore, to properly understand some of the most severe symptoms of this musculoskeletal disease and others, it is important to develop a method that accurately measures muscle protein FSR and avoids a muscle biopsy.

Here, we employed heavy water labeling and tandem mass spectrometric analysis to directly measure muscle protein FSR in skeletal muscle and body fluid samples in a pre-clinical animal model of DMD, the *mdx* mouse [8]. We identified certain muscle-specific proteins that were present in the urine. The FSR of these proteins was then compared to their parent protein from *mdx* muscle tissue, as well as to global proteins found from that tissue, to understand how these urinary-derived proteins reflect whole muscle FSR values.

Results

Study Design, Time Course of Labeling, and *mdx* Mouse Muscle Global Proteomics To determine how protein fluxes in skeletal muscle change over time in response to different genotypes, the FSRs of individual proteins were measured *in-vivo* via $^{2}H_2O$ administration coupled with HPLC-MS and MS/MS analysis. At the end of Day 7, both groups of mice were sacrificed, and tissues were taken for analysis (Figure 1). The FSR of 54 proteins from whole muscle tissue that passed analytical criteria and are present in both groups were measured and compared for changes in global flux rates. The *mdx* mouse had a higher FSR for almost all proteins that were measurable in both *mdx* and control groups (43/54 proteins, $p<0.05$ by binomial analysis, Figure 2). Of those 54 proteins present in both groups, 42 individual proteins had a significantly different FSR value in the *mdx* mouse compared to controls after correction for multiple comparisons. All 42 had a significantly higher value in the *mdx* mouse muscle (Table 1).

Changes in Protein Ontology-Group Turnover Rates Functional clusters of protein groups were analyzed by gene ontology enrichment using DAVID software from NIH to determine which cellular processes were highly affected at each stage (Figure 3A - 3D). At the end of the labeling period, all 4 measured gene ontologies had a significant number of proteins with higher FSR values in the mdx mouse compared to the control mouse. The 4 gene ontology groups that were measured were: Glycolysis (10/10 increased, $p< 0.05$, Figure 3A), Mitochondria (13/14 increased, $p< 0.05$, Figure 3B), Cytoplasm (19/19 increased, $p< 0.05$, Figure 3C), and Myofibril (11/11 increased, $p< 0.05$, Figure 3D). Along with analysis for the number of higher FSR proteins in each gene ontology, the average FSR value of both groups in each ontology was measured and was significantly different compared via Student's Unpaired T-Test (Figure 3A - 3D).

Individual Protein Flux Rates in Skeletal Muscle and Urine for Potential Biomarkers From the 42 individual proteins in the *mdx* mouse muscle that were significantly different to control after comparison for multiple corrections, a few stood out as potential candidates to represent changes in whole muscle flux rates for non-invasive collection methods. myosin-4 (My-4), titin, carbonic anhydrase 3 (CA3), creatine kinase, muscle form (CK-MM), and myosin light chain 1/3 are all muscle-specific proteins and have supporting literature that they can be detected in circulating (blood/serum) or excreted (urine) bodily fluids [9, 10]. For every protein, their individual FSRs were measured to be significantly higher in the mdx mouse muscle in comparison to controls (Figure 4A). In urine, only My-4 and titin had significantly increased FSR values in the *mdx* mouse in comparison to controls (Figure 4B).

Correlation Between Muscle and Urinary Derived Proteins At the end of the labeling period, both skeletal muscle and urine show an increase in FSR value for My-4 peptides in the *mdx* mouse, when compared to control. This is also seen in titin peptides, where both the skeletal muscle and urine show an increase in FSR value in the *mdx* mouse, when compared to control (Figure 4A-B). A correlation graph that plots the skeletal muscle and urine My-4 peptides from both *mdx* and control groups shows a significant correlation between skeletal muscle and urinary-derived My-4 proteins (Figure 5B). The same significant correlation is seen in a graph that plots the skeletal muscle and urinary derived titin peptides from both *mdx* and control groups (Figure 5A). A plot of change in urinary titin and My-4 FSR values vs average changes in

skeletal muscle FSR is shown (Figures 5C and 5D). Each point on the correlation graphs represents an average of peptides from one subject in each group. Changes in My-4 and titin peptides FSR between *mdx* and control from both skeletal muscle and urine were compared to changes in all 54 proteins measured from muscle to create a correlation table that is included in Supplementary Data (Tables S1-S2).

Discussion

In this work, we used a pre-clinical animal model of DMD, the *mdx* mouse, to determine whether any urinary proteins derived specifically from skeletal muscle reflect global protein turnover changes measured directly from skeletal muscle tissue. Our goal here was to test models for deeper discovery of non-invasive methods for measuring whole-body muscle protein synthesis rates. Our results show that My-4 and titin protein fragments found in the urine of *mdx* mice reflect the systematic increase in skeletal muscle FSR values that is seen in the animal model of disease.

Previous work from our research group has provided some relevant findings. First, muscle-specific proteins can be measured from circulation as "virtual biopsy" or "liquid biopsy" markers that reflect global muscle protein turnover rates [9], and, second, a muscle-specific protein found in the urine of DMD patients, titin, can be measured for protein turnover and correlate well to turnover rates of their cognate proteins and global proteins in skeletal muscle [10]. Other research groups have explored the urinary abundance of titin as a diagnostic tool to non-invasively measure DMD disease progression [11, 12], as has been tested for serum creatine kinase levels [13]. However, no one had previously reported protein turnover rates from urinary-derived muscle proteins, like My-4 and titin, and relate with what is directly occurring parent muscle tissue. In this study, we have done so directly *in-vivo* by administering $^{2}H_{2}O$ for 7 days to label newly synthesized proteins and analyzing samples with HPLC-MS and MS/MS to determine FSR values of potential non-invasive biomarkers. Doing so, we were able to see an across-the-board increase in fractional replacement rates in *mdx* mice for proteins present in skeletal muscle tissue from both groups. This is also accompanied by a striking increase in the number of significant proteins after correction for multiple comparisons. This data demonstrates that the *mdx* mouse has a signature of higher global protein FSR rates in comparison to control groups.

Along with a global increase in FSR rates, ontology-based group protein rates were also significantly increased for every group measured in *mdx* muscle, both by binomial analysis and grouped unpaired T-Test. This reinforces previous works that directly measured muscle protein FSR rates of *mdx* mice directly *in-vivo* using stable isotope labeling methods [15]. This robust animal model of increased muscle protein FSR made it possible to look for muscle-specific proteins found in urine and compare FSR to muscle tissue. Certain muscle proteins of interest were selected as potential non-invasive candidates based on previous literature that demonstrates their ability to be detected in circulation. My-4 was found to be present in higher concentrations in circulating serum of *mdx* mice [15]. As previously mentioned, our research group has demonstrated that carbonic anhydrase 3 (CA3) and creatine kinase, muscle isoform (CK-M) can be extracted from blood plasma samples to reflect changes in whole muscle protein FSR values [9]. Also, titin and Myosin light chain 1/3 were found in the urine of a clinical DMD patient population to correlate well with changes in anthropometrics (muscle mass by D3-creatine dilution) and serum testosterone levels [10]. These 5 markers were selected to be investigated here.

From urinary protein extracts, only My-4 and titin showed significant increases in *mdx* mice, consistent with changes in cognate protein and global protein flux rates in skeletal muscle.

The correlation between skeletal muscle-derived and urinary-derived protein fragments for My-4 and titin were strong in the *mdx* and control group (Figure 5). Both proteins show a significant increase in turnover rate (FSR) in both skeletal muscle, where they originate, and urine, where they are excreted from circulation and can be measured non-invasively. Moreover, when the proteins from individual subjects from both *mdx* and control groups are plotted for Myosin-4 and Titin, there is a significantly strong correlation between changes observed in muscle-derived FSR measurements and urinary-derived FSR measurements. To extrapolate these two markers further as reflective of changes to FSR in the whole muscle tissue proteome, a correlation matrix was generated for both muscle and urine My-4 and Titin and can be viewed in the Supplementary Tables (Tables S1-S2). The explanation for the lack of significant FSR change in *mdx* from control for the other candidate peptides tested in urine is unknown. The urinary peptides may derive disproportionately from non-skeletal muscle tissues. This question and a deeper search for other urinary proteins that reflect skeletal muscle protein turnover are areas for further research.

Conclusion

In summary, we present a new approach based on stable isotope labeling for discovering non-invasive biomarkers of changes in skeletal muscle protein flux rates from urine. My-4 and titin are two muscle-specific proteins that were measurable in urine and reflect the changes in skeletal muscle fluxes in *mdx* mice. This approach may be helpful for monitoring in a non-invasive manner disease progression, severity and response to therapy in patients suffering from musculoskeletal diseases.

Acknowledgments

The authors would like to thank all of those who contributed to producing the data in this work, including members of the Hellerstein Lab, for their efforts.

Materials and Methods

Mouse Models and $^{2}H_2O$ Labeling Time Course 5 male 8-week-old *C57BL/10ScSn-Dmdmdx/J* (*mdx*) mice and their aged-matched healthy C57/BL6 counterparts were purchased from Jackson Laboratory and housed at UC Berkeley's Northwest Animal Facility. All mice were housed according to the Animal Care and Use Committee (ACUC) standards in the animal facility at UC Berkeley. Mice were split into two groups (n=5/group), depending on their genotype, and received unrestricted access to a standard chow diet and 8% Deuterium drinking water ($^{2}H_2O$). $^{2}H_2O$ was provided to continually label the mice for 7 days after an initial bolus intraperitoneal injection of 99% $^{2}H_2O$/0.9% saline solution, at the start of the labeling period (Day 0), to allow for stable enrichment levels during the entire labeling time course. If a mouse appears to have issues accessing food or water at any time during incubation, then they were removed from the study and sacrificed. Urine was collected at the same time (11 AM) daily, as previously described [16], for the length of the labeling period. On Day 7, animals were sacrificed and target tissues (multiple muscles including muscle [gastrocnemius], blood [serum], and liver) were collected along for the following procedures.

Body Water Determination Mouse liver sections were distilled overnight upside down on a bead bath at 85°C to evaporate out body water. Deuterium present in the body water was exchanged onto acetone, and deuterium enrichment in the body water was measured via gas chromatography mass spectrometry (GC-MS), as previously described [17].

In-Solution Digestion of Muscle Tissue Around 20 mg of muscle tissue was weighed out and kept frozen on dry ice while mined into fine pieces. The sample was then added to a centrifuge tube along with 250 µL Homogenization Buffer (1x PBS containing 1mM PMSF, 5mM EDTA, 1x Protease Inhibitors). Samples were homogenized via bead beater until a homogeneous suspension was obtained. After sonication, sample supernatant was obtained by spinning down debris on a cooled (4°C) centrifuge at 10,000 g for 10 min. A small portion of each sample was diluted, and protein concentration was then determined by the Pierce BCA protein assay kit (Thermo Fisher #23225) with BSA as standards. Up to 100 µg of protein was taken and volume adjusted up to 100 µL in 50 mM Ammonium Bicarbonate (pH 8.1) with 25 µL 2,2,2-Trifluoroethanol (Sigma #T63002). 5 µL of Dithiothreitol (DTT) was added and samples were incubated at 60°C for 1 hour. Once samples were taken off and cooled to room temperature, Iodoacetamide (IAA) was added to make a final concentration of 20 mM, samples were vortexed briefly, and incubated at room temperature in the dark for 30 minutes. More DTT was added to make a final concentration of 4 mM to quench excess IAA and samples were diluted in 50 mM Ammonium Bicarbonate (pH 8.1) so that the final concentration of DTT was < 5%. Proteomics-Grade Trypsin was added at a ratio of 1:50 trypsin to protein (Sigma Aldrich, #T6567). Samples were incubated at 37°C overnight. The next day, formic acid was added at 5% of the final volume. Samples underwent Solid-Phase Extraction using Agilent C18 clean up columns (#A57203) to remove digested peptides from the digestion buffer. Peptides were eluted using 30% acetonitrile and speedvac'd until dry and re-suspended in 25 µL of 0.1 % formic acid/3% acetonitrile/96.9% LC-MS grade water and transferred to LC-MS vials to be analyzed via LC-MS.

In-Solution Digestion of Urinary Proteins Up to 200 µL of urine was taken for protein extraction, following immiscible phase (Methanol/Chloroform) extraction protocol that was

previously described [18]. Protein extracts were then dried and resuspended in 100 µL 8M Urea in 50 mM Ammonium Bicarbonate (pH 8.1) with agitation on vortexer at medium speed for 30 minutes at room temperature. A small portion of each sample was diluted to make Urea in buffer < 1M , and protein concentration was then determined by the Pierce BCA protein assay kit (Thermo Fisher #23225) with BSA as standards. Up to 100 µg of protein was taken from the sample and volume adjusted up to 100 µL in 8M Urea in 50 mM Ammonium Bicarbonate (pH 8.1). Tris-(2-carboxyethyl)-phosphine (TCEP) was added to make a final concentration of 10 mM and samples were agitated on a vortexer for 20 minutes at room temperature. Iodoacetamide (IAA) was added to make a final concentration of 20 mM, samples were vortexed briefly, and incubated at room temperature in the dark for 30 minutes. TCEP was added to make a final concentration of 4 mM to quench excess IAA and samples were diluted in 50 mM Ammonium Bicarbonate (pH 8.1) so that the final concentration of Urea was < 1M. Proteomics-Grade Trypsin was added at a ratio of 1:50 trypsin to protein (Sigma Aldrich, #T6567). Samples were incubated at 37°C overnight. The next day, formic acid was added at 5% of the final volume. Samples underwent Solid-Phase Extraction using Agilent C18 clean up columns (#A57203) to remove digested peptides from the digestion buffer. Peptides were eluted using 30% acetonitrile and speedvac'd until dry and re-suspended in 25 µL of 0.1 % formic acid/3% acetonitrile/96.9% LC-MS grade water and transferred to LC-MS vials to be analyzed via LC-MS.

Liquid chromatography-mass spectrometry (LC-MS) analysis Trypsin-digested peptides were analyzed on a 6550 quadropole time of flight (Q-ToF) mass spectrometer equipped with Chip Cube nano ESI source (Agilent Technologies). High-performance liquid chromatography (HPLC) separated the peptides using capillary and nano binary flow. Mobile phases were 95% acetonitrile/0.1% formic acid in LC-MS grade water. Peptides were eluted at 350 nl/minute flow rate with an 18-minute LC gradient. Each sample was analyzed once for protein/peptide identification in data-dependent MS/MS mode and once for peptide isotope analysis in MS mode. Acquired MS/MS spectra were extracted and searched using Spectrum Mill Proteomics Workbench software (Agilent Technologies) and a mouse protein database (www.uniprot.org). Search results were validated with a global false discovery rate of 1%. A filtered list of peptides was collapsed into a nonredundant peptide formula database containing peptide elemental composition, mass, and retention time. This was used to extract mass isotope abundances (M0 - M3) of each peptide from MS-only acquisition files with MassHunter Qualitative Analysis software (Agilent Technologies). Mass isotopomer distribution analysis (MIDA) was used to calculate peptide elemental composition and curve-fit parameters for predicting peptide isotope enrichment based on precursor body water enrichment (p) and the number (n) of amino acid C-H positions per peptide actively incorporating hydrogen (H) and deuterium (2H) from body water. Subsequent data handling was performed using python-based scripts, with input of precursor body water enrichment for each subject, to yield fractional synthesis rate (FSR) data at the protein level. FSR data were filtered to exclude protein measurements with fewer than 2 peptide isotope measurements per protein. Details of FSR calculations and data filtering criteria have been described in detail previously [19].

Calculation of fractional replacement (f) and replacement rate constant (k) for individual proteins Details of f calculations were previously described [19].

Statistical analysis Data filtering and calculations were performed according to previous reports [19]. Only those proteins that met analytic filtering criteria and that were present in at least 2

animals per group were included in comparisons and statistical analyses [20]. Individual proteins were also grouped into different functional clusters based on gene ontology origin using DAVID software from NIH website (https://david.ncifcrf.gov/tools.jsp) to determine which processes were affected at each stage [21]. The methods used to determine statistical significance of protein turnover comparisons are listed in the respective figure legend under their respective figures, * $p<0.05$, ** $p<0.01$, *** $p<0.005$, **** $p<0.001$. All statistical analysis was carried out by GraphPad Prism software (version 9.4).

References

1. Houang EM, Sham YY, Bates FS, Metzger JM. “Muscle membrane integrity in Duchenne muscular dystrophy: recent advances in copolymer-based muscle membrane stabilizers”. *Skeletal Muscle*, vol. 8, no. 31, December 2018.

2. Balch WE, Morimoto RI, Dillin A, Kelly JW. Adapting Proteostasis for Disease Intervention. *Science*. 2008;319(5865):916-919. doi:10.1126/science.1141448

3. Mah JK, Korngut L, Dykeman J, Day L, Pringsheim T, Jette N. A systematic review and meta-analysis on the epidemiology of Duchenne and Becker muscular dystrophy. *Neuromuscul Disord*. 2014;24(6):482-491. doi:10.1016/j.nmd.2014.03.008

4. Rennie, M.J., *et al.* Effects of Duchenne muscular dystrophy on muscle protein synthesis. *Nature* **296**, 165-167 (1982).

5. Takeda S, Clemens PR, Hoffman EP. Exon-Skipping in Duchenne Muscular Dystrophy. *J Neuromuscul Dis*. 8(Suppl 2):S343-S358. doi:10.3233/JND-210682

6. Matsuo M. Antisense Oligonucleotide-Mediated Exon-skipping Therapies: Precision Medicine Spreading from Duchenne Muscular Dystrophy. *JMA J*. 2021;4(3):232-240. doi:10.31662/jmaj.2021-0019

7. Blake DJ, Tinsley JM, Davies KE. Utrophin: A Structural and Functional Comparison to Dystrophin. *Brain Pathology*. 1996;6(1):37-47. doi:10.1111/j.1750-3639.1996.tb00781.x

8. Sicinski P, Geng Y, Ryder-Cook AS, Barnard EA, Darlison MG, Barnard PJ. The molecular basis of muscular dystrophy in the mdx mouse: a point mutation. *Science*. 1989;244(4912):1578-1580. doi:10.1126/science.2662404

9. Shankaran M, King CL, Angel TE, et al. Circulating protein synthesis rates reveal skeletal muscle proteome dynamics. *J Clin Invest*. 2016;126(1):288-302. doi:10.1172/JCI79639

10. Evans WJ, Shankaran M, Smith EC, Morris C, Nyangau E, Bizieff A, Matthews M, Mohamed H, Hellerstein M. Profoundly lower muscle mass and rate of contractile protein synthesis in boys with Duchenne muscular dystrophy. J Physiol. 2021 Dec;599(23):5215-5227. doi: 10.1113/JP282227. Epub 2021 Oct 11. PMID: 34569076.

11. Awano H, Matsumoto M, Nagai M, et al. Diagnostic and clinical significance of the titin fragment in urine of Duchenne muscular dystrophy patients. *Clinica Chimica Acta*. 2018;476:111-116. doi:10.1016/j.cca.2017.11.024

12. Robertson AS, Majchrzak MJ, Smith CM, et al. Dramatic elevation in urinary amino terminal titin fragment excretion quantified by immunoassay in Duchenne muscular dystrophy patients and in dystrophin deficient rodents. *Neuromuscul Disord*. 2017;27(7):635-645. doi:10.1016/j.nmd.2017.05.009

13. Ozawa E, Hagiwara Y, Yoshida M. Creatine kinase, cell membrane and Duchenne muscular dystrophy. *Molecular and Cellular Biochemistry.* 1999;190(1-2):143–151.

14. MacLennan PA, Edwards RH. Protein turnover is elevated in muscle of mdx mice in vivo. *Biochem J*. 1990;268(3):795-797.

15. Hathout Y, Marathi RL, Rayavarapu S, et al. Discovery of serum protein biomarkers in the mdx mouse model and cross-species comparison to Duchenne muscular dystrophy patients. *Hum Mol Genet*. 2014;23(24):6458-6469. doi:10.1093/hmg/ddu366

16. Kurien BT, Scofield RH. Mouse urine collection using clear plastic wrap. *Lab Anim*. 1999;33(1):83-86. doi:10.1258/002367799780578525

17. Yang D, Diraison F, Beylot M, et al. Assay of low deuterium enrichment of water by isotopic exchange with [U-13C3] acetone and gas chromatography-mass spectrometry. *Anal Biochem*. 1998;258(2):315-321. doi:10.1006/abio.1998.2632

18. Saito S, Hirao Y, Quadery AF, Xu B, Elguoshy A, Fujinaka H, Koma S, Yamamoto K, Yamamoto T. The Optimized Workflow for Sample Preparation in LC-MS/MS-Based Urine Proteomics. Methods Protoc. 2019 Jun 7;2(2):46. doi: 10.3390/mps2020046.

19. Holmes WE, Angel TE, Li KW, Hellerstein MK. Dynamic Proteomics: In Vivo Proteome-Wide Measurement of Protein Kinetics Using Metabolic Labeling. *Methods Enzymol*. 2015;561:219-276. doi:10.1016/bs.mie.2015.05.018

20. Thompson ACS, Bruss MD, Price JC, et al. Reduced in vivo hepatic proteome replacement rates but not cell proliferation rates predict maximum lifespan extension in mice. *Aging Cell*. 2016;15(1):118-127. doi:10.1111/acel.12414

21. Huang DW, Sherman BT, Lempicki RA. Systematic and integrative analysis of large gene lists using DAVID bioinformatics resources. *Nat Protoc*. 2009;4(1):44-57. doi:10.1038/nprot.2008.211

Figure and Table Legends

Figure 1 Study Design and Time Course of Labeling

Overview of $^{2}H_2O$ labeling time course and experimental procedures. All mice were sacrificed on Day 7 of labeling.

Figure 2 *mdx* Mouse Muscle Global Proteomics

Heatmap showing 54 proteins that are present in skeletal muscle of both *mdx* and control groups. Values are fractional replacement rate (f-Value) of label (^{2}H) into proteins.

Table 1 Statistical Comparisons of Skeletal Muscle Proteins

FSR values of all 54 proteins from skeletal muscle that are present in both groups with values that are significantly different are highlighted in green. Significance determined by Student's Unpaired T-Test with Benjamini-Hochberg correction for multiple comparisons. Green highlighted text $p<0.05$.

Figure 3 Changes in Protein Ontology-Group Turnover Rates

Protein Group analysis of proteins found in both groups and separated into ontologies based on NIH DAVID analysis. Ontologies include **A.)** Glycolysis **B.)** Mitochondria **C.)** Cytoplasm **D.)** Myofibril. Significance determined by both Binomial Test of the proportion of proteins showing a higher or lower value of FSR in relation to uninjected (control) and Student's Unpaired T-Test of protein group averages, * $p<0.05$, ** $p<0.01$, *** $p<0.005$, **** $p<0.001$.

Figure 4 Individual Protein Flux Rates in Skeletal Muscle and Urine for Potential Biomarkers

A.) Individual skeletal muscle-derived proteins of interest, based on previous literature, with their corresponding FSR values from skeletal muscle tissue in both *mdx* and control groups. **B.)** Individual skeletal muscle-derived proteins of interest, based on previous literature, with their corresponding FSR values from urine tissue in both *mdx* and control groups. Significance determined by Student's Unpaired T-Test of protein group averages, * $p<0.05$, ** $p<0.01$, *** $p<0.005$, **** $p<0.001$.

Figure 5 Correlation Between Muscle and Urinary Derived Proteins

A.) Correlation graph of Titin peptides between muscle and urine FSR values from both *mdx* and control groups. **B.)** Correlation graph of My-4 peptides between muscle and urine FSR values from both *mdx* and control groups. **C.)** Correlation graph of Titin peptides, from both *mdx* and control groups, comparing change in urine FSR to average change in all measured skeletal muscle proteins. **D.)** Correlation graph of My-4 peptides, from both *mdx* and control groups, comparing change in urine FSR to average change in all measured skeletal muscle proteins. For correlation graphs, significance was determined by simple linear regression equation with R^2 value shown.

Supplemental Tables

Table S1 Correlation Matrix of Muscle and Urinary My-4 to All Measured Muscle Proteins

Correlation matrix of change in My-4 FSR muscle (left column) and urine (right column) to control to change in proteins from different group ontologies. **A.)** Mitochondria, **B.)** Glycolysis, **C.)** Cytoplasm, **D.)** Myofibril.

Table S2 Correlation Matrix of Muscle and Urinary Titin to All Measured Muscle Proteins

Correlation matrix of change in titin FSR from muscle FSR muscle (left column) and urine (right column) to control to change in proteins from different group ontologies. **A.)** Mitochondria, **B.)** Glycolysis, **C.)** Cytoplasm, **D.)** Myofibril.

Figures and Tables

<u>Figure 1</u> Study Design and Time Course of Labeling

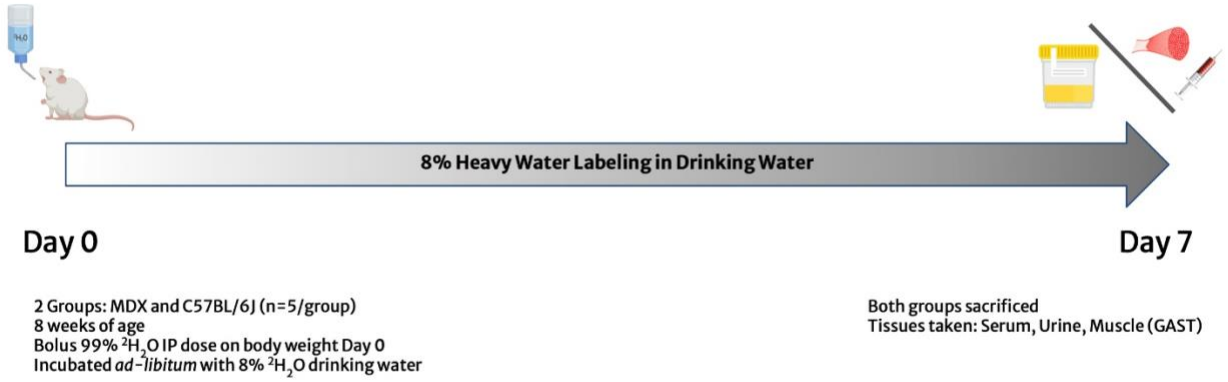

Figure 2 ***mdx*** **Mouse Muscle Global Proteomics**

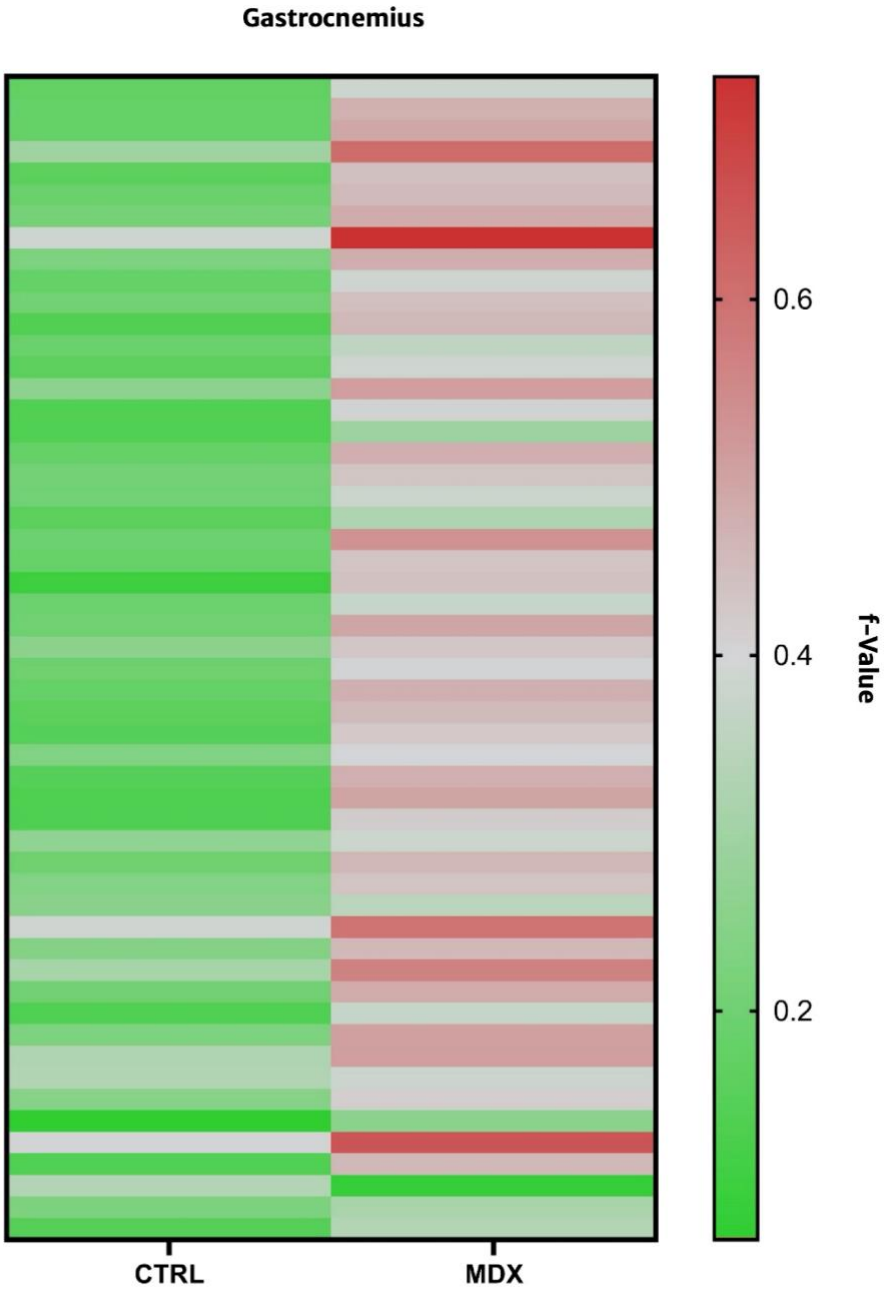

Table 1 Statistical Comparisons of Skeletal Muscle Proteins

Protein	Accession#	Mean Peptide Count	ttest	rank	adj p value
Sarcoplasmic/endoplasmic reticulum calcium ATPase 1	Q8R429	11.2	8.88432E-07	1	4.79753E-05
Fructose-bisphosphate aldolase A	P05064	40.0	2.34182E-06	2	6.3229E-05
Parvalbumin alpha	P32848	29.8	2.7747E-06	3	3.74585E-05
Glyceraldehyde-3-phosphate dehydrogenase	P16858	42.1	3.41755E-06	4	3.69095E-05
Myoglobin	P04247	14.5	3.65382E-06	5	3.28844E-05
Pyruvate kinase PKM	P52480	21.2	4.75004E-06	6	3.66431E-05
Aconitate hydratase, mitochondrial	Q99KI0	16.6	5.88253E-06	7	3.9707E-05
Nucleoside diphosphate kinase B	Q01768	4.4	6.46188E-06	8	3.87713E-05
Beta-enolase	P21550	42.4	8.7231E-06	9	4.28225E-05
Phosphoglycerate kinase 1	P09411	13.5	1.23391E-05	10	5.12548E-05
Creatine kinase M-type	P07310	87.7	1.2665E-05	11	0.000227971
Electron transfer flavoprotein subunit beta	Q9DCW4	2.4	1.68692E-05	12	6.50669E-05
Carbonic anhydrase 3	P16015	15.3	2.70768E-05	13	0.000121846
Troponin I, fast skeletal muscle	P13412	2.7	8.39016E-05	14	0.000302046
Myosin light chain 1/3, skeletal muscle isoform	P05977	11.1	8.77898E-05	15	0.000278862
Hemoglobin subunit alpha	P01942	8.0	9.82517E-05	16	0.000331599
Phosphoglycerate mutase 2	O70250	11.8	0.000101799	17	0.000305396
Phosphoglucomutase-1	Q9D0F9	6.8	0.00010324	18	0.000293419
Triosephosphate isomerase	P17751	7.5	0.000114846	19	0.000310083
Heat shock cognate 71 kDa protein	P63017	5.2	0.000165446	20	0.000425433
NPC intracellular cholesterol transporter 1	O35604	2.0	0.000191011	21	0.000468844
L-lactate dehydrogenase A chain	P06151	9.8	0.000225781	22	0.000530094
Tropomyosin beta chain	P58774	7.8	0.000328643	23	0.000739447
Glycogen phosphorylase, muscle form	Q9WUB3	21.3	0.000331356	24	0.000715729
Titin	A2ASS6	11.0	0.000448921	25	0.002424172
Peptidyl-prolyl cis-trans isomerase A	P17742	3.6	0.000706585	26	0.001467523
Glycogen phosphorylase, brain form	Q8CI94	4.1	0.00076354	27	0.001527081
Myosin-4	Q5SX39	12.8	0.000765046	28	0.001291015
Superoxide dismutase [Cu-Zn]	P08228	2.1	0.001372028	29	0.002646053
Creatine kinase U-type, mitochondrial	P30275	2.4	0.001681712	30	0.003131463
Malate dehydrogenase, mitochondrial	P08249	9.4	0.001807089	31	0.003252761
Troponin T, fast skeletal muscle	Q9QZ47	2.4	0.003107572	32	0.005413189
ATP synthase subunit beta, mitochondrial	P56480	6.1	0.008461032	33	0.013845326
Serum albumin	P07724	19.3	0.009291356	34	0.01475686
ATP-dependent 6-phosphofructokinase, muscle type	P47857	2.6	0.009365491	35	0.014449615
Adenylate kinase isoenzyme 1	Q9R0Y5	5.5	0.011666224	36	0.017499335
Creatine kinase S-type, mitochondrial	Q6P8J7	6.4	0.020599425	37	0.030064025

Myosin regulatory light chain 2, skeletal muscle isoform	P97457	4.3	0.021978955	38	0.031233252
Plasminogen activator inhibitor 1 RNA-binding protein	Q9CY58	2.1	0.022595738	39	0.031286407
Malate dehydrogenase, cytoplasmic	P14152	3.4	0.024875571	40	0.033582021
Alpha-enolase	P17182	4.9	0.02558962	41	0.033703402
Glucose-6-phosphate isomerase	P06745	5.1	0.028820049	42	0.037054348
Citrate synthase, mitochondrial	Q9CZU6	3.1	0.044021865	43	0.055283272
Tropomyosin alpha-1 chain	P58771	9.6	0.061825969	44	0.075877325
Superoxide dismutase [Mn], mitochondrial	P09671	2.3	0.075849194	45	0.091019033
3-ketoacyl-CoA thiolase, mitochondrial	Q8BWT1	2.1	0.098929476	46	0.116134602
Actin, cytoplasmic 1	P60710	3.1	0.108251724	47	0.124374321
Troponin C, skeletal muscle	P20801	2.3	0.129517392	48	0.145707066
Calmodulin-1	P0DP26	3.1	0.169597336	49	0.186903186
Aspartate aminotransferase, mitochondrial	P05202	3.7	0.185507935	50	0.200348569
Musculoskeletal embryonic nuclear protein 1	Q99JI1	2.0	0.368261516	51	0.389923958
ATP synthase subunit alpha, mitochondrial	Q03265	5.7	0.417603488	52	0.433665161
LIM domain-binding protein 3	Q9JKS4	4.4	0.482457627	53	0.491560601
Long-chain specific acyl-CoA dehydrogenase, mitochondrial	P51174	2.0	0.747617873	54	0.747617873

<u>Figure 3</u> Changes in Protein Ontology-Group Turnover Rates

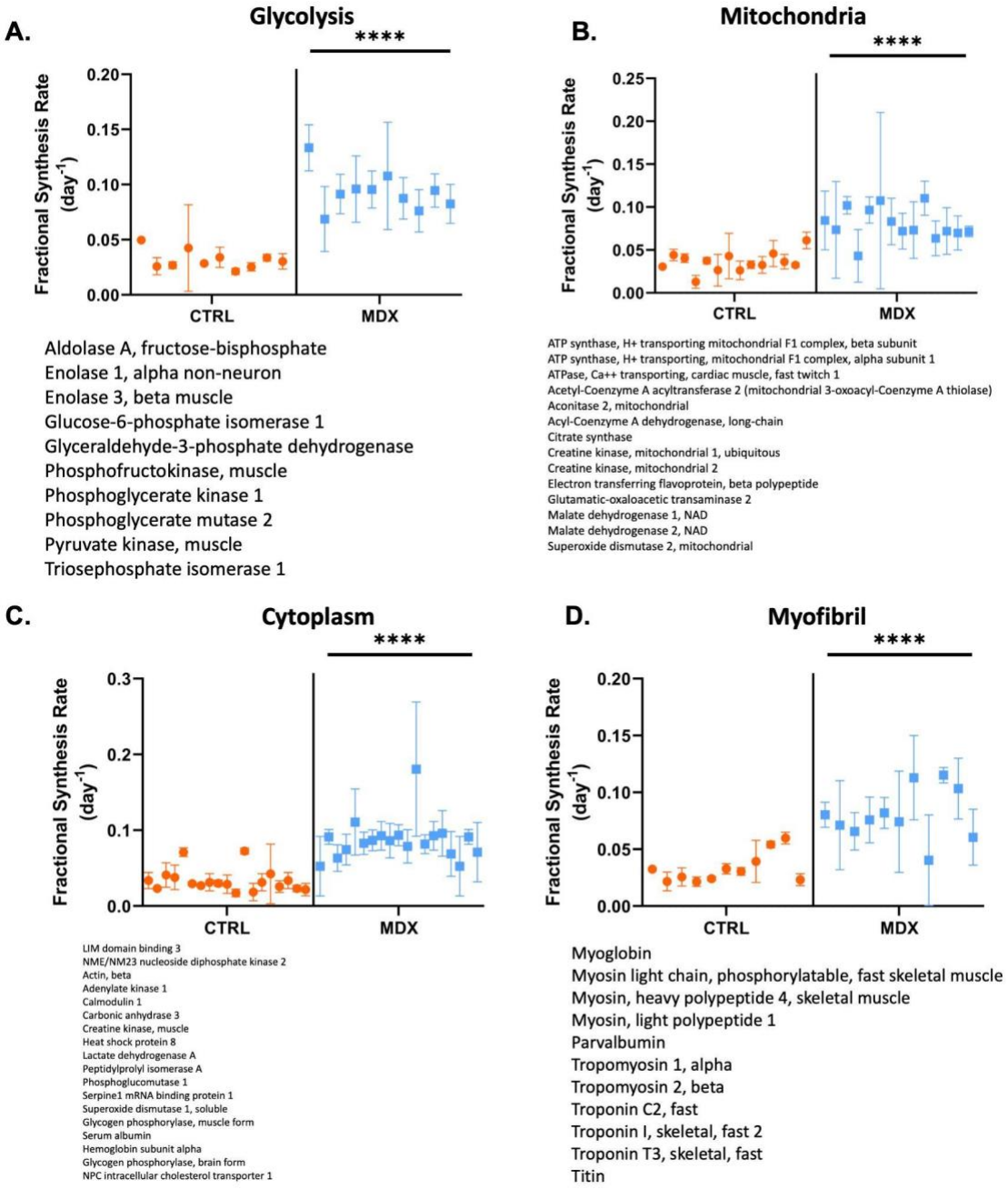

<u>Figure 4</u> Individual Protein Flux Rates in Skeletal Muscle and Urine for Potential Biomarkers

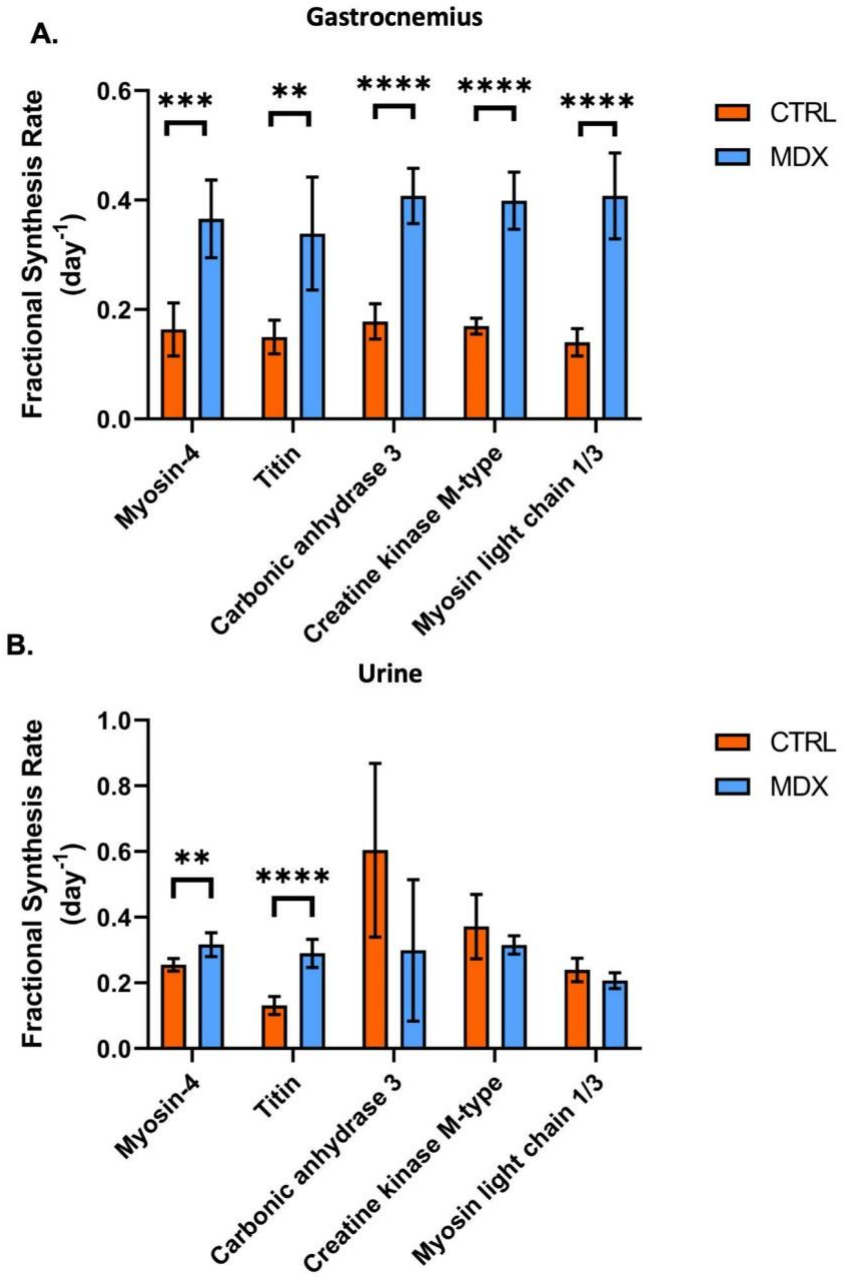

Figure 5 Correlation Between Muscle and Urinary Derived Proteins

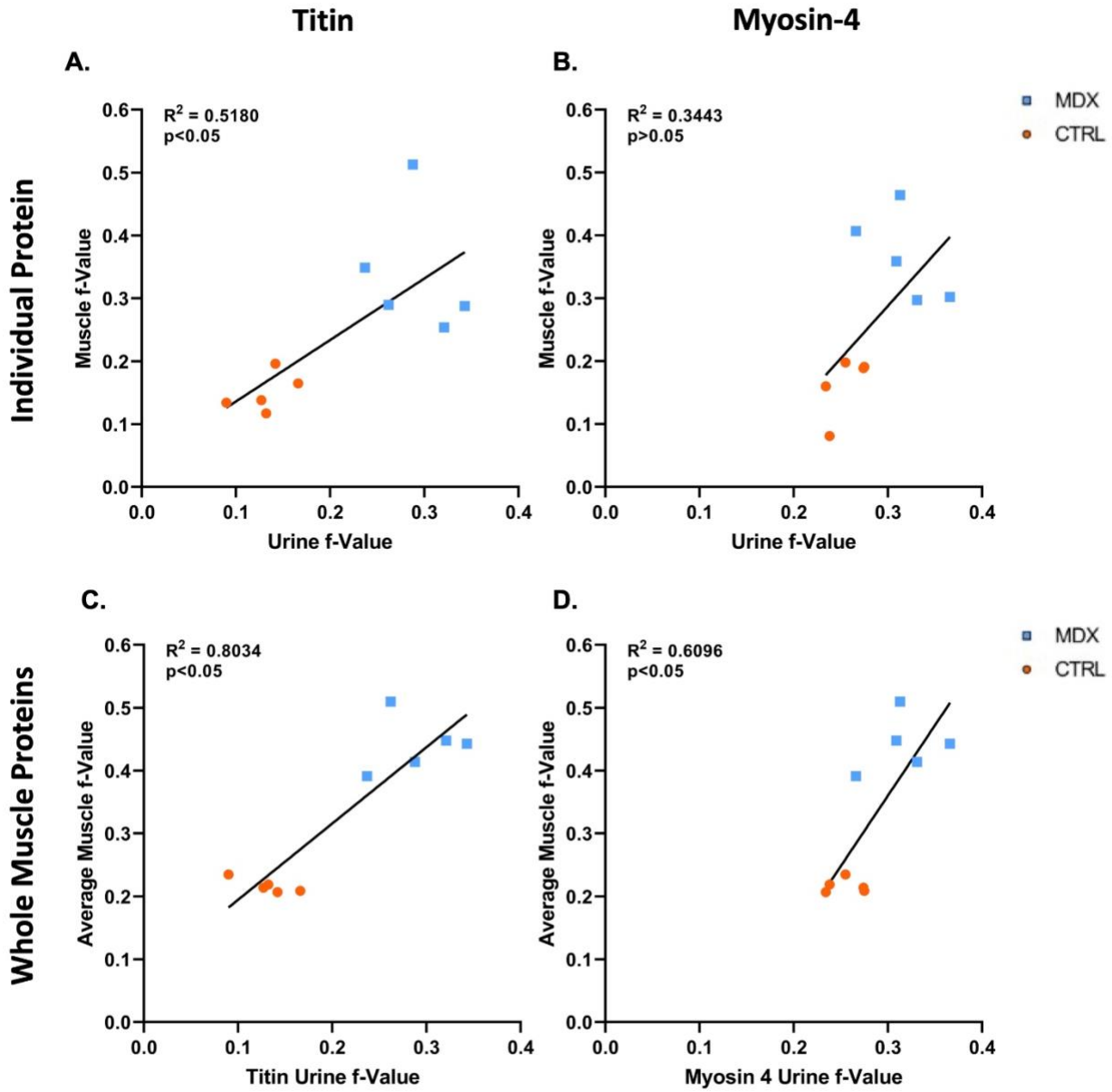

Table S1 Correlation Matrix of Muscle and Urinary My-4 to All Measured Muscle Proteins

A.

		R value	
Muscle Proteins (Gene) - Mitochondria	***Accession #***	***Myosin-4 (muscle)***	***Myosin-4 (urine)***
ATP synthase, H+ transporting mitochondrial F1 complex, beta subunit(Atp5b)	P56480	0.799444219	0.559235365
ATP synthase, H+ transporting, mitochondrial F1 complex, alpha subunit 1(Atp5a1)	Q03265	0.305231696	0.492696945
ATPase, Ca++ transporting, cardiac muscle, fast twitch 1(Atp2a1)	Q8R429	0.814176687	0.716988496
acetyl-Coenzyme A acyltransferase 2 (mitochondrial 3-oxoacyl-Coenzyme A thiolase)(Acaa2)	Q8BWT1	0.536202683	0.860591616
aconitase 2, mitochondrial(Aco2)	Q99KI0	0.94135552	0.722955582
acyl-Coenzyme A dehydrogenase, long-chain(Acadl)	P51174	-0.299642303	0.30456738
citrate synthase(Cs)	Q9CZU6	0.547206865	0.492480063
creatine kinase, mitochondrial 1, ubiquitous(Ckmt1)	P30275	0.877118905	0.65171565
creatine kinase, mitochondrial 2(Ckmt2)	Q6P8J7	0.716788449	0.678771788
electron transferring flavoprotein, beta polypeptide(Etfb)	Q9DCW4	0.948476371	0.774593301
glutamatic-oxaloacetic transaminase 2, mitochondrial(Got2)	P05202	0.516983997	0.775088729
malate dehydrogenase 1, NAD (soluble)(Mdh1)	P14152	0.578612421	0.672849918
malate dehydrogenase 2, NAD (mitochondrial)(Mdh2)	P08249	0.907243515	0.539346116
superoxide dismutase 2, mitochondrial(Sod2)	P09671	0.417009577	0.616062317

B.

		R value	
Muscle Proteins (Gene) - Glycolysis	***Accession #***	***Myosin-4 (muscle)***	***Myosin-4 (urine)***
aldolase A, fructose-bisphosphate(Aldoa)	P05064	0.875131853	0.810437864
enolase 1, alpha non-neuron(Eno1)	P17182	0.812764063	0.522503897
enolase 3, beta muscle(Eno3)	P21550	0.86673858	0.789777393
glucose-6-phosphate isomerase 1(Gpi1)	P06745	0.41732893	0.609560185
glyceraldehyde-3-phosphate dehydrogenase(Gapdh)	P16858	0.883659331	0.787901071
phosphofructokinase, muscle(Pfkm)	P47857	0.843638768	0.448830866
phosphoglycerate kinase 1(Pgk1)	P09411	0.809370098	0.816023464
phosphoglycerate mutase 2(Pgam2)	O70250	0.904773233	0.697894692
pyruvate kinase, muscle(Pkm)	P52480	0.90153719	0.827635838
triosephosphate isomerase 1(Tpi1)	P17751	0.885062826	0.748377625

C.

		R value	
Muscle Proteins (Gene) - Cytoplasm	***Accession #***	***Myosin-4 (muscle)***	***Myosin-4 (urine)***
LIM domain binding 3(Ldb3)	Q9JKS4	0.649863541	-0.209098568
NME/NM23 nucleoside diphosphate kinase 2(Nme2)	Q01768	0.885507353	0.864266293
actin, beta(Actb)	P60710	0.594502638	0.153664565
adenylate kinase 1(Ak1)	Q9R0Y5	0.76948025	0.511179138
calmodulin 1(Calm1)	P0DP26	0.225754208	0.402393777
carbonic anhydrase 3(Car3)	P16015	0.90194561	0.67395917
creatine kinase, muscle(Ckm)	P07310	0.80486123	0.854603765
heat shock protein 8(Hspa8)	P63017	0.66495075	0.811586434
lactate dehydrogenase A(Ldha)	P06151	0.664104177	0.854603723
peptidylprolyl isomerase A(Ppia)	P17742	0.923364599	0.699777551
phosphoglucomutase 1(Pgm1)	Q9D0F9	0.816933903	0.795102893
ribosomal protein SA(Rpsa)	P14206	-0.837093426	-0.887610082
serpine1 mRNA binding protein 1(Serbp1)	Q9CY58	0.860382261	0.785665234
superoxide dismutase 1, soluble(Sod1)	P08228	0.909366856	0.635286881
Glycogen phosphorylase, muscle form	Q9WUB3	0.728650987	0.865770183
Serum albumin	P07724	0.869547932	0.572565258
Hemoglobin subunit alpha	P01942	0.677098342	0.843702194
Glycogen phosphorylase, brain form	Q8CI94	0.887562944	0.668033013
NPC intracellular cholesterol transporter 1	O35604	0.894739939	0.770272575

D.

		R value	
Muscle Proteins (Gene) - Myofibril	***Accession #***	***Myosin-4 (muscle)***	***Myosin-4 (urine)***
myoglobin(Mb)	P04247	0.8755708	0.790669691
myosin light chain, phosphorylatable, fast skeletal muscle(Mylpf)	P97457	0.871121374	0.309308046
myosin, light polypeptide 1(Myl1)	P05977	0.91729196	0.770326224
parvalbumin(Pvalb)	P32848	0.815935543	0.871025965
tropomyosin 1, alpha(Tpm1)	P58771	0.828258759	0.22504349
tropomyosin 2, beta(Tpm2)	P58774	0.855064725	0.818395108
troponin C2, fast(Tnnc2)	P20801	0.547369577	0.750838378
troponin I, skeletal, fast 2(Tnni2)	P13412	0.960729575	0.729171475
troponin T3, skeletal, fast(Tnnt3)	Q9QZ47	0.647342828	0.775613536
Titin	A2ASS6	0.636705724	0.621967358
myosin, heavy polypeptide 4, skeletal muscle (muscle)	Q5SX39	1	0.588532369
Myosin-4 (urine)	Q5SX39	0.588532369	1

Table S2 Correlation Matrix of Muscle and Urinary Titin to All Measured Muscle Proteins

A.

		R value	
Muscle Proteins (Gene) - Mitochondria	***Accession #***	***Titin (muscle)***	***Titin (urine)***
ATP synthase, H+ transporting mitochondrial F1 complex, beta subunit(Atp5b)	P56480	0.292394755	0.744393442
ATP synthase, H+ transporting, mitochondrial F1 complex, alpha subunit 1(Atp5a1)	Q03265	0.037083412	0.4286218
ATPase, Ca++ transporting, cardiac muscle, fast twitch 1(Atp2a1)	Q8R429	0.853003145	0.890465902
acetyl-Coenzyme A acyltransferase 2 (mitochondrial 3-oxoacyl-Coenzyme A thiolase)(Acaa2)	Q8BWT1	0.926174288	0.690977501
aconitase 2, mitochondrial(Aco2)	Q99KI0	0.729817074	0.876094109
acyl-Coenzyme A dehydrogenase, long-chain(Acadl)	P51174	0.157599742	0.244679063
citrate synthase(Cs)	Q9CZU6	0.639754383	0.595115592
creatine kinase, mitochondrial 1, ubiquitous(Ckmt1)	P30275	0.485844835	0.811901506
creatine kinase, mitochondrial 2(Ckmt2)	Q6P8J7	0.346718223	0.741099739
electron transferring flavoprotein, beta polypeptide(Etfb)	Q9DCW4	0.720331428	0.857776816
glutamatic-oxaloacetic transaminase 2, mitochondrial(Got2)	P05202	0.396821625	0.432631838
malate dehydrogenase 1, NAD (soluble)(Mdh1)	P14152	0.54411473	0.699873373
malate dehydrogenase 2, NAD (mitochondrial)(Mdh2)	P08249	0.457323214	0.769942809
superoxide dismutase 2, mitochondrial(Sod2)	P09671	0.271515526	0.628956371

B.

		R value	
Muscle Proteins (Gene) - Glycolysis	***Acession #***	***Titin (muscle)***	***Titin (urine)***
aldolase A, fructose-bisphosphate(Aldoa)	P05064	0.723295943	0.926887638
enolase 1, alpha non-neuron(Eno1)	P17182	0.242265383	0.669136289
enolase 3, beta muscle(Eno3)	P21550	0.754421742	0.891652479
glucose-6-phosphate isomerase 1(Gpi1)	P06745	0.420173544	0.677210351
glyceraldehyde-3-phosphate dehydrogenase(Gapdh)	P16858	0.765656775	0.902844319
phosphofructokinase, muscle(Pfkm)	P47857	0.566445272	0.71761887
phosphoglycerate kinase 1(Pgk1)	P09411	0.848691895	0.909647016
phosphoglycerate mutase 2(Pgam2)	O70250	0.677367413	0.824556736
pyruvate kinase, muscle(Pkm)	P52480	0.714536152	0.913221317
triosephosphate isomerase 1(Tpi1)	P17751	0.687279943	0.854303963

C.

		R value	
Muscle Proteins (Gene) - Cytoplasm	***Acession #***	***Titin (muscle)***	***Titin (urine)***
LIM domain binding 3(Ldb3)	Q9JKS4	0.020975651	0.046677411
NME/NM23 nucleoside diphosphate kinase 2(Nme2)	Q01768	0.761135169	0.963650628
actin, beta(Actb)	P60710	0.406610632	0.417187229
adenylate kinase 1(Ak1)	Q9R0Y5	0.726116988	0.582043559
calmodulin 1(Calm1)	P0DP26	0.665441391	0.551629919
carbonic anhydrase 3(Car3)	P16015	0.735424104	0.885796939
creatine kinase, muscle(Ckm)	P07310	0.745504147	0.945636435
heat shock protein 8(Hspa8)	P63017	0.73893163	0.919939594
lactate dehydrogenase A(Ldha)	P06151	0.73753988	0.968361971
peptidylprolyl isomerase A(Ppia)	P17742	0.835412247	0.785205424
phosphoglucomutase 1(Pgm1)	Q9D0F9	0.683441935	0.91139306
ribosomal protein SA(Rpsa)	P14206	-0.996552088	-0.94545105
serpine1 mRNA binding protein 1(Serbp1)	Q9CY58	0.594888454	0.757274593
superoxide dismutase 1, soluble(Sod1)	P08228	0.813939817	0.837361023
Glycogen phosphorylase, muscle form	Q9WUB3	0.819970821	0.879017579
Serum albumin	P07724	0.465778851	0.59889899
Hemoglobin subunit alpha	P01942	0.772233626	0.915873534
Glycogen phosphorylase, brain form	Q8CI94	0.736849696	0.803273657
NPC intracellular cholesterol transporter 1	O35604	0.8621602	0.858897829

D.

		R value	
Muscle Proteins (Gene) - Myofibril	***Accession #***	***Titin (muscle)***	***Titin (urine)***
myoglobin(Mb)	P04247	0.671631425	0.935698313
myosin light chain, phosphorylatable, fast skeletal muscle(Mylpf)	P97457	0.32341878	0.559377408
myosin, heavy polypeptide 4, skeletal muscle(Myh4)	Q5SX39	0.636705724	0.723181666
myosin, light polypeptide 1(Myl1)	P05977	0.763212368	0.823256709
parvalbumin(Pvalb)	P32848	0.786166802	0.955803667
tropomyosin 1, alpha(Tpm1)	P58771	0.22875408	0.456418554
tropomyosin 2, beta(Tpm2)	P58774	0.827996031	0.875961813
troponin C2, fast(Tnnc2)	P20801	0.670168514	0.776820647
troponin I, skeletal, fast 2(Tnni2)	P13412	0.890094973	0.917661173
troponin T3, skeletal, fast(Tnnt3)	Q9QZ47	0.480648109	0.892702437
Titin (muscle)	A2ASS6	0.717881079	1
Titin (urine)	A2ASS6	1	0.717881079

Section 2

Satellite Cells Influence on Skeletal Muscle Regeneration and Whole Tissue Protein Dynamics

Review of the Existing Literature

Overview of Muscle Regeneration

Muscle tissue comprises about 30 - 40% of total body mass in healthy humans and provides many important functions including structural support, execution of movement, involuntary process (breathing, digestion, heart rate, etc.) and substrate metabolism [1]. Most of this tissue is composed of mature myocytes that are differentiated and not currently entered into the cell cycle. This is due to muscle being a low proliferative tissue type that has lower rates of cellular turnover in comparison to other tissue types. However, a small portion of the cells that make up muscle are quiescent muscle satellite cells (MuSCs) that give this tissue the ability to exert a regenerative capacity in response to damage or injury [2]. Muscle regeneration is a dynamic process that requires the synchronized effort of multiple inputs to assist in taking the muscle from initial damage to complete repair and reintegration into existing tissue. This process can be divided into 5 unique stages that occur sequentially to take muscle from initial injury to full recovery and reintegration back into existing tissue [3]. These stages are time-dependent and interrelated, requiring a smooth transition from one stage to the next. The temporal regulation of this process depends on the type of tissue damage, the severity of injury, and characteristics of the host, like age or disease status. However, all forms of muscle regeneration will undergo these outlined stages to some degree.

The individual stages and their defining characteristics are as follows:

- **Initial Tissue Damage + Necrosis** There are multiple different categories of muscle damage that can occur depending on the type of stress the tissue is placed under [4]. However, the most common type of muscle damage that is seen in pathological disease is necrosis [5]. Necrotic damage is a non-regulated cell death pathway that is an uncontrolled breakdown of cellular structures and release of components. It involves the influx of extracellular components, like calcium, from tears in the sarcolemma, disruption of cellular organelles and their processes, and accumulation of debris in and around the cell [4]. Therefore, necrotic damage is much more dangerous to the health of surrounding tissue and more taxing on the body to repair. Necrotic tissue appears pale and has altered internal cellular architecture that leads to abnormal and truncated cell shape when visualized under histology. A faithful *in-vivo* marker of necrotic damage is the absorption of Evans Blue Dye, a dye administered via circulation that can enter through the damaged sarcolemma and appear on the inside of necrotic muscle fibers when visualized. As mentioned, this type of damage is what is primarily seen in pathologic diseases, such as Duchenne's muscular dystrophy (DMD), and persistent necrotic damage can lead to detrimental long-term tissue damage including fibrotic deposition and muscle atrophy [6].

Therefore, warranting further exploration of the cellular and molecular mechanisms that are involved in regenerating muscle from necrotic damage.

- **Inflammatory Response** Necrotic damage can elicit a wide range of host inflammatory responses to initiate the regeneration process from MuSCs. The inflammatory response to injured muscle plays a major role in maintaining properly functioning skeletal muscle. This involves the recruitment of specific myeloid cell populations within the injured area [7-11]. Neutrophils are generally the first myeloid cell type to invade the site of injury and are present almost immediately after initial necrotic tissue damage. They release high concentrations of free radicals and proteases to degrade damaged tissue, as well as other pro-inflammatory cytokines that attract other inflammatory cell populations, like monocytes and macrophages [10]. The number of neutrophils in the tissue usually drops after 24 hours, and they are no longer detectable in damaged tissue by 48 hours [12, 13]. This allows for other myeloid cell types to enter and mediate the inflammatory response. Macrophages that are attracted to the damaged tissue by neutrophils will rapidly increase within 24 hours after injury and are the predominant inflammatory cell type within the injured area at that time. There are two types of macrophages: the proinflammatory M1 species and the anti-inflammatory M2 species [14, 15]. The initial responding macrophages that enter the damaged tissue are the pro-inflammatory M1 type that are mainly responsible for removing tissue debris and activating MuSCs [16-22]. After a while, these proinflammatory M1 macrophages will change to the anti-inflammatory M2 type in the muscle to promote growth and regeneration of the tissue [23]. There are many proposed mechanisms as to how these macrophages can switch their function [23-31], however, it is a necessary process to occur to mediate proper skeletal muscle regeneration, and the lack of this switch can lead to improper regenerative events in the tissue [25, 32, 33]. Therefore, the initial inflammatory response to tissue damage is a well-regulated process that requires proper localization, cell population identity, and temporal coordination to occur. Disruption to one or multiple of these factors can result in a persistent and non-resolved inflammatory stage [34].

- **Regeneration (Proliferation of MuSCs)** Muscle exerts its regenerative capacity as a tissue through the stem cells that lay peripheral to the myofiber, in between the basal lamina and the sarcolemma, which is how they are known as “satellite cells” (MuSCs). These MuSCs maintain a state of mitotic quiescence until they are activated to enter the cell cycle and proliferate [35]. MuSCs can become activated in response to physiological stimuli, such as exercise, or pathological stimuli, such as necrotic damage, to produce a set of myoblasts that can either integrate into existing myofibers, repair damaged muscle fibers, or fuse to each other to form new myofibers [36]. There is also a small population that reverts to mitotic quiescence to maintain the MuSC pool for future regeneration events [37]. Until recently, MuSCs were thought to only occupy two functional stages of quiescence or active proliferation in the cell cycle. However, work done by Rodgers et al. demonstrates that MuSCs can occupy a third stage, known as the $G_{\text{“Alert”}}$ phase, that exists between the two [38]. The $G_{\text{“Alert”}}$ phase is designed to prepare MuSCs for a regenerative event and is mediated by circulating factors that are released from distant tissue injury of another muscle group [39, 40]. MuSCs in the $G_{\text{“Alert”}}$ phase demonstrate a different functional characteristic than quiescent tissue, which is validated by altered

transcriptional profiles [38]. The work laid out in this dissertation, in part, seeks to expand the understanding of the G"Alert" phase in MuSCs by exploring the changes in genome and proteome of whole muscle tissue that is distant to an acute injury model. Overall, once MuSCs become activated and proliferate, their fate is determined to be one of two paths depending upon the expression of MyoD. MuSCs may downregulate MyoD expression and revert to quiescence to maintain the MuSC pool for future regeneration events. Alternatively, MuSCs can maintain MyoD expression but downregulate Pax7, a marker of MuSC activity, and activate myogenin expression to commit to differentiation into myoblasts [41-44]. The latter is the route for the majority of activated MuSCs to help regenerate damaged muscle tissue.

- **Remodeling (Differentiation to myocytes)** For MuSCs to transition from a proliferative state in the cell cycle to differentiate towards myoblasts, there must be a downregulation of proliferative-associated genes as well as a withdrawal from the cell-cycle [45-47]. Three key genes that are involved in this process are Notch, Numb, and Wnt. Numb has been known to inhibit Notch signaling in actively proliferating MuSCs, thus promoting myogenic differentiation [48-53]. Differentiation occurs due to a transition from Notch signaling to Wnt signaling in the MuSC. Crosstalk via GSK3beta, which is maintained in an active form by Notch but is inhibited by Wnt, has been found to be the main driver of this transition in progenitor cells [54, 55]. Recent work has found that Notch can also promote homeostasis of the quiescent MuSC pool by preventing entry into the cell cycle upon activating signals [51, 52]. This divergent behavior of Notch to promote or to block the cell cycle progression is most likely dependent upon cellular context and other pathways that may interact with it. There are many cellular markers that are uniquely expressed by the MuSC at this time, with the most known and well-studied being an embryonic form of myosin heavy chain (EmyHC). Traditionally only expressed during embryogenesis, EmyHC is also expressed transiently during the switch from MuSC proliferation to the differentiation towards myocytes. Therefore, it is commonly used as a visual marker of this transitional stage to confirm MuSC exit from proliferation towards a myogenic lineage [56]. Overall, during this stage of the regeneration process, the MuSC undergoes alterations in signaling from both external and internal cues to exit the cell cycle and promote differentiation towards forming a new myoblast that can reintegrate with undamaged tissue.

- **Maturation of Novel Myofibers into Existing Tissue** The final stage that occurs in a complete regeneration event is the remodeling of surrounding structures to accommodate newly differentiated muscle tissue from MuSCs. This stage is defined by angiogenesis and production of several types of extracellular matrix (ECM) proteins, like collagens, fibronectin, elastin, proteoglycans, and laminin [57-60]. These structures are designed to provide nutrient-rich blood flow, act as scaffolding to stabilize the newly formed tissue, and guide the formation of neuromuscular junctions (NMJs) for reinnervation [61]. Interestingly, the fibrotic response at this stage is overall beneficial because it adds quick support for tissue strength and helps protect the injury site. However, the overproduction or dysregulation of fibrotic production can lead to pathogenic scar formation and loss of muscle function. Therefore, it must be tightly regulated and temporally controlled to produce the correct effects for this process. The regeneration event is considered

complete when the damaged tissue can rescue its contractile ability and functional performance as it was before the injury. Therefore, the effectiveness of this process is in part limited by the ability of the new tissue to become innervated. At around two weeks after initial damage, new NMJs can be spotted on the muscle tissue, effectively marking the end of the final stage of this process. Nerve signaling will help the nascent muscle tissue further develop by promoting growth in size and contractile ability. Together, this process marks the end of a regenerative event that takes muscle from initial damage to complete integration to existing tissue. The novel myofibers will continue to grow and mature after this stage, however, that is part of a normal myofibers characteristics and therefore not considered part of its regeneration from damage.

"Priming" G$_{\text{"Alert"}}$ phase

The regeneration potential of old or damaged tissue is robust in lower vertebrates, but is gradually lost in higher vertebrates, such as mammals [62-66]. Humans still exert the capacity to regenerate tissues, but not to the extent that other species can [67, 68]. However, this does not mean that humans do not possess a sophisticated regeneration capacity that can recapitulate many of the same processes that are seen in embryogenesis. As previously mentioned, the MuSCs in non-injured muscles demonstrate altered characteristics due to injury in a distant tissue [38]. While studies have been done to discover the cause of this biological phenomenon, the results are still inconclusive [39, 40]. It is hypothesized that some circulating factors that are released from the injured tissue will be sensed by other undamaged tissues and "prime" the MuSC in them for a subsequent regenerative event. This "primed" state is referring to the functional state that MuSCs will enter that exists between quiescence and the cell cycle, known as the "G$_{\text{Alert}}$" phase. In this state, tissue has a higher capacity to regenerate from MuSCs since they are already "primed" and readily enter the cell cycle quicker. These altered dynamics to cell cycle entry prove great therapeutic potential for recovery from musculoskeletal injuries such as traumatic damage or surgery. Generally, proper tissue recovery from injury is mediated in part by the speed and overall ability for stem cells to enter the cell-cycle [40]. Disruption of this process can lead to improper regeneration of damaged tissue and the pathological manifestation of prolonged injury. Therefore, promoting MuSC entry into the cell cycle and differentiating to new myofibers is another therapeutic avenue to target the root cause of many muscle wasting disorders, such as dystrophy or sarcopenia [69-72].

References

1. Frontera WR, Ochala J. Skeletal muscle: a brief review of structure and function. *Calcif Tissue Int*. 2015;96(3):183-195. doi:10.1007/s00223-014-9915-y

2. Mauro A. Satellite cell of skeletal muscle fibers. *J Biophys Biochem Cytol*. 1961;9(2):493-495. doi:10.1083/jcb.9.2.493

3. Musarò A. The Basis of Muscle Regeneration. *Advances in Biology*. 2014;2014:e612471. doi:10.1155/2014/612471

4. D'Arcy MS. Cell death: a review of the major forms of apoptosis, necrosis and autophagy. *Cell Biology International*. 2019;43(6):582-592. doi:10.1002/cbin.11137

5. Elmore S. Apoptosis: A Review of Programmed Cell Death. *Toxicol Pathol*. 2007;35(4):495-516. doi:10.1080/01926230701320337

6. Mah JK, Korngut L, Dykeman J, Day L, Pringsheim T, Jette N. A systematic review and meta-analysis on the epidemiology of Duchenne and Becker muscular dystrophy. *Neuromuscul Disord*. 2014;24(6):482-491. doi:10.1016/j.nmd.2014.03.008

7. Grounds MD. Phagocytosis of necrotic muscle in muscle isografts is influenced by the strain, age, and sex of host mice. *J Pathol*. 1987;153(1):71-82. doi:10.1002/path.1711530110

8. Tidball JG, Wehling-Henricks M. Macrophages promote muscle membrane repair and muscle fibre growth and regeneration during modified muscle loading in mice in vivo. *J Physiol*. 2007;578(Pt 1):327-336. doi:10.1113/jphysiol.2006.118265

9. Summan M, Warren GL, Mercer RR, et al. Macrophages and skeletal muscle regeneration: a clodronate-containing liposome depletion study. *Am J Physiol Regul Integr Comp Physiol*. 2006;290(6):R1488-1495. doi:10.1152/ajpregu.00465.2005

10. Tidball JG. Inflammatory processes in muscle injury and repair. *Am J Physiol Regul Integr Comp Physiol*. 2005;288(2):R345-353. doi:10.1152/ajpregu.00454.2004

11. Teixeira CFP, Zamunér SR, Zuliani JP, et al. Neutrophils do not contribute to local tissue damage, but play a key role in skeletal muscle regeneration, in mice injected with Bothrops asper snake venom. *Muscle Nerve*. 2003;28(4):449-459. doi:10.1002/mus.10453

12. Fielding RA, Manfredi TJ, Ding W, Fiatarone MA, Evans WJ, Cannon JG. Acute phase response in exercise. III. Neutrophil and IL-1 beta accumulation in skeletal muscle. *Am J Physiol*. 1993;265(1 Pt 2):R166-172. doi:10.1152/ajpregu.1993.265.1.R166

13. Belcastro AN, Arthur GD, Albisser TA, Raj DA. Heart, liver, and skeletal muscle myeloperoxidase activity during exercise. *J Appl Physiol (1985)*. 1996;80(4):1331-1335. doi:10.1152/jappl.1996.80.4.1331

14. Geissmann F, Jung S, Littman DR. Blood monocytes consist of two principal subsets with distinct migratory properties. *Immunity*. 2003;19(1):71-82. doi:10.1016/s1074-7613(03)00174-2

15. Geissmann F, Auffray C, Palframan R, et al. Blood monocytes: distinct subsets, how they relate to dendritic cells, and their possible roles in the regulation of T-cell responses. *Immunol Cell Biol*. 2008;86(5):398-408. doi:10.1038/icb.2008.19

16. St Pierre BA, Tidball JG. Differential response of macrophage subpopulations to soleus muscle reloading after rat hindlimb suspension. *J Appl Physiol (1985)*. 1994;77(1):290-297. doi:10.1152/jappl.1994.77.1.290

17. Arnold L, Henry A, Poron F, et al. Inflammatory monocytes recruited after skeletal muscle injury switch into antiinflammatory macrophages to support myogenesis. *J Exp Med*. 2007;204(5):1057-1069. doi:10.1084/jem.20070075

18. Saclier M, Cuvellier S, Magnan M, Mounier R, Chazaud B. Monocyte/macrophage interactions with myogenic precursor cells during skeletal muscle regeneration. *FEBS J*. 2013;280(17):4118-4130. doi:10.1111/febs.12166

19. McLennan IS. Resident macrophages (ED2- and ED3-positive) do not phagocytose degenerating rat skeletal muscle fibres. *Cell Tissue Res*. 1993;272(1):193-196. doi:10.1007/BF00323586

20. Honda H, Kimura H, Rostami A. Demonstration and phenotypic characterization of resident macrophages in rat skeletal muscle. *Immunology*. 1990;70(2):272-277.

21. Pimorady-Esfahani A, Grounds MD, McMenamin PG. Macrophages and dendritic cells in normal and regenerating murine skeletal muscle. *Muscle Nerve*. 1997;20(2):158-166. doi:10.1002/(sici)1097-4598(199702)20:2<158::aid-mus4>3.0.co;2-b

22. Du H, Shih CH, Wosczyna MN, et al. Macrophage-released ADAMTS1 promotes muscle stem cell activation. *Nat Commun*. 2017;8(1):1-11. doi:10.1038/s41467-017-00522-7

23. Deng B, Wehling-Henricks M, Villalta SA, Wang Y, Tidball JG. IL-10 triggers changes in macrophage phenotype that promote muscle growth and regeneration. *J Immunol*. 2012;189(7):3669-3680. doi:10.4049/jimmunol.1103180

24. Lawrence T, Natoli G. Transcriptional regulation of macrophage polarization: enabling diversity with identity. *Nat Rev Immunol*. 2011;11(11):750-761. doi:10.1038/nri3088

25. Mounier R, Théret M, Arnold L, et al. AMPKα1 regulates macrophage skewing at the time of resolution of inflammation during skeletal muscle regeneration. *Cell Metab*. 2013;18(2):251-264. doi:10.1016/j.cmet.2013.06.017

26. Sag D, Carling D, Stout RD, Suttles J. Adenosine 5'-monophosphate-activated protein kinase promotes macrophage polarization to an anti-inflammatory functional phenotype. *J Immunol*. 2008;181(12):8633-8641. doi:10.4049/jimmunol.181.12.8633

27. Krishnan V, Yaden BC. Macrofinancing efficient remodeling of damaged muscle tissue. *Cell Metab*. 2013;18(2):149-151. doi:10.1016/j.cmet.2013.07.011

28. Bordon Y. Macrophages: metabolic master prompts a change of tack. *Nat Rev Immunol*. 2013;13(10):706. doi:10.1038/nri3542

29. Takeuch O, Akira S. Epigenetic control of macrophage polarization. *European Journal of Immunology*. 2011;41(9):2490-2493. doi:10.1002/eji.201141792

30. Banerjee S, Cui H, Xie N, et al. miR-125a-5p Regulates Differential Activation of Macrophages and Inflammation. *J Biol Chem*. 2013;288(49):35428-35436. doi:10.1074/jbc.M112.426866

31. Banerjee S, Xie N, Cui H, et al. MicroRNA let-7c regulates macrophage polarization. *J Immunol*. 2013;190(12):6542-6549. doi:10.4049/jimmunol.1202496

32. Tidball JG, Villalta SA. Regulatory interactions between muscle and the immune system during muscle regeneration. *Am J Physiol Regul Integr Comp Physiol*. 2010;298(5):R1173-1187. doi:10.1152/ajpregu.00735.2009

33. Villalta SA, Nguyen HX, Deng B, Gotoh T, Tidball JG. Shifts in macrophage phenotypes and macrophage competition for arginine metabolism affect the severity of muscle pathology in muscular dystrophy. *Hum Mol Genet*. 2009;18(3):482-496. doi:10.1093/hmg/ddn376

34. Douglas MR, Morrison KE, Salmon M, Buckley CD. Why does inflammation persist: a dominant role for the stromal microenvironment? *Expert Rev Mol Med*. 2002;4(25):1-18. doi:10.1017/S1462399402005264

35. Forcina L, Miano C, Pelosi L, Musarò A. An Overview About the Biology of Skeletal Muscle Satellite Cells. *Current Genomics*. 20(1):24-37.

36. Gayraud-Morel B, Chrétien F, Tajbakhsh S. Skeletal muscle as a paradigm for regenerative biology and medicine. *Regen Med*. 2009;4(2):293-319. doi:10.2217/17460751.4.2.293

37. Zammit PS, Golding JP, Nagata Y, Hudon V, Partridge TA, Beauchamp JR. Muscle satellite cells adopt divergent fates: a mechanism for self-renewal? *J Cell Biol*. 2004;166(3):347-357. doi:10.1083/jcb.200312007

38. Rodgers JT, King KY, Brett JO, et al. mTORC1 controls the adaptive transition of quiescent stem cells from G0 to GAlert. *Nature*. 2014;510(7505):393-396. doi:10.1038/nature13255

39. Rodgers JT, Schroeder MD, Ma C, Rando TA. HGFA Is an Injury-Regulated Systemic Factor that Induces the Transition of Stem Cells into GAlert. *Cell Reports*. 2017;19(3):479-486. doi:10.1016/j.celrep.2017.03.066

40. Lee G, Espirito Santo AI, Zwingenberger S, et al. Fully reduced HMGB1 accelerates the regeneration of multiple tissues by transitioning stem cells to GAlert. *Proceedings of the National Academy of Sciences*. 2018;115(19):E4463-E4472. doi:10.1073/pnas.1802893115

41. Boldrin L, Muntoni F, Morgan JE. Are Human and Mouse Satellite Cells Really the Same? *J Histochem Cytochem*. 2010;58(11):941-955. doi:10.1369/jhc.2010.956201
42. Day K, Shefer G, Richardson JB, Enikolopov G, Yablonka-Reuveni Z. Nestin-GFP reporter expression defines the quiescent state of skeletal muscle satellite cells. *Dev Biol*. 2007;304(1):246-259. doi:10.1016/j.ydbio.2006.12.026

43. Nagata Y, Kobayashi H, Umeda M, et al. Sphingomyelin levels in the plasma membrane correlate with the activation state of muscle satellite cells. *J Histochem Cytochem*. 2006;54(4):375-384. doi:10.1369/jhc.5A6675.2006

44. Relaix F, Zammit PS. Satellite cells are essential for skeletal muscle regeneration: the cell on the edge returns centre stage. *Development*. 2012;139(16):2845-2856. doi:10.1242/dev.069088

45. Zammit PS, Partridge TA, Yablonka-Reuveni Z. The skeletal muscle satellite cell: the stem cell that came in from the cold. *J Histochem Cytochem*. 2006;54(11):1177-1191. doi:10.1369/jhc.6R6995.2006

46. Yablonka-Reuveni Z, Rudnicki MA, Rivera AJ, Primig M, Anderson JE, Natanson P. The Transition from Proliferation to Differentiation Is Delayed in Satellite Cells from Mice Lacking MyoD. *Dev Biol*. 1999;210(2):440-455. doi:10.1006/dbio.1999.9284

47. Yablonka-Reuveni Z, Day K, Vine A, Shefer G. Defining the transcriptional signature of skeletal muscle stem cells. *J Anim Sci*. 2008;86(14 Suppl):E207-216. doi:10.2527/jas.2007-0473

48. Conboy IM, Rando TA. The regulation of Notch signaling controls satellite cell activation and cell fate determination in postnatal myogenesis. *Dev Cell*. 2002;3(3):397-409. doi:10.1016/s1534-5807(02)00254-x

49. Kuang S, Kuroda K, Le Grand F, Rudnicki MA. Asymmetric self-renewal and commitment of satellite stem cells in muscle. *Cell*. 2007;129(5):999-1010. doi:10.1016/j.cell.2007.03.044

50. Schuster-Gossler K, Cordes R, Gossler A. Premature myogenic differentiation and depletion of progenitor cells cause severe muscle hypotrophy in Delta1 mutants. *Proceedings of the National Academy of Sciences*. 2007;104(2):537-542. doi:10.1073/pnas.0608281104

51. Bjornson CRR, Cheung TH, Liu L, Tripathi PV, Steeper KM, Rando TA. Notch signaling is necessary to maintain quiescence in adult muscle stem cells. *Stem Cells*. 2012;30(2):232-242. doi:10.1002/stem.773

52. Mourikis P, Sambasivan R, Castel D, Rocheteau P, Bizzarro V, Tajbakhsh S. A critical requirement for notch signaling in maintenance of the quiescent skeletal muscle stem cell state. *Stem Cells*. 2012;30(2):243-252. doi:10.1002/stem.775

53. Wen Y, Bi P, Liu W, Asakura A, Keller C, Kuang S. Constitutive Notch Activation Upregulates Pax7 and Promotes the Self-Renewal of Skeletal Muscle Satellite Cells. *Mol Cell Biol*. 2012;32(12):2300-2311. doi:10.1128/MCB.06753-11

54. Brack AS, Conboy IM, Conboy MJ, Shen J, Rando TA. A temporal switch from notch to Wnt signaling in muscle stem cells is necessary for normal adult myogenesis. *Cell Stem Cell*. 2008;2(1):50-59. doi:10.1016/j.stem.2007.10.006

55. Wagers AJ. Wnt not, waste not. *Cell Stem Cell*. 2008;2(1):6-7. doi:10.1016/j.stem.2007.12.005

56. Schiaffino S, Rossi AC, Smerdu V, Leinwand LA, Reggiani C. Developmental myosins: expression patterns and functional significance. *Skeletal Muscle*. 2015;5(1):22. doi:10.1186/s13395-015-0046-6

57. Pelosi L, Giacinti C, Nardis C, et al. Local expression of IGF-1 accelerates muscle regeneration by rapidly modulating inflammatory cytokines and chemokines. *FASEB J*. 2007;21(7):1393-1402. doi:10.1096/fj.06-7690com

58. Mutsaers SE, Bishop JE, McGrouther G, Laurent GJ. Mechanisms of tissue repair: from wound healing to fibrosis. *Int J Biochem Cell Biol*. 1997;29(1):5-17. doi:10.1016/s1357-2725(96)00115-x

59. Grounds MD. Complexity of Extracellular Matrix and Skeletal Muscle Regeneration. In: Schiaffino S, Partridge T, eds. *Skeletal Muscle Repair and Regeneration*. Advances in Muscle Research. Springer Netherlands; 2008:269-302. doi:10.1007/978-1-4020-6768-6_13

60. Mann CJ, Perdiguero E, Kharraz Y, et al. Aberrant repair and fibrosis development in skeletal muscle. *Skeletal Muscle*. 2011;1(1):21. doi:10.1186/2044-5040-1-21

61. Lluri G, Langlois GD, McClellan B, Soloway PD, Jaworski DM. Tissue inhibitor of metalloproteinase-2 (TIMP-2) regulates neuromuscular junction development via a beta1 integrin-mediated mechanism. *J Neurobiol*. 2006;66(12):1365-1377. doi:10.1002/neu.20315

62. Brockes JP. Amphibian limb regeneration: rebuilding a complex structure. *Science*. 1997;276(5309):81-87. doi:10.1126/science.276.5309.81

63. Tanaka EM. Regeneration: if they can do it, why can't we? *Cell*. 2003;113(5):559-562. doi:10.1016/s0092-8674(03)00395-7

64. Iten LE, Bryant SV. Forelimb regeneration from different levels of amputation in the newt,Notophthalmus viridescens: Length, rate, and stages. *Wilhelm Roux Arch Entwickl Mech Org*. 1973;173(4):263-282. doi:10.1007/BF00575834
65. Tanaka EM, Gann AAF, Gates PB, Brockes JP. Newt Myotubes Reenter the Cell Cycle by Phosphorylation of the Retinoblastoma Protein. *J Cell Biol*. 1997;136(1):155-165.

66. Kragl M, Knapp D, Nacu E, et al. Cells keep a memory of their tissue origin during axolotl limb regeneration. *Nature*. 2009;460(7251):60-65. doi:10.1038/nature08152

67. Alesci A, Pergolizzi S, Lo Cascio P, Fumia A, Lauriano ER. Neuronal regeneration: Vertebrates comparative overview and new perspectives for neurodegenerative diseases. *Acta Zoologica*. 2022;103(2):129-140. doi:10.1111/azo.12397

68. Cutie S, Huang GN. Vertebrate cardiac regeneration: evolutionary and developmental perspectives. *Cell Regen*. 2021;10(1):6. doi:10.1186/s13619-020-00068-y

69. Conboy IM, Rando TA. Aging, Stem Cells and Tissue Regeneration: Lessons from Muscle. *Cell Cycle*. 2005;4(3):407-410. doi:10.4161/cc.4.3.1518

70. Chang NC, Chevalier FP, Rudnicki MA. Satellite Cells in Muscular Dystrophy – Lost in Polarity. *Trends in Molecular Medicine*. 2016;22(6):479-496. doi:10.1016/j.molmed.2016.04.002

71. Morgan JE, Zammit PS. Direct effects of the pathogenic mutation on satellite cell function in muscular dystrophy. *Experimental Cell Research*. 2010;316(18):3100-3108. doi:10.1016/j.yexcr.2010.05.014

72. Alway SE, Myers MJ, Mohamed JS. Regulation of Satellite Cell Function in Sarcopenia. *Frontiers in Aging Neuroscience*. 2014;6. Accessed May 10, 2023. https://www.frontiersin.org/articles/10.3389/fnagi.2014.00246

Chapter 3

Changes in Protein Fluxes in Skeletal Muscle During Sequential Stages of Muscle Regeneration After Acute Injury

Keywords: Muscle Damage/Injury; *In-Vivo* Regeneration; Satellite Cells; Proteomics; Stable Isotope Labeling; Mass Spectrometry; Protein Turnover

Alec Bizieff [1], Maggie Cheng [1,] Kelvin Chang [1,] Hussein Mohammed [1], Naveed Ziari [1], Edna Nyangau [1], Mark Fitch [1], and Marc K. Hellerstein [1]

[1] Department of Nutritional Sciences & Toxicology, University of California, Berkeley

Correspondence:
Marc K. Hellerstein
march@berkeley.edu
University of California, Berkeley
Berkeley, CA, United States

Abstract

Changes in protein turnover play an important role in dynamic physiological processes, including skeletal muscle regeneration that occurs as an essential part of proper tissue repair after injury. The inability of muscle tissue to recapitulate this regenerative process can facilitate the development of pathology and clinical symptoms in various musculoskeletal diseases, including muscular dystrophies and pathological atrophy. Here, we employed a workflow that couples deuterated water (^2H_2O) administration with high-resolution mass spectrometry (MS) to systematically measure *in-vivo* protein turnover rates across the muscle proteome at unique sequential stages along the regeneration timeline. We compared the turnover kinetics of over 100 proteins in response to cardiotoxin (CTX) induced muscle damage and regeneration. This analysis is compared to gene expression data from bulk RNA-sequencing (RNA-seq). The data reveal quantitative protein flux signatures in response to necrotic damage at the molecular level, in addition to widespread differences in cell proliferation, energy metabolism, and contractile gene expression. Interestingly, the mRNA changes correlated poorly with changes in protein synthesis rates, consistent with post-transcriptional control mechanisms. In summary, the experiments described here reveal the signatures of protein flux changes during skeletal muscle regeneration and their timing, as well as the inability of mRNA expression measurements to reveal changes in directly measured protein turnover rate. The approach described here could identify biomarkers or therapeutic targets for the therapeutic modulation of muscle regeneration.

Introduction

A unique feature of skeletal muscle tissue is that it can recapitulate certain elements of embryonic myogenesis upon injury by replacing damaged tissue with newly formed ones. This is an important process that allows tissue to recover from and adapt to repeated bouts of stress, like those incurred during physical activity or exercise [1]. The regenerative capacity of skeletal muscle comes from a small portion of peripherally located progenitor stem cells, known as muscle satellite cells (MuSCs) [2, 3, 4]. An impairment in this repair process is what generally leads to the signs and symptoms of musculoskeletal diseases such as muscular dystrophy and pathological atrophy [5, 38]. Understanding this process of skeletal muscle regeneration may lead to rational countermeasures against the impairment of regenerative capacity that is seen in pathologic conditions.

Traditional abundance-based measurements can establish changes in protein expression. However, the transition from MuSCs to mature myofiber is a dynamic process that involves synchronized, time-dependent changes in protein fluxes. Since proteins are not a static entity, traditional abundance-based measurements cannot capture the dimension of time-dependent change in protein fluxes [37]. Skeletal muscle regeneration has been previously divided into distinct stages that follow this sequential order: initial tissue damage, inflammation-mediated immune response, activation/proliferation of MuSCs, differentiation of MuSCs to myofibers, and maturation of novel myofibers into existing tissue [6]. To undergo complete skeletal muscle regeneration, the rates of protein synthesis and/or degradation (flux) must be altered in the transition from one defined stage to the next. Therefore, a kinetic signature in the form of a fraction of newly synthesized proteins may be an identifiable characteristic of each stage.

Here, we employed a workflow to measure the kinetic signatures of each stage of muscle regeneration by *in-vivo* by labeling proteins with deuterium (^2H) from deuterated "heavy" water (^2H_2O). Protein mass isotopomers were identified with high performance liquid chromatography (HPLC) coupled single (MS) and tandem (MS/MS) mass spectrometry and used to measure changes in protein flux rates, as previously described [7, 8, 9]. We asked whether the use of this stable isotope labeling flux proteomics approach would identify global, group, and individual protein kinetic changes at each stage. This information on protein turnover rates can then be compared to gene level expression values for global, individual, and group protein response during proper *in-vivo* muscle regeneration. Doing so will prove critical in setting a benchmark and identifying potential therapeutic targets of complete muscle regeneration.

Results

Time Course Layout & Visualization of Damage To induce damage, and subsequent *in-vivo* regeneration of the skeletal muscle, we injected CTX into the Tibialis Anterior (TA) muscle of one hind limb of each mouse in each experimental group [35, 36]. Mice injected with CTX were separated into groups differing in timing of ^2H_2O labeling relative to the time of initial injury (Figure 1A). The "Proliferation Stage" was administered CTX and ^2H_2O on the same day (Day 10) and labeled continuously until sacrifice 4 days post-CTX injection (dpi) to capture the protein flux changes that occur during initial tissue damage, inflammation-mediated immune response, and activation/proliferation of MuSCs. The "Differentiation Stage" was injected with CTX on Day 7 and ^2H_2O from 4 to 7 dpi (Day 11 to Day 14) to capture the protein flux changes that occur in the tissue during MuSCs differentiation into newly formed myofibers. There is a break in ^2H_2O labeling from day 7 to 10 dpi to avoid redundancy in global proteome kinetic analysis. The "Maturation Stage" received a CTX injection on Day 0 and ^2H_2O from 10 to 14 dpi (Day 10 to Day 14) to capture the reintegration of new myofibers into existing muscle, as well as the construction of surrounding structures to support newly formed tissue. Control groups (Uninjected) received no CTX injection but were administered ^2H_2O for 3 days (Day 11 to Day 14) to label proteins and were sacrificed for tissue collection alongside all other CTX injected groups on Day 14. All groups were sacrificed on Day 14 to avoid variation of multiple analyses. Analysis of Hematoxylin & Eosin (H&E) staining of this stage at 4 dpi demonstrated widespread myofiber fragmentation and extensive immune cell infiltration at the site of CTX injection (Figure 1B) that decreased at the beginning stages of newly formed myofibers reintegrating back into unaffected tissue was evident at 7 dpi (Figure 1C). Visual analysis at 14 dpi shows almost complete regeneration of damaged tissue, which is almost indistinguishable from unaffected tissue (Figure 1D). Muscle regeneration has been found to be virtually complete after 14 dpi, as previously reported [10,11], and further analysis of later stages are not expected to net significantly different findings.

DNA turnovers, Visual Confirmation of Regeneration, & Gene Expression of Myogenic Genes Visual quantification measurements were made to confirm the completion of skeletal muscle regeneration from initial CTX damage. Under visual analysis of H&E staining, the quantifiable fraction of damaged tissue decreased significantly (Proliferation Stage: avg. 38%, Differentiation Stage: avg 30% †, Maturation: no visible signs of damage †*. † $p<0.001$ from Proliferation Stage, * $p<0.001$ from Differentiation Stage) as a fraction of the entire tissue cross-sectional area (Figure 2A). Another visual marker of skeletal muscle regeneration, myofibers

with central nuclei, began forming as soon as 4 dpi, in congruence with previous findings (Figure 2C) [11]. However, during the Differentiation Stage the prevalence of central nuclei is significantly higher than the Proliferation Stage (Figure 2C, $p<0.001$), and decreases significantly after the Differentiation Stage transitions to the Maturation Stage (Figure 2C, $p<0.001$). Along with visible quantifications of muscle regeneration, we also observed changes in activity of cellular proliferation, which is measured by incorporation rates of ^{2}H into DNA [12]. To avoid the infiltration of immune cells that proliferate around the damaged tissue in our measurements of ^{2}H incorporation to DNA, purified muscle fibers were isolated from bulk tissue of all groups via enzymatic digestion and physical separation and then selectively depleted via MACS with CD45+ magnetic beads, as previously described [13]. The Proliferation Stage showed a high rate of incorporation of ^{2}H in DNA, however, there is a significant drop in ^{2}H incorporation into DNA during the Differentiation Stage and Maturation Stage in comparison to the Proliferation Stage (Proliferation Stage: avg. 44%, Differentiation Stage: avg 10% †, Maturation: avg 3% †. † $p<0.001$ from Proliferation Stage) (Figure 2E). These results were substantiated with measurements of gene expression from bulk RNA-sequencing values for known genes of myogenesis (Figure 2F) [6]. At the Proliferation Stage, MyoD, MyoG, and Myf5 all have significantly increased gene expression values, and MyoD and Myf5 still show significant increases by the Differentiation Stage. But once the Maturation Stage is reached, there is no significant expression of myogenic genes, and all genes are almost back to control levels. Genes found in bulk RNA-seq data for cell cycling (Ki67, PCNA) were also measured, and interestingly only PCNA during the Differentiation Stage stood out as significant when compared to control (data not shown).

Proteomics Comparison: To determine how protein fluxes in skeletal muscle change over time in response to damage, fractional synthesis rates (FSR) of proteins were measured *in-vivo* via $^{2}H_2O$ administration coupled with HPLC-MS and MS/MS analysis. Since there is a systemic response to local tissue injury [14], we used muscle tissue from a separate mouse that wasn't injured as a control for most comparisons. We also purified muscle fibers from bulk muscle tissue via enzymatic digestion and physical separation to remove the influence of interstitial and other cell types from circulation on our analyses [13]. Global, group, and individual protein flux analysis were still carried out on purified muscle fibers between injured muscle and muscle from the contralateral limb of the same mouse and can be found in the Supplemental Figures section (Figures S1 - S3).

Comparison of Global Protein Turnover Rates at Each Stage At the end of the Proliferation Stage (4 dpi), the FSR of 73 proteins that are present in both the CTX injured and the control limbs were measured. There was no significant global difference in protein FSR values between injured and control muscle tissue during this phase of regeneration (Figure 3A). At the end of the Differentiation Stage, the FSR of 127 proteins that are present in both the CTX injured and the control limbs, were measured. Global proteome analysis shows a significant increase in protein FSR values between injured and control muscle tissue, indicating a more pronounced response to injury at this stage of regeneration ($p<0.001$, Figure 3B). At the end of the Maturation Stage, the FSR of 125 proteins that are present in both the CTX injured and the control limbs, were measured at the end of the Maturation Stage (14 dpi). Global proteome analysis shows a significant increase in protein FSR values between injured and control muscle tissue during this phase of regeneration ($p<0.001$, Figure 3C). Average FSR values for every protein with standard deviation (SD) in all the measured stages can be found in Table 1.

Changes in Protein Group Turnover Rates in Each Stage Functional clusters of protein groups were analyzed by gene ontology enrichment using DAVID software from NIH to determine which cellular processes were highly affected at each stage (Figure 4A - 4C). In the Proliferation Stage, only the Myofibril cluster had a significant number of proteins with higher FSR values in the injured limb compared to control limb (13/18 increased, $p<0.05$). Other functional clusters [Cytoplasm (9/15 increased, $p>0.05$), Glycolysis (5/10 increased, $p>0.05$), Mitochondria (7/10 decreased, $p>0.05$), and Oxidative Phosphorylation (7/12 decreased, $p>0.05$)] were not significantly affected in this stage. In the Differentiation Stage, all measured functional clusters [Cytoplasm (24/25 increased, $p<0.05$), Myofibril (19/19 increased, $p<0.05$), Glycolysis (12/12 increased, $p<0.05$), Mitochondria (24/25 increased, $p<0.05$), and Oxidative Phosphorylation (35/35 increased, $p<0.05$)] had a significant increase in the number of proteins with a higher FSR value in the injured limb compared to control limb (Figure 4B). In the Maturation Stage, all measured functional cluster protein groups [Cytoplasm (22/23 increased, $p<0.05$), Myofibril (17/19 increased, $p<0.05$), Glycolysis (12/12 increased, $p<0.05$), Mitochondria (23/23 increased, $p<0.05$), and Oxidative Phosphorylation (38/39 increased, $p<0.05$)] saw significant increases in the number of proteins with a higher FSR value in the injured limb compared to control limb (Figure 4C).

Individual Protein Turnover Rates at Each Stage. In the Proliferation Stage, there were 8 individual proteins that stood out as statistically significant after correction for multiple comparisons between CTX injected and control muscle (Figure 5A). Proteins from skeletal muscle that have been previously identified as systemic markers of whole muscle FSR values (CA3) [15], proteins involved in accessing cellular components to DNA to either promote or silence the DNA replication processes (Histone H2B Type 1-M) [16], and individual glycolytic enzymes, like TPI, showed a significant change in FSR during this stage of regeneration. In the Differentiation Stage, there were 14 individual proteins that are significant after correction for multiple comparisons that include different myosin heavy chain isoforms including Myosin 3, also known as Embryonic Myosin Heavy Chain (EmyHC) and Myosin Light Chain 1/3 [17, 18, 19]. A few more glycolytic enzymes than just TPI (Phosphoglycerate Mutase 2 (PGM-2), Glyceraldehyde-3-Dehydrogenase (G3PDH), & Lactate Dehydrogenase A (LDH-A)) had significantly increased FSR values during this stage of regeneration as well. In the Maturation Stage, there were 91 individual proteins that stood out as having significantly different FSR values in the injured limb compared to control limb after correction for multiple comparisons (Figure 5C). Previously mentioned individual proteins of interest, (CA3, as well as Creatine Kinase-Muscle isoform (CK-M), and Myosin Light Chain 1/3) had significantly increased protein turnover at this stage of regeneration as well [15]. Interestingly, Myosin 3 also had a significant increase in FSR in the injured muscle at this time point, after nascent myofibers began to mature [18]. Also, Histone H2B Type 1-M is seen to have a significant increase in this stage as well. All measured glycolysis proteins, including the ones mentioned above (TPI, PGM-2, G3PDH, LDH-A), were significantly increased as well.

Global Gene Expression Changes at Each Stage. Gene expression values were normalized to fragment per kilobase millions (FPKM) values, which were used to compare global gene expression profiles of each stage of muscle regeneration. In the Proliferation Stage, 17198 individual gene expression values were measured. Of those 17198 genes, 2555 genes (14.9%) were significantly upregulated, 2423 genes (14.1%) were significantly downregulated, and 12220 (71.0%) genes did not change significantly ($-\text{Log}_{10}(p)>1.301$, Figure 6A). In the

Differentiation Stage, 16940 individual gene expression values were measured. Of those 16940 genes, 2397 genes (14.2%) were significantly upregulated, 2362 genes (13.9%) were significantly downregulated, and 12181 genes (71.9%) did not change significantly ($-Log_{10}(p)>1.301$, Figure 6B). In the Maturation Stage, 16474 individual gene expression values were measured. Of those 16474 genes, 778 genes (4.7%) were significantly upregulated, 771 genes (4.7%) were significantly downregulated, and 14925 genes (90.6%) did not change significantly ($-Log_{10}(p)>1.301$, Figure 6C).

Group Ontology Gene Expression at Each Stage for Matched Proteins. UniProt unique protein identification numbers (Accession #) were used to find Gene IDs for all proteins that were measured in functional cluster protein groups from DAVID by NIH software. FPKM values for each of those individual genes identified were ratioed to generate a Log_2(Fold Change) to measure the magnitude of change between each stage of muscle regeneration and control tissue. These values were then split up into the same functional cluster protein groups, as seen in Figure 4. In the Proliferation Stage, all of the functional clusters that were measured had a significant number of proteins with lower FSR values in the injured limb compared to control limb [Myofibril (15/18 decreased, $p<0.05$), Glycolysis (9/10 decreased, $p<0.05$), Mitochondria (8/9 decreased, $p<0.05$), and Oxidative Phosphorylation (12/12 decreased, $p<0.05$)], except for Cytoplasm (9/14 decreased, $p>0.05$) (Figure 7A). In the Differentiation Stage, again most of the functional clusters that were measured had a significant number of proteins with lower FSR values in the injured limb compared to control limb [Cytoplasm (16/23 decreased, $p<0.05$), Glycolysis (10/12 decreased, $p<0.05$), Mitochondria (23/24 decreased, $p<0.05$), and Oxidative Phosphorylation (33/37 decreased, $p<0.05$)], except for Myofibril (10/19 decreased, $p>0.05$), (Figure 7B). In the Maturation Stage, 3 of the measured functional cluster protein groups [Myofibril (13/18 increased, $p<0.05$), Glycolysis (11/12 increased, $p<0.05$), Oxidative Phosphorylation (34/39 increased, $p<0.05$)] saw significant increases in the number of proteins with a higher FSR value in the injured limb compared to control limb, while 2 did not [Cytoplasm (13/21 increased, $p>0.05$), Mitochondria (11/22 decreased, $p>0.05$)] (Figure 7C).

Correlations of Changes in Gene Expression to Changes in Protein FSR To correlate changes in gene expression FPKM values with their protein FSR values, a 2-dimensional graph was created to plot the Log_2FC of FPKM values on the Y axis and Log_2FC of protein FSR values on the X axis for each stage of muscle regeneration. In the Proliferation Stage, there is no significant correlation between the magnitude of change in FPKM and FSR values ($R^2 = 0.01819$, $p>0.05$, Figure 8A). In the Differentiation Stage, there is also no significant correlation between the magnitude of change in FPKM and FSR values ($R^2 = 0.00184$, $p>0.05$, Figure 8B). In the Maturation Stage as well, there is no significant correlation between the magnitude of change in FPKM and FSR values ($R^2 = 0.00220$, $p>0.05$, Figure 8C). These results indicate that there is no significant correlation between the magnitude of change in gene expression values and the magnitude of change in protein turnover at any of the stages in muscle regeneration.

Myh3 Gene Expression, EmyHC Protein Abundance, and My3 Protein Turnover. To support our analysis of protein flux changes, we incorporated static abundance measurements of certain proteins that are only transiently expressed during muscle regeneration, along with our genome data, to confirm which stage of new myofiber genesis we are exploring. EmyHC protein expression was analyzed by immunofluorescence intensity on muscle sections that were taken at the end of each regeneration stage (Figure 9A). The Proliferation Stage showed modest EmyHC

expression, however, a significant increase in EmyHC expression was seen between the Proliferation Stage and the Differentiation Stage (Figure 9B, $p<0.001$). By the end of the Maturation Stage, the level of EmyHC expression was significantly lower than both the Proliferation Stage (Figure 9B, $p<0.001$) and the Differentiation Stage (Figure 9B, $p<0.001$), as most myofibers had undergone their initial formation stages and began to mature back into unaffected tissue. Myh3, the gene for EmyHC, expression was also measured at the Proliferation Stage, and showed a significant increase in comparison to control values (Figure 9C, $p<0.005$). However, Myh3 gene expression no longer showed a significant difference from control levels at the Differentiation Stage and was significantly reduced from the Proliferation Stage ($p<0.005$). These gene expression levels of Myh3 were also observed in the Maturation Stage, with levels that were like the control group and significantly lower than the Proliferation Stage (Figure 9C, $p<0.001$).

In addition, we investigated the relationship between kinetic measurements, protein abundance measurements, and gene expression values for this protein during the process of muscle regeneration. EmyHC FSR did not show a significant increase from control during the Proliferation Stage (Figure 9D, $p>0.05$), when protein abundance level measurements were only moderately increased (Figure 9B) and Myh3 gene expression levels were significantly increased (Figure 9C, $p<0.001$). However, as with EmyHC abundance measurements, there was a significant increase in the EmyHC FSR value in the injured limb during the Differentiation Stage in comparison to the injured limb of the Proliferation Stage, as well as the control limb in the Differentiation Stage (Figure 9D, $p<0.001$). However, at this stage Myh3 gene expression was significantly decreased from the Proliferation Stage (Figure 9C, $p<0.005$). In the Maturation Stage, there was a significant decrease in EmyHC FSR from the injured limb of the Differentiation Stage to the injured limb of the Maturation Stage ($p<0.01$). The same significant decrease between the two stages can be seen with EmyHC protein abundance (Figure 9B, $p<0.001$). Myh3 gene expression was also significantly lower from previous stages (Proliferation Stage) and not significantly different from the control group. Interestingly, EmyHC from the injured limb during the Maturation Stage was still significantly higher in FSR values than control. This is different from what is seen in EmyHC protein abundance during the Maturation Stage, as it was the lowest of all the stages we measured. Also, there is no significant difference between the EmyHC FSR values of the injured limb from the Proliferation Stage and the injured limb from the Maturation Stage, which is different from what is seen in EmyHC abundance (Figure 9B).

Discussion

Here, we describe how both protein flux changes and gene expression values are affected on a global, group, and individual levels during sequential stages of muscle regeneration from CTX injury. This was achieved through paired "omics" approaches, including $^{2}H_2O$ labeling of proteins coupled to high resolution MS analysis to measure *in-vivo* protein turnover rates and bulk RNA-sequencing of CTX injured tissue. To first validate our model of CTX-mediated initial muscle damage and subsequent regeneration, we used quantitative measurements of histology, DNA replication, and EmyHC expression profiles.

We utilized visual analysis of the injured tissue at each stage to confirm our model of induced injury caused sufficient necrotic damage and subsequent regeneration of that damaged

muscle tissue. Previous work done by Mahdy et al. demonstrated histological analysis of CTX mediated muscle damage and regeneration on or around similar time points as our study [35]. The authors show early, widespread tissue damage with fragmented myofibers and cellular edema that is followed by later stage nascent myofiber formation and transient presence of central nuclei. Yan et al. also reported visual confirmation of new myofiber formation from MuSCs, with the abundance of central nuclei being the highest around 5 - 10 dpi [10]. In the later stages of muscle regeneration, the new myofibers have left their beginning stages of formation from MuSCs and have begun to mature into surrounding unaffected tissue. While this process generally begins after 7 dpi, we decided to delay the start of our measurement of protein fluxes until 10 dpi to allow for this process to develop. Visual analysis of the Maturation Stage shows significant decreases in measurements of histology and central nuclei, which indicates the early stage of myofiber genesis has ended. This point of muscle regeneration is where new tissue begins to develop the structures that surround the new myofiber to help integrate it back into the unaffected tissue [36]. By around 14 dpi, both articles report newly formed myofibers are visibly indistinguishable from unaffected tissue, thus confirming the final stages of the regeneration process end around this time point.

To support our visual confirmation of unique stages of skeletal muscle damage and regeneration, ^{2}H incorporation into DNA was measured from purified muscle fibers to determine cell-cycle activity. Previous work shows that MuSCs cultured from mouse tissue *ex-vivo* that are responding to an injury model have high BrdU incorporation up to 3 dpi [14], and that all cell populations actively incorporating BrdU at 3 dpi are MuSCs [10]. Our analysis shows high rates of cell-cycle activity from purified muscle fibers via high ^{2}H incorporation into DNA during the early stages of initial muscle damage (4dpi), but a striking and significant decrease in ^{2}H incorporation into DNA as the cell-cycle was exited to differentiate and the process of muscle regeneration occurred. Interestingly, we only saw significant changes in the expression of the cell-cycling genes that we measured, including PCNA or Ki67, in the Differentiation Stage when PCNA had significant upregulation. However, gene expression of myogenic markers that are involved with newly formed myofibers, like MyoD and Myf5 [6], were high at early stages (Proliferation and Differentiation), but all decreased back to control levels by the Maturation Stage.

Interestingly, we did not see a significant difference in global protein flux rate changes during the Proliferation Stage, which encompasses the phases of initial cellular damage, the subsequent immune system response, and the activation/proliferation of MuSCs around damaged tissue. However, in later time points that capture the stages of novel myofiber genesis from the differentiation of MuSCs (Differentiation Stage) and reintegration of these new myofibers into existing tissue (Maturation Stage), we see a very significant increase in global protein turnover rates at both stages in the CTX injured tissue compared to control. These results in global protein flux rate trends are a striking contrast to what we (see below) and others [10] have observed with global gene expression analysis of damaged or regenerating muscle. The Proliferation Stage showed the highest total number of genes and percent of all genes discovered to be either significantly upregulated or downregulated. However, as the regeneration process occurs, the total number of genes and percent of all genes discovered being either significantly upregulated or downregulated decreased from Proliferation Stage to Differentiation Stage, and from Differentiation Stage to Maturation Stage. This trend of decreasing global gene expression as the muscle regeneration process occurs is in line with other works [10] but is opposite of what we see

in protein turnover, which shows persistently high global changes into the later stages of muscle regeneration.

Along with global protein turnover measurements, proteins were grouped into functional clusters based on NIH DAVID ontology software to provide us with a deeper understanding of which specific cellular processes were most affected during each stage of the regeneration timeline. During the Proliferation Stage, only the proteins in the Myofibril functional cluster had a significant change in the direction of protein flux rates. This overall variance and lack of direction in group flux rates analysis may be due to the still persistent widespread tissue damage that is seen during this stage, which could influence turnover in specific protein groups [11]. In the Differentiation Stage, once the MuSCs began to differentiate towards new myofibers, there was a much more uniform effect seen with all measured functional clusters showing an across-the-board significant increase in protein turnover. At the Maturation Stage, group protein analysis shows significant increases in the number of proteins with higher turnover values for each functional cluster we measured. This is supported by the increase in global protein turnover rates at this stage as the myofiber still requires additional structure formation around it to integrate back into the unaffected tissue. This indicates that initial damage from CTX is still affecting the tissue, even at the later stages of regeneration while the tissue is maturing.

Gene expression values were also grouped into the same functional clusters as proteins based on matching genes to individual proteins in the groups. Interestingly, all the functional clusters that were measured for gene expression values in the Proliferation Stage were significantly decreased, except for Cytoplasm. Same with the Differentiation Stage, where we saw a different response in gene expression level than in protein turnover as all the functional clusters that were measured, besides Myofibril, had significantly more genes with a lower expression value compared to control. In the Maturation Stage, there are fewer groups than from the previous stages that we measured that have significant directional changes in gene expression and the overall magnitude of average change is less than the previous groups that we measured. This could be explained by the reduced global effect on gene expression at this stage as well. In summary, we found changes in group gene expression values that both fit previous findings from global abundance measurements at certain stages of regeneration but that did not at all correlate with actual protein synthesis rates.

On the individual protein level, we saw varying results in the number and types that were significant at each stage of regeneration. While there was not a significant change in global protein turnover values during the Proliferation Stage, a few individual proteins stand out as being significantly different. Proteins from skeletal muscle that have been previously validated as a systemic marker of whole muscle FSR values (CA3) [15], proteins involved in access of cellular components to DNA to either promote or silence the DNA replication processes (Histone H2B Type 1-M) [16], and individual glycolytic enzymes, like TPI, showed a significant change in FSR during this stage of regeneration. All data for other individual histone proteins can be found in Table 1. Along with significant increases in global protein flux rates at the Differentiation Stage, there were some individual proteins that stood out as significant as well. After correction for multiple comparisons, 14 proteins stood out as individually significant. Proteins of interest that are significant at this stage include different myosin heavy chain isoforms including Myosin 3 and Myosin Light Chain 1/3. These might provide insight into the status of whole tissue response to injury at this stage [17, 18, 19]. Also, a handful of glycolytic enzymes (TPI, PGM-2,

G3PDH, LDH-A) showed increases at this stage of regeneration, which have been previously found to be upregulated during the conversion of MuSC's to myofibers [20]. Thus, suggests an increased demand for energy metabolism during this stage to support new myofiber formation, as further corroborated by functional cluster protein group changes mentioned above. In the later stages of a regenerative event, when nascent myofibers are tasked with maturing into surrounding tissue, we see a significant increase in both global protein flux rates and individual protein flux values. In the Maturation Stage, 91 individual proteins had a significantly different flux rate and all 91 proteins that were significantly different in the regenerating limb had a higher turnover value. Previously mentioned individual proteins of interest (CA3, CK-M, Myosin Light Chain 1/3) that could serve as non-invasive markers had significantly increased protein turnover at this stage of regeneration as well. Interestingly, Myosin 3 protein fluxes were still high at this stage, after nascent myofibers began to mature [18]. Also, Histone H2B Type 1-M is seen to have a significant increase in this stage as well. We were able to examine individual protein flux changes along the entire muscle regeneration timeline, which provides us with more information on potential biomarkers of whole tissue FSR values or targets to further assess what is occurring along the in this temporally regulated process.

Knowing what individual protein turnover values stood out as significant after correction for multiple comparisons, we explored the relationship between protein turnover values and their gene expression values at the end of each labeling period. A correlation graph that compares the magnitude of change of an individual protein's turnover value and the magnitude of change in gene expression values was made for each stage. For the Proliferation Stage, 71 proteins that had available turnover and gene expression data, there was no significant correlation between the two types of measurements. In the Differentiation Group, 124 proteins that had available turnover and gene expression data, there was no significant correlation between the two types of measurements. In the Maturation Stage, 121 proteins that had available turnover and gene expression data, there was no significant correlation between the two types of measurements. Across all stages that we measured during muscle regeneration, there was no significant correlation between protein turnover values and gene expression values. This divergence in change between protein turnover and gene expression may be explained by post-transcriptional levels of control over protein synthesis (e.g., initiation or elongation translational changes, microRNA effects, etc.) or by delays in gene transcript turnover, whereas protein synthesis rates measure the current flux rate of each protein. This evidence of translational control during muscle regeneration is an important finding [21, 22, 23]. In fact, a few recent studies from our research group showed a clear dissociation between protein turnover and gene expression levels in various tissues, like skeletal muscle and liver [24, 25].

Specific time-dependent protein abundance, along with gene expression profiles, were also measured to substantiate our findings at each measured stage of the regeneration process. As mentioned previously, EmyHC is a protein that is transiently expressed from the gene Myh3 during the nascent stages of new myofiber formation, after proliferating MuSCs begin to differentiate [18]. Previous findings [26] support our results of a moderate abundance of EmyHC protein at 4 dpi, but a significantly higher protein abundance measurement at 7 dpi. These protein abundance values of EmyHC start to decrease after about 7 dpi, as new myofibers begin to mature into existing tissue [18] and return to almost baseline by the end of our regeneration time course at 14 dpi. EmyHC protein abundance patterns have also been found to mirror that of central nuclei abundance in the earlier stages of regeneration [27]. We see a similar correlation in

expression between markers of new myofibers, EmyHC and central nuclei, which decrease from their high co-abundance at the Differentiation Stage, almost back to baseline levels by the Maturation Stage. However, protein abundances lag a bit behind gene expression values as there is a highly significant increase in Myh3 gene expression, which starts to decrease after 4 dpi and is no longer significant from control by 7 dpi or 14 dpi.

Conclusion

In this paper, we have presented a new approach and technology for categorization of *in-vivo* protein turnover rates in response to a model of necrotic damage and subsequent regeneration, by using time dependent measurements. These results provide a deeper look into the local response to skeletal muscle regeneration and all the intricate processes that are required to take the tissue from initial damage to complete repair. Signature changes in protein turnover rates and a striking lack of correlation between mRNA changes and protein synthesis rates are clearly shown. Hopefully, this information will enable researchers and medical professionals to better understand this process to treat those with diseases where it is impaired.

Acknowledgments

The authors would like to thank all of those who contributed to this work, including members of the Hellerstein Lab and Conboy Lab, for their efforts. Special consideration and thanks go to Mike and Irina Conboy for promoting the core ideas and sharing the key techniques that aided in the development and completion of these studies.

Methods and Materials

Mouse Experiments:

CTX Time Course 20 male 8-week-old C57/BL6 mice were purchased from Jackson Laboratory and housed at UC Berkeley's Northwest Animal Facility. All mice were housed according to the Animal Care and Use Committee (ACUC) standards in the animal facility at UC Berkeley. The mice were assigned to a group (n=5) at random that reflected what stage of muscle regeneration is being measured (Proliferation Stage, Differentiation Stage, Maturation Stage, or Control). CTX induced muscle regeneration groups received a dose of 50 µL 0.1mg/mL CTX in sterile PBS/0.2% Meloxicam in the form of an intramuscular injection to the Tibialis Anterior (TA) muscle to one limb while the TA from the other limb was not injected. Day of injection will be Day 0, and subsequent days following will allow for the toxin induced model of muscle regeneration to occur. One group of mice did not receive CTX injection to serve as "uninjected controls" but did receive 3 days of stable isotope labeling alongside experimental groups. All groups of mice had unrestricted access to a standard chow diet and 8% Deuterium drinking water (^2H_2O). ^2H_2O was provided to continually label the mice after a bolus intraperitoneal injection of 99% ^2H_2O/0.9% saline solution to allow for stable enrichment levels during the entire labeling time course. If a mouse appears to have issues accessing food or water due to CTX injection at any time during incubation, then they would be removed from study and sacrificed. At specific time points along the muscle regeneration timeline after initial CTX injection pertaining to unique stages (Proliferation Stage: 4 days after injection, Differentiation Stage: 7 days after injection, Maturation Stage: 14 days after injection), animals will be sacrificed, and tissues will be taken for analysis. To avoid bias from multiple analysis, all animals were sacrificed on Day 14 of the study. Muscle histology and protein expression via immunofluorescence will be utilized to confirm each stage of muscle regeneration. After sacrifice, target tissues (multiple muscles including TA, blood [serum], kidneys, liver) will be collected along with urine, as previously described [28], for the following procedures.

Immunofluorescence Briefly, tissues were harvested and snap-frozen in OCT. 10 µm sections were taken from the muscle's mid-belly with a cryostat and placed on positively charged frosted slides for imaging. Slides with tissue sections were washed 3 times with PBS-T (0.1% Triton-X 100) for 5 minutes each and then air dried for 15 minutes at room temperature. Slides were blocked in buffer (10% Normal Donkey Serum (NDS) + 1% Bovine Serum Albumin (BSA) in PBS-T) for 1 hour at room temperature. Primary antibodies (Embryonic Myosin Heavy Chain: #F1.652 clone, Developmental Studies Hybridoma Bank, University of Iowa, deposited by Blau, HM) 1:10. β-Laminin: #AF-3837, R&D Systems, 1:20) were added in the same buffer used to block the slides and allowed to incubate in a dark, humid container overnight at 4°C. The next day, samples were washed 3 times with PBS-T for 5 minutes each. Secondary antibodies (Donkey anti Goat, Alexa Fluor 488, Abcam, #AB150129, 1:500. Donkey anti Mouse, Alexa Fluor 647, Abcam, #AB150107, 1:500) were added in the same buffer used to block the samples for 1 hour at room temperature, in the dark. Samples were washed 3 more times with PBS-T for 5 minutes each, dried, and mounted with 3 drops of Fluoromount (Sigma Aldrich #F4680) mounting media and cover slips. A Zeiss Axioscope fluorescence microscope was used for fluorescent imaging.

Tissue Histology Hematoxylin and eosin staining was performed on 10 µm sections of regenerating muscle on positively charged glass slides, as previously described [34] (DMD_M.1.2.007). Images were collected with a Zeiss Plan-Apochromat 20x/0.8NA (WD=0.55mm) M27 Biomarker Technology Core microscope. Imaging was conducted in a Zeiss Axio Scan.Z1 whole slide scanner objective lens in the brightfield mode with Hitachi HV-F202 camera.

Visual Quantification of Images Quantification of images for visible muscle damage, tissue regeneration, and protein expression via immunofluorescence was carried out using ImageJ software (https://imagej.nih.gov/). The individual doing analysis was blinded by a Python script that generated random images codes for file names. Images were later decoded after visual quantification for analysis of each stage.

Body Water Determination Mouse blood was distilled overnight upside down on a bead bath at 85°C to evaporate out body water. Deuterium present in the body water was exchanged onto acetone, and deuterium enrichment in the body water was measured via gas chromatography mass spectrometry (GC-MS), as previously described [29].

RNA-sequencing

RNA Bulk Isolation Whole RNA transcripts were isolated from frozen purified muscle fibers, according to manufacturer's instructions (Qiagen RNA Extraction Mini Kit, #74104), and RNA concentrations were obtained using a Nanodrop.

Sample collection and preparation From the RNA sample to the final data, each step, including sample test, library preparation, and sequencing, influences the quality of the data, and data quality directly impacts the analysis results. To guarantee the reliability of the data, quality control (QC) is performed at each step of the procedure.

RNA quantification and qualification RNA degradation and contamination was monitored on 1% agarose gels. RNA purity was checked using the NanoPhotometer® spectrophotometer (IMPLEN, CA, USA). RNA integrity and quantitation were assessed using the RNA Nano 6000 Assay Kit of the Bioanalyzer 2100 system (Agilent Technologies, CA, USA).

Library preparation for transcriptome sequencing A total amount of 1 µg RNA per sample was used as input material for the RNA sample preparations. Sequencing libraries were generated using NEBNext® UltraTM RNA Library Prep Kit for Illumina® (NEB, USA) following manufacturer's recommendations and index codes were added to attribute sequences to each sample. Briefly, mRNA was purified from total RNA using poly-T oligo-attached magnetic beads. Fragmentation was carried out using divalent cations under elevated temperature in NEBNext First Strand Synthesis Reaction Buffer (5X). First strand cDNA was synthesized using random hexamer primer and M-MuLV Reverse Transcriptase (RNase H-). Second strand cDNA synthesis was subsequently performed using DNA Polymerase I and RNase H. Remaining overhangs were converted into blunt ends via exonuclease/polymerase activities. After adenylation of 3' ends of DNA fragments, NEBNext Adaptor with hairpin loop structure were ligated to prepare for hybridization. To select cDNA fragments of preferentially 150~200 bp in length, the library fragments were purified with AMPure XP system (Beckman Coulter,

Beverly, USA). Then 3 µl USER Enzyme (NEB, USA) was used with size-selected, adaptor-ligated cDNA at 37 °C for 15 min followed by 5 min at 95 °C before PCR. Then PCR was performed with Phusion High-Fidelity DNA polymerase, Universal PCR primers and Index (X) Primer. At last, PCR products were purified (AMPure XP system) and library quality was assessed on the Agilent Bioanalyzer 2100 system.

Clustering and sequencing The clustering of the index-coded samples was performed on an Illumina Novaseq sequencer according to the manufacturer's instructions. After cluster generation, the libraries were sequenced on the same machine and paired-end reads were generated.

Sample Digestion for Proteomics

Muscle Fiber Isolation and CD45+ Cell Depletion via MACS Tissues were snap-frozen after harvest in 0.5 mL of 10% DMSO in FBS and stored at -80℃ until processing. Samples were thawed, buffer was removed, and individual muscle fibers were physically separated from whole muscle tissue, as previously described [13]. Purified muscle fibers were then depleted of infiltrating CD45+ cells by undergoing magnetic assisted cell sorting (MACS) mediated selective depletion, according to manufacturer's instructions (Miltenyi Biotec #130-052-301), before being processed for in-solution digestion.

Myofiber SDS Solubilization + In-Solution Digestion of Tissue After MACS-mediated CD45+ cell depletion, a 150 µL aliquot of purified myofibers was brought up to 500 µL in 0.1% SDS solution and allowed to disassociate on a vortexer overnight at medium speed. The next day, samples were pulled off the vortexer, mixed with 7:1 v/v 100% ethanol:sample, vortexed, and placed at -20℃ overnight to precipitate out proteins. The next day, samples were centrifuged 16,000 g for 30 minutes at 4℃ to pellet out all protein. Supernatant was removed and protein pellet was resuspended in 100 µL 8M Urea in 50 mM Ammonium Bicarbonate (pH 8.1) with agitation on vortexer at medium speed for 30 minutes at room temperature. A small portion of each sample was diluted, and protein concentration was then determined by the Pierce BCA protein assay kit (Thermo Fisher #23225) with BSA as standards. Up to 100 µg of protein was taken and volume adjusted up to 100 µL in 8M Urea in 50 mM Ammonium Bicarbonate (pH 8.1). Tris-(2-carboxyethyl)-phosphine (TCEP) was added to make a final concentration of 10 mM and samples were agitated on a vortexer for 20 minutes at room temperature. Iodoacetamide (IAA) was added to make a final concentration of 20 mM, samples were vortexed briefly, and incubated at room temperature in the dark for 30 minutes. TCEP was added to make a final concentration of 4 mM to quench excess IAA and samples were diluted in 50 mM Ammonium Bicarbonate (pH 8.1) so that the final concentration of Urea was < 1M. Proteomics-Grade Trypsin was added at a ratio of 1:50 trypsin to protein (Sigma Aldrich, #T6567). Samples were incubated at 37°C overnight. The next day, formic acid was added at 5% of the final volume. Samples underwent Solid-Phase Extraction using Agilent C18 clean up columns (#A57203) to remove digested peptides from the digestion buffer. Peptides were eluted using 30% acetonitrile and speedvac'd until dry and re-suspended in 25 µL of 0.1 % formic acid/3% acetonitrile/96.9% LC-MS grade water and transferred to LC-MS vials to be analyzed via LC-MS.

Mitochondria Isolation for Proteomics After MACS-mediated CD45+ cell type depletion, a 150 µL aliquot of purified myofibers was used to isolate mitochondrial proteins according to

manufacturer's instructions (Thermo Fisher #89801). Protein pellets were resuspended in 50 mM Ammonium Bicarbonate (pH 8.1) and protein concentration was then determined by the Pierce BCA protein assay kit with BSA as standards. Up to 100 µg of protein was taken and volume adjusted to 100 µL in 50 mM Ammonium Bicarbonate (pH 8.1). TCEP was added to make a final concentration of 10 mM and samples were agitated on a vortexer for 20 minutes at room temperature. IAA was added to make a final concentration of 20 mM, samples were vortexed briefly, and incubated at room temperature in the dark for 30 minutes. TCEP was added to make a final concentration of 4 mM to quench excess IAA and samples were diluted in 50 mM Ammonium Bicarbonate (pH 8.1) up to 400 µL. Proteomics-Grade Trypsin was added at a ratio of 1:50 trypsin to protein. Samples were incubated at 37°C overnight. The next day, formic acid was added at 5% of the final volume. Samples were centrifuged at 10,000 g for 10 minutes at room temperature, and the supernatant was collected. Supernatant was speedvac'd until dry and re-suspended in 50 µL of 0.1 % formic acid/3% acetonitrile/96.9% LC-MS grade water and transferred to LC-MS vials to be analyzed via LC-MS.

DNA Incorporation of ^{2}H After MACS mediated CD45+ cell type depletion, a 150 µL aliquot of purified myofibers was used to extract DNA. DNA was derivatized and analyzed for deuterium enrichment in deoxyribose via gas chromatography mass spectrometry, as previously described [12,30].

Liquid chromatography-mass spectrometry (LC-MS) analysis Trypsin-digested peptides were analyzed on a 6550 quadropole time of flight (Q-ToF) mass spectrometer equipped with Chip Cube nano ESI source (Agilent Technologies). High performance liquid chromatography (HPLC) separated the peptides using capillary and nano binary flow. Mobile phases were 95% acetonitrile/0.1% formic acid in LC-MS grade water. Peptides were eluted at 350 nl/minute flow rate with an 18-minute LC gradient. Each sample was analyzed once for protein/peptide identification in data-dependent MS/MS mode and once for peptide isotope analysis in MS mode. Acquired MS/MS spectra were extracted and searched using Spectrum Mill Proteomics Workbench software (Agilent Technologies) and a mouse protein database (www.uniprot.org). Search results were validated with a global false discovery rate of 1%. A filtered list of peptides was collapsed into a nonredundant peptide formula database containing peptide elemental composition, mass, and retention time. This was used to extract mass isotope abundances (M_0 - M_3) of each peptide from MS-only acquisition files with Mass Hunter Qualitative Analysis software (Agilent Technologies). Mass isotopomer distribution analysis (MIDA) was used to calculate peptide elemental composition and curve-fit parameters for predicting peptide isotope enrichment based on precursor body water enrichment (p) and the number (n) of amino acid C-H positions per peptide actively incorporating hydrogen (H) and deuterium (^{2}H) from body water. Subsequent data handling was performed using python-based scripts, with input of precursor body water enrichment for each subject, to yield fractional synthesis rate (FSR) data at the protein level. FSR data were filtered to exclude protein measurements with fewer than 2 peptide isotope measurements per protein. Details of FSR calculations and data filtering criteria have been described in detail previously [9].

Calculation of fractional replacement (f) and replacement rate constant (k) for individual proteins Details of f calculations were previously described [9]**.**

Statistical analysis Data filtering and calculations were performed according to previous reports [9]. Only those proteins that met analytic filtering criteria and that were present in at least 2 animals per group were included in comparisons and statistical analyses [31]. Individual proteins were also grouped into different functional clusters based on gene ontology origin using DAVID software from NIH website (https://david.ncifcrf.gov/tools.jsp) to determine which processes were affected at each stage [32]. Statistical significance of protein turnover comparisons was assessed by one of the following tests: 1.) Global changes in protein turnover were compared across groups with a Student's T-Test, 2.) Individual proteins were compared across groups with a Student's T-Test and Benjamini-Hochberg correction for multiple comparisons, or 3.) a Binomial Test of the proportion of proteins showing a higher or lower value of FSR in relation to control for comparison of functional clusters across the regeneration timeline, as described previously [33], * $p<0.05$, ** $p<0.01$, *** $p<0.005$, **** $p<0.001$. All statistical analysis was carried out by GraphPad Prism software (version 9.4).

References

1. Hinkson IV, Elias JE. The dynamic state of protein turnover: It's about time. *Trends Cell Biol*. 2011;21(5):293-303. doi:10.1016/j.tcb.2011.02.002

2. Forcina L, Cosentino M, Musarò A. Mechanisms Regulating Muscle Regeneration: Insights into the Interrelated and Time-Dependent Phases of Tissue Healing. *Cells*. 2020;9(5):1297. doi:10.3390/cells9051297

3. Mauro A. Satellite cell of skeletal muscle fibers. *J Biophys Biochem Cytol*. 1961;9(2):493-495. doi:10.1083/jcb.9.2.493

4. Shi X, Garry DJ. Muscle stem cells in development, regeneration, and disease. *Genes Dev*. 2006;20(13):1692-1708. doi:10.1101/gad.1419406

5. Balch WE, Morimoto RI, Dillin A, Kelly JW. Adapting Proteostasis for Disease Intervention. *Science*. 2008;319(5865):916-919. doi:10.1126/science.1141448

6. Musarò A. The Basis of Muscle Regeneration. *Advances in Biology*. 2014;2014:e612471. doi:10.1155/2014/612471

7. Hellerstein MK, Neese RA. Mass isotopomer distribution analysis: a technique for measuring biosynthesis and turnover of polymers. *Am J Physiol*. 1992;263(5 Pt 1):E988-1001. doi:10.1152/ajpendo.1992.263.5.E988

8. Hellerstein MK, Neese RA. Mass isotopomer distribution analysis at eight years: theoretical, analytic, and experimental considerations. *American Journal of Physiology-Endocrinology and Metabolism*. 1999;276(6):E1146-E1170. doi:10.1152/ajpendo.1999.276.6.E1146

9. Holmes WE, Angel TE, Li KW, Hellerstein MK. Dynamic Proteomics: In Vivo Proteome-Wide Measurement of Protein Kinetics Using Metabolic Labeling. *Methods Enzymol*. 2015;561:219-276. doi:10.1016/bs.mie.2015.05.018

10. Yan Z, Choi S, Liu X, et al. Highly Coordinated Gene Regulation in Mouse Skeletal Muscle Regeneration*. *Journal of Biological Chemistry*. 2003;278(10):8826-8836. doi:10.1074/jbc.M209879200

11. Ramadasan-Nair R, Gayathri N, Mishra S, et al. Mitochondrial Alterations and Oxidative Stress in an Acute Transient Mouse Model of Muscle Degeneration. *J Biol Chem*. 2014;289(1):485-509. doi:10.1074/jbc.M113.493270

12. Busch R, Neese RA, Awada M, Hayes GM, Hellerstein MK. Measurement of cell proliferation by heavy water labeling. *Nat Protoc*. 2007;2(12):3045-3057. doi:10.1038/nprot.2007.420

13. Conboy MJ, Conboy IM. Preparation of adult muscle fiber-associated stem/precursor cells. *Methods Mol Biol*. 2010;621:149-163. doi:10.1007/978-1-60761-063-2_10

14. Rodgers JT, King KY, Brett JO, et al. mTORC1 controls the adaptive transition of quiescent stem cells from G0 to GAlert. *Nature*. 2014;510(7505):393-396. doi:10.1038/nature13255

15. Shankaran M, King CL, Angel TE, et al. Circulating protein synthesis rates reveal skeletal muscle proteome dynamics. *J Clin Invest*. 2016;126(1):288-302. doi:10.1172/JCI79639

16. Brown VD, Wang ZF, Williams AS, MarZluff WF. Structure of a cluster of mouse histone genes. *Biochimica et Biophysica Acta (BBA) - Gene Structure and Expression*. 1996;1306(1):17-22. doi:10.1016/0167-4781(96)00013-9

17. Evans WJ, Shankaran M, Smith EC, et al. Profoundly lower muscle mass and rate of contractile protein synthesis in boys with Duchenne muscular dystrophy. *J Physiol*. 2021;599(23):5215-5227. doi:10.1113/JP282227

18. Schiaffino S, Rossi AC, Smerdu V, Leinwand LA, Reggiani C. Developmental myosins: expression patterns and functional significance. *Skeletal Muscle*. 2015;5(1):22. doi:10.1186/s13395-015-0046-6

19. Dalle S, Hiroux C, Poffé C, Ramaekers M, Deldicque L, Koppo K. Cardiotoxin-induced skeletal muscle injury elicits profound changes in anabolic and stress signaling, and muscle fiber type composition. *J Muscle Res Cell Motil*. 2020;41(4):375-387. doi:10.1007/s10974-020-09584-5

20. Ohlendieck K. Proteomics of skeletal muscle glycolysis. *Biochimica et Biophysica Acta (BBA) - Proteins and Proteomics*. 2010;1804(11):2089-2101. doi:10.1016/j.bbapap.2010.08.001

21. Liu Y, Beyer A, Aebersold R. On the Dependency of Cellular Protein Levels on mRNA Abundance. *Cell*. 2016;165(3):535-550. doi:10.1016/j.cell.2016.03.014

22. Greenbaum D, Colangelo C, Williams K, Gerstein M. Comparing protein abundance and mRNA expression levels on a genomic scale. *Genome Biology*. 2003;4(9):117. doi:10.1186/gb-2003-4-9-117

23. Maier T, Güell M, Serrano L. Correlation of mRNA and protein in complex biological samples. *FEBS Lett*. 2009;583(24):3966-3973. doi:10.1016/j.febslet.2009.10.036

24. Chen TC, Kuo T, Dandan M, et al. The role of striated muscle Pik3r1 in glucose and protein metabolism following chronic glucocorticoid exposure. *J Biol Chem*. 2021;296:100395. doi:10.1016/j.jbc.2021.100395

25. Ward CP, Peng L, Yuen S, et al. ER Unfolded Protein Response in Liver In Vivo Is Characterized by Reduced, Not Increased, De Novo Lipogenesis and Cholesterol Synthesis Rates with Uptake of Fatty Acids from Adipose Tissue: Integrated Gene Expression, Translation Rates and Metabolic Fluxes. *Int J Mol Sci*. 2022;23(3):1073. doi:10.3390/ijms23031073

26. Mehdipour M, Skinner C, Wong N, et al. Rejuvenation of three germ layers tissues by exchanging old blood plasma with saline-albumin. *Aging (Albany NY)*. 2020;12(10):8790-8819. doi:10.18632/aging.103418

27. Daou N, Hassani M, Matos E, et al. Displaced Myonuclei in Cancer Cachexia Suggest Altered Innervation. *Int J Mol Sci*. 2020;21(3):1092. doi:10.3390/ijms21031092

28. Kurien BT, Scofield RH. Mouse urine collection using clear plastic wrap. *Lab Anim*. 1999;33(1):83-86. doi:10.1258/002367799780578525

29. Yang D, Diraison F, Beylot M, et al. Assay of low deuterium enrichment of water by isotopic exchange with [U-13C3] acetone and gas chromatography-mass spectrometry. *Anal Biochem*. 1998;258(2):315-321. doi:10.1006/abio.1998.2632

30. Rogers-Broadway KR, Karydis LI, Dobson RC, Steele AJ. Ex-Vivo Signal Transduction Studies in Chronic Lymphocytic Leukemia. *Methods Mol Biol*. 2019;1881:1-17. doi:10.1007/978-1-4939-8876-1_1

31. Thompson ACS, Bruss MD, Price JC, et al. Reduced in vivo hepatic proteome replacement rates but not cell proliferation rates predict maximum lifespan extension in mice. *Aging Cell*. 2016;15(1):118-127. doi:10.1111/acel.12414

32. Huang DW, Sherman BT, Lempicki RA. Systematic and integrative analysis of large gene lists using DAVID bioinformatics resources. *Nat Protoc*. 2009;4(1):44-57. doi:10.1038/nprot.2008.211

33. Evans W, Shankaran M, Nyangau E, et al. Effects of Fortetropin on the Rate of Muscle Protein Synthesis in Older Men and Women: A Randomized, Double-Blinded, Placebo-Controlled Study. *J Gerontol A Biol Sci Med Sci*. 2020;76(1):108-114. doi:10.1093/gerona/glaa162

34. Experimental protocols for DMD animal models. TREAT-NMD. DMD_M.1.2.007. Accessed March 22, 2023. https://treat-nmd.org/resources-support/research-overview/preclinical-research/experimental-protocols-for-dmd-animal-models/

35. Mahdy MAA, Lei HY, Wakamatsu JI, Hosaka YZ, Nishimura T. Comparative study of muscle regeneration following cardiotoxin and glycerol injury. *Annals of Anatomy - Anatomischer Anzeiger*. 2015;202:18-27. doi:10.1016/j.aanat.2015.07.002

36. Wang Y, Lu J, Liu Y. Skeletal Muscle Regeneration in Cardiotoxin-Induced Muscle Injury Models. *Int J Mol Sci*. 2022;23(21):13380. doi:10.3390/ijms232113380

37. Claydon AJ, Beynon R. Proteome Dynamics: Revisiting Turnover with a Global Perspective. *Molecular & Cellular Proteomics*. 2012;11(12):1551-1565. doi:10.1074/mcp.O112.022186

38. Sousa-Victor P, García-Prat L, Muñoz-Cánoves P. Control of satellite cell function in muscle regeneration and its disruption in aging. *Nat Rev Mol Cell Biol*. 2022;23(3):204-226. doi:10.1038/s41580-021-00421-2

Figure Legend:

<u>Figure 1</u> Time Course Layout & Visualization of Damage
A.) Overview of $^{2}H_2O$ labeling time course and definition of each stage based on days after CTX injection. Visualization of muscle regeneration **B.)** 4 days **C.)** 7 days **D.)** 14 days after CTX injection. All images taken at 5x magnification.

<u>Figure 2</u> DNA turnover, Visual Confirmation of Regeneration, & Gene Expression of Myogenic Genes
A.) Visualization of muscle damage 4 days after CTX injection. Image taken at 10x magnification. **B.)** Quantification of damaged muscle tissue as a fraction of whole tissue surface area. Values are expressed as: % of damaged tissue area in μM^2 / % of whole tissue area in μM^2. Significance determined by One-Way ANOVA with Benjamini-Hochberg correction for multiple comparisons. * $p<0.05$, ** $p<0.01$, *** $p<0.005$, **** $p<0.001$.**C.)** Visualization of central nuclei expression 7 days after CTX injection. Image taken at 10x magnification. **D.)** Quantification of individual myofibers expressing central nuclei. Values are expressed as: number of myofibers with central nuclei / 100 μM^2 of tissue. Significance determined by One-Way ANOVA with Benjamini-Hochberg correction for multiple comparisons. * $p<0.05$, ** $p<0.01$, *** $p<0.005$, **** $p<0.001$. **E.)** Measuring the fractional replacement rate (f-Value) of DNA with ^{2}H in newly dividing myocytes during various stages of muscle regeneration. Significance was determined by One-Way ANOVA with Benjamini Hochberg correction for multiple comparisons. * $p<0.05$, ** $p<0.01$, *** $p<0.005$, **** $p<0.001$. **F.)** Myogenic gene expression measured in FPKM in all stages and control group. Significance determined by Student's Unpaired T-Test, * $p<0.05$, ** $p<0.01$, *** $p<0.005$, **** $p<0.001$**.**

<u>Table 1</u> Protein Turnover Values in Each Stage
Average % turnover per day ± standard deviation of each individual protein in each group. Proteins with **bold text** and a * in their boxes are significant by Student's unpaired T-Test with Benjamini Hochberg correction for multiple comparisons when compared to their control value, * $p<0.05$. OxPhos = Oxidative Phosphorylation

<u>Figure 3</u> Global Protein Turnover Rates at Each Stage
A.) Overview of global proteome FSR changes between CTX and control muscle tissue after 4 days of CTX injection. **B.)** Overview of global proteome FSR changes between CTX and control muscle tissue after 7 days of CTX injection. **C.)** Overview of global proteome FSR changes between CTX and control muscle tissue after 14 days of CTX injection. For all figures, significance determined by Student's Unpaired T-Test, * $p<0.05$, ** $p<0.01$, *** $p<0.005$, **** $p<0.001$**.**

<u>Figure 4</u> Changes in Protein Group Turnover Rates in Each Stage
A.) Protein Group analysis of proteins found during the Proliferation Stage (4 dpi) and separated into ontologies based on NIH DAVID analysis. **B.)** Protein Group analysis of proteins found during the Maturation Stage (7 dpi) and separated into ontologies based on NIH DAVID analysis. **C.)** Protein Group analysis of proteins found during the Maturation Stage (14 dpi) and separated into ontologies based on NIH DAVID analysis. Significance determined by Binomial

Test of the proportion of proteins showing a higher or lower value of FSR in relation to uninjected (control), * $p<0.05$.

Figure 5 Significantly Different Individual Protein Turnover Rates at Each Stage
A.) Comparison of change in individual protein FSR value between CTX injected and control limbs for proteins that are significantly different after Benjamini Hochberg correction for multiple comparisons at 4 days after CTX injection (Proliferation Stage) **B.)** Comparison of change in individual protein FSR value between CTX injected and control limbs for proteins that are significantly different after Benjamini Hochberg correction for multiple comparisons at 7 days after CTX injection (Differentiation Stage). **C.)** Comparison of change in individual protein FSR value between CTX injected and control limbs for proteins that are significantly different after Benjamini Hochberg correction for multiple comparisons at 14 days after CTX injection (Maturation Stage). Significance determined by Student's Paired T-Test with Benjamini Hochberg correction for multiple comparisons, * $p<0.05$, ** $p<0.01$, *** $p<0.005$, **** $p<0.001$.

Figure 6 Global Gene Expression Rates at Each Stage
A.) Volcano plot of global gene expression (FPKM) on the X-axis and Log_{10}(p value) on the Y-axis for all genes found during the Proliferation Stage (4 dpi). **B.)** Volcano plot of global gene expression (FPKM) on the X-axis and Log_{10}(p value) on the Y-axis for all genes found during the Proliferation Stage (7 dpi). **C.)** Volcano plot of global gene expression (FPKM) on the X-axis and Log_{10}(p value) on the Y-axis for all genes found during the Proliferation Stage (14 dpi). All values with a -log10(p value) of below 1.301 were non-significant and are colored gray.

Figure 7 Matched Group Ontology Gene Expression at Each Stage to Individual Proteins
A.) Functional Clusters of gene expression based on protein groups (used in Figure 4) from NIH DAVID software at the Proliferation Stage (4 dpi). **B.)** Functional Clusters of gene expression based on protein groups (used in Figure 4) from NIH DAVID software at the Differentiation Stage (7 dpi) **C.)** Functional Clusters of gene expression based on protein groups (used in Figure 4) from NIH DAVID software at the Maturation Stage (14 dpi). For all groups, significance is determined by Binomial Test of the proportion of proteins showing a higher or lower value of FSR in relation to control, * $p<0.05$.

Figure 8 Correlations of Gene Expression to Protein FSR
A.) Correlation graphs between log transformed fold change in gene expression (FPKM, Y Axis) and log transformed fold change in protein turnover (FSR, X Axis) for Proliferation Stage (4 dpi) B.) Correlation graphs between log transformed fold change in gene expression (FPKM, Y Axis) and log transformed fold change in protein turnover (FSR, X Axis) for Differentiation Stage (7 dpi) **C.)** Correlation graphs between log transformed fold change in gene expression (FPKM, Y Axis) and log transformed fold change in protein turnover (FSR, X Axis) for Maturation Stage (14 dpi). For all graphs, significance was determined by simple linear regression equation with R^2 value shown.

Figure 9 Myh3 Gene Expression, EmyHC Protein Abundance, and My3 Protein Turnover
A.) Visualization of EmyHC (green) expression, counterstained with β-Laminin (red), at 7 days post CTX injection (Proliferation Stage). **B.)** Quantification of individual myofibers expressing

Embryonic Myosin Heavy Chain (EmyHC). Values are expressed as: number of myofibers / 100 uM^2 of tissue. **C.)** Gene expression (FPKM) of Myh3 during various stages of muscle regeneration. Significance determined by One-Way ANOVA with Benjamini-Hochberg correction for multiple comparisons. * $p<0.05$, ** $p<0.01$, *** $p<0.005$, **** $p<0.001$. **D.)** Myosin 3 (EmyHC) turnover per day (K) value during various stages of muscle regeneration. Significance determined by One-Way ANOVA with Benjamini-Hochberg correction for multiple comparisons. * $p<0.05$, ** $p<0.01$, *** $p<0.005$, **** $p<0.001$.

Supplemental Figure Legend

Figure S1 Proteomic Signature of Proliferation Stage, Compared to Contralateral Muscle **A.)** Overview of global proteome FSR changes between CTX and control (contralateral) muscle tissue after 4 days of CTX injection. Significance determined by Student's Paired T-Test with Benjamini Hochberg correction for multiple comparisons, * $p<0.05$, ** $p<0.01$, *** $p<0.005$, **** $p<0.001$. **B.)** Comparison of change in individual protein FSR value between CTX injected and control limbs for proteins that are significantly different after Benjamini Hochberg correction for multiple comparisons at 4 days after CTX injection (Proliferation Stage). **C.)** Protein Group analysis of proteins found during this stage and separated into ontologies based on NIH DAVID software analysis. Significance determined by Binomial Test of the proportion of proteins showing a higher or lower value of FSR in relation to control, * $p<0.05$.

Figure S2 Proteomic Signature of Differentiation Stage, Compared to Contralateral Muscle **A.)** Overview of global proteome FSR changes between CTX and control (contralateral) muscle tissue after 7 days of CTX injection (Differentiation Stage). Significance determined by Student's Paired T-Test with Benjamini Hochberg correction for multiple comparisons, * $p<0.05$, ** $p<0.01$, *** $p<0.005$, **** $p<0.001$. **B.)** Protein Group analysis of proteins found during this stage and separated into ontologies based on NIH DAVID software analysis. Significance determined by Binomial Test of the proportion of proteins showing a higher or lower value of FSR in relation to control, * $p<0.05$.

Figure S3 Proteomic Signature of Maturation Stage, Compared to Contralateral Muscle **A.)** Overview of global proteome FSR changes between CTX and control (contralateral) muscle tissue after 14 days of CTX injection. Significance determined by Student's Paired T-Test with Benjamini Hochberg correction for multiple comparisons, * $p<0.05$, ** $p<0.01$, *** $p<0.005$, **** $p<0.001$. **B.)** Comparison of change in individual protein FSR value between CTX injected and control limbs for proteins that are significantly different after Benjamini Hochberg correction for multiple comparisons at 14 days after CTX injection (Maturation Stage). **C.)** Protein Group analysis of proteins found during this stage and separated into ontologies based on NIH DAVID software analysis. Significance determined by Binomial Test of the proportion of proteins showing a higher or lower value of FSR in relation to control, * $p<0.05$.

Figures and Tables

<u>Figure 1</u> Time Course Layout & Visualization of Damage

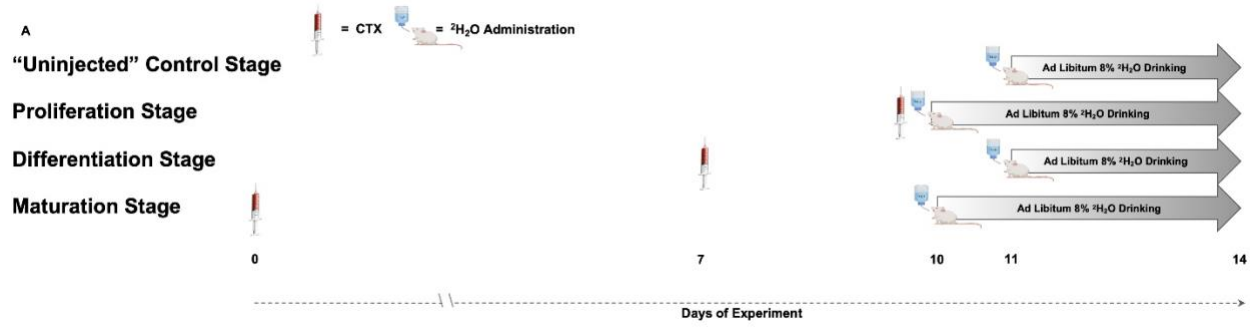

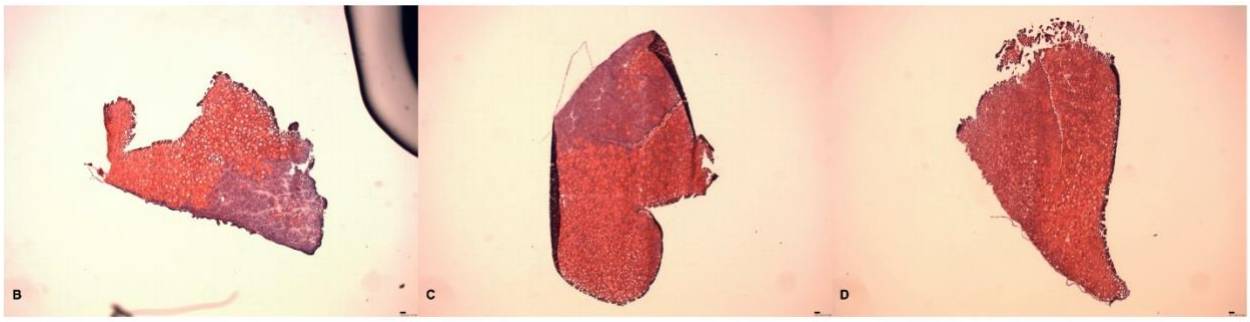

4 Days post-CTX | 7 Days post-CTX | 14 Days post-CTX

<u>Figure 2</u> DNA turnover, Visual Confirmation of Regeneration, & Gene Expression of Myogenic Genes

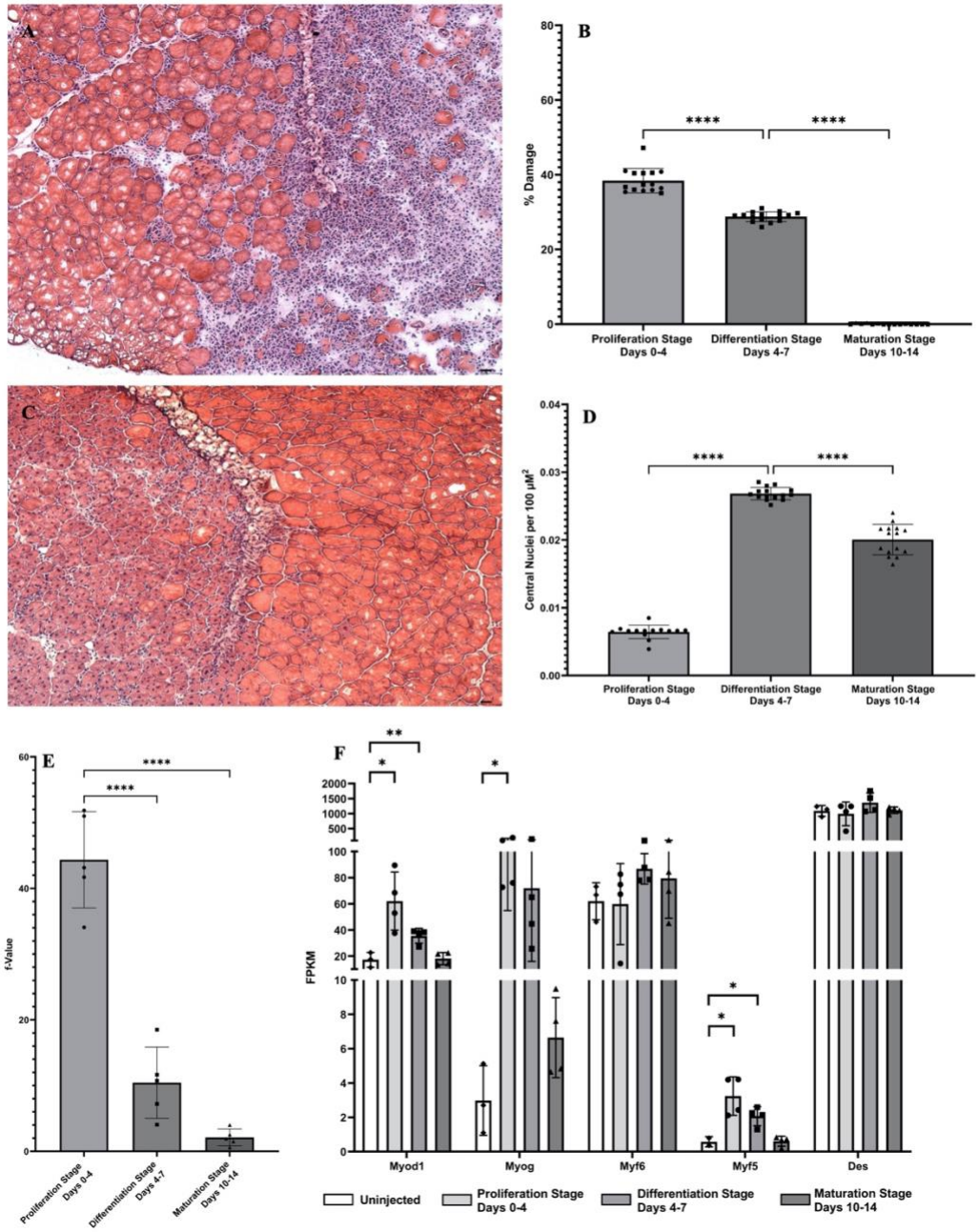

Table 1 Protein Turnover Values in Each Stage

#	Protein	Accession #	Ontology	Proliferation Stage	Differentiation Stage	Maturation Stage	Control
1	Succinate dehydrogenase iron-sulfur subunit	Q9CQA3	Mitochondria	**0.808 ± 0.115% ***	1.954 ± 1.042%		4.721 ± 0.422%
2	Cytochrome b-c1 complex subunit 1	Q9CZ13	OxPhos	**5.596 ± 0.541% ***	12.412 ± 9.133%	**6.976 ± 1.078% ***	2.664 ± 0.422%
3	Carbonic anhydrase 3	P16015	Cytoplasm	**0.670 ± 0.394% ***	8.890 ± 4.592%	**11.078 ± 4.185% ***	2.601 ± 0.406%
4	Triosephosphate isomerase	P17751	Glycolysis	**5.724 ± 1.021% ***	**14.663 ± 7.041% ***	**9.012 ± 2.761% ***	2.442 ± 0.388%
5	Aconitate hydratase	Q99KI0	Mitochondria	**1.635 ± 0.379% ***	12.255 ± 7.028%	**7.080 ± 1.327% ***	3.035 ± 0.347%
6	Collagen alpha 1(III) chain	P08121	Cytoplasm	**1.654 ± 0.271% ***	9.080 ± 4.471%	6.479 ± 3.281%	4.899 ± 0.871%
7	Trifunctional enzyme subunit alpha	Q8BMS1	Mitochondria	**0.267 ± 0.249% ***	12.798 ± 9.815%	6.165 ± 3.573%	3.062 ± 1.035%
8	Histone H2B type 1-M	P10854	Histone	**4.202 ± 1.405% ***	6.151 ± 1.995%	**3.112 ± 1.227% ***	1.066 ± 0.478%
9	Phosphoglycerate kinase 1	P09411	Glycolysis	1.020 ± 0.52%	12.825 ± 6.042%	**10.109 ± 3.629% ***	2.604 ± 0.595%
10	NADH dehydrogenase iron-sulfur protein 6	P52503	OxPhos	2.673 ± 0.083%	8.162 ± 2.842%	6.157 ± 2.794%	3.514 ± 0.437%
11	ATP synthase subunit beta	P56480	OxPhos	0.649 ± 0.759%	13.602 ± 8.869%	**7.125 ± 1.152% ***	2.160 ± 0.195%
12	Myosin light chain 1/3, skeletal muscle isoform	P05977	Myofibril	2.769 ± 0.588%	**18.116 ± 9.806% ***	**8.845 ± 2.706% ***	1.703 ± 0.283%
13	Phosphatidylethanolamine-binding protein 1	P70296	Cytoplasm	23.658 ± 10.397%	17.715 ± 15.136%	7.51 ± 4.171%	3.586 ± 2.677%
14	Phosphoglucomutase-1	Q9D0F9	Glycolysis	1.329 ± 0.513%	12.066 ± 6.393%	**8.285 ± 3.023% ***	2.342 ± 0.399%
15	Albumin	P07724	Extracellular	1.424 ± 0.878%	13.691 ± 4.993%	**15.629 ± 2.807% ***	7.128 ± 3.629%
16	Myosin regulatory light chain 2, skeletal muscle isoform	P97457	Myofibril	3.144 ± 0.913%	**15.749 ± 8.367% ***	**8.751 ± 3.235% ***	1.717 ± 0.263%
17	Myosin-binding protein C, fast-type	Q5XKE0	Myofibril	20.593 ± 11.934%	22.170 ± 14.392%	**12.214 ± 5.419% ***	2.642 ± 0.985%
18	ATP synthase subunit g	Q9CPQ8	OxPhos	1.891 ± 0.362%	6.708 ± 3.219%	**6.953 ± 1.743% ***	0.644 ± 0.555%
19	L-lactate dehydrogenase A chain	P06151	Glycolysis	5.692 ± 2.301%	**15.812 ± 8.103% ***	**10.292 ± 3.334% ***	2.186 ± 0.442%
20	Hemoglobin subunit alpha	P01942	Extracellular	5.674 ± 2.723%	1.829 ± 0.147%	2.522 ± 0.502%	1.804 ± 0.491%
21	Collagen alpha 1(I) chain	P11087	Cytoplasm	2.334 ± 1.142%	6.409 ± 5.525%	4.682 ± 1.466%	3.910 ± 0.311%
22	Vertnin	Q3SYK4	Cytoplasm	1.300 ± 0.312%	1.723 ± 0.078%	**1.062 ± 0.078% ***	2.030 ± 0.476%
23	Glyceraldehyde-3-phosphate dehydrogenase	P16858	Glycolysis	1.221 ± 0.768%	**14.165 ± 6.491% ***	**10.292 ± 3.231% ***	2.414 ± 0.416%
24	Cytochrome c, somatic	P62897	OxPhos	0.379 ± 0.304%	12.135 ± 5.266%	**8.427 ± 0.991% ***	2.965 ± 0.941%
25	Calsequestrin-1	O09165	Cytoplasm	2.422 ± 1.152%	16.316 ± 10.359%	**7.922 ± 2.732% ***	1.067 ± 0.545%
26	Actin, alpha skeletal muscle	P68134	Myofibril	2.745 ± 1.511%	15.038 ± 7.593%	**6.514 ± 1.614% ***	1.136 ± 0.510%
27	Titin	A2ASS6	Myofibril	1.257 ± 0.947%	7.304 ± 5.401%	2.240 ± 1.205%	2.388 ± 0.611%
28	Malate dehydrogenase	P08249	Mitochondria	38.498 ± 31.447%	11.888 ± 7.637%	**6.811 ± 1.574% ***	2.171 ± 0.412%
29	Myosin light chain 3	P09542	Myofibril	2.029 ± 0.489%	13.340 ± 11.791%	8.709 ± 3.725%	3.654 ± 1.621%
30	ADP/ATP translocase 1	P48962	Mitochondria	2.271 ± 0.783%	20.589 ± 9.866%	**9.328 ± 1.604% ***	3.912 ± 1.588%
31	Parvalbumin alpha	P32848	Extracellular	7.899 ± 3.726%	12.598 ± 10.416%	**11.055 ± 2.638% ***	4.406 ± 1.471%
32	Aspartate aminotransferase	P05201	Cytoplasm	7.616 ± 5.416%	9.385 ± 4.313%	6.651 ± 4.126%	2.419 ± 0.991%
33	NADH dehydrogenase 1 beta subcomplex subunit 10	Q9DCS9	OxPhos	0.678 ± 0.197%	14.674 ± 7.989%	**6.729 ± 1.887% ***	1.739 ± 0.895%
34	Glycogen phosphorylase, muscle form	Q9WUB3	Glycolysis	3.023 ± 0.667%	18.813 ± 7.782%	**12.908 ± 3.501% ***	3.732 ± 0.561%

35	Myozenin-1	Q9JK37	Myofibril	6.098 ± 2.751%	4.098 ± 2.064%	2.262 ± 1.449%	3.517 ± 1.355%
36	Pyruvate kinase PKM	P52480	Glycolysis	4.596 ± 1.726%	15.914 ± 7.028%	**11.808 ± 3.548% ***	3.038 ± 0.533%
37	Myoglobin	P04247	Extracellular	2.635 ± 0.248%	12.661 ± 6.126%	**9.071 ± 3.379% ***	3.216 ± 0.700%
38	Fructose-bisphosphate aldolase A	P05064	Glycolysis	2.848 ± 0.989%	17.324 ± 6.718%	**14.635 ± 4.516% ***	3.739 ± 0.572%
39	Parkinson disease protein 7 homolog	Q99LX0	Cytoplasm	4.725 ± 3.626%	9.929 ± 2.413%	**8.499 ± 4.634% ***	1.454 ± 0.852%
40	Troponin T, fast skeletal muscle	Q9QZ47	Myofibril	2.339 ± 1.719%	23.964 ± 10.275%	**12.996 ± 3.924% ***	3.483 ± 0.242%
41	LIM domain-binding protein 3	Q9JKS4	Cytoplasm	2.589 ± 0.743%	**13.857 ± 6.588% ***	**7.606 ± 2.068% ***	1.676 ± 1.034%
42	Actin, alpha cardiac muscle 1	P68033	Myofibril	2.162 ±1.218%	15.755 ± 7.358%	**6.709 ± 1.859% ***	1.310 ± 0.585%
43	Histone H4	P62806	Histone	4.315 ± 1.31%	8.854 ± 3.891%	**3.732 ± 1.013%**	6.602 ± 3.354%
44	Sarcoplasmic/endoplasmic reticulum calcium ATPase 1	Q8R429	Cytoplasm	3.372 ± 0.913%	12.162 ± 6.198%	**11.181 ± 2.325% ***	2.817 ± 0.330%
45	Alpha-actinin-3	O88990	Myofibril	6.104 ± 5.176%	18.834 ± 16.162%	**9.670 ± 2.019% ***	3.317 ± 0.560%
46	Phosphoglycerate mutase 2	O70250	Glycolysis	1.863 ± 0.543%	**12.236 ± 5.528% ***	**9.897 ± 3.362% ***	2.199 ± 0.390%
47	Cytochrome b-c1 complex subunit 7	Q9D855	OxPhos	5.99 ± 4.283%	14.071 ± 10.397%	9.180 ± 4.145%	3.208 ± 0.168%
48	ATP synthase subunit O	Q9DB20	OxPhos	0.933 ± 0.428%	12.058 ± 6.922%	**8.408 ± 1.559% ***	1.938 ± 1.097%
49	ATP synthase subunit d	Q9DCX2	OxPhos	2.636 ± 2.595%	14.703 ± 10.311%	**8.299 ± 0.921% ***	4.226 ± 1.229%
50	Tropomyosin beta chain	P58774	Myofibril	3.483 ± 1.545%	20.450 ± 9.492%	**9.634 ± 2.737% ***	2.7645 ± 0.676%
51	Aspartate aminotransferase	P05202	Mitochondria	3.321 ± 1.854%	13.195 ± 9.701%	**5.799 ± 0.211% ***	1.958 ± 1.162%
52	Dihydrolipoyl dehydrogenase	O08749	Mitochondria	4.188 ± 1.905%	15.802 ± 9.119%	**10.881 ± 1.704% ***	5.727 ± 1.009%
53	ADP/ATP translocase 2	P51881	Mitochondria	2.256 ± 1.237%	**12.591 ± 3.295% ***	7.058 ± 2.584%	3.200 ± 1.467%
54	Glucose-6-phosphate isomerase	P06745	Glycolysis	2.091 ± 1.296%	14.763 ± 6.794%	**9.576 ± 3.205% ***	1.549 ± 0.269%
55	Nucleoside diphosphate kinase B	Q01768	Cytoplasm	3.518 ± 1.34%	10.913 ± 4.194%	3.092 ± 0.888%	2.918 ± 0.759%
56	Myosin-3	P13541	Myofibril	3.098 ± 0.502%	**17.741 ± 6.788% ***	**8.632 ± 2.026% ***	2.845 ± 0.454%
57	Creatine kinase M-type	P07310	Cytoplasm	2.088 ± 0.683%	12.766 ± 7.031%	**10.725 ± 3.614% ***	2.334 ± 0.334%
58	Adenylate kinase isoenzyme 1	Q9R0Y5	Cytoplasm	6.56 ± 6.691%	13.356 ± 8.524%	10.091 ± 3.218%	2.676 ± 1.245%
59	Pyruvate dehydrogenase E1 component subunit beta	Q9D051	Mitochondria	1.402 ± 0.531%	17.912 ± 17.817%	**10.069 ± 3.588% ***	1.7367 ± 0.485%
60	Centrosomal protein of 162 kDa	Q6ZQ06	Cytoplasm	0.998 ± 0.807%	1.029 ± 0.223%		0.503 ± 0.101%
61	Troponin C, skeletal muscle	P20801	Myofibril	4.432 ± 2.101%	23.207 ± 12.899%	**12.944 ± 0.351% ***	3.645 ± 0.702%
62	Myosin-7	Q91Z83	Myofibril	2.919 ± 0.552%	19.078 ± 8.624%	**10.105 ± 3.507% ***	2.692 ± 0.692%
63	NADH-ubiquinone oxidoreductase 75 kDa subunit	Q91VD9	OxPhos	2.253 ± 1.163%	13.502 ± 9.761%	**9.697 ± 0.154% ***	2.645 ± 1.129%
64	Tropomyosin alpha-1 chain	P58771	Myofibril	3.292 ± 1.068%	**24.316 ± 11.703% ***	**12.135 ± 3.619% ***	3.051 ± 0.435%
65	Desmoglein-4	Q7TMD7	Extracellular	2.278 ± 0.358%	6.637 ± 1.868%	**6.252 ± 1.573% ***	2.543 ± 1.875%
66	Troponin I, fast skeletal muscle	P13412	Myofibril	2.772 ± 3.786%	14.408 ± 9.648%	**11.275 ± 3.391% ***	3.120 ± 0.638%
67	ATP synthase subunit alpha	Q03265	OxPhos	3.069 ± 2.453%	13.685 ± 8.443%	**7.798 ± 0.997% ***	2.821 ± 0.628%
68	Beta-enolase	P21550	Glycolysis	2.993 ± 0.806%	15.768 ± 6.887%	**9.799 ± 2.771% ***	2.928 ± 0.528%
69	Myosin-4	Q5SX39	Myofibril	2.617 ± 0.525%	13.03 ± 6.334%	**8.540 ± 2.271% ***	2.579 ± 0.395%
70	Collagen alpha-2(I) chain	Q01149	Cytoplasm	1.749 ± 0.882%	6.855 ± 5.648%	4.358 ± 0.173%	1.853 ± 0.134%
71	Cytochrome b-c1 complex subunit 2	Q9DB77	OxPhos	3.741 ± 0.687%	12.696 ± 8.177%	**7.910 ± 1.345% ***	3.716 ± 0.187%

72	Myosin-1	Q5SX40	Myofibril	2.662 ± 0.771%	**18.191 ± 10.073% ***	**7.138 ± 1.637% ***	2.675 ± 0.572%
73	Superoxide dismutase [Mn]	P09671	Mitochondria	1.881 ± 0.811%	7.240 ± 5.53%	**5.747 ± 2.585% ***	1.869 ± 0.356%
74	Heat shock cognate 71 kDa protein	P63017	Cytoplasm		18.396 ± 6.43%	**9.970 ± 0.024% ***	5.112 ± 2.252%
75	Alpha-enolase	P17182	Glycolysis		11.379 ± 3.973%	**7.056 ± 2.348% ***	3.629 ± 0.958%
76	Histone H2A type 1-B	C0HKE1	Histone		5.011 ± 1.761%	**1.908 ± 0.636% ***	0.155 ± 0.068%
77	Ubiquinone biosynthesis protein COQ9	Q8K1Z0	Mitochondria		**11.913 ± 4.233% ***	**10.460 ± 3.135% ***	2.646 ± 0.885%
78	E3 ubiquitin-protein ligase UBR4	A2AN08	Cytoplasm		**13.175 ± 5.817% ***	**7.763 ± 2.892% ***	2.687 ± 0.388%
79	E3 ubiquitin-protein ligase UBR3	Q5U430	Cytoplasm		**27.949 ± 15.189% ***	**17.507 ± 7.163% ***	1.223 ± 1.009%
80	Very long-chain specific acyl-CoA dehydrogenase	P50544	Mitochondria		16.838 ± 7.417%	8.786 ± 3.464%	3.402 ± 1.956%
81	Creatine kinase S-type	Q6P8J7	Mitochondria		7.134 ± 2.504%	**8.734 ± 2.252% ***	2.673 ± 0.425%
82	Cytochrome c oxidase subunit 6C	Q9CPQ1	OxPhos		14.812 ± 6.971%	**7.436 ± 3.237%**	2.863 ± 0.368%
83	Sarcalumenin	Q7TQ48	Cytoplasm		13.037 ± 7.622%	**6.788 ± 2.051% ***	1.861 ± 0.849%
84	NADH dehydrogenase flavoprotein 1	Q91YT0	OxPhos		13.358 ± 6.28%	**8.120 ± 2.029% ***	2.638 ± 0.931%
85	Keratin, type II cytoskeletal 1	P04104	Cytoplasm		12.781 ± 2.845%	8.523 ± 3.349%	6.156 ± 2.426%
86	Voltage-dependent anion-selective channel protein 2	Q60930	Mitochondria		17.969 ± 10.852%	**16.622 ± 9.964% ***	1.172 ± 0.341%
87	2-oxoglutarate dehydrogenase	Q60597	Mitochondria		12.728 ± 4.676%	**10.484 ± 0.553%**	4.590 ± 2.8085%
88	MICOS complex subunit Mic60	Q8CAQ8	Mitochondria		12.908 ± 6.049%	**13.049 ± 3.866% ***	2.017 ± 0.955%
89	ATP synthase-coupling factor 6	P97450	OxPhos		13.338 ± 8.724%	**4.843 ± 1.787% ***	0.727 ± 0.437%
90	Cytochrome c oxidase subunit 4 isoform 1	P19783	OxPhos		13.407 ± 6.626%	**9.101 ± 1.772% ***	3.773 ± 1.137%
91	Isocitrate dehydrogenase [NAD] subunit alpha	Q9D6R2	OxPhos		12.691 ± 6.118%	**5.350 ± 2.844%**	3.388 ± 1.499%
92	Malate dehydrogenase	P14152	Cytoplasm		10.222 ± 6.133%	**9.054 ± 3.799% ***	3.049 ± 0.749%
93	Citrate synthase	Q9CZU6	Mitochondria		13.995 ± 8.577%	**8.780 ± 1.445% ***	2.581 ± 0.272%
94	Cytochrome c oxidase subunit NDUFA4	Q62425	OxPhos		19.203 ± 9.895%	**13.529 ± 3.471% ***	4.204 ± 1.703%
95	Voltage-dependent anion-selective channel protein 1	Q60932	Mitochondria		12.654 ± 8.096%	**10.117 ± 2.361% ***	2.609 ± 0.838%
96	Cytochrome c oxidase subunit 2	P00405	OxPhos		12.272 ± 9.047%	**6.237 ± 1.392% ***	1.093 ± 0.249%
97	Cytochrome c oxidase subunit 6B1	P56391	OxPhos		15.028 ± 10.416%	**8.420 ± 1.31% ***	2.232 ± 0.255%
98	Alpha-actinin-2	Q9JI91	Myofibril		15.588 ± 9.833%	**8.145 ± 1.074% ***	3.641 ± 0.774%
99	Cytochrome c oxidase subunit 5B	P19536	OxPhos		13.394 ± 9.383%	**7.503 ± 1.776% ***	2.547 ± 0.453%
100	Myelin protein P0	P27573	Cytoplasm		9.877 ± 7.41%	**9.217 ± 2.874% ***	2.321 ± 1.902%
101	NADH dehydrogenase 1 beta subcomplex subunit 1	P0DN34	OxPhos		16.550 ± 11.136%	**8.989 ± 1.226% ***	3.945 ± 0.583%
102	Cytochrome b-c1 complex subunit Rieske	Q9CR68	OxPhos		12.612 ± 8.751%	**8.267 ± 1.666% ***	2.817 ± 0.305%
103	ATP synthase subunit gamma	Q91VR2	OxPhos		12.435 ± 8.037%	**6.224 ± 1.147% ***	1.698 ± 0.066%
104	Cytochrome c1, heme protein	Q9D0M3	OxPhos		11.024 ± 7.245%	**6.761 ± 0.793% ***	3.057 ± 0.585%
105	Cytochrome b-c1 complex subunit 6	P99028	OxPhos		12.398 ± 9.641%	**5.770 ± 0.133% ***	1.871 ± 0.452%
106	Cytochrome b-c1 complex subunit 8	Q9CQ69	OxPhos		14.625 ± 10.285%	9.990 ± 0.663%	4.041 ± 0.685%
107	Elongation factor 1-alpha 2	P62631	Cytoplasm		17.518 ± 14.891%	**10.873 ± 2.597% ***	4.156 ± 2.371%

108	NADH dehydrogenase [ubiquinone] 1 alpha subcomplex subunit 7	Q9Z1P6	OxPhos		18.110 ± 12.195%	**11.246 ± 1.436% ***	5.817 ± 0.602%
109	Cytochrome c oxidase subunit 5A	P12787	OxPhos		14.048 ± 10.802%	**8.566 ± 0.965% ***	3.395 ± 0.516%
110	NADH dehydrogenase 1 alpha subcomplex subunit 8	Q9DCJ5	OxPhos		15.487 ± 12.898%	**11.041 ± 1.409% ***	3.267 ± 0.563%
111	Triadin	E9Q9K5	Cytoplasm		15.377 ± 13.226%	**8.131 ± 1.473% ***	3.556 ± 0.703%
112	Calcium-binding mitochondrial carrier protein Aralar1	Q8BH59	Mitochondria		10.569 ± 5.878%	**8.784 ± 2.103% ***	2.452 ± 1.022%
113	NADH dehydrogenase iron-sulfur protein 3	Q9DCT2	OxPhos		7.959 ± 4.907%	7.905 ± 3.656%	3.710 ± 0.145%
114	NADH dehydrogenase 1 beta subcomplex subunit 9	Q9CQJ8	OxPhos		13.572 ± 10.199%	2.870 ± 1.765%	3.540 ± 1.634%
115	ATP-dependent 6-phosphofructokinase, muscle type	P47857	Glycolysis		12.190 ± 10.024%	**16.549 ± 4.776% ***	5.001 ± 1.547%
116	NADH dehydrogenase iron-sulfur protein 5	Q99LY9	OxPhos		13.174 ± 10.451%	**7.292 ± 1.487% ***	3.188 ± 0.748%
117	NADH dehydrogenase iron-sulfur protein 8	Q8K3J1	OxPhos		14.293 ± 13.812%	6.928 ± 3.745%	1.944 ± 0.159%
118	Succinate dehydrogenase flavoprotein subunit	Q8K2B3	Mitochondria		10.575 ± 5.816%	7.172 ± 3.902%	5.272 ± 2.281%
119	ATP synthase subunit delta	Q9D3D9	OxPhos		4.852 ± 3.366%	3.765 ± 1.253%	1.343 ± 0.017%
120	NADH dehydrogenase flavoprotein 2	Q9D6J6	OxPhos		7.424 ± 5.079%	4.547 ± 0.277%	3.601 ± 0.433%
121	ATP synthase F (0) complex subunit B1	Q9CQQ7	OxPhos		12.538 ± 8.688%	7.485 ± 1.505%	6.824 ± 6.658%
122	Glycerol-3-phosphate dehydrogenase	Q64521	Mitochondria		12.417 ± 9.942%	11.004 ± 2.957%	4.086 ± 1.487%
123	Cytochrome c oxidase subunit 6A2	P43023	OxPhos		18.43 ± 11.419%	12.832 ± 3.977%	7.717 ± 3.418%
124	NADH dehydrogenase 1 alpha subcomplex subunit 9	Q9DC69	OxPhos		9.906 ± 5.739%	8.373 ± 1.546%	5.375 ± 1.076%
125	Hemoglobin subunit beta 1	P02088	Extracellular		2.987 ± 0.566%	2.933 ± 0.685%	2.598 ± 0.668%
126	Electron transfer flavoprotein subunit alpha	Q99LC5	OxPhos		8.782 ± 9.531%	9.228 ± 2.616%	4.549 ± 0.808%
127	Phosphate carrier protein	Q8VEM8	Mitochondria		2.824 ± 1.441%	6.119 ± 3.707%	3.548 ± 2.193%

<u>Figure 3</u> Global Protein Turnover Rates at Each Stage

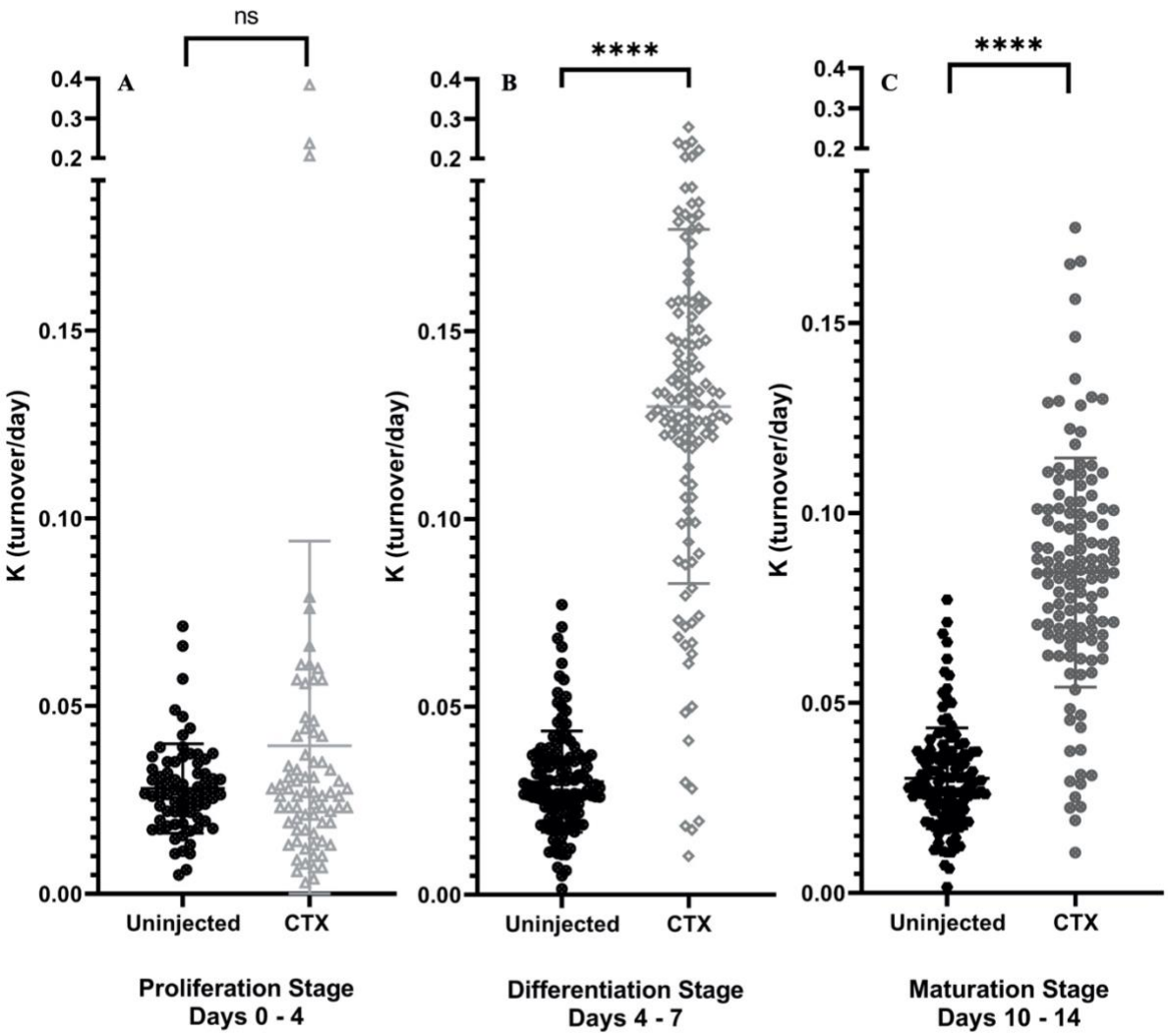

<u>Figure 4</u> Changes in Protein Group Turnover Rates in Each Stage

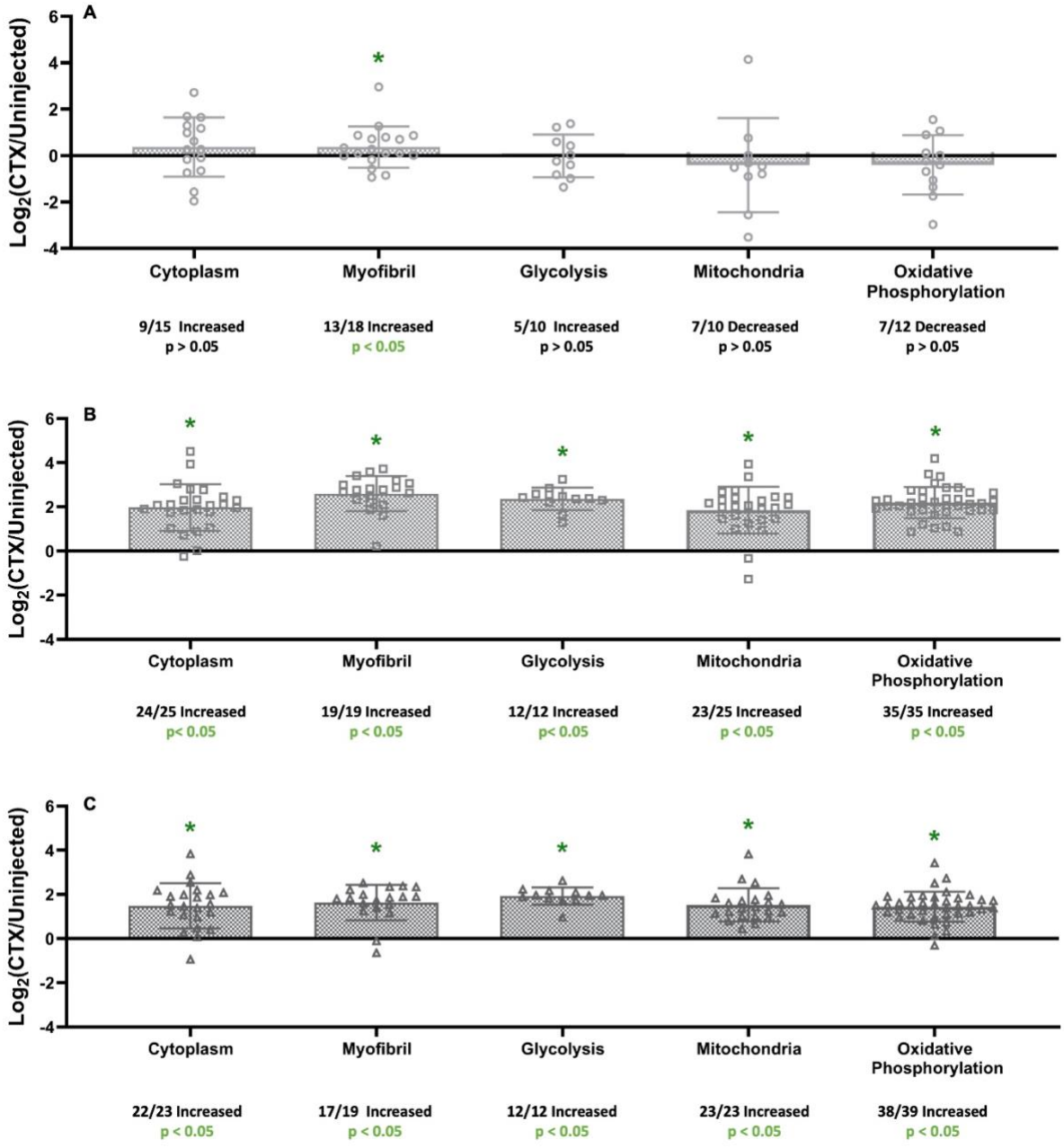

<u>Figure 5</u> Significantly Different Individual Protein Turnover Rates at Each Stage

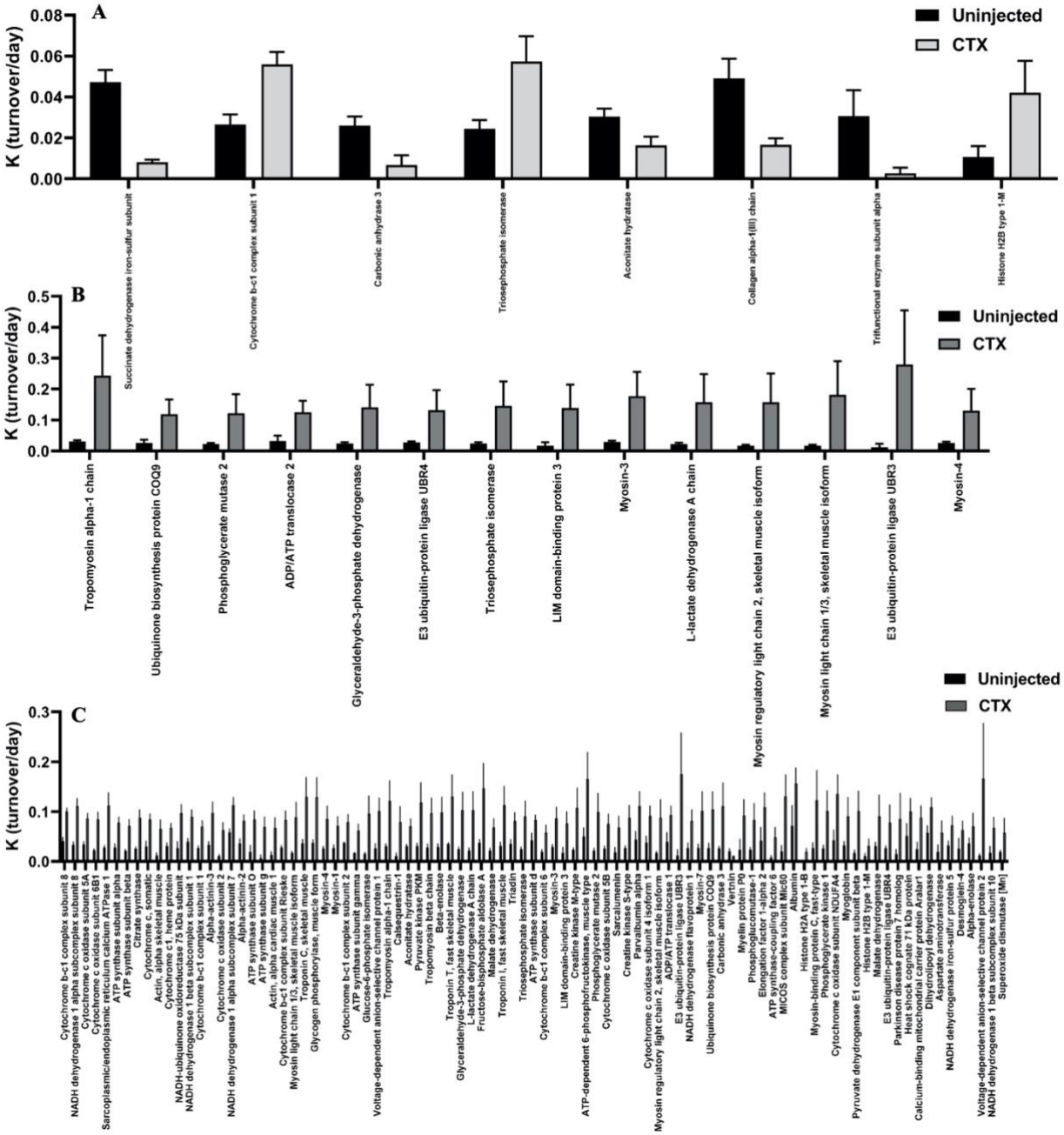

<u>Figure 6</u> Global Gene Expression at Each Stage

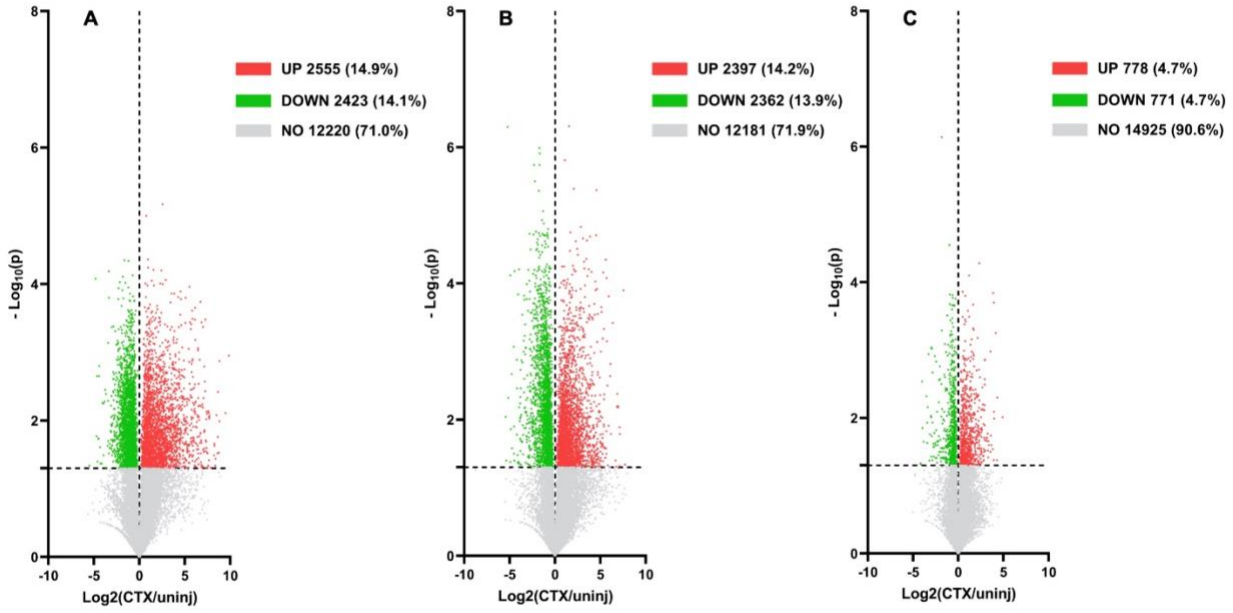

<u>Figure 7</u> Gene Expression at Each Stage to Matched Individual Proteins in Group Ontologies

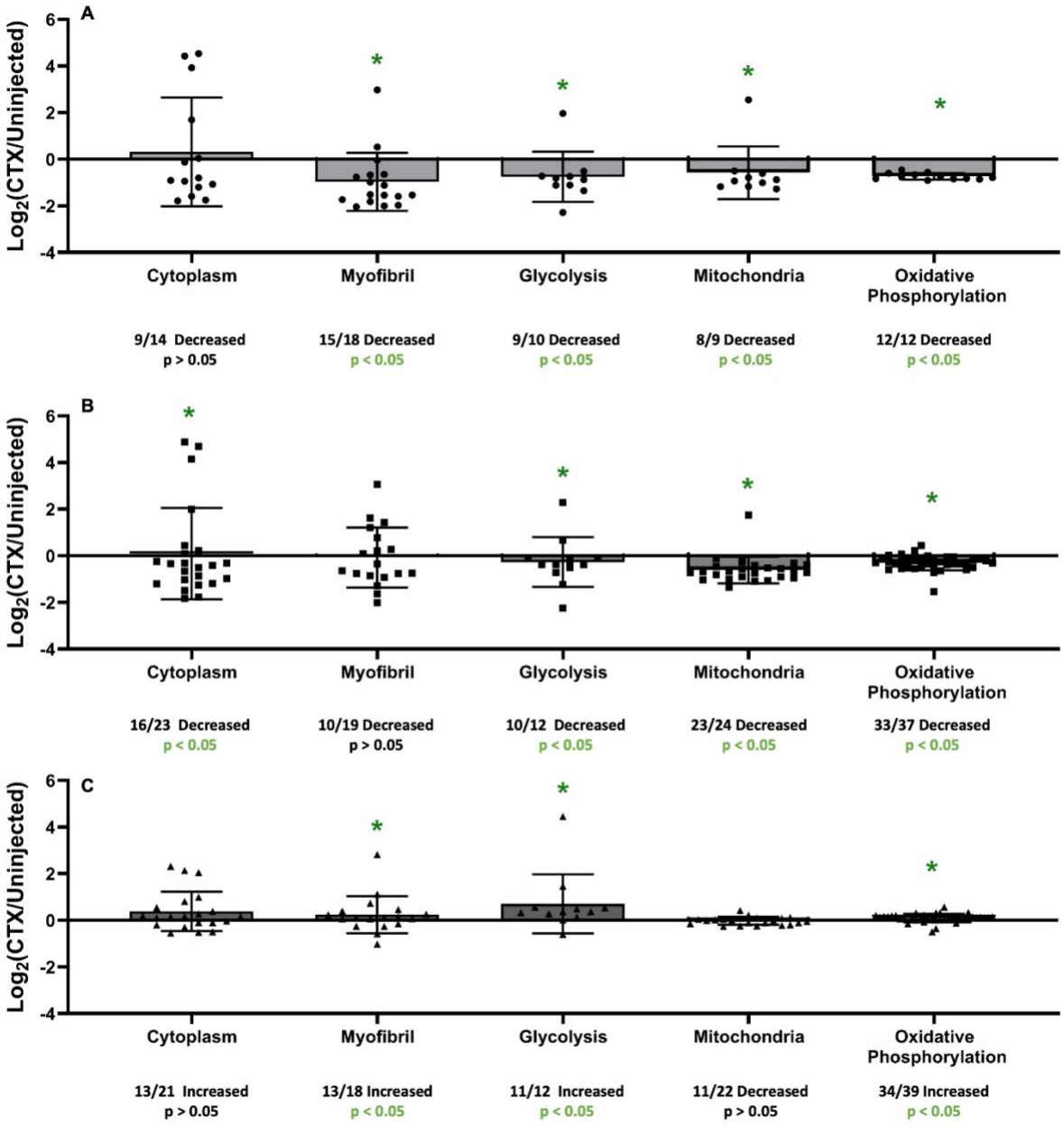

<u>Figure 8</u> Correlations of Gene Expression to Protein FSR

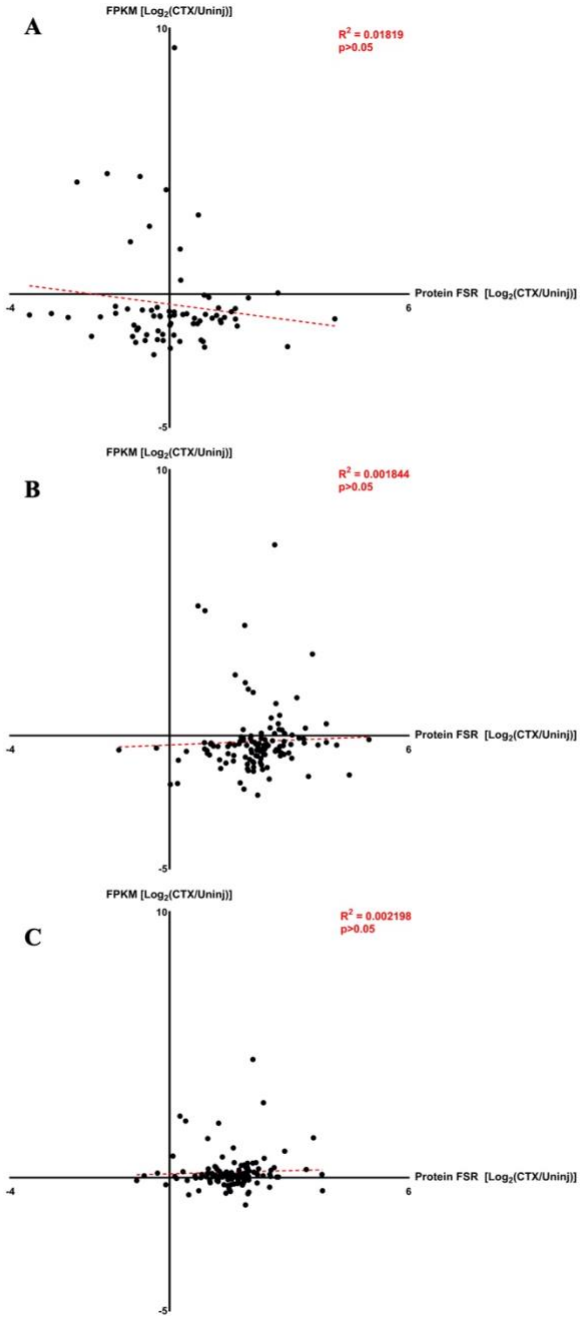

Figure 9 Myh3 Gene Expression, EmyHC Protein Abundance, and My3 Protein Turnover

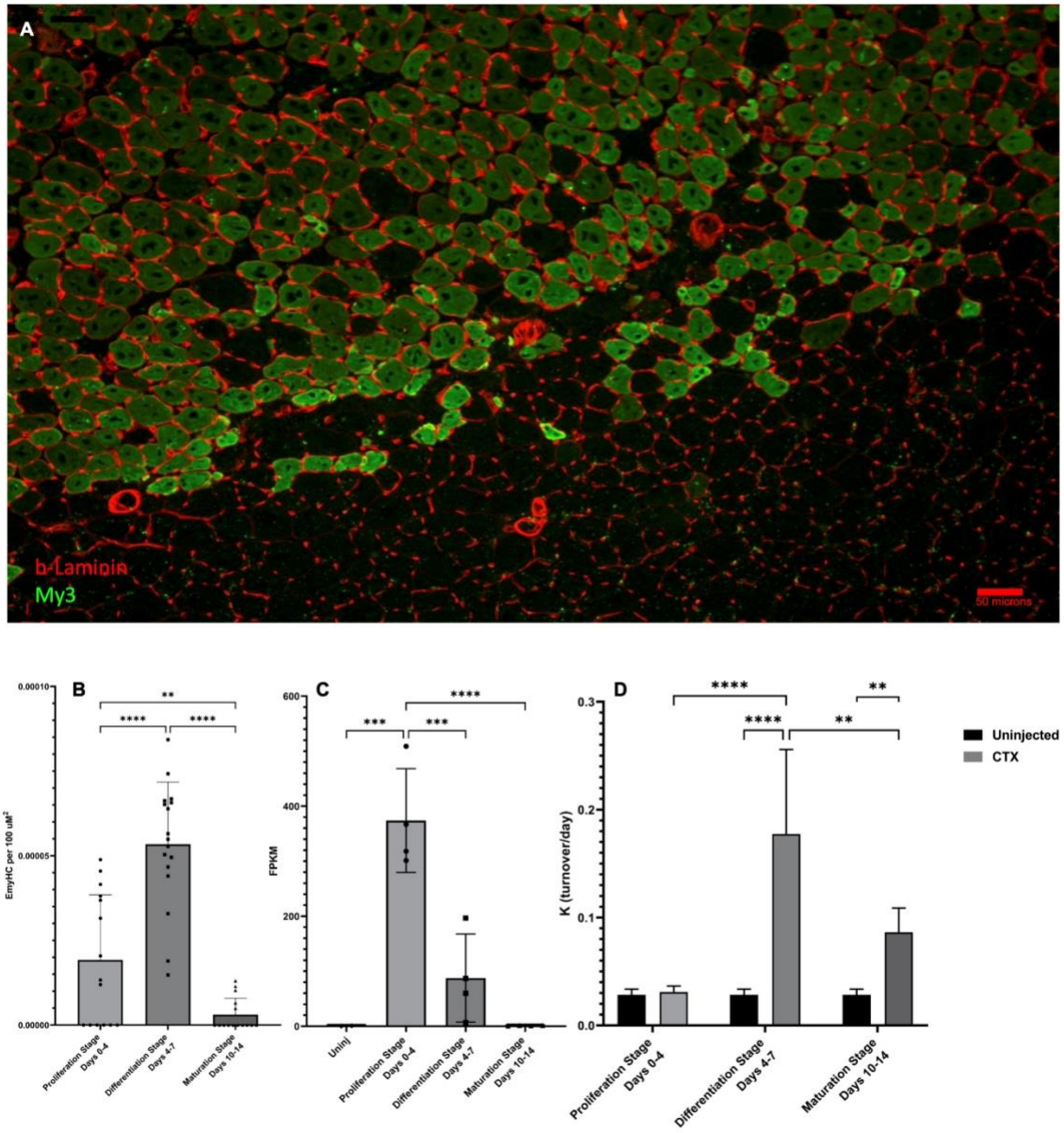

<u>Figure S1</u> Proteomic Signature of Proliferation Stage, Compared to Contralateral Muscle

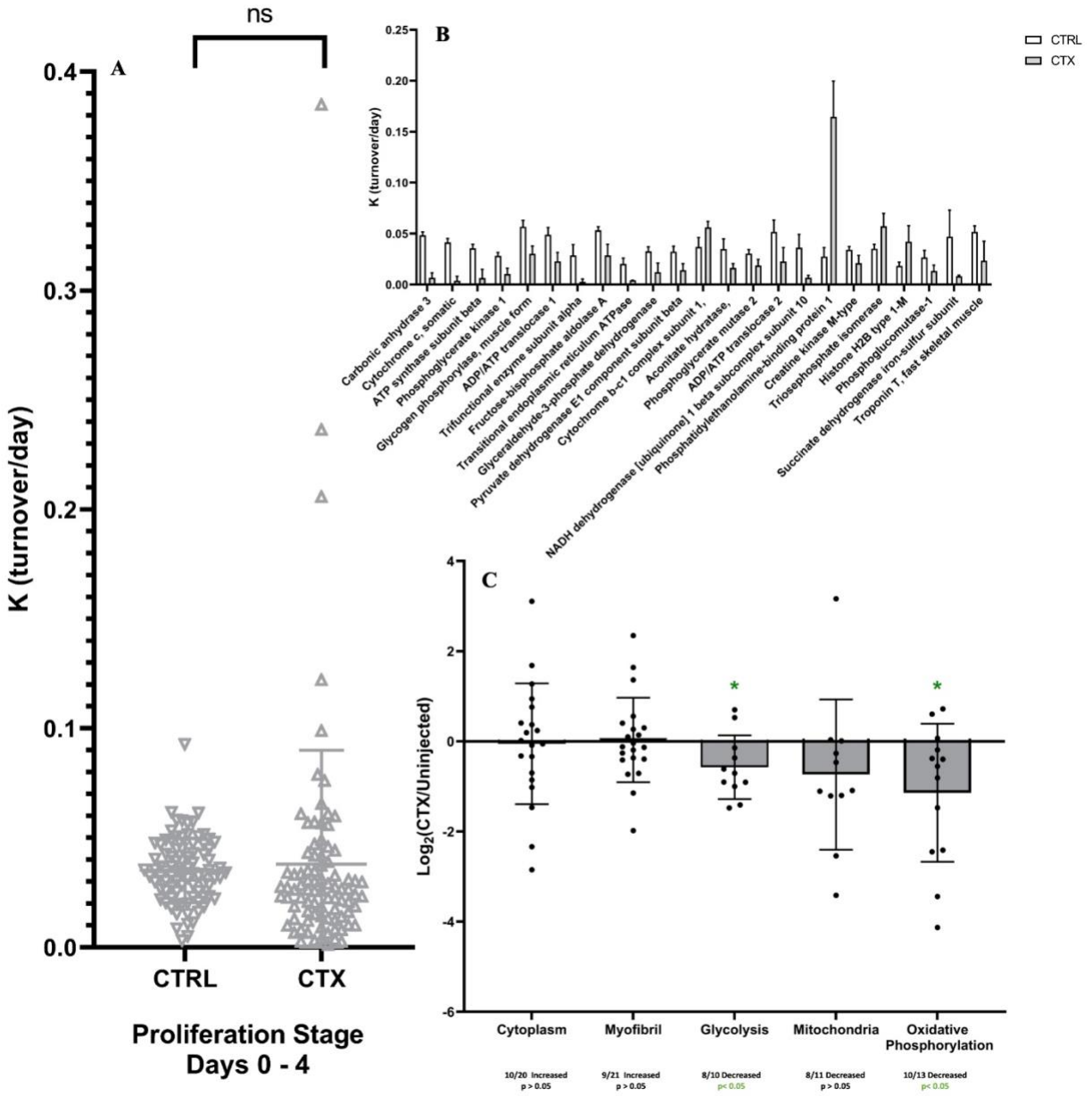

<u>Figure S2</u> Proteomic Signature of Differentiation Stage, Compared to Contralateral Muscle

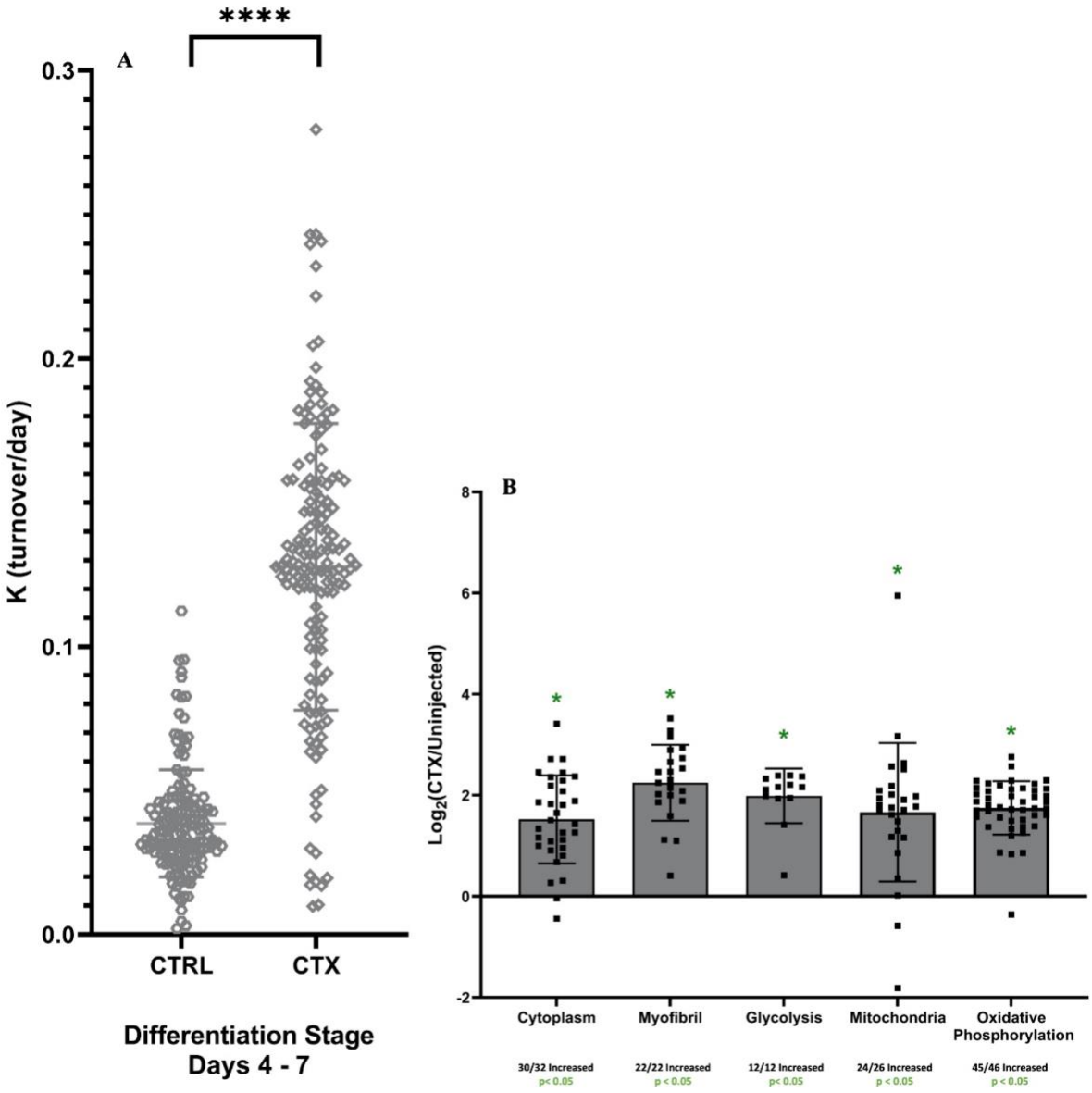

<u>Figure S3</u> Proteomic Signature of Maturation Stage, Compared to Contralateral Muscle

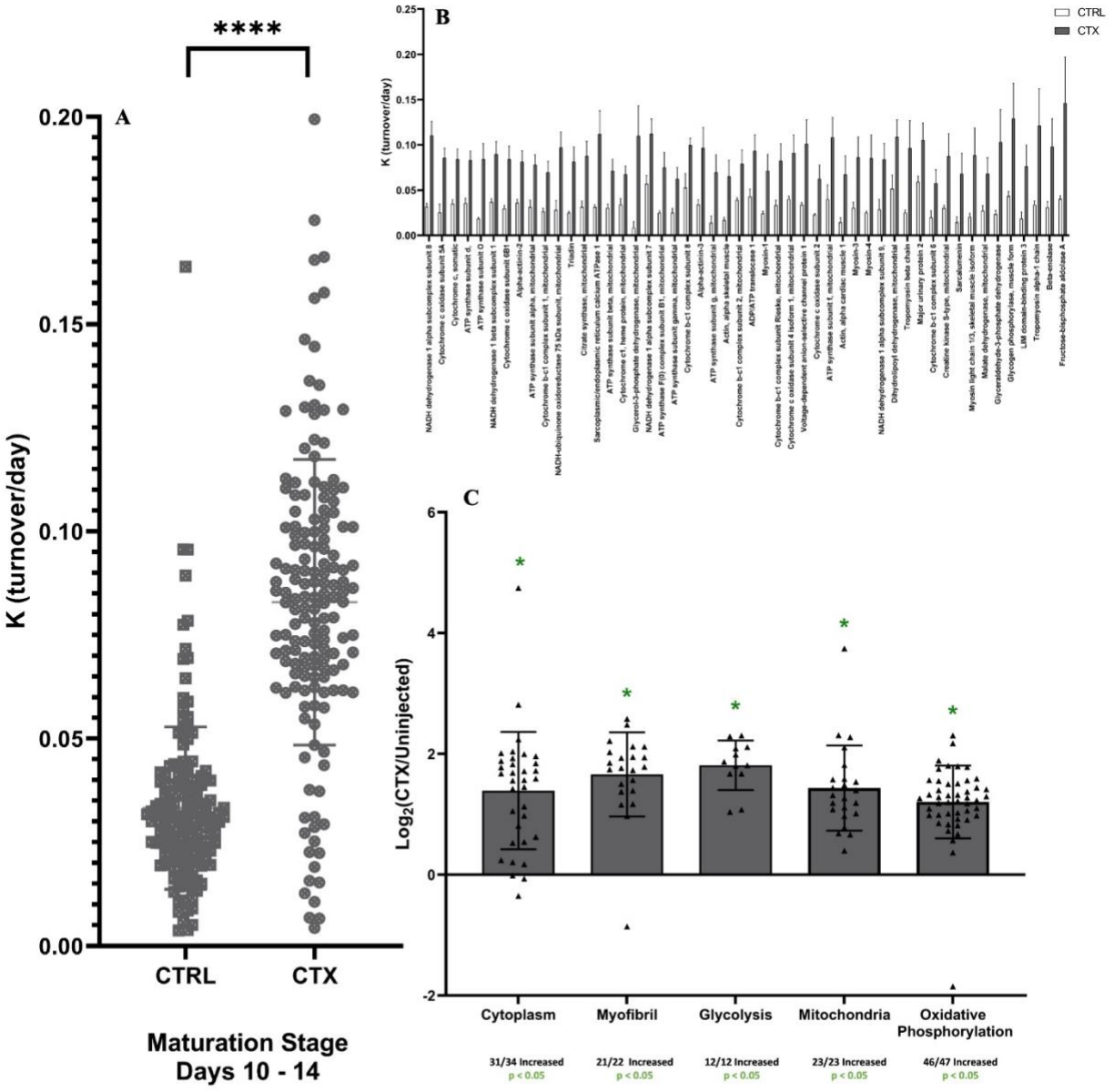

Chapter 4

Changes in Protein Fluxes in Non-Injured Muscle Tissue Distant from an Acute Myotoxic Injury

Keywords: Muscle Damage/Injury; *In-Vivo* Regeneration; Satellite Cells; Proteomics; Stable Isotope Labeling; Mass Spectrometry; Protein Turnover

Alec Bizieff [1], Maggie Cheng [1,] Kelvin Chang [1,] Hussein Mohammed [1], Naveed Ziari [1], Edna Nyangau [1], Mark Fitch [1], and Marc K. Hellerstein [1]

[1] Department of Nutritional Sciences & Toxicology, University of California, Berkeley

Correspondence:
Marc K. Hellerstein
march@berkeley.edu
University of California, Berkeley
Berkeley, CA United States

Abstract

Skeletal muscle repair and regeneration after damage or injury is an important biological process that helps maintain healthy and functional contractile tissue on the body. The process requires stimulation of local repair mechanisms in the damaged tissue. An interesting question is whether muscle tissues distant from an acute muscle injury are altered through circulating factors. It has been reported that satellite cells (MuSCs) in tissue distant from acute injury can enter a functional state between quiescence and active proliferation. However, little is known about how global, ontology-grouped, or individual protein flux rates are affected in tissue distant from acute injury, and how protein flux rates correlate to gene expression. We employed an approach that couples deuterated water (^2H_2O) administration with liquid chromatography-mass spectrometry (LC-MS) to measure *in-vivo* protein turnover at unique sequential stages along the muscle regeneration timeline in muscle that was distant to cardiotoxin-induced injury. We compared the turnover kinetics of over 100 proteins in distant muscle and compared bulk RNA-sequencing (RNA-seq) data. Significant alterations and signatures were observed sequentially for both protein turnover and gene expression profiles. Protein turnover in the liver was not altered, suggesting that contralateral muscle changes are not explained by systemic inflammation. Interestingly, the mRNA changes did not reveal changes in directly measured protein turnover rates. In summary, there are systemic effects on protein turnover in skeletal muscle distant from myotoxic injury and these are not revealed at the mRNA level, consistent with post-transcriptional effects.

Introduction

An important feature of skeletal muscle is its capacity to regenerate new myofibers after damage or injury to the tissue. The regenerative capacity of muscle tissue is attributed to a small portion of progenitor stem cells that are peripherally located on the myofiber, known as satellite cells (MuSCs) [1, 2, 3]. Upon activation, the MuSCs exit from quiescence to enter the cell cycle, proliferate, and then exit to either replenish the quiescent MuSC pool or differentiate towards mature myofibers that can reintegrate into existing tissue. The MuSC's ability to transition from a stage of quiescence to activation in response to damage is a crucial step that ultimately determines the efficiency and completeness of a regenerative event. In certain ailments like musculoskeletal disease and sarcopenia, there is a documented impairment of MuSC's ability to exit this dormant state and actively contribute to tissue repair [4, 5, 39]. A betterer understanding of this process may lead to the development of therapies that can combat the pathology of many of the previously mentioned ailments.

Until recently, it was thought that MuSCs would occupy only one of two states: actively proliferating in the cell-cycle or maintaining quiescence in the G_0 phase. However, a recent paper by Rodgers et al. reported that MuSCs can enter an intermediate stage between the two to prepare for a future regenerative event by transitioning from quiescent to a "primed" $G_{"Alert"}$ phase when prompted by circulating factors [6, 7]. They and others [38] have shown that entry of MuSCs in a tissue that is distant from local muscle damage to the $G_{"Alert"}$ phase is mTOR dependent. They also demonstrated that tissues will regenerate more efficiently and quicker if first entered into the $G_{"Alert"}$ phase before damage [6]. However, no one has fully examined or categorized global, ontology-grouped, or individual changes in protein flux rates of whole muscle tissue that has entered the $G_{"Alert"}$ phase in response to distant injury.

In this study, we elucidated changes in protein flux rates that occur during the $G_{"Alert"}$ phase in muscle that is distant to different stages of a regeneration event from acute injury. This was done directly *in-vivo* by labeling newly synthesized proteins in muscle tissue distant to acute muscle damage with deuterium (^2H) from deuterated water (^2H_2O) and quantifying mass isotopomer patterns and content by liquid chromatography (LC) coupled - tandem mass spectrometry (MS/MS). Each protein's replacement (turnover) rate could then be calculated, as previously described [8, 9, 10]. This information on protein turnover rates was then compared to gene expression values from RNA-seq.

Results

Pilot Study (First 3 Days After Distant Muscle Injury) To understand how systemic factors from acute injury affect distant muscle tissue, we ran an initial experiment with a small cohort of mice ("Pilot Stage", n=10), designed to capture the protein flux changes that occur in muscle from a limb that is contralateral to an injected cardiotoxin (CTX) injury model (CNTRA) [35, 37]. Mice were randomly split into two even groups (CTX injected and uninjured control) and local tissue damage was induced by injection of CTX into the tibialis anterior (TA) muscle of one hind limb in each mouse in the injury group. Both groups received ^2H_2O from the initial day of CTX injection (Day 11) until 3 days post CTX injection (dpi) (Day 14) (Figure 1A). The fractional synthesis rate (FSR) of 151 proteins that were present in both the CNTRA limb and control limb were measured at the end of the Pilot Stage. Average FSR values with standard deviation (SD) for every protein can be found in Table 1. There was a statistically significant increase in global protein FSR values between the tissue from the CNTRA limb and control muscle tissue (Figure 1B). There were no individual proteins in the CNTRA limb that stood out as significantly different after correction for multiple comparisons. Interestingly, when looking for specific individual proteins of early-stage novel myofiber formation [11], there is a significant increase in Myosin 3 FSR in the limb contralateral to injury when compared to control muscle (Figure 1C). Functional clusters of protein groups were also analyzed to determine if any gene ontologies were significantly affected at this stage (Figure 1E). In this stage, all the measured functional clusters had a significant number of proteins with higher FSR values in the contralateral limb to injury compared to control limb [Cytoplasm (22/33 increased, $p<0.05$), Myofibril (17/19 increased, $p<0.05$), Glycolysis (9/12 increased, $p<0.05$), Mitochondria (28/39 increased, $p<0.05$), Oxidative Phosphorylation (30/39 increased, $p<0.05$)]. We observed no significant increase in cell proliferation rates based on new synthesis of cellular DNA [31] at this early stage post-CTX, despite partial cell cycle activity being reported as a characteristic of G_{Alert} [6] (Figure 1D). These pilot results demonstrated a modest, but significant, effect of local skeletal muscle injury on tissues distant to that injury. We then carried out a systematic time course of responses in muscle tissue distant to CTX injury.

Proteomics Comparisons To determine how protein flux rates in skeletal muscle that is distant from a local injury respond to different stages of regeneration over time, FSR of proteins were measured *in-vivo* via ^2H_2O administration coupled HPLC-MS and MS/MS analysis. We also purified muscle fibers from bulk muscle tissue via enzymatic digestion and physical separation to remove the influence of interstitial and other cell types from circulation on our analyses [13]. Mice injected with CTX were separated into groups of ^2H_2O labeling relative to the time of initial injury to capture different events occurring along the muscle regeneration timeline (Figure 1A). The following labeling protocol was used, to ensure that all mice were sacrificed at the

same age. The "Proliferation Stage" captured the initial damage, inflammation-mediated immune response of activation/proliferation of MuSCs through administration of CTX and $^{2}H_2O$ concurrently on day 10 and continuous label until sacrifice 4 dpi (Day 14). The "Differentiation Stage" mice were injected with CTX on Day 7 but with $^{2}H_2O$ from 4 to 7 dpi (Day 11 to Day 14) to capture the period of differentiation into newly formed myofibers. The "Maturation Stage" mice received a CTX injection on Day 0 and $^{2}H_2O$ from 10 to 14 dpi (Day 10 to Day 14) to capture the period of reintegration of new myofibers into existing muscle, as well as the construction of surrounding structures to support newly formed tissue in the damaged limb. Muscle regeneration from MuSCs has been found to be virtually complete after 14 dpi [12, 13, 37]. Control groups (Uninjected) received no CTX injection but were administered $^{2}H_2O$ for 3 days (Day 11 to Day 14) and were sacrificed for tissue collection alongside all other CTX injected groups on Day 14.

Comparison of Global Protein Turnover Rates at Each Stage. The FSRs of 73 proteins present in both the CNTRA limb and control limb were measured at the end of the Proliferation Stage (4 dpi). Proteome analysis showed a significant increase in global protein FSR values between contralateral and control muscle tissue during this stage of regeneration ($p<0.01$, Figure 2A). At the end of the Differentiation Stage, the FSRs of 127 proteins present in both the CNTRA limb and the control limb were measured. Global proteome analysis shows a significant increase in protein FSR values from contralateral to control muscle tissue during this phase of regeneration ($p<0.001$, Figure 2B). The FSR of 126 proteins present in both the CNTRA limb and the control limb was at the end of the Maturation Stage. There was no significant difference in global protein FSR values from contralateral to control muscle tissue during this late stage of regeneration (Figure 2C). Average values for every protein with standard deviation (SD) values can be found in Table 1.

Changes at each stage in protein turnover rates in gene ontology groups. Functional clusters of protein groups were analyzed by gene ontology enrichment using DAVID from NIH to determine which cellular processes were highly affected at each stage (Figure 3A-C). The ontology groups analyzed were Cytoplasmic, Myofibril, Glycolysis, Mitochondria, and Oxidative Phosphorylation. During the Proliferation Stage, almost all (4/5) groups showed a significant number of proteins with higher FSR values in the limb contralateral to injury, compared to control limb [Myofibril (16/18 increased, $p<0.05$), Glycolysis (9/9 increased, $p<0.05$), Mitochondria (10/12 increased, $p<0.05$), Oxidative Phosphorylation (8/10 increased, $p<0.05$)] (Figure 3A). In the Differentiation Stage, when proteins were grouped into functional clusters, again almost all measured processes (4/5) had a significant increase in the number of proteins with a higher FSR value in the injured limb compared to control limb [Myofibril (18/19 increased, $p<0.05$), Glycolysis (11/12 increased, $p<0.05$), Mitochondria (21/25 increased, $p<0.05$), Oxidative Phosphorylation (28/36 increased, $p<0.05$)](Figure 3B). In the Maturation Stage, the only two functional clusters with significant increases in the number of proteins with a higher FSR value in the injured limb compared to control limb were Myofibril (14/19 increased, $p<0.05$) and Mitochondria (16/23 increased, $p<0.05$) (Figure 3C).

Individual Protein Turnover Rates at Each Stage. In the Proliferation Stage, there were 26 individual proteins that stood out as statistically significant after correction for multiple comparisons between the CNTRA limb and control (Figure 4A). Two validated "virtual biopsy" markers (proteins in plasma that are derived from and reflect muscle protein turnover) [14],

Creatine Kinase-Muscle isoform (CK-M) and Carbonic Anhydrase 3 (CA3), are significantly lower in distant muscle tissue during this phase of the regeneration process. Myosin Light Chain 1/3 is another potential blood measurement of muscle FSR [15] and is significantly different between CNTRA and control. Also, several glycolytic enzymes, Glucose-6-phosphate Isomerase (G6P), Lactate Dehydrogenase Alpha Chain (LDH-A), Fructose-bisphosphate Aldolase (FBP), Pyruvate Kinase (PKM), Pyruvate Dehydrogenase (PDH), Phosphoglycerate Mutase 2 (PGM2), Beta-Enolase (B-Enolase) have a higher FSR in the contralateral muscle at this stage. Collagen Alpha Chain, Type III is an extracellular protein mainly involved with connective tissue but can also serve as a ligand for signal transduction [16] and was significantly increased. In the Differentiation Stage only a few individual proteins (4) stood out as having significantly different FSR values in CNTRA compared to control after correction for multiple comparisons at the, (Figure 4B). Despite having few individual proteins stand out after correction for multiple comparisons, global protein analysis revealed significantly higher FSR in the contralateral limb compared to control limb. In the Maturation Stage, there were 4 individual proteins that stood out as having significantly different FSR values in the contralateral limb compared to control limb after correction for multiple comparisons (Figure 4C). Individual proteins from the Collagen families (Collagen Alpha Chain 1, Collagen Alpha Chain 3) showed decreased FSR values in the contralateral limb. Average values for every protein with standard deviation (SD) values can be found in Table 1.

Global Gene Expression Changes at Each Stage Gene expression was normalized to fragment per kilobase millions (FPKM) values, which were used to compare global gene expression profiles of each stage of muscle regeneration. In the Proliferation Stage, 16585 individual gene expression values were measured. Of those 16585 genes, 615 genes (3.7%) were significantly upregulated, 610 genes (3.7%) were significantly downregulated, and 15360 (92.6%) genes did not change significantly ($-\text{Log}_{10}(p)>1.301$, Figure 5A). In the Differentiation Stage, 16388 individual gene expression values were measured. Of those 16388 genes, 649 genes (4.0%) were significantly upregulated, 632 genes (3.9%) were significantly downregulated, and 15107 genes (92.1%) did not change significantly ($-\text{Log}_{10}(p)>1.301$, Figure 5B). In the Maturation Stage, 16178 individual gene expression values were measured. Of those 16178 genes, 348 genes (2.2%) were significantly upregulated, 453 genes (2.8%) were significantly downregulated, and 15377 genes (95.0%) did not change significantly ($-\text{Log}_{10}(p)>1.301$, Figure 5C).

Group Ontology Gene Expression at Each Stage UniProt unique protein identification numbers (Accession #) were used to find Gene IDs for all proteins measured in functional cluster protein groups from DAVID by NIH. FPKM values for each of those individual genes identified were ratioed to generate a Log_2(Fold Change) (Log_2(FC)) to measure the magnitude of change between the contralateral limb at each stage of muscle regeneration and control tissue. These values were then split up into the same functional cluster protein groups as seen in Figure 3. The mRNA changes are shown for all proteins in each gene ontology for which FSR was measured. Changes in mRNA are statistically analyzed for these proteins and shown below the individual graphs in Figure 6. The changes in gene expression were generally not significant and did not parallel the changes in FSRs for the same proteins in each ontology (shown in Figure 3).

Correlations of changes in gene expression to changes in protein FSRs. To correlate gene expression FPKM values to their protein FSR values, a 2-dimensional graph was created to plot the Log_2FC of FPKM values on the Y axis and Log_2FC of protein FSR values on the X axis for

each stage of muscle regeneration. In the Proliferation Stage, there is no significant correlation between the magnitude of change in FPKM and FSR values ($R^2 = 0.02522$, $p>0.05$, Figure 7A). In the Differentiation Stage, there is also no significant correlation between the magnitude of change in FPKM and FSR values ($R^2 = 0.00249$, $p>0.05$, Figure 7B). Also, in the Maturation Stage, there is no significant correlation between the magnitude of change in FPKM and FSR values ($R^2 = 0.02336$, $p>0.05$, Figure 7C).

My3 Protein Turnover, Myh3 Gene Expression, and Myogenic Gene Expression Myosin 3, also known as Embryonic Myosin Heavy Chain (EmyHC), is an isoform of the Myosin Heavy Chain super family that is expressed in newly differentiated myofibers from MuSCs, but not in later stages of the myofiber maturation process [17]. We used FSR values of this individual protein across the regeneration time course to provide us with a surrogate measurement of the myogenic potential of MuSCs in the limb contralateral to injury [11, 36]. As mentioned above, the Pilot Study showed a significant increase in protein FSR values of EmyHC in the contralateral limb (Figure 1C). The Proliferation Stage was the only stage in the time-course study to show a significant increase in EmyHC protein FSR values in the contralateral limb (Figure 8A). However, gene expression analysis of Myh3, the gene for EmyHC, from bulk RNA-seq data showed no significant changes in expression in the contralateral limb at any stage in comparison to control (Figure 8B). These findings were compared to measurements of gene expression from bulk RNA-sequencing values for known genes of myogenesis (MyoD, MyoG, Myf5/6, and Desmin) (Figure 8C) [18]. Interestingly, none of the genes of myogenesis we measured stood out as significant in the contralateral limb at any stage when compared to control muscle.

Non-Muscle Tissue (Liver) Global Protein Turnover Rates Global protein flux rate analysis of non-muscle tissue (liver) was analyzed to determine if the systemic response to local tissue damage affects non-muscle tissues as well. There was no statistically significant change in global protein FSR rates of the liver tissue in injured mice, when compared to tissue from uninjured controls, at any time point after acute injury that we measured (Supplemental Figure S1).

Discussion

In this work, we describe how protein flux changes and gene expression values in whole tissue respond on a global, ontology-grouped, and individual level in muscle tissue that is distant from a local CTX injury. This was achieved through ^2H_2O labeling coupled to high resolution MS analysis to measure *in-vivo* protein turnover rates. We also measured bulk RNA-seq mediated gene expression profiles and measurements of muscle cell proliferation from ^2H incorporation into DNA [31]. Previous work from Rodgers et al. shows fundamental changes in MuSCs that are in G_{Alert} [6, 7] and provides the necessary groundwork for which this study is based upon. In the Pilot Study, measurements are taken 3 days after CTX injection and ^2H_2O label presence, which is the same time point after injury as seen in Rodgers et al. Global proteome analysis reveals a significant increase in protein flux values in the whole CNTRA muscle at certain stages, when compared to control. We measured group protein analysis to have a significant increase in the number of proteins with a higher FSR value in the CNTRA limb for all five of the functional clusters measured. We did not detect a significant increase in cell proliferation (^2H incorporation into DNA) [31], although Rodgers et al. did see a significant increase in BrdU labeling of *ex-vivo* MuSCs isolated from the contralateral limb up to 3 days after local injury [6].

In this study, changes in global protein turnover values were observed in the contralateral limb, with more pronounced changes in stages closer to the initial injury. During the first 4 dpi (Proliferation Stage), we saw a significant increase in global protein flux rates in the contralateral limb. Rodgers et al. directly examined the MuSCs from a similar model of injury and found significant transcriptome analysis up to 3 dpi [6]. Our global gene expression analysis at this stage shows moderate numbers of gene transcripts being either significantly upregulated or downregulated expression. During the Differentiation Stage there was still a significant increase in global protein flux rates in the contralateral limb, suggesting that the systemic response to local injury can have significant effects on other whole muscle tissues up to 1 week after injury. Global gene expression values also showed modest changes at this stage, with a slightly higher number of gene transcripts being significantly upregulated and downregulated than the previous stage. However, by the time the damaged tissue begins to mature during the Maturation Stage, the contralateral limb does not show a significant difference in protein flux rates from control. This was also observed in global gene expression analysis, with this stage having the lowest number of significantly upregulated and downregulated gene transcripts in comparison to the previous two stages. These results suggest that there is a systemic influence of local injury on uninjured tissue that diminishes as the damaged tissue regenerates.

There were varying results in the types and number of individual proteins at each stage that were significant after correction for multiple comparisons. In the Proliferation Stage, all the individual proteins that were significant after correction for multiple comparisons had higher flux rates in the contralateral limb in comparison to a control (26/26). As discussed above, two proteins of interest that stood out as significant after corrections in this stage were CK-M and CA3, which we have previously shown to be circulating flux markers of whole muscle FSR values [14]. Also, Myosin Light Chain 1/3 was another potential plasma marker of whole muscle FSR that was found to correlate well with global protein flux rates here in muscle tissue, as individual flux rates were significantly increased. Individual protein analysis gave a hint of response of group changes. For example, there were many individual enzymes from glycolysis, such as G6P, LDH-α, FBP, PKM, PDH, PGM2, and β-Enolase, that all showed a significant increase in the contralateral limb. This finding is more evidence supporting tissue preparation for regeneration, as increased glycolysis is required for new myofiber synthesis in directly damaged muscle [21] and is the main energy source of active MuSCs [22]. Despite the strong significant increase in global protein flux rates at the Differentiation Stage, there was only a modest number of individual proteins (4) that individually stood out as significant after correction for multiple comparisons. All the individual proteins (4/4) that had significant changes in flux rates after corrections for multiple comparisons in the Differentiation Stage showed an increase in flux rate in comparison to the control group. However, in contrast with the large global effect that is observed in the limb contralateral to injury at this stage, there were no individual proteins of interest that stood out as significant in the CNTRA limb at this stage. We observed no significant difference in global protein flux rates at the Maturation Stage. This is accompanied by a few subtle changes in individual protein flux rates that overall lack a uniform direction. There were only 4 individual proteins that were significant after correction for multiple comparisons at this stage. Proteins of interest that had significant differences in the limb contralateral to injury were Collagen Alpha Chain 1 and Collagen Alpha Chain 3 [16]. Both proteins were significantly decreased in protein FSR value at this stage, which is surprising because during this stage of the muscle regeneration, new myofibers reintegrate into existing tissue by developing the surrounding support structures, like blood vessels, nerves, and extracellular matrix [18].

Along with measuring changes in global protein flux rates and gene expression profiles, proteins and genes were grouped into functional gene ontology clusters and analyzed to understand how DAVID-defined biological processes are potentially affected by different stages of skeletal muscle damage and regeneration [20]. During the Proliferation Stage, the CNTRA limb showed a significant increase in almost all the measured functional clusters from skeletal muscle for protein flux rates. The only cluster that did not show a significant directional change for FSR values was the Cytoplasm group, which is a somewhat ambiguous collection of various cytoplasmic proteins. However, when gene transcripts were organized into the same groups based on their relation to the individual proteins in that group, fewer effects were observed. Three functional clusters showed significant directional changes in group gene expression levels, with only two of them being in the same direction as the protein groups (a significant number of proteins/genes increased turnover/expression compared to control). Interestingly, group gene expression levels in the CNTRA limb in the Differentiation Stage did not reflect changes in grouped protein FSR changes, as only one functional cluster showed a significant number of genes with a higher expression level than control. In the later stages of muscle regeneration (Maturation Stage), the contralateral limb only shows modest results for functional cluster analysis with only two groups having a significant increase in the number of proteins with higher FSR values. Functional clusters for gene expression were also only observed in two groups, different from the two protein functional clusters, with a higher expression level than control.

Moreover, we wanted to explore the relationship between protein turnover values and their static gene expression values at the end of the labeling period. A correlation graph that compares the magnitude of change of an individual protein's turnover value and the magnitude of change in gene expression values was made for each stage. For the Proliferation Stage, for the 69 proteins that had available turnover and gene expression data, there was no significant correlation between the two types of measurements. In the Differentiation Group, for the 118 proteins that had available turnover and gene expression data, there was no significant correlation between the two types of measurements. In the Maturation Stage, for the 118 proteins that had available turnover and gene expression data, there was no significant correlation between the two types of measurements. This divergence in change between protein turnover and gene expression may be explained by post-transcriptional levels of control over protein synthesis (e.g., initiation or elongation translational changes, microRNA effects, etc.) or by delays in gene transcript turnover, whereas protein synthesis rates measure the integrated previous 3-to-4-day flux rate for each protein. Evidence of translational control during muscle regeneration is an important finding [23, 24, 25]. Of note, previous studies from our research group have shown a clear dissociation between protein turnover and gene expression levels in various tissues including skeletal muscle and liver [26, 27].

To expand upon our individual protein findings, we decided in advance to target Myosin 3, also known as Embryonic Myosin Heavy Chain (EmyHC). EmyHC exists transiently during embryonic development and its presence in muscle tissue outside of embryogenesis has been commonly used as an abundance-based marker to indicate MuSCs differentiation towards a new myofiber [11, 36.] In this study, EmyHC turnover in whole tissue was used as an added proxy of the magnitude of MuSCs exit from a quiescent state. In the Pilot Study, there was a significant increase in EmyHC turnover in the contralateral limb at 3 dpi. This time point has been proven in previous studies [6] and in our own work to be when MuSCs of the contralateral limb are in the $G_{\text{"Alert"}}$ phase. However, there was no active cell-cycling that could be measured from ^{2}H

incorporation into DNA at this stage. Taken together, increased EmyHC turnover at this stage could be used as a surrogate measure of MuSCs activity, independent of other markers of active MuSC proliferation. In the time-course study, the only phase where EmyHC was measured to have a significant increase in turnover in the contralateral limb was during the Proliferation Stage. Gene expression levels of the gene for EmyHC (Myh3), were measured in the contralateral limb at each stage of muscle regeneration, but at no stage showed significant changes from control. Other myogenic genes and markers of MuSC activity were also examined in the contralateral limb at each stage of muscle regeneration, but also didn't show significant changes in expression levels at any stage.

Conclusion

In summary, we present a new approach based on protein flux rates for analyzing the systemic effect of local muscle tissue damage in a limb contralateral to injury. Signature changes in protein turnover rates and a striking lack of correlation between mRNA changes and protein synthesis rates are clearly shown. Hopefully, this information will help us better identify the factors responsible for and the pathways involved in this distant response to muscle damage.

Acknowledgments

The authors would like to thank all of those who contributed to this work, including members of the Hellerstein Lab and Conboy Lab, for their efforts. Special consideration and thanks go to Mike and Irina Conboy for promoting the core ideas and sharing the key techniques that aided in the development and completion of these studies.

Methods and Materials

Mouse Experiments:

CTX Time Course 20 male 8-week-old C57/BL6 mice were purchased from Jackson Laboratory and housed at UC Berkeley's Northwest Animal Facility. All mice were housed according to the Animal Care and Use Committee (ACUC) standards in the animal facility at UC Berkeley. The mice were assigned to a group (n=5) at random that reflected what stage of muscle regeneration is being measured (Pilot Stage, Proliferation Stage, Differentiation Stage, Maturation Stage, or Control). CTX induced muscle regeneration groups received a dose of 50 µL 0.1mg/mL CTX will be administered in sterile PBS/0.2% Meloxicam in the form of intramuscular injection to the Tibialis Anterior (TA) muscle to one limb while the other TA will not be injected to serve as "contralateral" to the injected one (CNTRA). Day of injection will count as Day 0, and subsequent days following will allow for the toxin induced model of muscle regeneration to occur. One group of mice did not receive CTX injection to serve as "uninjected controls" (Uninj) but did receive 3 days of stable isotope labeling alongside experimental groups. All groups of mice had unrestricted access to a standard chow diet and 8% Deuterium drinking water (^2H_2O). ^2H_2O was provided to continually label the mice after a bolus intraperitoneal injection of 99.1% ^2H_2O/0.9% saline solution to allow for stable enrichment levels during the entire labeling time course. If a mouse appears to have issues accessing food or water due to CTX injection at any time during incubation, then they will be removed from study and sacrificed. At specific time points along the muscle regeneration timeline after initial CTX injection pertaining to unique stages (Pilot Stage: 3 days after injection, Proliferation Stage: 4 days after injection, Differentiation Stage: 7 days after injection, Maturation Stage: 14 days after injection), animals will be sacrificed, and tissues will be taken for analysis. To avoid bias from multiple analysis, all animals were sacrificed on Day 14 of the study. Muscle histology and protein expression via immunofluorescence will be utilized to confirm each stage of muscle regeneration. After sacrifice, target tissues (multiple muscles including TA, blood (serum), kidneys, liver) will be collected along with urine, as previously described [28], for the following procedures.

Body Water Determination Mouse blood was distilled overnight upside down on a bead bath at 85°C to evaporate out body water. Deuterium present in the body water was exchanged onto acetone, and deuterium enrichment in the body water was measured via gas chromatography mass spectrometry (GC-MS), as previously described [29].

RNA-sequencing

RNA Bulk Isolation Whole RNA transcripts were isolated from frozen purified muscle fibers, according to manufacturer's instructions (Qiagen RNA Extraction Mini Kit, #74104), and RNA concentrations were obtained using a Nanodrop.

Sample collection and preparation From the RNA sample to the final data, each step, including sample test, library preparation, and sequencing, influences the quality of the data, and data quality directly impacts the analysis results. To guarantee the reliability of the data, quality control (QC) is performed at each step of the procedure.

RNA quantification and qualification RNA degradation and contamination was monitored on 1% agarose gels. RNA purity was checked using the NanoPhotometer® spectrophotometer (IMPLEN, CA, USA). RNA integrity and quantitation were assessed using the RNA Nano 6000 Assay Kit of the Bioanalyzer 2100 system (Agilent Technologies, CA, USA).

Library preparation for transcriptome sequencing A total amount of 1 μg RNA per sample was used as input material for the RNA sample preparations. Sequencing libraries were generated using NEBNext® UltraTM RNA Library Prep Kit for Illumina® (NEB, USA) following manufacturer's recommendations and index codes were added to attribute sequences to each sample. Briefly, mRNA was purified from total RNA using poly-T oligo-attached magnetic beads. Fragmentation was carried out using divalent cations under elevated temperature in NEBNext First Strand Synthesis Reaction Buffer (5X). First strand cDNA was synthesized using random hexamer primer and M-MuLV Reverse Transcriptase (RNase H-). Second strand cDNA synthesis was subsequently performed using DNA Polymerase I and RNase H. Remaining overhangs were converted into blunt ends via exonuclease/polymerase activities. After adenylation of 3' ends of DNA fragments, NEBNext Adaptor with hairpin loop structure were ligated to prepare for hybridization. In order to select cDNA fragments of preferentially 150~200 bp in length, the library fragments were purified with AMPure XP system (Beckman Coulter, Beverly, USA). Then 3 μl USER Enzyme (NEB, USA) was used with size-selected, adaptor-ligated cDNA at 37 °C for 15 min followed by 5 min at 95 °C before PCR. Then PCR was performed with Phusion High-Fidelity DNA polymerase, Universal PCR primers and Index (X) Primer. At last, PCR products were purified (AMPure XP system) and library quality was assessed on the Agilent Bioanalyzer 2100 system.

Clustering and sequencing The clustering of the index-coded samples was performed on an Illumina Novaseq sequencer according to the manufacturer's instructions. After cluster generation, the libraries were sequenced on the same machine and paired-end reads were generated.

Sample Digestion for Proteomics

Muscle Fiber Isolation and CD45+ Cell Depletion via MACS Tissues were snap-frozen after harvest in 0.5 mL of 10% DMSO in FBS and stored at -80℃ until processing. Samples were thawed, buffer was removed, and individual muscle fibers were physically separated from whole muscle tissue, as previously described [13]. Purified muscle fibers were then depleted of infiltrating CD45+ cells by undergoing magnetic assisted cell sorting (MACS) mediated selective depletion, according to manufacturer's instructions (Miltenyi Biotec #130-052-301), before being processed for in-solution digestion.

Myofiber SDS Solubilization + In-Solution Digestion of Tissue After MACS-mediated CD45+ cell depletion, a 150 µL aliquot of purified myofibers was brought up to 500 µL in 0.1% SDS solution and allowed to disassociate on a vortexer overnight at medium speed. The next day, samples were pulled off the vortexer, mixed with 7:1 v/v 100% ethanol:sample, vortexed, and placed at -20℃ overnight to precipitate out proteins. The next day, samples were centrifuged 16,000 g for 30 minutes at 4℃ to pellet out all protein. Supernatant was removed and protein pellet was resuspended in 100 µL 8M Urea in 50 mM Ammonium Bicarbonate (pH 8.1) with agitation on vortexer at medium speed for 30 minutes at room temperature. A small portion of

each sample was diluted, and protein concentration was then determined by the Pierce BCA protein assay kit (Thermo Fisher #23225) with BSA as standards. Up to 100 µg of protein was taken and volume adjusted up to 100 µL in 8M Urea in 50 mM Ammonium Bicarbonate (pH 8.1). Tris-(2-carboxyethyl)-phosphine (TCEP) was added to make a final concentration of 10 mM and samples were agitated on a vortexer for 20 minutes at room temperature. Iodoacetamide (IAA) was added to make a final concentration of 20 mM, samples were vortexed briefly, and incubated at room temperature in the dark for 30 minutes. TCEP was added to make a final concentration of 4 mM to quench excess IAA and samples were diluted in 50 mM Ammonium Bicarbonate (pH 8.1) so that the final concentration of Urea was < 1M. Proteomics-Grade Trypsin was added at a ratio of 1:50 trypsin to protein (Sigma Aldrich, #T6567). Samples were incubated at 37°C overnight. The next day, formic acid was added at 5% of the final volume. Samples underwent Solid-Phase Extraction using Agilent C18 clean up columns (#A57203) to remove digested peptides from the digestion buffer. Peptides were eluted using 30% acetonitrile and speedvac'd until dry and re-suspended in 25 µL of 0.1 % formic acid/3% acetonitrile/96.9% LC-MS grade water and transferred to LC-MS vials to be analyzed via LC-MS.

Mitochondria Isolation for Proteomics After MACS-mediated CD45+ cell type depletion, a 150 µL aliquot of purified myofibers was used to isolate mitochondrial proteins according to manufacturer's instructions (Thermo Fisher #89801). Protein pellets were resuspended in 50 mM Ammonium Bicarbonate (pH 8.1) and protein concentration was then determined by the Pierce BCA protein assay kit (Thermo Fisher, #23225) with BSA as standards. Up to 100 µg of protein was taken and volume adjusted to 100 µL in 50 mM Ammonium Bicarbonate (pH 8.1). TCEP was added to make a final concentration of 10 mM and samples were agitated on a vortexer for 20 minutes at room temperature. IAA was added to make a final concentration of 20 mM, samples were vortexed briefly, and incubated at room temperature in the dark for 30 minutes. TCEP was added to make a final concentration of 4 mM to quench excess IAA and samples were diluted in 50 mM Ammonium Bicarbonate (pH 8.1) up to 400 µL. Proteomics-Grade Trypsin was added at a ratio of 1:50 trypsin to protein (Sigma Aldrich, #T6567). Samples were incubated at 37°C overnight. The next day, formic acid was added at 5% of the final volume. Samples were centrifuged at 10,000 g for 10 minutes at room temperature, and the supernatant was collected. Supernatant was speedvac'd until dry and re-suspended in 50 µL of 0.1 % formic acid/3% acetonitrile/96.9% LC-MS grade water and transferred to LC-MS vials to be analyzed via LC-MS.

Non-Muscle Tissue (Liver) Proteomics Tissue was snap-frozen after harvest and stored at -80°C until processing. 50 µg of sample was homogenized in 500 µL 1x PBS/1 mM PMSF/5 mM EDTA/1x Protease Inhibitor (Thermo Fisher, #78429) using Qiagen TissueLyser II (#85300). Samples were sonicated in a bath sonicator for 1 minute and centrifuged at 10,000 g for 10 minutes at 4°C to pellet out debris. Supernatant was collected and protein concentration was then determined by the Pierce BCA protein assay kit with BSA as standards. Up to 100 µg of protein was taken and volume adjusted to 100 µL in 50 mM Ammonium Bicarbonate (pH 8.1). TCEP was added to make a final concentration of 10 mM and samples were agitated on a vortexer for 20 minutes at room temperature. IAA was added to make a final concentration of 20 mM, samples were vortexed briefly, and incubated at room temperature in the dark for 30 minutes. TCEP was added to make a final concentration of 4 mM to quench excess IAA and samples were diluted in 50 mM Ammonium Bicarbonate (pH 8.1) up to 400 µL. Proteomics-Grade Trypsin was added at a ratio of 1:50 trypsin to protein. Samples were incubated at 37°C overnight. The

next day, formic acid was added at 5% of the final volume. Samples underwent Solid-Phase Extraction using Agilent C18 clean up columns to remove digested peptides from the digestion buffer. Peptides were eluted using 30% acetonitrile and speedvac'd until dry and re-suspended in 25 µL of 0.1 % formic acid/3% acetonitrile/96.9% LC-MS grade water and transferred to LC-MS vials to be analyzed via LC-MS.

Measuring Muscle Cell Proliferation Rates (Incorporation of ^{2}H into DNA). After MACS-mediated CD45+ cell type depletion, a 150 µL aliquot of purified myofibers was used to extract DNA. DNA was derivatized and analyzed for deuterium enrichment in deoxyribose from purine deoxyribonucleosides via gas chromatography mass spectrometry, as previously described [31, 32].

Liquid chromatography-mass spectrometry (LC-MS) analysis Trypsin-digested peptides were analyzed on a 6550 quadropole time of flight (Q-ToF) mass spectrometer equipped with Chip Cube nano ESI source (Agilent Technologies). High performance liquid chromatography (HPLC) separated the peptides using capillary and nano binary flow. Mobile phases were 95% acetonitrile/0.1% formic acid in LC-MS grade water. Peptides were eluted at 350 nl/minute flow rate with an 18-minute LC gradient. Each sample was analyzed once for protein/peptide identification in data-dependent MS/MS mode and once for peptide isotope analysis in MS mode. Acquired MS/MS spectra were extracted and searched using Spectrum Mill Proteomics Workbench software (Agilent Technologies) and a mouse protein database (www.uniprot.org). Search results were validated with a global false discovery rate of 1%. A filtered list of peptides was collapsed into a nonredundant peptide formula database containing peptide elemental composition, mass, and retention time. This was used to extract mass isotope abundances (M_0 - M_3) of each peptide from MS-only acquisition files with Mass Hunter Qualitative Analysis software (Agilent Technologies). Mass isotopomer distribution analysis (MIDA) was used to calculate peptide elemental composition and curve-fit parameters for predicting peptide isotope enrichment based on precursor body water enrichment (p) and the number (n) of amino acid C-H positions per peptide actively incorporating hydrogen (H) and deuterium (^{2}H) from body water. Subsequent data handling was performed using python-based scripts, with input of precursor body water enrichment for each subject, to yield fractional synthesis rate (FSR) data at the protein level. FSR data were filtered to exclude protein measurements with fewer than 2 peptide isotope measurements per protein. Details of FSR calculations and data filtering criteria have been described in detail previously [10].

Calculation of fractional replacement (f) and replacement rate constant (k) for individual proteins Details of f calculations were previously described [10].

Statistical analysis Data filtering and calculations were performed according to previous reports [10]. Only those proteins that met analytic filtering criteria and that were present in at least 2 animals per group were included in comparisons and statistical analyses [33]. Individual proteins were also grouped into different functional clusters based on gene ontology origin using DAVID from NIH website (https://david.ncifcrf.gov/tools.jsp) to determine which processes were affected at each stage [34]. Statistical significance of protein turnover comparisons was assessed by one of the following tests: 1.) Global changes in protein turnover were compared across groups with a Student's Unpaired T-Test, 2.) Individual proteins were compared across groups with a Student's Unpaired T-Test and Benjamini-Hochberg correction for multiple comparisons, or 3.) a Binomial Test of the proportion of proteins showing a higher or lower value of FSR in relation

to control for comparison of functional clusters across the regeneration timeline, as described previously [20], * $p<0.05$, ** $p<0.01$, *** $p<0.005$, **** $p<0.001$. All statistical analysis was carried out by GraphPad Prism software (version 9.4).

References

1. Forcina L, Cosentino M, Musarò A. Mechanisms Regulating Muscle Regeneration: Insights into the Interrelated and Time-Dependent Phases of Tissue Healing. *Cells*. 2020;9(5):1297. doi:10.3390/cells9051297

2. Mauro A. Satellite cell of skeletal muscle fibers. *J Biophys Biochem Cytol*. 1961;9(2):493-495. doi:10.1083/jcb.9.2.493

3. Shi X, Garry DJ. Muscle stem cells in development, regeneration, and disease. *Genes Dev*. 2006;20(13):1692-1708. doi:10.1101/gad.1419406

4. Alway SE, Myers MJ, Mohamed JS. Regulation of Satellite Cell Function in Sarcopenia. Frontiers in Aging Neuroscience. 2014;6. Accessed May 10, 2023. https://www.frontiersin.org/articles/10.3389/fnagi.2014.00246

5. Morgan JE, Zammit PS. Direct effects of the pathogenic mutation on satellite cell function in muscular dystrophy. Experimental Cell Research. 2010;316(18):3100-3108. doi:10.1016/j.yexcr.2010.05.014

6. Rodgers JT, King KY, Brett JO, et al. mTORC1 controls the adaptive transition of quiescent stem cells from G0 to GAlert. Nature. 2014;510(7505):393-396. doi:10.1038/nature13255

7. Rodgers JT, Schroeder MD, Ma C, Rando TA. HGFA Is an Injury-Regulated Systemic Factor that Induces the Transition of Stem Cells into GAlert. Cell Reports. 2017;19(3):479-486. doi:10.1016/j.celrep.2017.03.066

8. Hellerstein MK, Neese RA. Mass isotopomer distribution analysis: a technique for measuring biosynthesis and turnover of polymers. *Am J Physiol*. 1992;263(5 Pt 1):E988-1001. doi:10.1152/ajpendo.1992.263.5.E988

9. Hellerstein MK, Neese RA. Mass isotopomer distribution analysis at eight years: theoretical, analytic, and experimental considerations. *American Journal of Physiology-Endocrinology and Metabolism*. 1999;276(6):E1146-E1170. doi:10.1152/ajpendo.1999.276.6.E1146

10. Holmes WE, Angel TE, Li KW, Hellerstein MK. Dynamic Proteomics: In Vivo Proteome-Wide Measurement of Protein Kinetics Using Metabolic Labeling. *Methods Enzymol*. 2015;561:219-276. doi:10.1016/bs.mie.2015.05.018

11. Schiaffino S, Rossi AC, Smerdu V, Leinwand LA, Reggiani C. Developmental myosins: expression patterns and functional significance. *Skeletal Muscle*. 2015;5(1):22. doi:10.1186/s13395-015-0046-6

12. Yan Z, Choi S, Liu X, et al. Highly Coordinated Gene Regulation in Mouse Skeletal Muscle Regeneration*. Journal of Biological Chemistry. 2003;278(10):8826-8836. doi:10.1074/jbc.M209879200

13. Ramadasan-Nair R, Gayathri N, Mishra S, et al. Mitochondrial Alterations and Oxidative Stress in an Acute Transient Mouse Model of Muscle Degeneration. *J Biol Chem*. 2014;289(1):485-509. doi:10.1074/jbc.M113.493270

14. Shankaran M, King CL, Angel TE, et al. Circulating protein synthesis rates reveal skeletal muscle proteome dynamics. *J Clin Invest*. 2016;126(1):288-302. doi:10.1172/JCI79639

15. Evans WJ, Shankaran M, Smith EC, et al. Profoundly lower muscle mass and rate of contractile protein synthesis in boys with Duchenne muscular dystrophy. *J Physiol*. 2021;599(23):5215-5227. doi:10.1113/JP282227

16. Type I, II, III, IV, V, and VI collagens serve as extracellular ligands for the isoforms of platelet-derived growth factor (AA, BB, and AB). | Literature citations | UniProt. Accessed March 22, 2023. https://www.uniprot.org/citations/8900172

17. Dalle S, Hiroux C, Poffé C, Ramaekers M, Deldicque L, Koppo K. Cardiotoxin-induced skeletal muscle injury elicits profound changes in anabolic and stress signaling, and muscle fiber type composition. *J Muscle Res Cell Motil*. 2020;41(4):375-387. doi:10.1007/s10974-020-09584-5

18. Musarò A. The Basis of Muscle Regeneration. *Advances in Biology*. 2014;2014:e612471. doi:10.1155/2014/612471

19. Lee G, Espirito Santo AI, Zwingenberger S, et al. Fully reduced HMGB1 accelerates the regeneration of multiple tissues by transitioning stem cells to GAlert. *Proceedings of the National Academy of Sciences*. 2018;115(19):E4463-E4472. doi:10.1073/pnas.1802893115

20. Evans W, Shankaran M, Nyangau E, et al. Effects of Fortetropin on the Rate of Muscle Protein Synthesis in Older Men and Women: A Randomized, Double-Blinded, Placebo-Controlled Study. *J Gerontol A Biol Sci Med Sci*. 2020;76(1):108-114. doi:10.1093/gerona/glaa162

21. Sousa-Victor P, García-Prat L, Muñoz-Cánoves P. Control of satellite cell function in muscle regeneration and its disruption in ageing. *Nat Rev Mol Cell Biol*. 2022;23(3):204-226. doi:10.1038/s41580-021-00421-2

22. Ryall JG, Dell'Orso S, Derfoul A, et al. The NAD(+)-dependent SIRT1 deacetylase translates a metabolic switch into regulatory epigenetics in skeletal muscle stem cells. Cell Stem Cell. 2015;16(2):171-183. doi:10.1016/j.stem.2014.12.004

23. Liu Y, Beyer A, Aebersold R. On the Dependency of Cellular Protein Levels on mRNA Abundance. Cell. 2016;165(3):535-550. doi:10.1016/j.cell.2016.03.014

24. Greenbaum D, Colangelo C, Williams K, Gerstein M. Comparing protein abundance and mRNA expression levels on a genomic scale. Genome Biology. 2003;4(9):117. doi:10.1186/gb-2003-4-9-117

25. Maier T, Güell M, Serrano L. Correlation of mRNA and protein in complex biological samples. FEBS Lett. 2009;583(24):3966-3973. doi:10.1016/j.febslet.2009.10.036

26. Chen TC, Kuo T, Dandan M, et al. The role of striated muscle Pik3r1 in glucose and protein metabolism following chronic glucocorticoid exposure. *J Biol Chem*. 2021;296:100395. doi:10.1016/j.jbc.2021.100395

27. Ward CP, Peng L, Yuen S, et al. ER Unfolded Protein Response in Liver In Vivo Is Characterized by Reduced, Not Increased, De Novo Lipogenesis and Cholesterol Synthesis Rates with Uptake of Fatty Acids from Adipose Tissue: Integrated Gene Expression, Translation Rates and Metabolic Fluxes. *Int J Mol Sci*. 2022;23(3):1073. doi:10.3390/ijms23031073

28. Kurien BT, Scofield RH. Mouse urine collection using clear plastic wrap. *Lab Anim*. 1999;33(1):83-86. doi:10.1258/002367799780578525

29. Yang D, Diraison F, Beylot M, et al. Assay of low deuterium enrichment of water by isotopic exchange with [U-13C3]-acetone and gas chromatography-mass spectrometry. *Anal Biochem*. 1998;258(2):315-321. doi:10.1006/abio.1998.2632

30. Conboy MJ, Conboy IM. Preparation of adult muscle fiber-associated stem/precursor cells. *Methods Mol Biol*. 2010;621:149-163. doi:10.1007/978-1-60761-063-2_10

31. Busch R, Neese RA, Awada M, Hayes GM, Hellerstein MK. Measurement of cell proliferation by heavy water labeling. *Nat Protoc*. 2007;2(12):3045-3057. doi:10.1038/nprot.2007.420

32. Rogers-Broadway KR, Karydis LI, Dobson RC, Steele AJ. Ex-Vivo Signal Transduction Studies in Chronic Lymphocytic Leukemia. *Methods Mol Biol*. 2019;1881:1-17. doi:10.1007/978-1-4939-8876-1_1

33. Thompson ACS, Bruss MD, Price JC, et al. Reduced in vivo hepatic proteome replacement rates but not cell proliferation rates predict maximum lifespan extension in mice. *Aging Cell*. 2016;15(1):118-127. doi:10.1111/acel.12414

34. Huang DW, Sherman BT, Lempicki RA. Systematic and integrative analysis of large gene lists using DAVID bioinformatics resources. *Nat Protoc*. 2009;4(1):44-57. doi:10.1038/nprot.2008.211

35. Mahdy MAA, Lei HY, Wakamatsu JI, Hosaka YZ, Nishimura T. Comparative study of muscle regeneration following cardiotoxin and glycerol injury. *Annals of Anatomy - Anatomischer Anzeiger*. 2015;202:18-27. doi:10.1016/j.aanat.2015.07.002

36. Mehdipour M, Skinner C, Wong N, et al. Rejuvenation of three germ layers tissues by exchanging old blood plasma with saline-albumin. *Aging (Albany NY)*. 2020;12(10):8790-8819. doi:10.18632/aging.103418

37. Wang Y, Lu J, Liu Y. Skeletal Muscle Regeneration in Cardiotoxin-Induced Muscle Injury Models. *Int J Mol Sci*. 2022;23(21):13380. doi:10.3390/ijms232113380

38. Ge Y, Wu AL, Warnes C, et al. mTOR regulates skeletal muscle regeneration in vivo through kinase-dependent and kinase-independent mechanisms. *Am J Physiol Cell Physiol*. 2009;297(6):C1434-C1444. doi:10.1152/ajpcell.00248.2009

39. Chang NC, Chevalier FP, Rudnicki MA. Satellite Cells in Muscular Dystrophy – Lost in Polarity. *Trends in Molecular Medicine*. 2016;22(6):479-496. doi:10.1016/j.molmed.2016.04.002

Figure Legend

Figure 1 Pilot Study Measurements & Time Course Design
A.) Overview of $^{2}H_2O$ labeling time course and definition of each stage based on days after CTX injection. **B.)** Overview of global proteome FSR changes between contralateral limb and control (uninjected limb) muscle tissue after 3 days of CTX injection in Pilot Study. Significance determined by Student's Unpaired T-Test, * p<0.05, ** p<0.01, *** p<0.005, **** p<0.001**. C.)** Myosin 3 (EmyHC) turnover per day (K) value during various stages of muscle regeneration. Significance determined by Student's Unpaired T-Test, * p<0.05, ** p<0.01, *** p<0.005, **** p<0.001**. D.)** Measuring the fractional replacement rate (f-Value) of DNA in newly dividing myocytes in the contralateral limb in comparison to control samples. Significance determined by Student's Paired T-Test, * p<0.05, ** p<0.01, *** p<0.005, **** p<0.001**. E.)** Protein Group analysis of proteins found during this stage and separated into ontologies based on NIH DAVID analysis. Significance determined by Binomial Test of the proportion of proteins showing a higher or lower value of FSR in relation to control, * p<0.05.

Table 1 Individual Protein Turnover Values ± SD
Average % turnover per day ± standard deviation (SD) of each individual protein in each group. Proteins with **bold text** and a * in their boxes are significant by Student's Unpaired T-Test with Benjamini Hochberg correction for multiple comparisons when compared to their control value, * p<0.05.

Figure 2 Changes in Global Protein Turnover Rates at Each Stage
A.) Overview of global proteome FSR changes between contralateral (CNTRA) and control muscle tissue after 4 days of CTX injection. **B.)** Overview of global proteome FSR changes between CNTRA and control muscle tissue after 7 days of CTX injection. **C.)** Overview of global proteome FSR changes between CNTRA and control muscle tissue after 14 days of CTX injection. For all figures, significance determined by Student's Unpaired T-Test, * p<0.05, ** p<0.01, *** p<0.005, **** p<0.001**.**

Figure 3 Changes in Ontology-Grouped Protein Turnover Rates in Each Stage
A.) Protein Group analysis of proteins found during the Proliferation Stage (4 dpi) and separated into functional clusters based on NIH DAVID analysis. **B.)** Protein Group analysis of proteins found during the Differentiation Stage (7 dpi) and separated into functional clusters based on NIH DAVID analysis. **C.)** Protein Group analysis of proteins found during the Maturation Stage (14 dpi) and separated into functional clusters based on NIH DAVID analysis. Significance determined by Binomial Test of the proportion of proteins showing a higher or lower value of FSR in relation to uninjected (control), * p<0.05.

Figure 4 Significantly Different Individual Protein Turnover Rates at Each Stage
A.) Comparison of change in individual protein FSR value between CNTRA and control limbs for proteins that are significantly different after Benjamini Hochberg correction for multiple comparisons at 4 days after CTX injection (Proliferation Stage) **B.)** Comparison of change in individual protein FSR value between CNTRA and control limbs for proteins that are significantly different after Benjamini Hochberg correction for multiple comparisons at 7 days after CTX injection (Differentiation Stage). **C.)** Comparison of change in individual protein FSR

value between CNTRA and control limbs for proteins that are significantly different after Benjamini Hochberg correction for multiple comparisons at 14 days after CTX injection (Maturation Stage). Significance determined by Student's Unpaired T-Test with Benjamini Hochberg correction for multiple comparisons, * $p<0.05$, ** $p<0.01$, *** $p<0.005$, **** $p<0.001$.

Figure 5 Global Gene Expression Rates at Each Stage

A.) Volcano plot of global gene expression (FPKM) on the X-axis and Log_{10}(p value) on the Y-axis for all genes found during the Proliferation Stage (4 dpi). **B.)** Volcano plot of global gene expression (FPKM) on the X-axis and Log_{10}(p value) on the Y-axis for all genes found during the Proliferation Stage (7 dpi). **C.)** Volcano plot of global gene expression (FPKM) on the X-axis and Log_{10}(p value) on the Y-axis for all genes found during the Proliferation Stage (14 dpi). All gene expression values with a -log10(p value) of below 1.301 were non-significant and are colored in gray.

Figure 6 Matched Group Ontology Gene Expression at Each Stage to Individual Proteins

A.) Functional Clusters of gene expression in CNTRA limb based on protein groups (used in Figure 3) from NIH DAVID at the Proliferation Stage (4 dpi). **B.)** Functional Clusters of gene expression in CNTRA limb based on protein groups (used in Figure 3) from NIH DAVID at the Differentiation Stage (7 dpi) **C.)** Functional Clusters of gene expression in CNTRA limb based on protein groups (used in Figure 3) from NIH DAVID at the Maturation Stage (14 dpi). For all groups, significance of mRNA data was determined by Binomial Test for the number of proteins showing a higher or lower value of FSR in relation to control, * $p<0.05$.

Figure 7 Correlations of Gene Expression to Protein FSR

A.) Correlation graphs between log transformed fold change in gene expression (FPKM, Y Axis) and log transformed fold change in protein turnover (FSR, X Axis) for Proliferation Stage (4 dpi) **B.)** Correlation graphs between log transformed fold change in gene expression (FPKM, Y Axis) and log transformed fold change in protein turnover (FSR, X Axis) for Differentiation Stage (7 dpi) **C.)** Correlation graphs between log transformed fold change in gene expression (FPKM, Y Axis) and log transformed fold change in protein turnover (FSR, X Axis) for Maturation Stage (14 dpi). For all graphs, significance was determined by simple linear regression equation with R^2 value shown.

Figure 8 My3 Protein Turnover, Myh3 Gene Expression, and Myogenic Gene Expression
A.) Myosin 3 (EmyHC) turnover per day (K) value during various stages of muscle regeneration. Significance determined by One-Way ANOVA with Benjamini-Hochberg correction for multiple comparisons. * $p<0.05$, ** $p<0.01$, *** $p<0.005$, **** $p<0.001$. **B.)** Gene expression (FPKM) of Myh3 during various stages of muscle regeneration. Significance determined by One-Way ANOVA with Benjamini-Hochberg correction for multiple comparisons. * $p<0.05$, ** $p<0.01$, *** $p<0.005$, **** $p<0.001$. **C.)** Myogenic gene expression was measured in FPKM in all stages and control group. Significance determined by One-Way ANOVA with Benjamini-Hochberg correction for multiple comparisons. * $p<0.05$, ** $p<0.01$, *** $p<0.005$, **** $p<0.001$.

Supplemental Figure Legend

Figure S1 Proteomic Signature of Non-Muscle (Liver) Tissue at all Stages
A.) Overview of global proteome FSR changes between CTX and control (uninjected) liver tissue after 4 days of CTX injection for 304 proteins present in both tissues. **B.)** Overview of global proteome FSR changes between CTX and control (uninjected) liver tissue after 7 days of CTX injection for 308 proteins present in both tissues. **C.)** Overview of global proteome FSR changes between CTX and control (uninjected) liver tissue after 14 days of CTX injection for 304 proteins present in both tissues. Significance determined by Student's Paired T-Test, * $p<0.05$, ** $p<0.01$, *** $p<0.005$, **** $p<0.001$.

Figures and Tables

<u>Figure 1</u> Pilot Study Measurements & Time Course Design

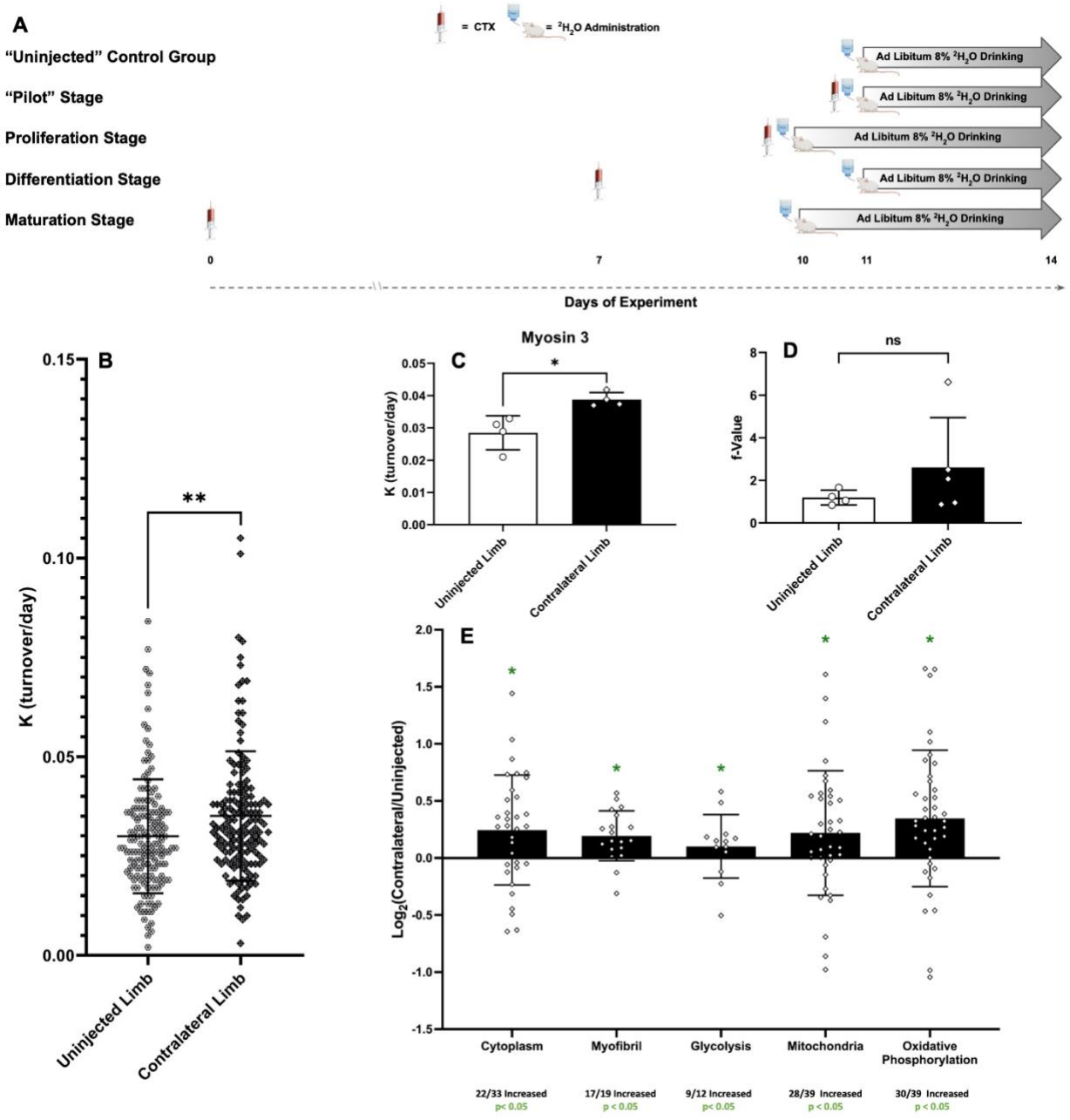

Table 1 Individual Protein Turnover Values ± SD

#	Protein	Accession #	Ontology	Pilot Stage	Proliferation Stage	Differentiation Stage	Maturation Stage	Control
1	Carbonic anhydrase 3	P16015	Cytoplasm	3.114 ± 0.186%	**4.823 ± 0.299%***	3.700 ± 0.354%	3.234 ± 0.449%	2.601% ± 0.406%
2	Sarcoplasmic/endoplasmic reticulum calcium ATPase 1	Q8R429	Cytoplasm	3.415 ± 0.648%	**4.258 ± 0.085%***	3.426 ± 0.441%	3.151 ± 0.217%	2.817 ± 0.330%
3	Glucose-6-phosphate isomerase	P06745	Glycolysis	2.318 ± 0.648%	**3.198 ± 0.346%***	2.854 ± 0.791%	1.957 ± 0.648%	1.550 ± 0.270%
4	L-lactate dehydrogenase A chain	P06151	Glycolysis	3.060 ± 0.550%	**3.947 ± 0.289%***	3.153 ± 0.353%	2.932 ± 0.327%	2.186 ± 0.442%
5	Malate dehydrogenase, mitochondrial	P08249	Mitochondria	2.312 ± 0.210%	**4.296 ± 0.366%***	2.617 ± 0.512%	2.734 ± 0.499%	2.172 ± 0.413%
6	Troponin T, fast skeletal muscle	Q9QZ47	Myofibril	3.872 ± 0.402%	**5.175 ± 0.521%***	**4.353 ± 0.286%***	3.885 ± 0.455%	3.483 ± 0.242%
7	Myosin light chain 1/3, skeletal muscle isoform	P05977	Myofibril	2.437 ± 0.512%	**3.035 ± 0.391%***	2.434 ± 0.222%	2.038 ± 0.360%	1.704 ± 0.283%
8	ATP synthase subunit beta, mitochondrial	P56480	OxPhos	2.464 ± 0.374%	**3.542 ± 0.379%***	3.131 ± 0.803%	3.034 ± 0.365%	2.161 ± 0.195%
9	Calsequestrin-1	O09165	Cytoplasm	1.782 ± 0.337%	**2.569 ± 0.272%***	**2.477 ± 0.139%***	2.035 ± 0.497%	1.068 ± 0.545%
10	Fructose-bisphosphate aldolase A	P05064	Glycolysis	4.149 ± 0.342%	**5.326 ± 0.311%***	4.531 ± 0.476%	4.012 ± 0.330%	3.740 ± 0.572%
11	Glycogen phosphorylase, muscle form	Q9WUB3	Glycolysis	4.127 ± 0.339%	**5.660 ± 0.573%***	4.741 ± 0.668%	4.339 ± 0.466%	3.732 ± 0.561%
12	Creatine kinase M-type	P07310	Cytoplasm	2.564 ± 0.253%	**3.392 ± 0.304%***	3.014 ± 0.325%	2.658 ± 0.302%	2.335 ± 0.335%
13	Aspartate aminotransferase, cytoplasmic	P05201	Cytoplasm	4.061 ± 2.072%	**5.740 ± 0.789%***	4.988 ± 1.953%	3.202 ± 1.771%	2.420 ± 0.991%
14	Pyruvate kinase PKM	P52480	Glycolysis	3.512 ± 0.703%	**5.070 ± 0.753%***	4.136 ± 0.469%	3.703 ± 0.348%	3.038 ± 0.533%
15	Parkinson disease	Q99LX0	Cytoplasm	2.652 ± 0.831%	**3.992 ± 0.931%***	3.673 ± 1.959%	3.883 ± 2.255%	1.455 ± 0.853%

	protein 7 homolog							
16	Collagen alpha-1(I) chain	P11087	Cytoplasm	3.793 ± 0.598%	**2.303 ± 0.737%***	2.952 ± 0.941%	**1.304 ± 0.221%***	3.901 ± 0.311%
17	Triosephosphate isomerase	P17751	Glycolysis	2.607 ± 0.312%	**3.519 ± 0.386%***	3.270 ± 0.479%	2.585 ± 0.244%	2.443 ± 0.389%
18	Tropomyosin alpha-1 chain	P58771	Myofibril	3.644 ± 0.638%	**4.244 ± 0.460%***	4.204 ± 0.501%	3.364 ± 0.393%	3.051 ± 0.435%
19	Myosin regulatory light chain 2, skeletal muscle isoform	P97457	Myofibril	1.572 ± 0.360%	**2.554 ± 0.388%***	2.050 ± 0.316%	2.011 ± 0.353%	1.718 ± 0.264%
20	Pyruvate dehydrogenase E1 component subunit beta, mitochondrial	Q9D051	Mitochondria	1.440 ± 0.418%	**3.240 ± 0.464%***	3.018 ± 0.926%	2.898 ± 0.608%	1.737 ± 0.486%
21	ATP synthase subunit alpha, mitochondrial	Q03265	OxPhos	3.184 ± 0.495%	**4.498 ± 0.613%***	3.235 ± 0.460%	3.120 ± 0.678%	2.822 ± 0.628%
22	Troponin C, skeletal muscle	P20801	Myofibril	5.403 ± 0.328%	**5.815 ± 1.091%***	4.700± 1.244%	4.993 ± 0.805%	3.646 ± 0.703%
23	Vertnin	Q3SYK4	Cytoplasm	1.915 ± 0.314%	**1.137 ± 0.279%***	1.767 ± 0.287%	0.898 ± 0.205%	2.030 ± 0.476%
24	Phosphoglycerate mutase 2	O70250	Glycolysis	2.024 ± 0.546%	**3.040 ± 0.349%***	2.728 ± 0.675%	2.322 ± 0.382%	2.200 ± 0.390%
25	Beta-enolase	P21550	Glycolysis	3.039 ± 0.552%	**3.859 ± 0.243%***	3.640% ± 0.341%	3.078 ± 0.593%	2.929 ± 0.528%
26	Alpha-actinin-3	O88990	Myofibril	4.007 ± 0.377%	**5.064 ± 0.942%***	4.243 ± 0.913%	3.411 ± 0.467%	3.317 ± 0.560%
27	Glyceraldehyde-3-phosphate dehydrogenase	P16858	Glycolysis	2.587 ± 0.403%	3.245% ± 0.400%	2.693 ± 0.250%	2.376 ± 0.330%	2.414 ± 0.417%
28	Histone H2B type 1-M	P10854	Histone	3.236 ± 1.332%	1.843 ± 0.331%	2.487 ± 0.817%	1.943 ± 0.593%	1.067 ± 0.479%
29	Myosin-binding protein C, fast-type	Q5XKE0	Myofibril	2.809 ± 0.743%	4.042 ± 0.377%	3.502 ± 1.154%	2.993 ± 0.550%	2.642 ± 0.986%
30	Myoglobin	P04247	Extracellular	3.420 ± 0.895%	4.494 ± 0.708%	3.932 ± 0.412%	3.210 ± 0.343%	3.217 ± 0.700%
31	Myosin-7	Q91Z83	Myofibril	2.713 ± 0.641%	4.768 ± 1.466%	4.768 ± 1.113%	2.932 ± 0.622%	2.693 ± 0.693%
32	Myosin-3	P13541	Myofibril	3.876 ± 0.192%	3.708 ± 0.376%	3.732 ± 0.651%	3.290 ± 0.293%	2.846 ± 0.455%
33	ATP synthase subunit g, mitochondrial	Q9CPQ8	OxPhos	1.205 ± 0.203%	1.802 ± 0.692%	2.344 ± 0.867%	1.407 ± 0.666%	0.644 ± 0.556%

34	Actin, alpha cardiac muscle 1	P68033	Myofibril	1.382 ± 0.207%	1.960 ± 0.078%	1.767 ± 0.259%	1.445 ± 0.448%	1.310 ± 0.586%
35	Myosin-1	Q5SX40	Myofibril	3.224 ± 0.979%	3.545 ± 0.547%	3.292 ± 0.308%	2.414 ± 0.223%	2.676 ± 0.573%
36	Cytochrome c, somatic	P62897	OxPhos	3.796 ± 0.757%	4.124 ± 0.357%	3.994 ± 0.555%	3.513 ± 0.394%	2.965 ± 0.941%
37	Aspartate aminotransferase, mitochondrial	P05202	Mitochondria	1.963 ± 0.686%	3.244 ± 0.389%	2.119 ± 0.974%	2.199 ± 0.521%	1.959 ± 1.163%
38	Titin	A2ASS6	Myofibril	2.600 ± 1.040%	4.951 ± 2.441%	3.363 ± 1.257%	0.375 ± 0.421%	2.389 ± 0.612%
39	Hemoglobin subunit alpha	P01942	Extracellular	2.358 ± 0.481%	2.337 ± 0.256%	1.879 ± 0.166%	2.375 ± 0.569%	1.805 ± 0.491%
40	Cytochrome b-c1 complex subunit 1, mitochondrial	Q9CZ13	OxPhos	2.809 ± 0.224%	3.680 ± 0.837%	2.907 ± 0.536%	2.647 ± 0.306%	2.665 ± 0.422%
41	ADP/ATP translocase 2	P51881	Mitochondria	2.889 ± 0.257%	5.173 ± 1.042%	6.929 ± 0.872%	4.454 ± 1.437%	3.200 ± 1.468%
42	Desmoglein-4	Q7TMD7	Extracellular	3.318 ± 0.469%	4.710 ± 1.611%	3.880 ± 1.661%	4.858 ± 2.605%	2.543 ± 1.876%
43	Superoxide dismutase [Mn], mitochondrial	P09671	Mitochondria	2.188 ± 0.537%	2.262 ± 0.155%	1.835 ± 0.907%	1.332 ± 0.612%	1.870 ± 0.356%
44	Collagen alpha-1(III) chain	P08121	Cytoplasm	3.482 ± 1.204%	3.355 ± 1.852%	2.887 ± 0.943%	**2.009 ± 0.928%***	4.900 ± 0.872%
45	NADH-ubiquinone oxidoreductase 75 kDa subunit, mitochondrial	Q91VD9	OxPhos	2.977 ± 1.586%	3.948 ± 1.151%	3.453 ± 0.734%	2.818 ± 0.916%	2.645 ± 1.130%
46	ATP synthase subunit d, mitochondrial	Q9DCX2	OxPhos	3.074 ± 1.097%	3.004 ± 0.937%	4.523 ± 0.871%	3.561 ± 0.480%	4.227 ± 1.229%
47	Cytochrome b-c1 complex subunit 2, mitochondrial	Q9DB77	OxPhos	3.294 ± 0.854%	4.918 ± 1.452%	4.266 ± 1.163%	3.888 ± 0.241%	3.717 ± 0.187%
48	NADH dehydrogenase [ubiquinone] 1 beta subcomplex subunit 10	Q9DCS9	OxPhos	3.148 ± 1.993%	3.614 ± 0.924%	3.006 ± 1.034%	3.778 ± 1.228%	1.739 ± 0.895%

49	Nucleoside diphosphate kinase B	Q01768	Cytoplasm	4.757 ± 1.747%	2.074 ± 1.233%	2.391 ± 0.730%	2.141 ± 0.812%	2.919 ± 0.759%
50	ADP/ATP translocase 1	P48962	Mitochondria	3.859 ± 0.897%	4.890 ± 0.634%	6.287 ± 1.715%	4.309 ± 0.702%	3.913 ± 1.588%
51	Tropomyosin beta chain	P58774	Myofibril	3.066 ± 0.414%	3.248 ± 0.575%	3.074 ± 0.496%	2.508 ± 0.259%	2.765 ± 0.677%
52	ATP synthase subunit O, mitochondrial	Q9DB20	OxPhos	4.164 ± 2.046%	2.590 ± 0.525%	3.294 ± 1.092%	1.863 ± 0.124%	1.939 ± 1.097%
53	Centrosomal protein of 162 kDa	Q6ZQ06	Cytoplasm	0.322 ± 0.236%	0.311 ± 0.176%	0.459 ± 0.064%	0.386 ± 0.043%	0.504 ± 0.102%
54	Myosin-4	Q5SX39	Myofibril	3.013 ± 0.294%	2.843 ± 0.367%	3.064 ± 0.182%	2.513 ± 0.158%	2.579 ± 0.396%
55	Adenylate kinase isoenzyme 1	Q9R0Y5	Cytoplasm	3.811 ± 2.699%	3.408 ± 0.583%	2.432 ± 0.600%	2.741 ± 1.339%	2.676 ± 1.246%
56	Phosphoglucomutase-1	Q9D0F9	Glycolysis	2.637 ± 0.791%	2.659 ± 0.632%	2.609 ± 0.414%	2.086 ± 0.304%	2.343 ± 0.399%
57	Aconitate hydratase, mitochondrial	Q99KI0	Mitochondria	3.734 ± 0.654%	3.475 ± 0.903%	3.573 ± 0.328%	3.614 ± 0.761%	3.036 ± 0.348%
58	Albumin	P07724	Extracellular	10.053 ± 4.411%	9.283 ± 4.184%	8.334 ± 4.176%	3.430 ± 1.788%	7.128 ± 3.629%
59	Cytochrome b-c1 complex subunit 7	Q9D855	OxPhos	3.903 ± 0.846%	3.636 ± 0.937%	3.001 ± 0.467%	3.114 ± 0.655%	3.208 ± 0.169%
60	Phosphoglycerate kinase 1	P09411	Glycolysis	2.958 ± 1.001%	2.836 ± 0.278%	2.448 ± 0.193%	2.048 ± 0.293%	2.604 ± 0.595%
61	Myozenin-1	Q9JK37	Myofibril	3.881 ± 1.801%	4.142 ± 1.267%	3.082 ± 1.641%	4.098 ± 2.345%	3.517 ± 1.355%
62	Phosphatidylethanolamine-binding protein 1	P70296	Cytoplasm	2.316 ± 1.225%	2.747 ± 0.790%	5.064 ± 4.213%	2.349 ± 2.201%	3.587 ± 2.678%
63	LIM domain-binding protein 3	Q9JKS4	Cytoplasm	2.039 ± 1.138%	1.999 ± 0.587%	2.107 ± 0.308%	1.850 ± 0.670%	1.677 ± 1.035%
64	Collagen alpha-2(I) chain	Q01149	Cytoplasm	2.799 ± 0.912%	2.184 ± 0.294%	2.711 ± 1.321%	1.478 ± 0.531%	1.854 ± 1.341%
65	Parvalbumin alpha	P32848	Extracellular	5.065 ± 0.989%	4.743 ± 0.575%	2.979 ± 0.477%	2.118 ± 0.228%	4.407 ± 1.472%
66	Trifunctional enzyme subunit alpha, mitochondrial	Q8BMS1	Mitochondria	3.639 ± 1.250%	2.853 ± 0.922%	4.167 ± 1.379%	1.752 ± 1.302%	3.062 ± 1.035%
67	Myosin light	P09542	Myofibril	3.708 ± 0.461%	3.363 ± 1.985%	6.224 ± 4.612%	4.446 ± 3.417%	3.655 ± 1.621%

	chain 3							
68	Actin, alpha skeletal muscle	P68134	Myofibril	1.525 ± 0.521%	1.067 ± 0.462%	1.311 ± 0.606%	1.687 ± 0.275%	1.136 ± 0.510%
69	Histone H4	P62806	Histone	4.275 ± 1.722%	6.142 ± 3.350%	3.501 ± 1.922%	9.567 ± 9.870%	6.603 ± 3.354%
70	NADH dehydrogenase [ubiquinone] iron-sulfur protein 6, mitochondrial	P52503	OxPhos	3.395 ± 0.306%	3.471 ± 0.598%	3.567 ± 0.428%	3.110 ± 0.339%	3.515 ± 0.438%
71	Troponin I, fast skeletal muscle	P13412	Myofibril	3.168 ± 0.431%	3.165 ± 0.682%	3.891 ± 1.180%	3.403 ± 0.970%	3.121 ± 0.639%
72	Dihydrolipoyl dehydrogenase, mitochondrial	O08749	Mitochondria	3.153 ± 1.063%	5.782 ± 2.841%	6.419 ± 1.235%	5.145 ± 1.363%	5.728 ± 1.009%
73	Succinate dehydrogenase [ubiquinone] iron-sulfur subunit, mitochondrial	Q9CQA3	Mitochondria	4.339 ± 3.044%		6.857 ± 1.596%		4.721 ± 0.422%
74	Cytochrome c oxidase subunit 2	P00405	OxPhos	2.215 ± 0.428%		**2.063 ± 0.168%***	**2.298 ± 0.115%***	1.094 ± 0.250%
75	Cytochrome c oxidase subunit 6C	Q9CPQ1	OxPhos	4.558 ± 1.427%		4.358 ± 0.604%	**3.963 ± 0.109%***	2.863 ± 0.368%
76	ATP synthase-coupling factor 6, mitochondrial	P97450	OxPhos	2.288 ± 1.652%		**3.042 ± 0.715%***	2.322 ± 0.652%	0.727 ± 0.438%
77	Cytochrome c oxidase subunit 6B1	P56391	OxPhos	2.841 ± 0.518%		3.190 ± 0.822%	2.977 ± 0.281%	2.232 ± 0.256%
78	NADH dehydrogenase [ubiquinone] iron-sulfur protein 8, mitochondrial	Q8K3J1	OxPhos	6.143 ± 3.529%		2.912 ± 0.768%	3.012 ± 0.404%	1.945 ± 0.159%
79	Voltage-dependent anion-selective channel protein 2	Q60930	Mitochondria	1.870 ± 0.913%		3.147 ± 1.305%	3.431 ± 1.221%	1.172 ± 0.342%

80	Glycerol-3-phosphate dehydrogenase, mitochondrial	Q64521	Mitochondria	2.531 ± 1.101%		0.201 ± 0.099%	0.821 ± 0.642%	4.087 ± 1.488%
81	Triadin	E9Q9K5	Cytoplasm	4.672 ± 2.441%		3.000 ± 1.073%	2.479 ± 0.154%	3.556 ± 0.704%
82	Histone H2A type 1-B	C0HKE1	Histone	1.514 ± 1.988%		1.177 ± 0.479%	1.501 ± 0.620%	0.156 ± 0.069%
83	MICOS complex subunit Mic60	Q8CAQ8	Mitochondria	2.058 ± 0.543%		4.011 ± 1.867%	4.384 ± 0.985%	2.017 ± 0.956%
84	NADH dehydrogenase [ubiquinone] flavoprotein 1, mitochondrial	Q91YT0	OxPhos	2.741 ± 0.600%		4.366 ± 1.801%	4.031 ± 0.429%	2.639 ± 0.931%
85	ATP synthase subunit gamma, mitochondrial	Q91VR2	OxPhos	2.432 ± 0.946%		3.140 ± 0.869%	2.489 ± 0.449%	1.698 ± 0.066%
86	Ubiquinone biosynthesis protein COQ9, mitochondrial	Q8K1Z0	Mitochondria	3.793 ± 1.175%		3.170 ± 1.314%	3.934 ± 0.528%	2.647 ± 0.885%
87	NADH dehydrogenase [ubiquinone] 1 alpha subcomplex subunit 9, mitochondrial	Q9DC69	OxPhos	2.730 ± 1.986%		2.584 ± 2.531%	2.855 ± 1.005%	5.376 ± 1.077%
88	Keratin, type II cytoskeletal 1	P04104	Cytoplasm	7.891 ± 3.991%		6.559 ± 1.662%	3.181 ± 1.527%	6.157 ± 2.426%
89	E3 ubiquitin-protein ligase UBR3	Q5U430	Cytoplasm	1.772 ± 0.611%		2.620 ± 0.689%	2.488 ± 0.686%	1.223 ± 1.010%
90	Cytochrome c oxidase subunit 5B, mitochondrial	P19536	OxPhos	3.330 ± 0.820%		4.537 ± 0.404%	3.512 ± 0.813%	2.548 ± 0.453%
91	Voltage-dependent anion-selective channel protein 1	Q60932	Mitochondria	3.642 ± 1.323%		3.742 ± 0.676%	3.374 ± 0.234%	2.609 ± 0.838%
92	Cytochrome b-c1 complex	Q9CR68	OxPhos	4.259 ± 1.176%		3.787 ± 1.010%	3.331 ± 0.479%	2.817 ± 0.306%

	subunit Rieske, mitochondrial							
93	NADH dehydrogenase [ubiquinone] 1 beta subcomplex subunit 9	Q9CQJ8	OxPhos	1.716 ± 1.265%		3.718 ± 1.353%	1.587 ± 1.205%	3.540 ± 1.634%
94	Cytochrome c oxidase subunit NDUFA4	Q62425	OxPhos	6.893 ± 2.216%		5.726 ± 1.061%	5.981 ± 0.943%	4.204 ± 1.703%
95	Cytochrome c oxidase subunit 5A, mitochondrial	P12787	OxPhos	4.090 ± 0.837%		3.191 ± 1.460%	2.542 ± 0.820%	3.396 ± 0.516%
96	Citrate synthase, mitochondrial	Q9CZU6	Mitochondria	3.665 ± 0.889%		3.996 ± 1.199%	3.135 ± 0.582%	2.582 ± 0.272%
97	ATP-dependent 6-phosphofructokinase, muscle type	P47857	Glycolysis	7.281 ± 5.101%		9.122 ± 1.336%	7.845 ± 3.439%	5.001 ± 1.547%
98	Cytochrome b-c1 complex subunit 8	Q9CQ69	OxPhos	3.787 ± 0.708%		5.640 ± 1.832%	5.270 ± 1.410%	4.042 ± 0.686%
99	NADH dehydrogenase [ubiquinone] flavoprotein 2, mitochondrial	Q9D6J6	OxPhos	2.873 ± 0.887%		9.509 ± 0.754%	16.387 ± 12.359%	3.601 ± 0.434%
100	Creatine kinase S-type, mitochondrial	Q6P8J7	Mitochondria	3.096 ± 0.457%		3.163 ± 0.909%	3.010 ± 0.262%	2.674 ± 0.426%
101	ATP synthase F(0) complex subunit B1, mitochondrial	Q9CQQ7	OxPhos	3.450 ± 1.129%		3.825 ± 1.000%	2.485 ± 0.216%	6.825 ± 6.659%
102	Succinate dehydrogenase [ubiquinone] flavoprotein subunit, mitochondrial	Q8K2B3	Mitochondria	7.954 ± 2.955%		2.474 ± 0.890%	3.145 ± 1.551%	5.273 ± 2.281%

103	Very long-chain specific acyl-CoA dehydrogenase, mitochondrial	P50544	Mitochondria	5.614 ± 2.316%		7.521 ± 1.974%	5.465 ± 2.534%	3.403 ± 1.957%
104	Sarcalumenin	Q7TQ48	Cytoplasm	2.356 ± 1.545%		2.516 ± 0.868%	1.436 ± 0.548%	1.861 ± 0.849%
105	Elongation factor 1-alpha 2	P62631	Cytoplasm	3.813 ± 1.115%		3.211 ± 1.248%	2.855 ± 1.632%	4.157 ± 2.372%
106	ATP synthase subunit delta, mitochondrial	Q9D3D9	OxPhos	1.939 ± 0.655%		2.723 ± 1.296%	1.752 ± 0.622%	1.343 ± 0.017%
107	Cytochrome c1, heme protein, mitochondrial	Q9D0M3	OxPhos	3.610 ± 0.774%		4.604 ± 0.726%	3.403 ± 0.600%	3.057 ± 0.585%
108	NADH dehydrogenase [ubiquinone] iron-sulfur protein 5	Q99LY9	OxPhos	2.309 ± 1.021%		2.965 ± 0.512%	2.811 ± 0.366%	3.189 ± 0.748%
109	Myelin protein P0	P27573	Cytoplasm	1.705 ± 0.774%		4.633 ± 0.804%	3.061 ± 1.079%	2.322 ± 1.902%
110	NADH dehydrogenase [ubiquinone] 1 beta subcomplex subunit 1	P0DN34	OxPhos	4.934 ± 1.234%		4.080 ± 0.741%	3.714 ± 0.299%	3.946 ± 0.583%
111	Calcium-binding mitochondrial carrier protein Aralar1	Q8BH59	Mitochondria	3.569 ± 2.938%		8.266 ± 3.241%	3.852 ± 2.386%	2.453 ± 1.022%
112	Heat shock cognate 71 kDa protein	P63017	Cytoplasm	10.487 ± 3.247%		7.672 ± 2.389%	6.461 ± 3.667%	5.112 ± 2.252%
113	NADH dehydrogenase [ubiquinone] iron-sulfur protein 3, mitochondrial	Q9DCT2	OxPhos	4.987 ± 1.091%		2.477 ± 1.230%	3.245 ± 0.697%	3.711 ± 1.450%
114	Malate dehydrogenase, cytoplasmic	P14152	Cytoplasm	2.945 ± 0.640%		2.815 ± 0.687%	2.747 ± 0.952%	3.050 ± 0.750%
115	E3 ubiquiti	A2AN08	Cytoplasm	2.767 ± 0.393%		3.561 ± 0.552%	2.840 ± 0.434%	2.688 ± 0.388%

	n-protein ligase UBR4							
116	Hemoglobin subunit beta-1	P02088	Extracellular	3.137 ± 0.264%		2.217 ± 0.573%	2.386 ± 0.766%	2.598 ± 0.668%
117	2-oxoglutarate dehydrogenase, mitochondrial	Q60597	Mitochondria	6.795 ± 2.724%		4.549 ± 3.064%	5.190 ± 1.017%	4.591 ± 2.809%
118	Cytochrome c oxidase subunit 4 isoform 1, mitochondrial	P19783	OxPhos	3.778 ± 0.951%		4.756 ± 0.636%	4.000 ± 0.273%	3.773 ± 1.138%
119	Electron transfer flavoprotein subunit alpha, mitochondrial	Q99LC5	OxPhos	4.869 ± 0.896%		4.809 ± 3.391%	7.164 ± 10.266%	4.550 ± 0.808%
120	Phosphate carrier protein, mitochondrial	Q8VEM8	Mitochondria	4.449 ± 1.075%		4.228 ± 0.570%	2.540 ± 3.293%	3.548 ± 2.193%
121	NADH dehydrogenase [ubiquinone] 1 alpha subcomplex subunit 8	Q9DCJ5	OxPhos	5.806 ± 1.686%		4.420 ± 1.218%	3.164 ± 0.331%	3.268 ± 0.564%
122	Isocitrate dehydrogenase [NAD] subunit alpha, mitochondrial	Q9D6R2	OxPhos	4.598 ± 1.865%		3.193 ± 1.337%	3.109 ± 1.157%	3.388 ± 1.500%
123	Alpha-enolase	P17182	Glycolysis	3.105 ± 1.161%		4.255 ± 1.460%	3.434 ± 1.163%	3.630 ± 0.959%
124	NADH dehydrogenase [ubiquinone] 1 alpha subcomplex subunit 7	Q9Z1P6	OxPhos	6.368 ± 1.564%		6.960 ± 1.335%	5.705 ± 0.825%	5.817 ± 0.603%
125	Cytochrome b-c1 complex subunit 6, mitochondrial	P99028	OxPhos	2.759 ± 0.302%		1.829 ± 0.651%	1.953 ± 0.690%	1.871 ± 0.453%
126	Alpha-actinin-2	Q9JI91	Myofibril	2.935 ± 1.590%		4.277 ± 1.019%	3.622 ± 0.318%	3.642 ± 0.774%

127	Cytochrome c oxidase subunit 6A2, mitochondrial	P43023	OxPhos	6.078 ± 1.144%		3.784 ± 1.438%	7.749 ± 3.330%	7.717 ± 3.418%
128	Acyl carrier protein, mitochondrial	Q9CR21	Mitochondria	4.787 ± 0.262%				1.817 ± 0.387%
129	Zinc finger protein 76	Q8BMU0	Cytoplasm	4.242 ± 0.487%				3.560 ± 0.299%
130	Tropomyosin alpha-3 chain	P21107	Myofibril	2.928 ± 0.471%				2.259 ± 0.861%
131	1-phosphatidylinositol 4,5-bisphosphate phosphodiesterase gamma-1	Q62077	Cytoplasm	3.769 ± 1.207%				2.268 ± 1.371%
132	NADH dehydrogenase [ubiquinone] iron-sulfur protein 2, mitochondrial	Q91WD5	Mitochondria	6.354 ± 5.953%				2.083 ± 2.195%
133	Isocitrate dehydrogenase [NAD] subunit gamma 1, mitochondrial	P70404	Mitochondria	7.512 ± 3.719%				4.171 ± 2.017%
134	CMRF35-like molecule 2	Q8K249	Cytoplasm	3.335 ± 0.217%				3.914 ± 0.976%
135	B-cell lymphoma/leukemia 11B	Q99PV8	Cytoplasm	3.568 ± 1.576%				1.313 ± 0.537%
136	Voltage-dependent anion-selective channel protein 3	Q60931	Mitochondria	2.386 ± 0.465%				39.766 ± 32.619%
137	Dynein heavy chain 3, axonemal	Q8BW94	Cytoplasm	3.999 ± 1.434%				3.120 ± 1.360%
138	Dihydrolipoyllysine-residue acetyltransferase compon	Q8BMF4	Mitochondria	3.428 ± 3.859%				1.499 ± 1.230%

	ent of pyruvate dehydrogenase complex, mitochondrial							
139	Gamma-enolase	P17183	Glycolysis	5.933 ± 2.878%				8.412 ± 5.710%
140	MICOS complex subunit Mic19	Q9CRB9	Mitochondria	4.826 ± 2.581%				3.879 ± 1.297%
141	Succinate--CoA ligase [ADP/GDP-forming] subunit alpha, mitochondrial	Q9WUM5	Ox Phos	3.783 ± 1.477%				3.204 ± 1.670%
142	Low-density lipoprotein receptor	P35951	Cytoplasm	2.254 ± 0.671%				1.988 ± 0.753%
143	Gem-associated protein 5	Q8BX17	Cytoplasm	3.918 ± 1.272%				4.871 ± 4.249%
144	NADH dehydrogenase [ubiquinone] 1 alpha subcomplex subunit 11	Q9D8B4	Ox Phos	1.015 ± 0.657%				0.811 ± 0.239%
145	V-type proton ATPase catalytic subunit A	P50516	Mitochondria	0.982 ± 0.809%				1.270 ± 1.228%
146	Fumarate hydratase, mitochondrial	P97807	Mitochondria	1.838 ± 1.527%				2.307 ± 0.947%
147	3-ketoacyl-CoA thiolase, mitochondrial	Q8BWT1	Mitochondria	2.274 ± 1.337%				1.990 ± 1.514%
148	Electron transfer flavoprotein-ubiquinone oxidoreductase, mitochondrial	Q921G7	Mitochondria	2.806 ± 0.541%				2.667 ± 0.957%
149	Mitochondrial pyruvate carrier 2	Q9D023	Mitochondria	6.929 ± 0.977%				7.239 ± 1.821%
150	UBX domain-containing	Q99PL6	Cytoplasm	1.838 ± 0.298%				1.911 ± 0.741%

	protein 6							
151	Solute carrier family 13 member 5	Q67BT3	Mitochondria	0.933 ± 0.91%				0.93 ± 0.12%

Figure 2 Global Protein Turnover Rates at Each Stage

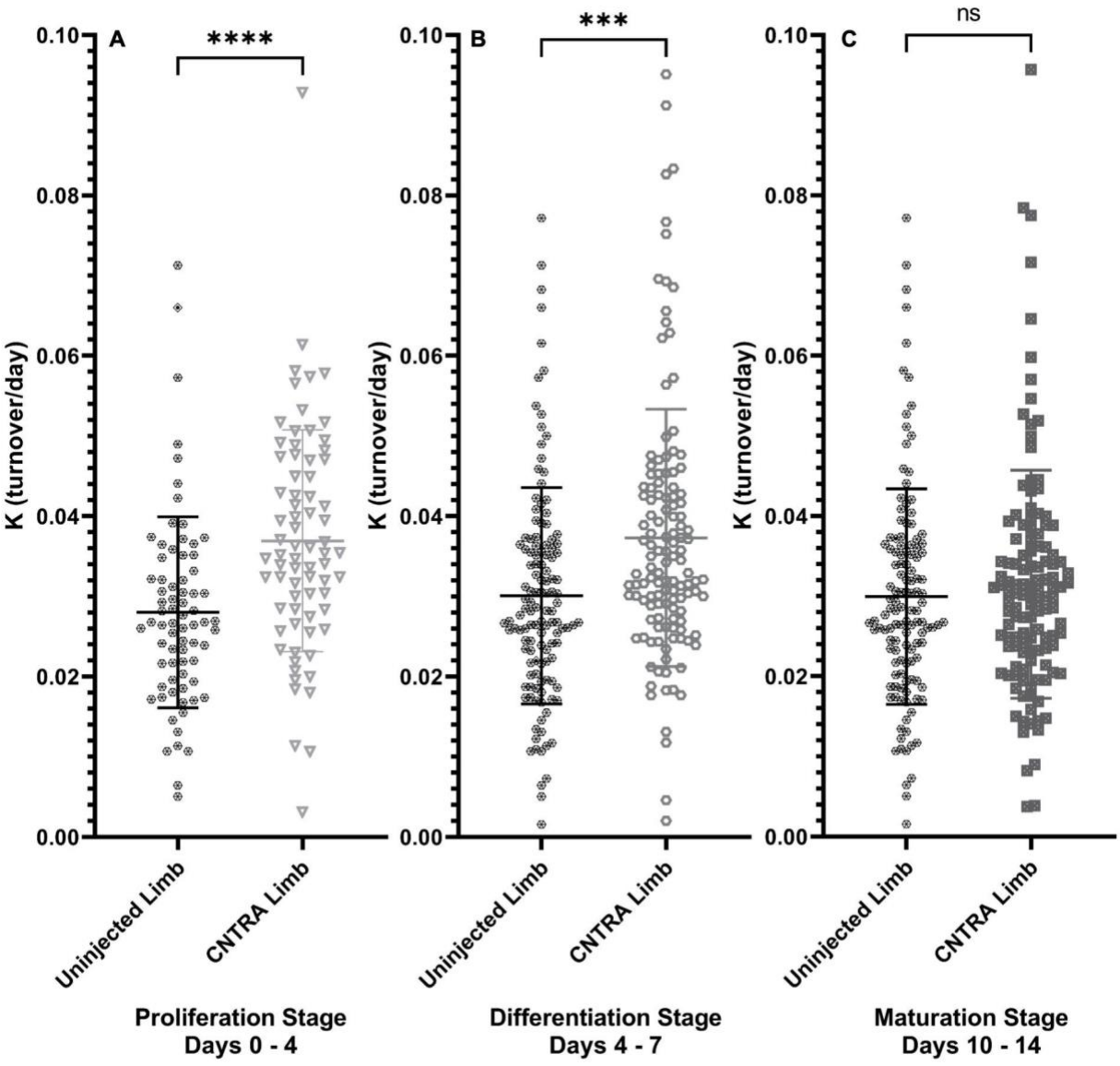

<u>Figure 3</u> Changes in Protein Ontology Group Turnover Rates at Each Stage

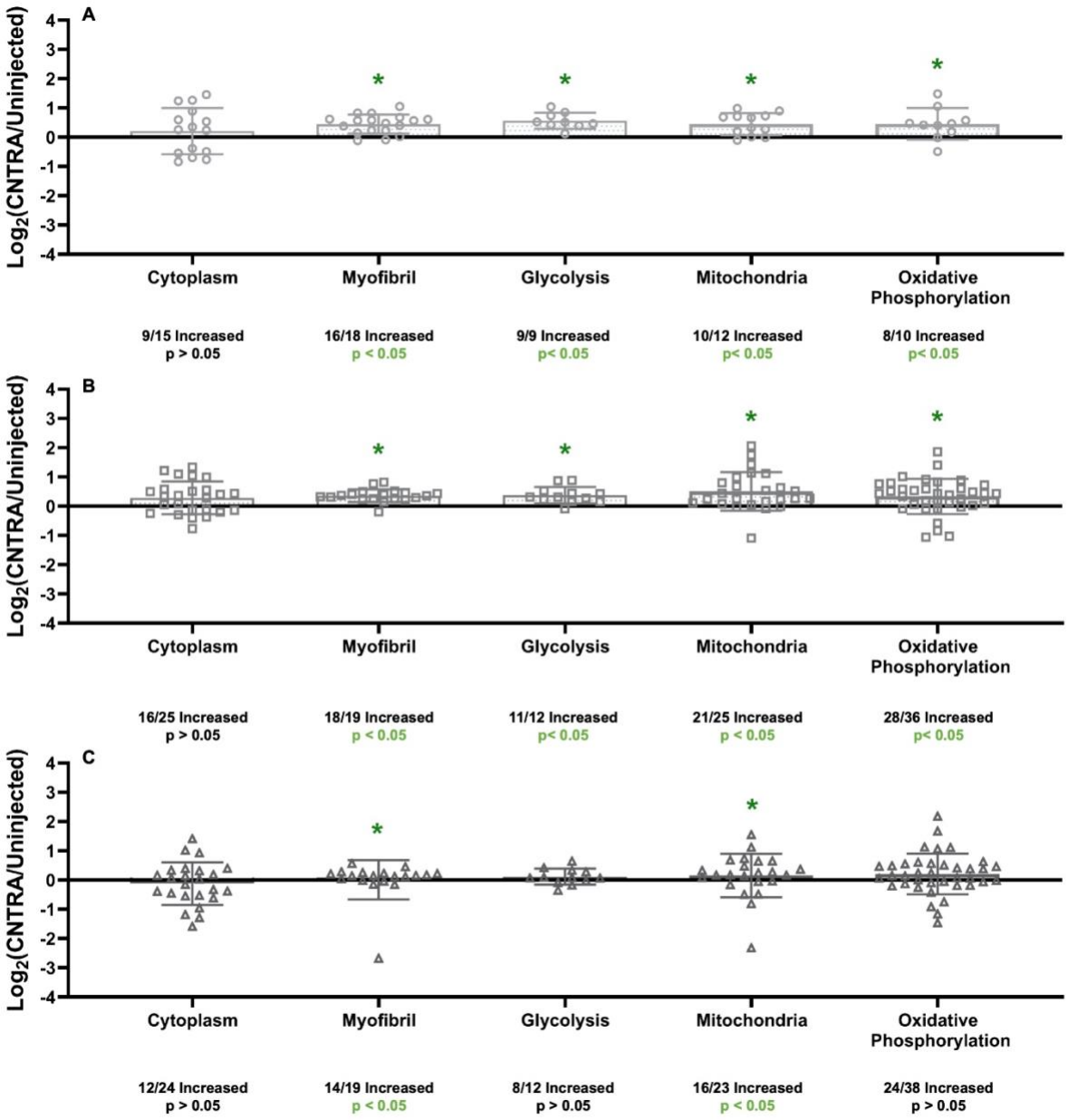

<u>Figure 4</u> Significantly Different Individual Protein Turnover Rates at Each Stage

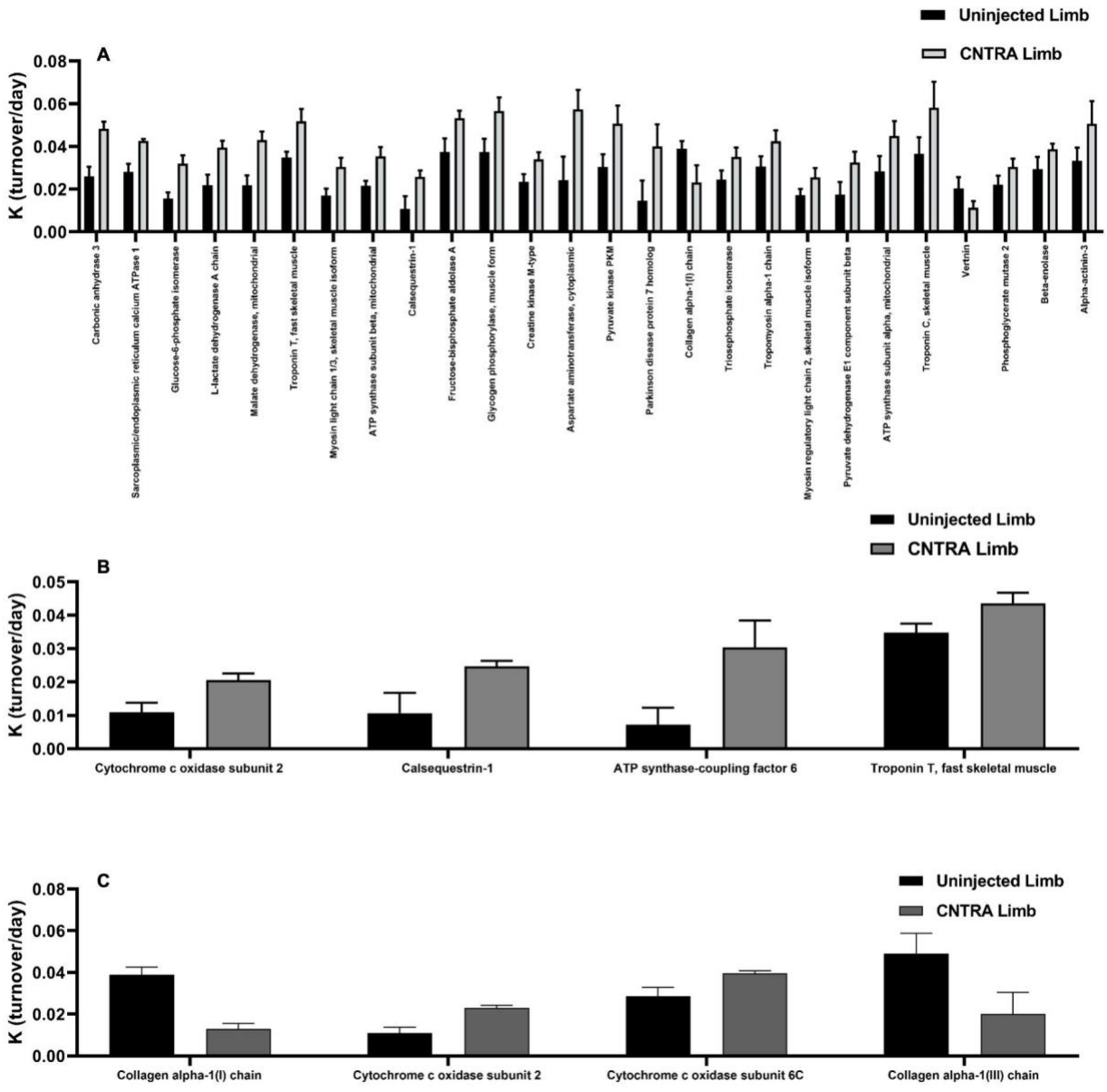

<u>Figure 5</u> Global Gene Expression Changes at Each Stage

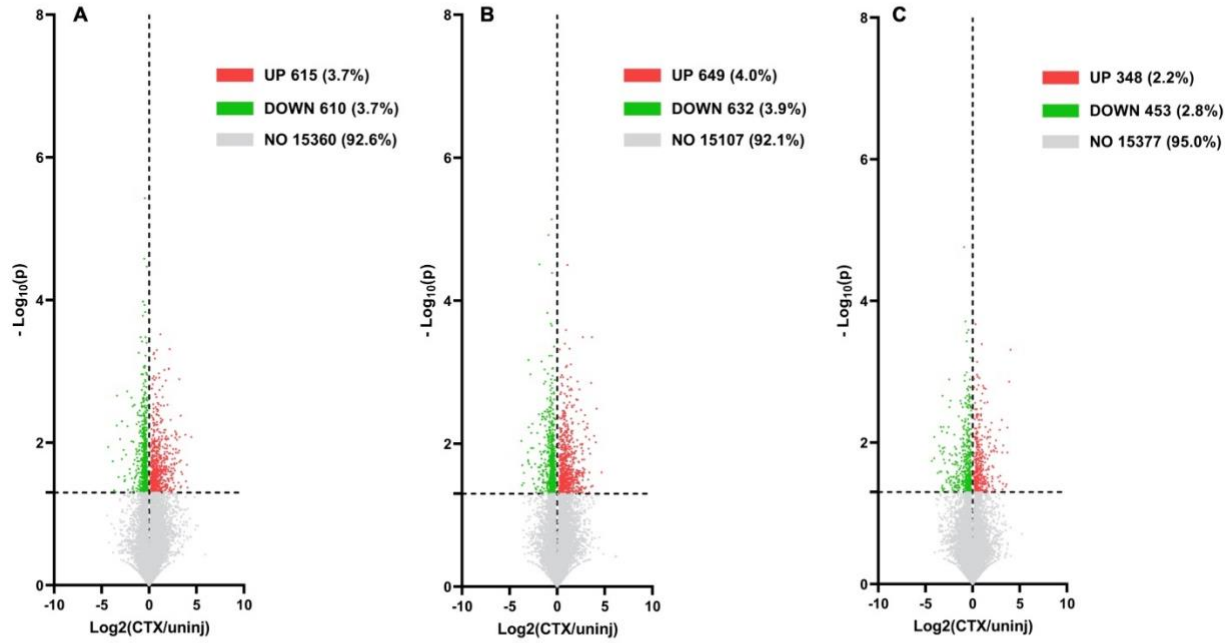

<u>Figure 6</u> Group Ontology Gene Expression at Each Stage

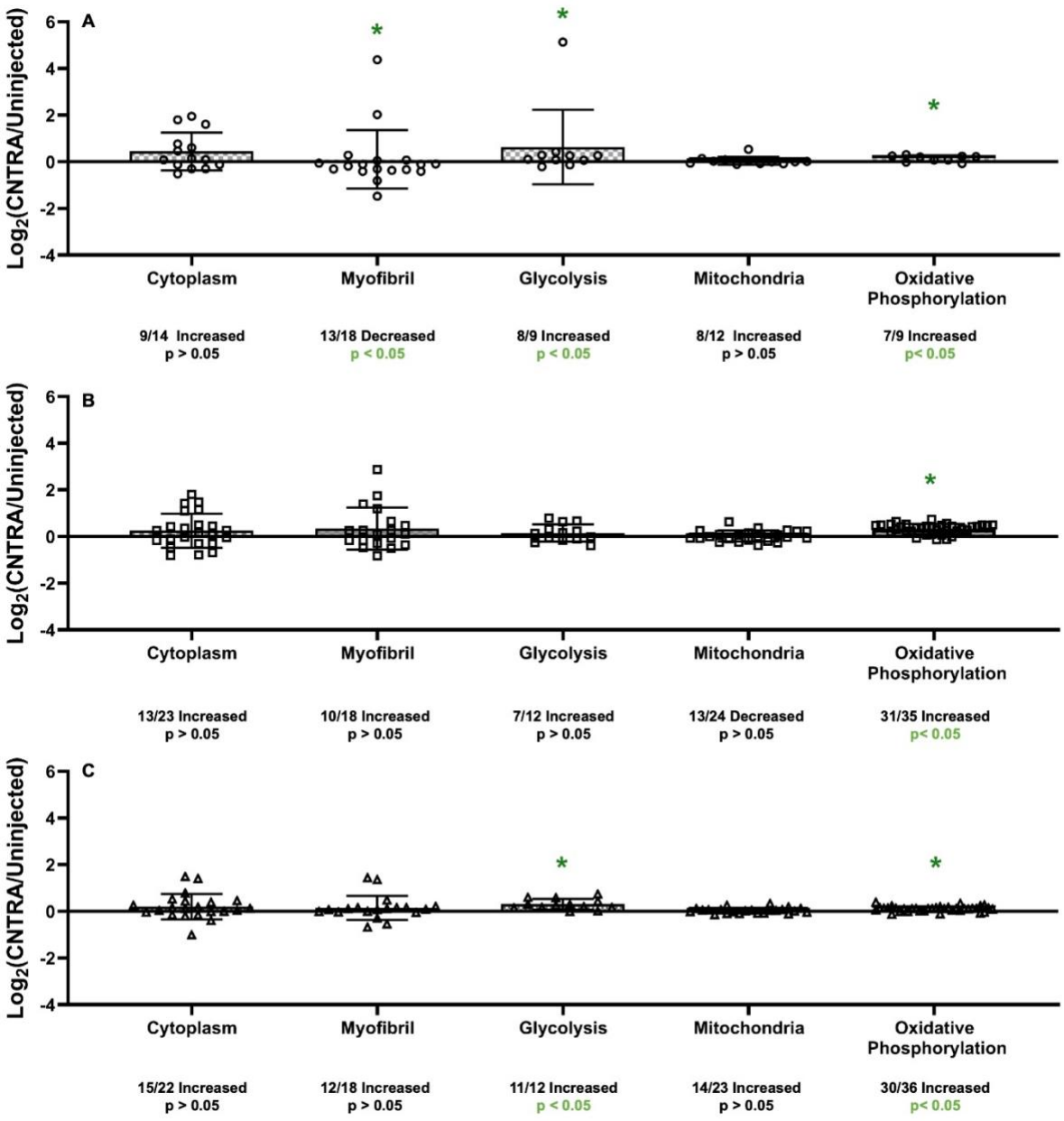

<u>Figure 7</u> Correlations of Changes in Gene Expression to Changes in Protein FSR

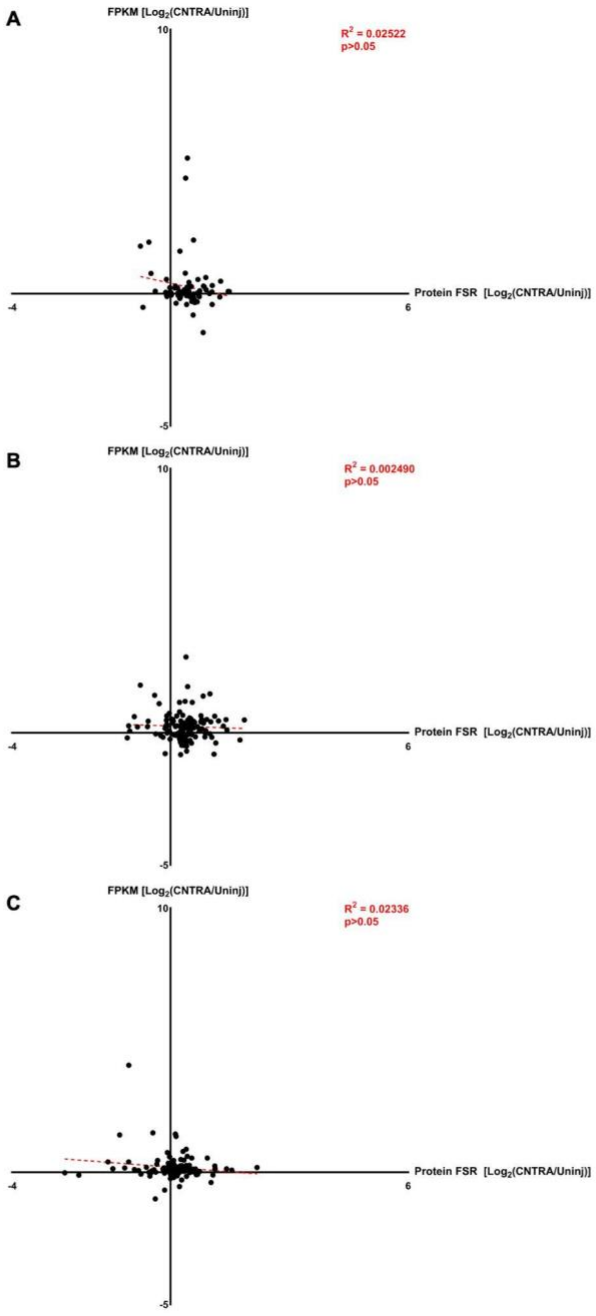

<u>Figure 8</u> My3 Protein Turnover, Myh3 Gene Expression, and Myogenic Gene Expression

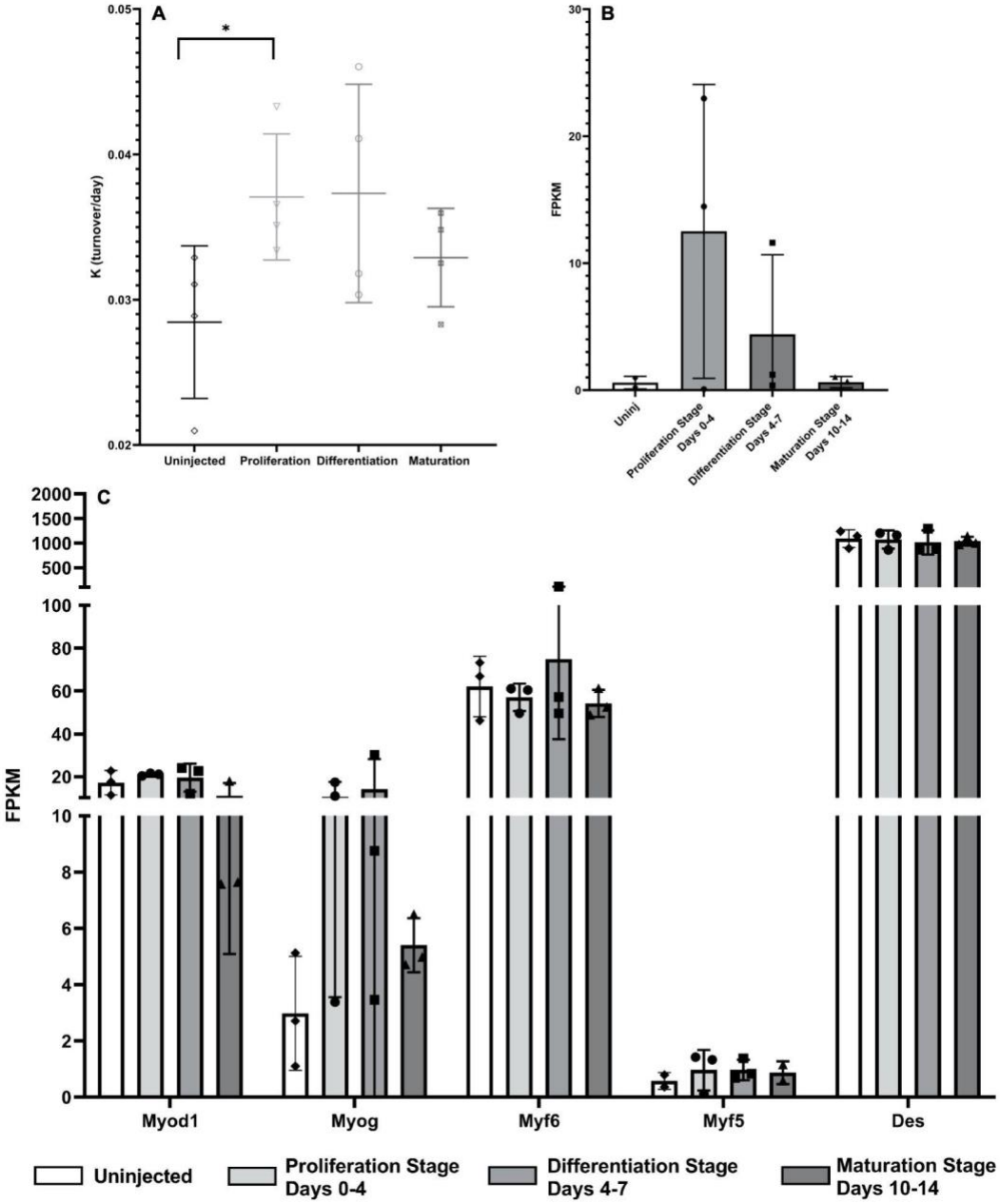

<u>Figure S1</u> Proteomic Signature of Non-Muscle (Liver) Tissue at all Stages